frontiers | Research Topics

Recent advances in immunosuppression-related swine diseases

Edited by
Gang Wang, Leyi Wang and Taofeng Du

Published in
Frontiers in Microbiology

ISSN 1664-8714
ISBN 978-2-8325-5216-2
DOI 10.3389/978-2-8325-5216-2

About Frontiers

Frontiers is more than just an open access publisher of scholarly articles: it is a pioneering approach to the world of academia, radically improving the way scholarly research is managed. The grand vision of Frontiers is a world where all people have an equal opportunity to seek, share and generate knowledge. Frontiers provides immediate and permanent online open access to all its publications, but this alone is not enough to realize our grand goals.

Frontiers journal series

The Frontiers journal series is a multi-tier and interdisciplinary set of open-access, online journals, promising a paradigm shift from the current review, selection and dissemination processes in academic publishing. All Frontiers journals are driven by researchers for researchers; therefore, they constitute a service to the scholarly community. At the same time, the *Frontiers journal series* operates on a revolutionary invention, the tiered publishing system, initially addressing specific communities of scholars, and gradually climbing up to broader public understanding, thus serving the interests of the lay society, too.

Dedication to quality

Each Frontiers article is a landmark of the highest quality, thanks to genuinely collaborative interactions between authors and review editors, who include some of the world's best academicians. Research must be certified by peers before entering a stream of knowledge that may eventually reach the public - and shape society; therefore, Frontiers only applies the most rigorous and unbiased reviews. Frontiers revolutionizes research publishing by freely delivering the most outstanding research, evaluated with no bias from both the academic and social point of view. By applying the most advanced information technologies, Frontiers is catapulting scholarly publishing into a new generation.

What are Frontiers Research Topics?

Frontiers Research Topics are very popular trademarks of the *Frontiers journals series*: they are collections of at least ten articles, all centered on a particular subject. With their unique mix of varied contributions from Original Research to Review Articles, Frontiers Research Topics unify the most influential researchers, the latest key findings and historical advances in a hot research area.

Find out more on how to host your own Frontiers Research Topic or contribute to one as an author by contacting the Frontiers editorial office: frontiersin.org/about/contact

Recent advances in immunosuppression-related swine diseases

Topic editors

Gang Wang — Shandong Agricultural University, China

Leyi Wang — University of Illinois at Urbana-Champaign, United States

Taofeng Du — Northwest A&F University, China

Citation

Wang, G., Wang, L., Du, T., eds. (2024). *Recent advances in immunosuppression-related swine diseases*. Lausanne: Frontiers Media SA.

doi: 10.3389/978-2-8325-5216-2

Table of contents

frontiers | Frontiers in Microbiology

TYPE Original Research
PUBLISHED 13 September 2023
DOI 10.3389/fmicb.2023.1241354

OPEN ACCESS

EDITED BY
Gang Wang,
Shandong Agricultural University, China

REVIEWED BY
Yihong Xiao,
Shandong Agricultural University, China
François J. M. A. Meurens,
Montreal University, Canada

*CORRESPONDENCE
Yin Wang
✉ 10334@sicau.edu.cn

†These authors have contributed equally to this work

RECEIVED 21 June 2023
ACCEPTED 23 August 2023
PUBLISHED 13 September 2023

CITATION
Jiang D, Tu T, Zhou Y, Li Y, Luo Y, Yao X, Yang Z, Ren M and Wang Y (2023) Epidemiological investigation and pathogenicity of porcine reproductive and respiratory syndrome virus in Sichuan, China.
Front. Microbiol. 14:1241354.
doi: 10.3389/fmicb.2023.1241354

Epidemiological investigation and pathogenicity of porcine reproductive and respiratory syndrome virus in Sichuan, China

Dike Jiang[1,2†], Teng Tu[1,2†], You Zhou[1,2], Yanwei Li[1,2], Yan Luo[1,2], Xueping Yao[1,2], Zexiao Yang[1,2], Meishen Ren[1,2] and Yin Wang[1,2*]

[1]Key Laboratory of Animal Diseases and Human Health of Sichuan Province, Sichuan Agricultural University, Chengdu, China, [2]College of Veterinary Medicine, Sichuan Agricultural University, Chengdu, China

Porcine reproductive and respiratory syndrome virus type 2 (PRRSV-2) lineage 8 was first detected in mainland China in 2006 and has since rapidly spread to become the primary epidemic strain in the country. In this study, samples such as lung tissue, hilar lymph nodes, abortion fetuses, and blood were collected from large-scale pig farms across 11 prefecture-level cities in Sichuan province between 2019 and 2020 for antigen detection and PRRS virus isolation. The antigen detection results indicated that the positive rate of HP-PRRSV (JXA1-Like strain) was 44.74% (51/114), NADC30-Like PRRSV was 17.54% (20/114), and classical PRRSV (VR2332-Like strain) was 37.72% (43/114). The predominant strain was HP-PRRSV. Positive samples were further inoculated into Marc-145 cells for virus isolation and identification, leading to the isolation of a new JXA1-Like PRRSV strain named SCSN2020. The strain was characterized by RT-qPCR, indirect immunofluorescence assay (IFA), plaque purification, electron microscopy, and whole genome sequencing. The total length of the viral genome was determined to be approximately 15,374 bp. A comparison of the SCSN2020 genome with VR2332 revealed that both strains had the same discontinuous 30-amino acid deletion on the Nsp2 gene. ORF5 genotyping classified the SCSN2020 strain as sublineage 8.7, with a whole genome sequence identity of 99.34% with JXA1. Furthermore, we evaluated the pathogenicity of the SCSN2020 strain in 28-day-old piglets and observed persistent fever from day 4 to day 10, weight loss started on day 7, dyspnea and severe lung lesions began started on day 14. The results of this study highlight the current PRRSV epidemic situation in Sichuan province and provide a scientific reference for subsequent prevention and control measures.

KEYWORDS

porcine reproductive and respiratory syndrome virus (PRRSV), ORF5, lineage 8, pathogenicity, epidemic situation

1. Introduction

Porcine reproductive and respiratory syndrome virus (PRRSV) is a major pathogen responsible for respiratory and reproductive diseases in pigs, significantly impacting the global pig industry. PRRSV is a single-stranded, positive-sense RNA virus that belongs to the *Arteriviridae* family (Mateu and Diaz, 2008; Guo et al., 2018). The genome size of PRRSV ranges between 15 and 15.5 Kb, encoding approximately 10 open reading frames (ORFs), including

ORF1a, ORF1b, ORF2a, ORF2b, ORF3, ORF4, ORF5a, ORF5, ORF6, and ORF7 (Johnson et al., 2011; Fang et al., 2012). ORF1a and ORF1b constitute about 75% of the genome and encode at least 16 non-structural proteins (Nsps), including Nsp1a, NSPSP1β, Nsp2, Nsp2TF, Nsp2N, Nsp3-Nsp6, Nsp7α, Nsp7β, and NSP8-NSP12 (van Dinten et al., 1999; Firth et al., 2011). Structural proteins are encoded by ORF2-7 located at the 3′ end of the genome, including six membrane-associated structural proteins—GP2, E, GP3, GP4, GP5, and M—as well as nucleocapsid proteins (N proteins; Meng et al., 1995; Kappes and Faaberg, 2015; Lunney et al., 2016). Of these, ORF5 encodes the surface glycoprotein GP5 of virus particles, which plays a vital role in virus attachment, endocytosis, assembly, and the production of neutralizing antibodies (Mardassi et al., 1996; Dokland, 2010; Hicks et al., 2018). Additionally, the ORF5 gene has been widely used to investigate the molecular prevalence of PRRS and strain lineage classification (Shi et al., 2010; Gao et al., 2017; Guo et al., 2018).

Porcine reproductive and respiratory syndrome virus (PRRSV) has two primary genotypes—PRRSV-1 (European type, Lelystad Virus) and PRRSV-2 (North American type, VR2332). In China, PRRSV-2 has been the dominant genotype since its first identification in 1996 (An et al., 2007; Kuhn et al., 2016). Based on the ORF5 gene, PRRSV can be further categorized into nine lineages, with the most common lineages in China being lineage 1 (NADC30-Like), lineage 3 (QYYZ-Like), lineage 5 (VR2332-Like), lineage 8 (CH-1R and JXA1), and lineage 9. In 1996, sublineage 5.1, or VR2332-Like PRRSV, emerged in China but did not cause a pandemic (Li et al., 2007; Tian et al., 2007; Liu et al., 2021). However, sublineage 8.7, commonly known as highly pathogenic PRRSV (HP-PRRSV) JXA1, emerged in 2006 with a high fever as the main pathogenic feature, resulting in significant losses to the pig industry. QYYZ-Like PRRSV was initially identified in Guangdong, China, in 2010 and had a low sequence identity with other Chinese lineage strains, initially classifying it as a new lineage (Lu et al., 2015; Zhou et al., 2019). Sublineage 1.8, also known as NADC30-Like PRRSV, first appeared in China in 2012 (Zhao et al., 2015; Zhou et al., 2015) and is currently the most prevalent strain in the country. Another rapidly spreading strain in China is sublineage 1.5 or NADC34-Like PRRSV, first reported in 2017 (Bao and Li, 2021; Zhao et al., 2022a). The NADC34-Like strains accounted for 11.5 and 28.6% of positive cases in 2020 and 2021, and have spread to eight provinces in China (Xu et al., 2022). However, changes in lineage, gene recombination, and mutation of epidemic strains pose significant challenges to the preventing and controlling in China (Wang H. M. et al., 2018; Yu et al., 2022). Studies have shown that sublineage 8.7 (JXA1-like) and sublineage 1.8 (NADC30-like) have become the dominant strains prevalent in China's swine herds, and NADC30-like strains have been highly regarded in recent years because of their high recombination and mutation rates. Multiple novel recombinant PRRSV strains from NADC30-Like outbreaks in China have recently been reported and exhibit different pathogenicity (Zhao et al., 2015; Liu J. K. et al., 2017; Chen et al., 2018). Additionally, the recombination of Chinese field strains and vaccine strains are emerging. These recombinant viruses exhibit significantly higher virulence than vaccine strains (Liu J. et al., 2017; Wang X. X. et al., 2018).

In this study, lung tissue, hilar lymph nodes, abortion fetuses, blood, and other pathogenic materials suspected of PRRSV infection were collected from large-scale pig farms in 11 prefecture-level cities in Sichuan province between January 2019 and January 2020 for pathogen detection and virus isolation. The highest positive rate was for HP-PRRSV, accounting for 44.74% (51/114) of samples. One strain of PRRSV was successfully isolated from the positive samples. Whole-genome sequencing and phylogenetic analysis classified the isolated strain as lineage 8 of PRRSV-2 (JXA1). Additionally, the pathogenicity of the isolated strain was evaluated through testing on 28-day-old piglets to provide scientific reference for subsequent prevention and control measures against PRRS in Sichuan province.

2. Materials and methods

2.1. Sample treatment

Clinical samples (including lung, hilar lymph node, abortion fetus, and blood) with suspected PRRSV infection were chopped up, freeze-thawed repeatedly, and then ground. After grinding was repeated three times, 2 mL PBS was added, centrifuged at 9710 × g for 5 min (4°C), and stored at −80°C. All clinical samples were collected from large-scale pig farms in Sichuan Province from 2019 to 2020.

2.2. Primer design and PRRSV detection in clinical samples

RNA was extracted using AG RNAex Pro RNA extraction reagent, and reverse transcription was performed using Evo M-MLV RT Kit (AG, Hunan, China). The reverse transcription reaction conditions were as follows: 37°C for 15 min, 85°C for 5 s, and 4°C ∞; the RNA reverse transcriptional reaction system is shown in Supplementary Table S1. Then the samples were detected by RT-qPCR and RT-PCR to confirm PRRSV positive. All primers are shown in Supplementary Table S2 (General Administration of Quality Supervision, Inspection and Quarantine of the People's Republic of China, Standardization Administration of China, 2018; Liao, 2019; Xu et al., 2019).

2.3. Isolation and identification of PRRSV

RT-qPCR-positive samples, including serum and lung tissue samples, were filtered through a 0.22 μm filter membrane to eliminate bacteria. For each sample, 1 mL of filtered supernatant was mixed with 1 mL of serum-free DMEM and added onto a monolayer of Marc-145 cells at a cell density between 80 and 90%. As described previously (Liu et al., 2022), a specific PRRSV polyclonal antibody labeled with fluorescein isothiocyanate (FITC) against PRRSV N protein (Bioss, Beijing, China) was used to detect PRRSV. As previously mentioned (Zhou et al., 2018a,b,c,d), the virus was purified by plaque analysis, and the virus titer was calculated according to the Reed-Muench method (Reed and Muench, 1938). Then, purified virus isolates were used to sequence their entire genomes. Meanwhile, to investigate the effect of different multiplicities of infection (MOI) on the growth of PRRSV in Marc-145 cells, we infected cells with MOI = 0.01 and MOI = 1 in triplicate. We incubated them for 1.5 h at 37°C. DMEM medium containing 2% serum was added for maintenance, and virus fluid was collected every 24 h and frozen at −80°C. After 5 days, we determined the virus titer and drew a growth curve. The PRRSV

strain isolated from Sichuan province in 2020 was designated as SCSN2020.

2.4. Observation of virus particles using electron microscopy

The PRRS virus suspension was dispatched to Wuhan Servicebio Biotechnology Company for transmission electron microscopy analysis. We loaded 20 μL of the virus suspension onto a copper grid with a carbon film using a pipet gun, allowing it to incubate for 3–5 min. Excess liquid was carefully absorbed using filter paper. Subsequently, we applied 2% phosphotungstic acid to the copper grid, staining it for 1–2 min. Excess liquid was removed using filter paper, and the grid was left to dry at room temperature. Finally, the copper grids were observed under a transmission electron microscope (TEM), and images were captured.

2.5. Whole genome sequencing and bioinformatics analysis of PRRSV isolate

PRRSV RNA was extracted, and cDNA was prepared according to the above procedures and then sent to Beijing Tsingke Biotech Company for whole genome sequencing. Mega 6 (Tempe, AZ, United States) was used to analyze the whole genome homology and amino acid sequence of the primary genes and related genes of PRRSV strains in each region and the isolated strains in this study in the NCBI database, and the genetic evolution tree was constructed. The SeqMan program of DNAstar software version 7.0 (DNASTAR Inc., Madison, United States) was used to assemble the full-length genome sequence of the isolated strain. The PRRSV genome, ORF, and derived protein sequences were analyzed using DNAstar's EditSeq and MegAlign programs.

2.6. Pathogenic experiment

Ten weaned piglets (about 28 days of age) were purchased from Chengdu Wangjiang Agriculture and Animal Husbandry Technology Company. All of them were negative for PRRSV antigen and antibody by RT-qPCR and ELISA assay. All the animals were randomly divided into two groups and separated into different rooms. All animals were individually housed under controlled temperature (26°C), humidity (60%), and lighting (12 h/day), with free access to water. Grouping of experimental animals: Ten weanling piglets were divided into the following groups: Group 1 (challenge group): Five weanling piglets were inoculated with 2 mL of virus solution (TCID50 = 10^5/mL) via nasal drip; Five piglets in group 2 (control group) were inoculated with 2 mL DMEM/mL via an intranasal drop.

Following the viral challenge, clinical indicators were regularly monitored on the weanling piglets, including daily recordings of rectal temperature and observations of various clinical manifestations such as appetite, mental state, and breathing. The scores of the resulting clinical signs were recorded and tabulated in Supplementary Table S3 (Sun, 2017). Additionally, piglet weights were measured and documented on days 3, 7, 10, and 14 post-challenge to track any changes in growth patterns. These comprehensive evaluations aimed to assess the viral infection's impact on the piglets' health and welfare and provide insights into potential treatment options for this particular virus strain.

Viral load measurement of the weanling piglets was conducted by collecting blood, nasal, and oral secretions at regular intervals after the viral challenge (0, 3, 7, 10, and 14 days). RT-qPCR assays were used to detect signs of detoxification in these samples. Additionally, viremia levels in serum were assessed using the TCID50 method. These evaluations aimed to provide insights into the piglets' viral clearance and detoxification mechanisms, thereby viral contributing to our understanding of how this particular virus strain interacts with its host.

If piglets died during the experiment, they were dissected immediately, and the gross pathological changes of each organ were observed. Lung and hilar lymph nodes were collected, rinsed with PBS to remove blood, soaked in 4% paraformaldehyde solution, fixed at room temperature for 24 h, and then embedded in the tissue, paraffin section and HE staining were used to observe the pathological changes. On day 14 of the challenge, the remaining pigs were euthanized and dissected, and tissues were collected and fixed as described above. Animal experiments in this study were approved by the Animal Ethics Committee of Sichuan Agricultural University (20220261). All experimental procedures and animal welfare standards strictly followed the guidelines of Animal Management at Sichuan Agricultural University.

2.7. Statistical analysis

Statistical analysis was performed with GraphPad Prism 8.0.2 (GraphPad Software, San Diego, CA, United States), and all data were using one-way ANOVA with the *t*-test. The level of significance was set at $p < 0.05$.

3. Results

3.1. RT-qPCR survey of clinical samples

Between 2019 and 2020, a total of 205 lung, hilar lymph nodes, serum, and abortion samples were collected in Sichuan to investigate the prevalence of PRRSV. Of these, 114 samples tested positive for PRRSV with an overall positivity rate of 55.61% (114/205). The highest positivity rate was observed in lung samples at 63.33% (38/60), as shown in Table 1. Specifically, 51 samples were positive for HP-PRRSV, 20 samples were positive for NADC30-like PRRSV, and 43 samples were positive for classical PRRSV; selected test results are presented in Supplementary Figure S1. In particular, the HP-PRRSV target band appeared at about 514 bp, while that of NADC30-like PRRSV appeared at approximately 334 bp (Supplementary Figure S1A). Additional RT-qPCR assays revealed that Supplementary Figures S1B–D corresponded to NADC30-like PRRSV, classical PRRSV, and HP-PRRSV, respectively.

3.2. Isolation and identification of PRRSV

3.2.1. Isolation and indirect immunofluorescence of PRRSV

The PRRSV-positive material was identified by RT-qPCR, which was inserted into Marc-145 cells and cultured in a 37°C CO2

TABLE 1 PRRSV detection results in each city of Sichuan Province from 2019 to 2020.

City	Lung (positive)	Hilar lymph nodes (positive)	Abortive fetal (positive)	Blood (positive)	Number of positive	Total sample number	Positive rate
Chengdu	4/7	2/5	–	2/6	8	18	44.44% (8/18)
Deyang	7/10	-	–	3/15	10	25	40% (10/25)
Guangyuan	2/3	1/1	2/3	3/5	8	12	66.67% (8/12)
Leshan	1/4	–	–	4/9	5	13	38.46% (5/13)
Meishan	2/3	–	–	7/10	9	13	69.23% (9/13)
Mianyang	1/2	0/1	1/2	3/6	5	11	45.45% (5/11)
Nanchong	1/2	–	–	3/9	3	11	27.27% (3/11)
Neijiang	3/5	–	–	7/10	10	15	66.67% (10/15)
Suining	15/20	3/5	9/16	18/25	45	66	68.18% (45/66)
Yaan	1/2	–	–	6/10	7	12	58.33% (7/12)
Yibin	1/2	–	–	3/7	4	9	44.44% (4/9)
Number of positives	38	6	12	58	114	–	–
Total sample	60	12	21	112	–	205	–
Positive rate	63.33% (38/60)	54.54% (6/11)	54.55% (12/22)	51.79% (58/112)	–	–	55.61% (114/205)

incubator for 4–5 days. qPCR was performed every three passages. The results showed that one strain of PRRSV was isolated and cultured into Marc-145 cells for 48 h, the cells began to become larger and showed typical warp-like lesions. At 72 h, the lesions could reach 80%, showing mass or grape-shaped lesions (Figure 1A). The control group cells were in good condition with clear cell edges (Figure 1B).

To confirm infection with the PRRSV strain isolated from swine samples, indirect immunofluorescence was used to identify infected Marc-145 cells that had been cultured for 48 h. The cells were stained with rabbit anti-PRRSV N protein followed by FITC-labeled sheep anti-rabbit IgG, and the results are shown in Figure 1C. The staining pattern indicated that the isolated PRRSV strain could proliferate on Marc-145 cells, confirming our previous observations of morphological changes suggestive of viral infection.

3.2.2. Results of $TCID_{50}$ determination

To determine the infectious titer of PRRSV isolates, cell supernatant was collected, and performed a $TCID_{50}$ assay using 96-well cell culture plates. The cell supernatant was diluted 10-fold and inoculated into the plates, which were then incubated at 37°C with CO2 for 4–5 days. We counted the number of cytopathic effects (CPEs) for each dilution and calculated the $TCID_{50}$ of PRRSV using the Reed-Muench formula. The resulting titer was determined to be $10^{-6.39}$/0.1 mL (Supplementary Table S4).

3.2.3. Plotting of viral one-step growth curves

To visualize virus growth over time, virus titers were plotted against corresponding time points by $TCID_{50}$ assay to generate growth curves for each MOI (Supplementary Figure S2). Our results showed that when Marc-145 cells were infected with the MOI = 1, the virus titer reached its highest point on the second day, with a PRRSV titer of $10^{-7.0}$/mL. In contrast, when cells were infected with a MOI of 0.1, the virus titer reached its highest level of $10^{-6.917}$/mL on the third day. The TCID50 of PRRSV on the fifth day were $10^{-5.833}$/mL (MOI = 1) and $10^{-5.917}$/mL (MOI = 0.1), respectively.

3.2.4. Results of virus plaque purification assay and transmission electron microscopy

A plaque assay and transmission electron microscopy analysis were performed to further characterize the isolated PRRSV strain. After 10-fold dilution of the virus solution, we inoculated 10^−4, 10^−5, and 10^−6 dilutions onto single-layer Marc-145 cells in six-well plate. After 5 days of culture in a 5% CO2 incubator at 37°C, uniform plaques appeared, displaying a typical PRRSV plaque pattern (Figure 2). The presence of these plaques confirms that the isolated PRRSV strain can infect and replicate within Marc-145 cells.

In addition, we sent the virus solution to Wuhan Servicebio Biotechnology Company for transmission electron microscopy identification. Figure 3 shows polymorphic spherical virions of about 50–70 nm were observed in the supernatant, consistent with other observations of PRRSV virus particles by electron microscopy (Arteriviridae and Roniviridae, 2017). Based on these identification techniques, we designated this strain as PRRSV SCSN20.

3.3. Whole genome sequencing and bioinformatics analysis of PRRSV SCSN2020

3.3.1. Whole genome sequencing and annotation of PRRSV SCSN2020

The sequencing results of PRRSV SCSN2020 were visualized using CG view. The full length of the PRRSV genome was 15,374 bp (GenBank accession number: OQ883907), with a GC content of 52.4%. ORF1a and ORF1b constituted 75% of the entire genome and were transcribed and translated into two polyproteins, pp1a, and pp1ab. pp1a was cleaved into Nsp1α, Nsp1β, Nsp2, Nsp3, Nsp4, Nsp5,

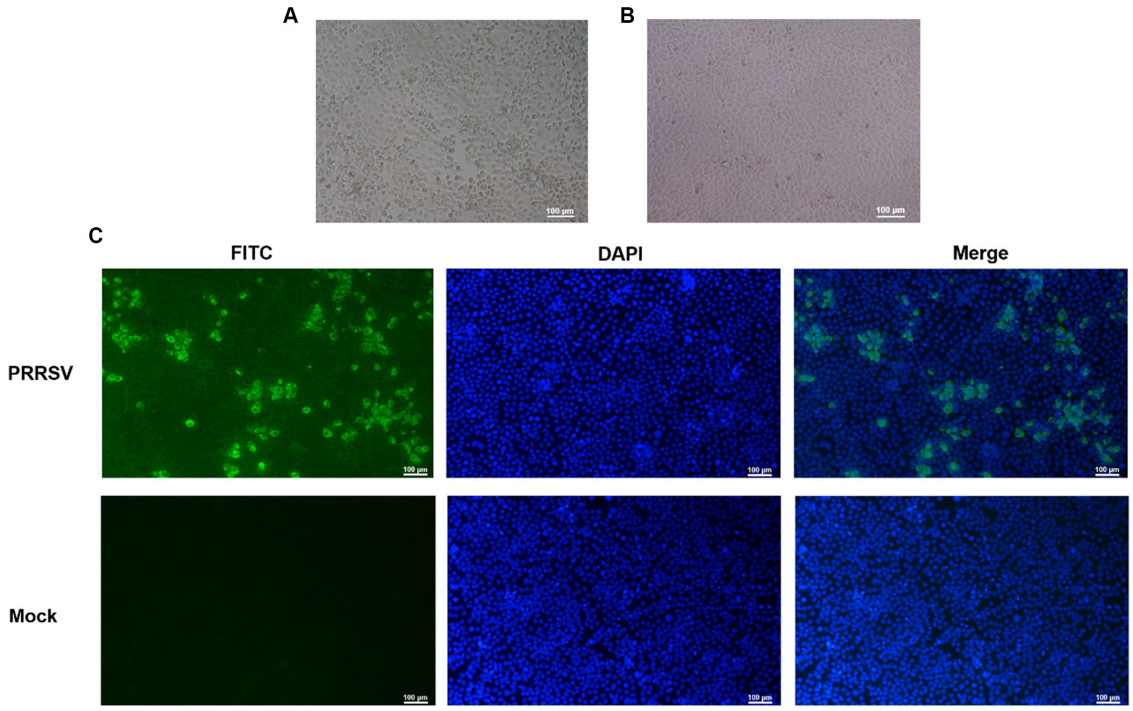

FIGURE 1
Identification of porcine reproductive and respiratory syndrome virus (PRRSV) isolates. **(A)** CPE diagram of Marc-145 cells infected with PRRSV isolates; **(B)** Blank control; **(C)** Results of indirect immunofluorescence assay.

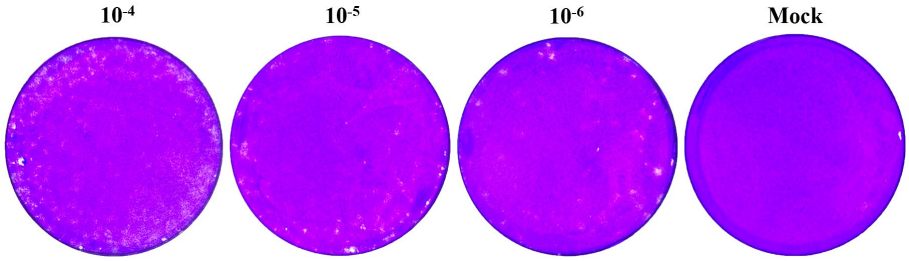

FIGURE 2
Plaque purification results.

Nsp6, Nsp7α, Nsp7β, and Nsp8, while pp1ab was cleaved into nonstructural proteins such as Nsp9, Nsp10, Nsp11, and Nsp12. Additionally, ORF2, ORF2b, ORF3, ORF4, ORF5a, ORF5, and ORF6 encode envelope proteins (E, GP2, GP3, GP4, GP5a, GP5, and M proteins) and N proteins, respectively (Figure 4A).

3.3.2. Genetic evolution analysis of PRRSV SCSN2020

To assess the genetic relatedness between PRRSV SCSN2020 and other reference strains, we compared the nucleotide identity rates of the isolated strain with those of CH-1a, CH-1R, JXA1, NADC30, NADC34, VR2332, and QYYZ strains (Table 2). The results showed high levels of similarity between the isolated strain and most reference strains, with nucleotide identity rates ranging from 82.21 to 99.34%. Specifically, the sequence identity rate with LV strain was 58.87%, confirming that the isolated strain belonged to the PRRSV-2 strain. Further comparison with the sequences of PRRSV in the GenBank database revealed that the PRRSV SCSN2020 strain was closely related to the JXA1 strain. Specifically, the nucleotide and protein sequences of the 5'UTR, ORF1a (Nsp1α, Nsp1β, and Nsp2-8), and ORF1b (Nsp9-Nsp12) of PRRSV SCSN2020 were highly similar to those of JXA1, with nucleotide identity rates ranging from 97.39 to 100% and protein identity rates ranging from 95.51 to 100%.

To establish the genetic relationship between PRRSV SCSN2020 and representative strains of other PRRSV lineages, a phylogenetic tree was constructed based on the ORF5 gene sequence. The results showed that the other strains could be divided into four lineages based on the ORF5 gene except for the LV strain. Lineage 8 was mainly JXA1-Like, CH-1a-Like, TJ-Like, etc. Lineage 1 was mainly NADC30-Like and NADC34-Like. The third lineage was QYYZ-Like. Lineage 5 is VR2332-Like. The SCSN2020 strain isolated in this study was classified as lineage 8.7 (Figures 4B,C).

Compared with the VR2332-Like strain, the NSP2 protein sequence of the SCSN2020 isolate was missing one aa at 481aa. 533-561aa, deletion of 29 aa; Consistent with JXA1-Like (Supplementary Figures S3A,B); there were two Hypervariable regions (HVR) in ORF5 (Supplementary Figure S3C), HVR1 aa 33–35, SCSN2020 was NNN; HVR2 57–60 was AQKF; In addition, SCSN2020 contained three transmembrane regions and two virulence sites (aa 13 and aa 151), and the primary amino acid was arginine (R).

3.4. Pathogenicity analysis of SN2020

3.4.1. Results of body temperature and body weight of piglets after the challenge

The results are presented in Figures 5A,B. In Figure 5A, it can be seen that the body temperature of the challenged piglets started to rise on the fourth day after the challenge. On the sixth day, it had increased to 40.65°C, and all the challenged pigs were above 40°C. From the 10th day onwards, the population temperature began to decrease. On the other hand, the control pigs showed no abnormalities throughout the experiment.

In Figure 5B, it can be observed that there was no significant difference between the control group and the challenge group for the first 3 days. However, from day 7 and day 14, the body weight of piglets in the challenge group was significantly lower than that in the control group ($p < 0.05$).

The body weight of piglets in the challenge group decreased by 1.10 and 1.66 kg, respectively. This indicates that the strain could decrease the weight growth of piglets, and the difference was more significant with the extension of time.

3.4.2. Clinical symptom score results of piglets after challenge

The results are presented in Figure 6. On the challenge's third day, pigs' feed intake decreased, and some pigs showed clinical signs such as runny noses and clumps. On day 4, the clinical signs worsened, and the pigs developed a decreased appetite, eyelid edema, and an indirect mild cough. By the seventh day, the pigs began to cluster, sneeze, cough, depression, and have other clinical signs. A few pigs also showed clinical signs such as ear redness and abdominal breathing.

On day 14, one of the pigs had dyspnea, stopped feeding, and had obvious abdominal breathing. These clinical signs suggest that the strain had adverse effects on the respiratory system of the piglets. The decrease in feed intake and appetite also indicates that the strain had negative impacts on the digestive system of the piglets.

3.4.3. Detection of detoxification of piglets after the challenge

The results are presented in Figure 7. On day 7 after the challenge, the amount of virus in blood reached the peak (2.05×10^5 copies/mL) and then began to slowly decline (Figure 7A). Similarly, the amount of virus in nasal swabs peaked at 9.58×10^3 copies per milliliter on day 10 after the challenge and then began to decline (Figure 7B). The virus titer in the serum of piglets was 10^4 TCID50/ml on day 7, $10^{4.35}$ TCID50/mL on day 10, and $10^{4.65}$ TCID50/mL on day 14 after infection (Figure 7C).

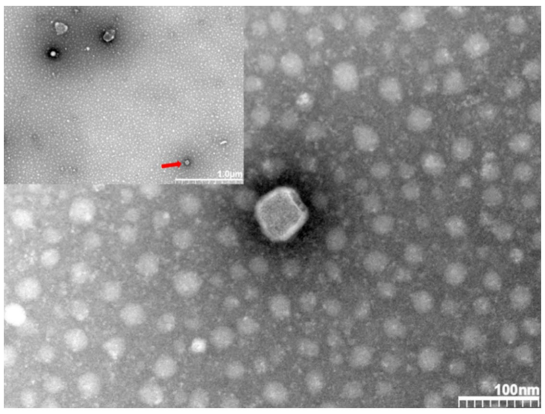

FIGURE 3
Transmission electron microscopic observation of virions.

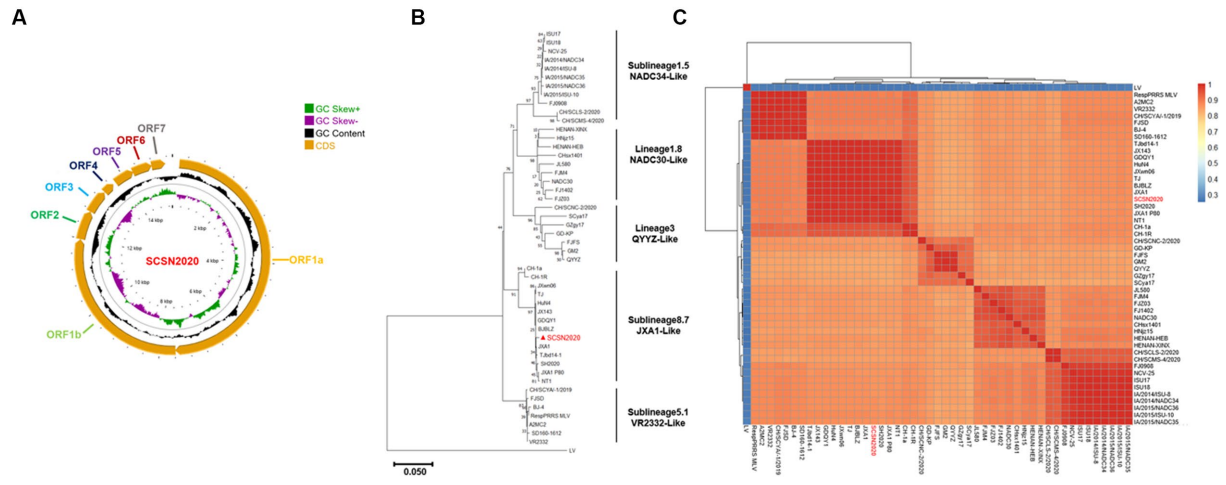

FIGURE 4
Whole genome sequencing and annotation of SCSN2020. SCSN2020 whole genome **(A)**, SCSN2020 phylogenetic tree based on PRRSV ORF5 gene **(B)**, cluster analysis of strains of each lineage of PRRSV **(C)**.

10.3389/fmicb.2023.1241354

TABLE 2 Sequence alignment results of PRRSV SCSN2020 with other reference strains.

Genome	CH-1A		CH-1R		JXA1		LV		NADC30		NADC34		VR2332		QYYZ	
	nt	aa	nt	aa	nt	aa	nt	aa	nt	aa	nt	aa	nt	aa	nt	aa
Complete genome	94.42		94.25		99.34		58.87		82.56		82.21		88.92		86.49	
5' UTR	97.37		95.79		100		54.05		91.62		92.59		91.58		95.26	
NSP1	94.34	92.43	94.26	92.43	99.04	99.22	55.33	48.07	84.86	85.9	84.25	86.42	89.03	90.08	88.42	88.51
NSP2	89.42	84.9	89.52	84.59	99.72	99.47	48.35	26.63	66.65	58.96	67.99	58.78	80.92	74.49	78.02	71.56
NSP3	95.07	98.43	95.07	98.43	99.63	99.55	58.92	57.81	83.41	91.03	82.88	91.03	90.88	98.43	82.06	88.57
NSP4	95.59	96.57	95.75	97.06	100	100	60.78	61.76	85.13	93.14	86.27	94.61	90.03	96.57	86.64	92.16
NSP5	94.51	95.29	93.92	94.71	100	100	63.8	71.76	90	94.12	84.34	88.89	89.61	95.29	81.96	90
NSP6	97.92	100	97.92	100	100	100	68.75	75	93.75	93.75	87.5	87.5	95.83	93.75	97.92	100
NSP7	96.01	96.91	95.62	96.53	99.23	100	52.48	40.51	82.63	84.94	82.11	86.87	89.45	89.58	93.82	94.21
NSP8	98.55	100	97.08	100	98.54	100	63.77	68.89	87.59	95.56	89.78	93.33	94.33	100	94.93	100
NSP9	96.46	98.59	96.41	98.44	99.06	98.91	66.74	73.02	87.19	97.03	87.24	96.88	92.29	97.66	91.25	97.34
NSP10	95.15	97.51	95.08	97.73	99.17	99.09	60.38	63.72	85.71	95.01	85.91	95.01	90.08	96.36	90.23	97.27
NSP11	94.79	97.77	95.09	98.66	98.81	99.11	66.52	76.44	91.07	96.43	86.31	96.43	90.48	95.54	88.39	94.64
NSP12	96.31	96.73	95.88	96.73	99.78	99.35	48.2	29.49	90.26	96.73	83.12	90.85	89.61	94.77	87.01	95.42
ORF2	95.86	95.31	95.34	94.92	98.84	98.83	63.31	59.38	85.77	85.55	86.8	85.16	92.63	91.8	89.26	88.28
ORF3	95.29	92.13	95.03	92.52	98.56	97.24	62.17	52.63	83.01	80.31	83.27	81.89	88.89	86.22	90.07	87.01
ORF4	96.65	98.31	96.46	97.75	97.39	95.51	65.04	67.76	86.96	89.89	86.22	90.45	89.76	91.01	94.23	95.51
ORF5	92.99	92.5	92.33	91	97.55	99	62.68	56.59	84.01	85.5	85.32	86.5	87.6	87.5	82.22	82
ORF6	97.33	97.7	96.95	97.13	99.81	100	69.14	78.74	88.76	93.1	88.95	93.68	95.24	97.7	90.66	96.55
ORF7	95.97	95.12	95.97	95.93	99.73	100	62.06	54.96	90.86	91.06	89.52	91.06	93.82	95.12	89.52	91.87
3' UTR	92.7		91.01		100		53.37		75.84		75.28		87.37		82.02	

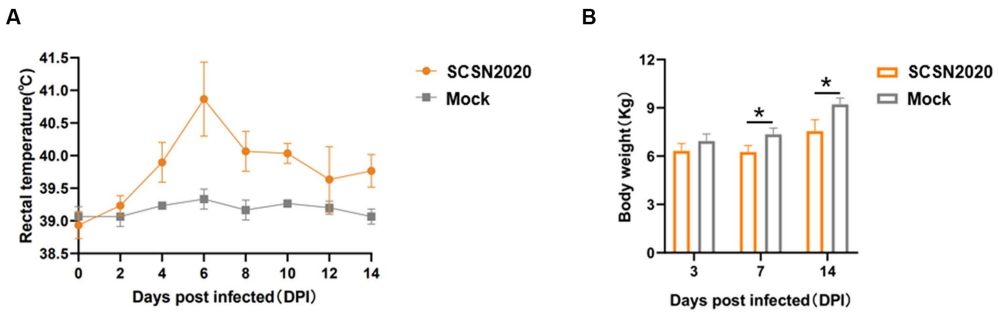

FIGURE 5
Changes in body temperature **(A)** and body weight **(B)** of piglets after challenge.

3.4.4. Pathological observation after dissection

The piglets in the challenge group showed obvious pneumonia, with tissue consolidation and multiple foci in the apical lobe of the lung, widening of the lung interstitium, and obvious bleeding points on the lung surface (Figure 8A). The hilar lymph nodes were enlarged and bleeding (Figure 8C). The results of pathological sections showed that the overall structure of the lung tissue of piglets in the challenge group was abnormal, with unclear alveolar tissue structure, significant collapse, thickening of the alveolar wall and parenchymal tissue, slight congestion of the lung interstitium, and significant infiltration of inflammatory cells (Figure 8A). The structure of pulmonary lymph nodes was not clearly defined, and the boundary between the cortex and medulla was unclear, with a large amount of diffuse lymphoid tissue visible (Figure 8C).

In contrast, the blank group showed normal lung tissue structure, with no alveolar fusion, expansion, atrophy, or other degeneration observed. There was no obvious loss, edema, or shedding of the alveolar epithelial cells in the tissue, no thickening of the alveolar wall, and no inflammatory cell infiltration. The lymphoid nodules were tightly packed with clear boundaries

between the cortex and medulla of the tissue, and abundant numbers of lymphocytes (Figures 8B,D).

4. Discussion

Porcine Reproductive and Respiratory Syndrome (PRRS) first emerged in China in 1996, rapidly spreading across the country and causing significant economic losses to the pig industry (An et al., 2007; Sui et al., 2018). Currently, vaccination represents the main strategy for preventing and controlling PRRS outbreaks. However, a contentious issue has arisen regarding the effectiveness of PRRSV vaccines; in clinical settings, such vaccines are frequently inefficient and ineffective (Guo et al., 2018). Nevertheless, given the prevalence of PRRS, vaccination remains the primary approach available. Commercially available vaccines in China include CH-1a/CH-1R, R98/R98 MLV, VR2332/Ingelvac PRRS MLV, JXA1/JXA1-R, TJ/TJM-F92, HuN4/ Hun4-F112, GD/GDr180, and among others (Leng et al., 2017; Wang H. M. et al., 2018; Ding et al., 2021). While these vaccines can partially control PRRS outbreaks and reduce the duration of clinical signs and viremia in pigs, they cannot provide full protection against PRRS infection, with vaccine efficacy limited to partial or modest protection against heterologous challenges.

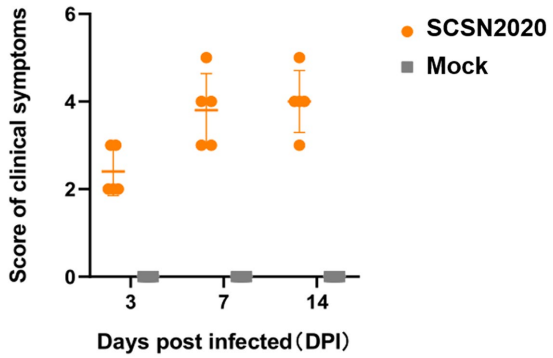

FIGURE 6
Changes in clinical symptom scores of piglets after the challenge.

However, mass vaccination with attenuated vaccines can pose safety risks and lead to genetic variations (Wang et al., 2015; Zhou et al., 2017). Studies indicate that vaccinated pigs can transmit vaccine viruses to unvaccinated pigs, thus propagating different vaccine strains within pig populations (Li et al., 2016, 2017; Bian et al., 2017; Wang X. X. et al., 2018). Large-scale vaccination with attenuated vaccines may also contribute to the emergence and spread of PRRSV-2 (Shi et al., 2013). Furthermore, "reverse virulence" has been reported during attenuated vaccine administration (Jiang et al., 2015). The misuse and overuse of vaccines have also contributed to the emergence of complex strains of PRRSV, notably NADC30-Like PRRSV, which predominantly recombines with HP-PRRSV (JXA1), classical PRRSV (CH-1R, VR2332), and attenuated vaccines (TJM-F92) to produce novel strains (Wang et al., 2016). In addition to the recombination between vaccine strains and other PRRS viruses, HP-PRRSV strains in China demonstrate recombination patterns across distinct lineages and sublineages. HP-PRRSV strains emerged in 2006, represented by JXA1, TJ, and HuN4, also parental strains of JXA1-R, TJM-F92, and HUN4-F112. In a previous study, we found that since 2016, the prevailing strains in Sichuan Province are mainly VR2332-Like, JXA1-Like, and NADC30-Like, and present different ways of recombination, mainly as follows: JXA1-Like+NADC30 -Like (Zhou et al., 2018a,b,c,d); VR2332-Like+JXA1-Like+NADC30-Like (Zhou et al., 2018a,b,c,d); JXA1-Like+NADC30-Like+QYYZ-Like (Zhou et al., 2018a,b,c,d). These studies further demonstrate that recombination may occur between PRRSV strains and vaccine strains. Lineage 3 surfaced in 2010, typified by QYYZ and GM2, among others. Subline 1.8 emerged in 2013, exemplified by NAD30-Like (Zhang et al., 2017,

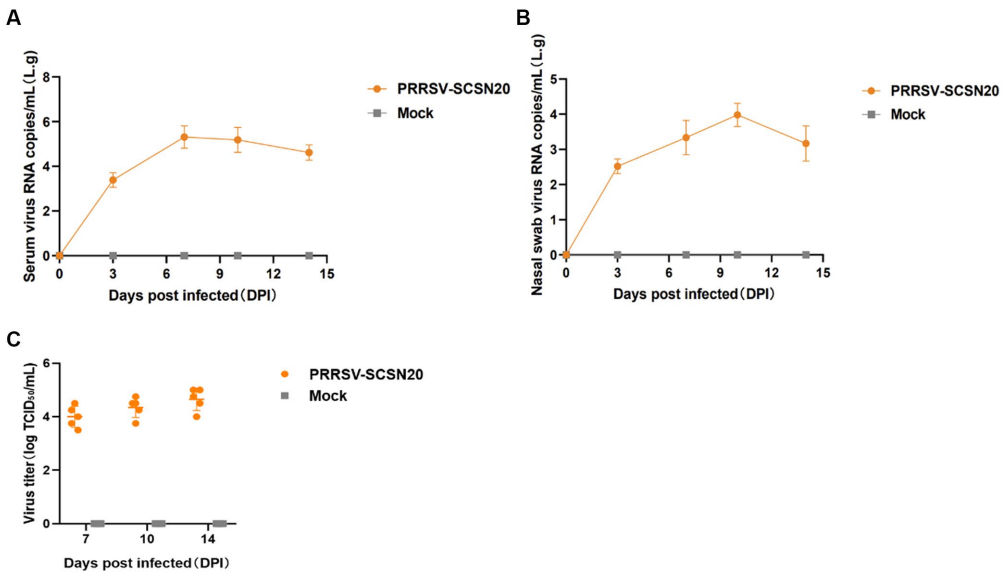

FIGURE 7
Shedding of virus and changes in blood virus titers in piglets after challenge. The amount of virus in blood in blood **(A)** and nasal swabs **(B)**, virus titer in the serum **(C)**.

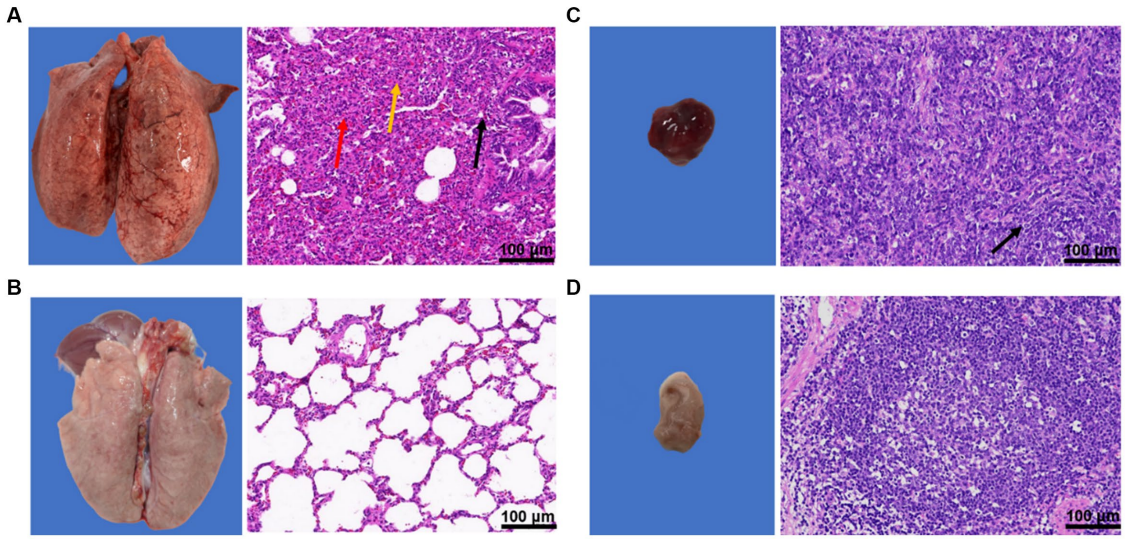

FIGURE 8
Results of pathological changes in lung and hilar lymph nodes of piglets after challenge. **(A)** lung and pathological sections of the challenge group; **(B)** Lung and pathological sections of the blank control group; **(C)** Lung lymph nodes and pathological sections of the challenge group; and **(D)** Lung lymph nodes and pathological sections of the blank control group.

2018; Zhou et al., 2018a,b,c,d). This study found that the positive rates of HP-PRRSV and NADC30 like PRRSV antigens were 44.74% (51/114) and 17.54% (20/114), respectively. As a large province of domestic pig stocking and slaughtering, Sichuan Province has widely used vaccines in pig herds, which also facilitates the recombination of PRRSV strains. At the same time, it has also brought enormous pressure to prevent and control PRRSV epidemics.

In addition to recombination, mutation is a crucial mechanism in the evolution of PRRSV (Guo et al., 2018). The exchange of gene segments usually occurs between different circulating strains and confers new biological characteristics to other variants, mainly including changes in pathogenicity and antigenicity (Sun et al., 2016; Bian et al., 2017). The Nsp2 and ORF5 regions of the PRRSV genome are highly susceptible to mutation, which makes them ideal targets for monitoring the development of PRRS gene mutations. Notably, HP-PRRSV has a 30-amino-acid discontinuous deletion (1aa + 29aa) in the NSP2 coding region (Tian et al., 2007), whereas NADC30-Like PRRSV presents a 131-amino-acid discontinuous deletion (111aaa + 1a + 19aa; Brockmeier et al., 2012). Meanwhile, NADC34-Like exhibits a continuous 100-amino-acid deletion (Bao and Li, 2021). Sequence comparison in this study found that compared with the genome of the VR2332 strain, the isolate SCSN2020 had 30 amino acid discontinuous deletions (1aa and 29aa) in the NSP2 coding region, which was located at positions 481 and 533–561, respectively.

The hypervariable region (HVR) of the PRRSV GP5 protein also shows significant variations. For instance, in aa 33–35 of HVR1, HP-PRRSV predominantly features NNN, while NADC34-Like mainly exhibits NNS or SSS, NADC30-Like primarily shows SNS, and QYYZ-Like features GNS; by contrast, VR2332 is characterized by NDS. Concerning HVR2 in aa 57–60, HP-PRRSV mainly exhibits AQKF or ANKF, whereas NADC34-Like mainly displays NKSF, NADC30-Like is more variable, showing mainly NEKF, STKF, NKKF, among others, and QYYZ-Like mainly exemplifies ATNF or ANKF. VR2332 is mainly ANKF. In PRRSV GP5, amino acids 13 and 151 act as virulence determinants (Allende et al., 2000; Luo et al., 2023). This study found that SCSN2020 mainly features arginine (R), with the remaining lineages predominantly displaying lysine (K), glutamine (Q), isoleucine (I), and arginine (R).

This study analyzed 205 suspected PRRSV samples collected from 11 prefecture-level cities in Sichuan province between 2019 and 2020. Of the 114 PRRSV-positive samples, the antigen-positive rate of HP-PRRSV (JXA1-Like strain) was 44.74% (51/114), NADC30-Like PRRSV was 17.54% (20/114), and classical PRRSV (VR2332-Like strain) was 37.72% (43/114), indicating that HP-PRRSV remains the prevalent strain in Sichuan province. Notably, 20 samples of NADC30-Like PRRSV were detected, with other studies indicating an increasing detection rate of this strain in the region (Zhou et al., 2018a,b,c,d; Zhao et al., 2022b). Furthermore, recent recombinant strains of PRRS in Sichuan province have mainly featured NADC30-Like PRRSV, while minor strains included JXA1-Like and TJ-Like HP-PRRSV. Previous studies have shown that HP-PRRSV, including JXA1, TJ, and HuN4, are lethal to piglets. These viruses are characterized by high fever, high morbidity (50–100%), and high mortality (20–100%; Tong et al., 2007; Liu et al., 2022). New recombinant strains can also lead to changes in PRRSV virulence. For example, the TJnh1501 strain is a recombinant virus between NADC30-Like and MLV vaccine (TJMF92), and its virulence is between HP-PRRSV (JXwn06) and MLV strains Between; SCN17 strain is recombined from NADC30-Like, JXA1-Like and MLV vaccine (VR2332), causing persistent fever and moderate interstitial pneumonia in pigs (Zhou et al., 2018a,b,c,d); FJLIUY-2017 strain is lineage 1 (NADC30-Like), lineage 3 (QYYZ-Like), lineage 5.1 (VR2332-Like), and lineage 8.7 (JXA1-Like; Liu et al., 2019). SCSN2020 isolated in this study was identified as JXA1-Like. Although no recombination occurred, our pathogenicity study revealed that piglets in the challenge group presented with typical PRRS clinical symptoms signs and pathological changes, including continuous increases in body temperature, weight loss, and viremia, as well as hunger, severe shortness of breath, and labored breathing from day 13.

These findings highlight the continued high pathogenicity of HP-PRRSV and underscore the need for vigilance in preventing and controlling its spread. Moreover, given Sichuan's status as a major pig-raising province in China, where swine vaccines are widely used, the potential for recombination between HP-PRRSV and NADC30-Like PRRSV is heightened. Recombinant strains exert significant pressure on PRRS prevention and control efforts. Hence, our study provides a scientific reference for future efforts to regulate and manage PRRSV outbreaks in Sichuan province.

5. Conclusion

In summary, we counted the prevalence of PRRSV in Southwest China from 2019 to 2020 and found that the highest positive rate of pathogen detection is still HP-PRRSV, and through isolation, purification, and whole-genome sequencing analysis, a strain of HP-PRRSV (SCSN2020) was obtained. Pathogenicity experiments found that the strain had typical PRRSV symptoms and pathological changes. In addition, multiple recombinations occurred between sublineage 8.7 (JXA1-Like) and lineage 1.8 (NADC30-Like) prevalent in China, and our study also reminds the importance of monitoring PRRSV in China.

Data availability statement

The datasets presented in this study can be found in online repositories. The names of the repository/repositories and accession number(s) can be found in the article/Supplementary material.

Ethics statement

The animal study was approved by Sichuan Agricultural University Institutional Animal Care and Use Committee. The study was conducted in accordance with the local legislation and institutional requirements.

Author contributions

DJ, MR, and TT: conceptualization. DJ: software. DJ and TT: methodology and writing—original draft preparation. YZ, MR, and Y Li: formal analysis. YZ: investigation. XY, Y Luo, and YW: resources. DJ and MR: data curation. DJ, ZY, and YW: writing—review and editing. DJ and YW: visualization. MR and YW: supervision. ZY, Y Luo, and XY: project administration. Y Luo and YW: funding acquisition. All authors contributed to the article and approved the submitted version.

Funding

This project was supported by the Sichuan Province Science and Technology Planning Program (2021ZDZX0010 and 2021YFSY0005).

Conflict of interest

The authors declare that the research was conducted in the absence of any commercial or financial relationships that could be construed as a potential conflict of interest.

Publisher's note

All claims expressed in this article are solely those of the authors and do not necessarily represent those of their affiliated organizations, or those of the publisher, the editors and the reviewers. Any product that may be evaluated in this article, or claim that may be made by its manufacturer, is not guaranteed or endorsed by the publisher.

Supplementary material

The Supplementary material for this article can be found online at: https://www.frontiersin.org/articles/10.3389/fmicb.2023.1241354/full#supplementary-material

References

Allende, R., Kutish, G. F., Laegreid, W., Lu, Z., Lewis, T. L., Rock, D. L., et al. (2000). Mutations in the genome of porcine reproductive and respiratory syndrome virus responsible for the attenuation phenotype. *Arch. Virol.* 145, 1149–1161. doi: 10.1007/s007050070115

An, T. Q., Zhou, Y. J., Liu, G. Q., Tian, Z. J., Li, J., Qiu, H. J., et al. (2007). Genetic diversity and phylogenetic analysis of glycoprotein 5 of PRRSV isolates in mainland China from 1996 to 2006: coexistence of two NA-subgenotypes with great diversity. *Vet. Microbiol.* 123, 43–52. doi: 10.1016/j.vetmic.2007.02.025

Arteriviridae and Roniviridae (2017). *Fenner's Veterinary Virology*. Elsevier 463–476. doi: 10.1016/B978-0-12-800946-8.00025-8

Bao, H., and Li, X. (2021). Emergence and spread of NADC34-like PRRSV in China. *Transbound. Emerg. Dis.* 68, 3005–3008. doi: 10.1111/tbed.14316

Bian, T., Sun, Y., Hao, M., Zhou, L., Ge, X., Guo, X., et al. (2017). A recombinant type 2 porcine reproductive and respiratory syndrome virus between NADC30-like and a MLV-like: genetic characterization and pathogenicity for piglets. *Infect. Genet. Evol.* 54, 279–286. doi: 10.1016/j.meegid.2017.07.016

Brockmeier, S. L., Loving, C. L., Vorwald, A. C., Kehrli, M. E., Baker, R. B., Nicholson, T. L., et al. (2012). Genomic sequence and virulence comparison of four type 2 porcine reproductive and respiratory syndrome virus strains. *Virus Res.* 169, 212–221. doi: 10.1016/j.virusres.2012.07.030

Chen, N., Ye, M., Li, S., Huang, Y., Zhou, R., Yu, X., et al. (2018). Emergence of a novel highly pathogenic recombinant virus from three lineages of porcine reproductive and respiratory syndrome virus 2 in China 2017. *Transbound. Emerg. Dis.* 65, 1775–1785. doi: 10.1111/tbed.12952

Ding, Y., Wubshet, A. K., Ding, X., Zhang, Z., Li, Q., Dai, J., et al. (2021). Evaluation of four commercial vaccines for the protection of piglets against the highly pathogenic porcine reproductive and respiratory syndrome virus (hp-PRRSV) QH-08 strain. *Vaccine* 9:1020. doi: 10.3390/vaccines9091020

Dokland, T. (2010). The structural biology of PRRSV. *Virus Res.* 154, 86–97. doi: 10.1016/j.virusres.2010.07.029

Fang, Y., Treffers, E. E., Li, Y., Tas, A., Sun, Z., van der Meer, Y., et al. (2012). Efficient −2 frameshifting by mammalian ribosomes to synthesize an additional arterivirus protein. *Proc. Natl. Acad. Sci. U. S. A.* 109, E2920–E2928. doi: 10.1073/pnas.1211145109

Firth, A. E., Zevenhoven-Dobbe, J. C., Wills, N. M., Go, Y. Y., Balasuriya, U. B. R., Atkins, J. F., et al. (2011). Discovery of a small arterivirus gene that overlaps the GP5 coding sequence and is important for virus production. *J. Gen. Virol.* 92, 1097–1106. doi: 10.1099/vir.0.029264-0

Gao, J. C., Xiong, J. Y., Ye, C., Chang, X. B., Guo, J. C., Jiang, C. G., et al. (2017). Genotypic and geographical distribution of porcine reproductive and respiratory syndrome viruses in mainland China in 1996-2016. *Vet. Microbiol.* 208, 164–172. doi: 10.1016/j.vetmic.2017.08.003

General Administration of Quality Supervision, Inspection and Quarantine of the People's Republic of China, Standardization Administration of China (2018). *GB/T*

35912–2018 Porcine Reproductive and Respiratory Syndrome Virus Real-Time RT-PCR. Beijing: Standards Press of China

Guo, Z., Chen, X. X., Li, R., Qiao, S., and Zhang, G. (2018). The prevalent status and genetic diversity of porcine reproductive and respiratory syndrome virus in China: a molecular epidemiological perspective. *Virol. J.* 15:2. doi: 10.1186/s12985-017-0910-6

Hicks, J. A., Yoo, D. W., and Liu, H. C. (2018). Interaction of porcine reproductive and respiratory syndrome virus major envelope proteins GP5 and M with the cellular protein Snapin. *Virus Res.* 249, 85–92. doi: 10.1016/j.virusres.2018.03.010

Jiang, Y. F., Xia, T. Q., Zhou, Y. J., Yu, L. X., Yang, S., Huang, Q. F., et al. (2015). Characterization of three porcine reproductive and respiratory syndrome virus isolates from a single swine farm bearing strong homology to a vaccine strain. *Vet. Microbiol.* 179, 242–249. doi: 10.1016/j.vetmic.2015.06.015

Johnson, C. R., Griggs, T. F., Gnanandarajah, J., and Murtaugh, M. P. (2011). Novel structural protein in porcine reproductive and respiratory syndrome virus encoded by an alternative ORF5 present in all arteriviruses. *J. Gen. Virol.* 92, 1107–1116. doi: 10.1099/vir.0.030213-0

Kappes, M. A., and Faaberg, K. S. (2015). PRRSV structure, replication and recombination: origin of phenotype and genotype diversity. *Virology* 479-480, 475–486. doi: 10.1016/j.virol.2015.02.012

Kuhn, J. H., Lauck, M., Bailey, A. L., Shchetinin, A. M., Vishnevskaya, T. V., Bào, Y., et al. (2016). Reorganization and expansion of the nidoviral family Arteriviridae. *Arch. Virol.* 161, 755–768. doi: 10.1007/s00705-015-2672-z

Leng, C., Zhang, W., Zhang, H., Kan, Y., Yao, L., Zhai, H., et al. (2017). ORF1a of highly pathogenic PRRS attenuated vaccine virus plays a key role in neutralizing antibody induction in piglets and virus neutralization in vitro. *Virol. J.* 14:159. doi: 10.1186/s12985-017-0825-2

Li, X., Bao, H., Wang, Y., and Tian, K. (2017). Widespread of NADC30-like PRRSV in China: another Pandora's box for Chinese pig industry as the outbreak of highly pathogenic PRRSV in 2006? *Infect. Genet. Evol.* 49, 12–13. doi: 10.1016/j.meegid.2016.12.021

Li, Y., Ji, G., Wang, J., Tan, F., Zhuang, J., Li, X., et al. (2016). Complete genome sequence of an NADC30-like porcine reproductive and respiratory syndrome virus characterized by recombination with other strains. *Genome Announc.* 4, e00330–e00316. doi: 10.1128/genomeA.00330-16

Li, Y., Wang, X., Bo, K., Wang, X., Tang, B., Yang, B., et al. (2007). Emergence of a highly pathogenic porcine reproductive and respiratory syndrome virus in the mid-eastern region of China. *Vet. J.* 174, 577–584. doi: 10.1016/j.tvjl.2007.07.032

Liao, C. Y. (2019). Isolation and identification of PRRSV NADC30-like CJS01 strain and establishment of its detection method. Sichuan Agricultural University, China.

Liu, J., Liu, C., Xu, Y., Yang, Y., Li, J., Dai, A., et al. (2022). Molecular characteristics and pathogenicity of a novel recombinant porcine reproductive and respiratory syndrome virus strain from NADC30-, NADC34-, and JXA1-like strains that emerged in China. *Microbiol. Spectr.* 10:e0266722. doi: 10.1128/spectrum.02667-22

Liu, J. K., Wei, E. H., Lin, Z. F., Fan, J. L., Xia, W., Dai, A., et al. (2019). Recombination in lineage 1, 3, 5 and 8 of porcine reproductive and respiratory syndrome viruses in China. *Infect. Genet. Evol.* 68, 119–126. doi: 10.1016/j.meegid.2018.12.006

Liu, J., Xu, Y., Lin, Z., Fan, J., Dai, A., Deng, X., et al. (2021). Epidemiology investigation of PRRSV discharged by faecal and genetic variation of ORF5. *Transbound. Emerg. Dis.* 68, 2334–2344. doi: 10.1111/tbed.13894

Liu, J. K., Zhou, X., Zhai, J. Q., Li, B., Wei, C. H., Dai, A. L., et al. (2017). Emergence of a novel highly pathogenic porcine reproductive and respiratory syndrome virus in China. *Transbound. Emerg. Dis.* 64, 2059–2074. doi: 10.1111/tbed.12617

Liu, J., Zhou, X., Zhai, J., Wei, C., Dai, A., Yang, X., et al. (2017). Recombination in JXA1-R vaccine and NADC30-like strain of porcine reproductive and respiratory syndrome viruses. *Vet. Microbiol.* 204, 110–120. doi: 10.1016/j.vetmic.2017.04.017

Lu, W. H., Tun, H. M., Sun, B. L., Mo, J., Zhou, Q. F., Deng, Y. X., et al. (2015). Re-emerging of porcine respiratory and reproductive syndrome virus (lineage 3) and increased pathogenicity after genomic recombination with vaccine variant. *Vet. Microbiol.* 175, 332–340. doi: 10.1016/j.vetmic.2014.11.016

Lunney, J. K., Fang, Y., Ladinig, A., Chen, N., Li, Y., Rowland, B., et al. (2016). Porcine reproductive and respiratory syndrome virus (PRRSV): pathogenesis and interaction with the immune system. *Annu. Rev. Anim. Biosci.* 4, 129–154. doi: 10.1146/annurev-animal-022114-111025

Luo, Q., Zheng, Y., Zhang, H., Yang, Z., Sha, H., Kong, W., et al. (2023). Research Progress on glycoprotein 5 of porcine reproductive and respiratory syndrome virus. *Animals* 13:813. doi: 10.3390/ani13050813

Mardassi, H., Massie, B., and Dea, S. (1996). Intracellular synthesis, processing, and transport of proteins encoded by ORFs 5 to 7 of porcine reproductive and respiratory syndrome virus. *Virology* 221, 98–112. doi: 10.1006/viro.1996.0356

Mateu, E., and Diaz, I. (2008). The challenge of PRRS immunology. *Vet. J.* 177, 345–351. doi: 10.1016/j.tvjl.2007.05.022

Meng, X. J., Paul, P. S., Halbur, P. G., and Lum, M. A. (1995). Phylogenetic analyses of the putative M (ORF 6) and N (ORF 7) genes of porcine reproductive and respiratory syndrome virus (PRRSV): implication for the existence of two genotypes of PRRSV in the U.S.a. and Europe. *Arch. Virol.* 140, 745–755. doi: 10.1007/BF01309962

Reed, L. J., and Muench, H. (1938). A simple method of estimating fifty per cent endpoints. *Am. J. Epidemiol.* 27, 493–497. doi: 10.1093/oxfordjournals.aje.a118408

Shi, M., Holmes, E. C., Brar, M. S., and Leung, F. C. (2013). Recombination is associated with an outbreak of novel highly pathogenic porcine reproductive and respiratory syndrome viruses in China. *J. Virol.* 87, 10904–10907. doi: 10.1128/JVI.01270-13

Shi, M., Lam, T. T., Hon, C. C., Murtaugh, M. P., Davies, P. R., Hui, R. K., et al. (2010). Phylogeny-based evolutionary, demographical, and geographical dissection of north American type 2 porcine reproductive and respiratory syndrome viruses. *J. Virol.* 84, 8700–8711. doi: 10.1128/JVI.02551-09

Sui, X., Guo, X., Jia, H., Wang, X., Lin, W., Li, M., et al. (2018). Genomic sequence and virulence of a novel NADC30-like porcine reproductive and respiratory syndrome virus isolate from the Hebei province of China. *Microb. Pathog.* 125, 349–360. doi: 10.1016/j.micpath.2018.08.048

Sun, Y. F. (2017). Surveillance, genomic characteristics and pathogenicity analysis of PRRSV NADC30 like strains isolated in Tianjin. China Agricultural University, China.

Sun, Z., Wang, J., Bai, X., Ji, G., Yan, H., Li, Y., et al. (2016). Pathogenicity comparison between highly pathogenic and NADC30-like porcine reproductive and respiratory syndrome virus. *Arch. Virol.* 161, 2257–2261. doi: 10.1007/s00705-016-2883-y

Tian, K., Yu, X., Zhao, T., Feng, Y., Cao, Z., Wang, C., et al. (2007). Emergence of fatal PRRSV variants: unparalleled outbreaks of atypical PRRS in China and molecular dissection of the unique hallmark. *PLoS One* 2:e526. doi: 10.1371/journal.pone.0000526

Tong, G. Z., Zhou, Y. J., Hao, X. F., Tian, Z. J., An, T. Q., Qiu, H. J., et al. (2007). Highly pathogenic porcine reproductive and respiratory syndrome, China. *Emerg. Infect. Dis.* 13, 1434–1436. doi: 10.3201/eid1309.070399

van Dinten, L. C., Rensen, S., Gorbalenya, A. E., and Snijder, E. J. (1999). Proteolytic processing of the open reading frame 1b-encoded part of arterivirus replicase is mediated by nsp4 serine protease and is essential for virus replication. *J. Virol.* 73, 2027–2037. doi: 10.1128/JVI.73.3.2027-2037.1999

Wang, L. J., Guo, Z., Qiao, S., Chen, X. X., and Zhang, G. (2016). Complete genome sequence of a mosaic NADC30-like porcine reproductive and respiratory syndrome virus in China. *Genome Announc.* 4, e01428–e01416. doi: 10.1128/genomeA.01428-16

Wang, H. M., Liu, Y. G., Tang, Y. D., Liu, T. X., Zheng, L. L., Wang, T. Y., et al. (2018). A natural recombinant PRRSV between HP-PRRSV JXA1-like and NADC30-like strains. *Transbound. Emerg. Dis.* 65, 1078–1086. doi: 10.1111/tbed.12852

Wang, X., Marthaler, D., Rovira, A., Rossow, S., and Murtaugh, M. P. (2015). Emergence of a virulent porcine reproductive and respiratory syndrome virus in vaccinated herds in the United States. *Virus Res.* 210, 34–41. doi: 10.1016/j.virusres.2015.07.004

Wang, X. X., Wang, F. X., Li, Z. G., Wen, Y. J., Wang, X., Song, N., et al. (2018). Development of an indirect enzyme-linked immunosorbent assay (ELISA) to differentiate antibodies against wild-type porcine reproductive and respiratory syndrome from the vaccine strain TJM-F92 based on a recombinant Nsp2 protein. *J. Virol. Methods* 251, 151–154. doi: 10.1016/j.jviromet.2017.09.001

Xu, H., Li, C., Li, W. S., Zhao, J., Gong, B. J., Sun, Q., et al. (2022). Novel characteristics of Chinese NADC34-like PRRSV during 2020-2021. *Transbound. Emerg. Dis.* 69, e3215–e3224. doi: 10.1111/tbed.14485

Xu, L., Zhao, J., Yang, X. Y., Yin, X. H., Zhang, J. Z., and Zhu, L. (2019). Establishment and application of RT-PCR methods for identifying porcine reproductive and respiratory syndrome virus (PRRSV) NADC30-like strain and HP-PRRSV strain. *Jiangsu J. Agric. Sci.* 35, 109–113. doi: 10.3969/j.issn.1000-4440.2019.01.016

Yu, Y., Zhang, Q., Cao, Z., Tang, Y. D., Xia, D., Wang, G., et al. (2022). Recent advances in porcine reproductive and respiratory syndrome virus NADC30-like research in China: molecular characterization, pathogenicity, and control. *Front. Microbiol.* 12:791313. doi: 10.3389/fmicb.2021.791313

Zhang, Q., Bai, J., Hou, H., Song, Z., Zhao, Y., and Jiang, P. (2017). A novel recombinant porcine reproductive and respiratory syndrome virus with significant variation in cell adaption and pathogenicity. *Vet. Microbiol.* 208, 150–158. doi: 10.1016/j.vetmic.2017.07.028

Zhang, H. L., Zhang, W. L., Xiang, L. R., Leng, C. L., Tian, Z. J., Tang, Y. D., et al. (2018). Emergence of novel porcine reproductive and respiratory syndrome viruses (ORF5 RFLP 1-7-4 viruses) in China. *Vet. Microbiol.* 222, 105–108. doi: 10.1016/j.vetmic.2018.06.017

Zhao, H., Han, Q., Zhang, L., Zhang, Z., Wu, Y., Shen, H., et al. (2017). Emergence of mosaic recombinant strains potentially associated with vaccine JXA1-R and predominant circulating strains of porcine reproductive and respiratory syndrome virus in different provinces of China. *Virol. J.* 14:67. doi: 10.1186/s12985-017-0735-3

Zhao, J., Xu, L., Xu, Z., Deng, H., Li, F., Sun, X., et al. (2022a). Emergence and spread of NADC34-like PRRSV in Southwest China. *Transbound. Emerg. Dis.* 69, e3416–e3424. doi: 10.1111/tbed.14463

Zhao, J., Xu, Z., Xu, T., Zhou, Y., Li, J., Deng, H., et al. (2022b). Molecular characterization of the Nsp2 and ORF5s of PRRSV strains in Sichuan China during 2012-2020. *Animals* 12:3309. doi: 10.3390/ani12233309

Zhao, K., Ye, C., Chang, X. B., Jiang, C. G., Wang, S. J., Cai, X. H., et al. (2015). Importation and recombination are responsible for the latest emergence of highly

pathogenic porcine reproductive and respiratory syndrome virus in China. *J. Virol.* 89, 10712–10716. doi: 10.1128/JVI.01446-15

Zhou, L., Kang, R., Ji, G., Tian, Y., Ge, M., Xie, B., et al. (2018a). Molecular characterization and recombination analysis of porcine reproductive and respiratory syndrome virus emerged in southwestern China during 2012-2016. *Virus Genes* 54, 98–110. doi: 10.1007/s11262-017-1519-y

Zhou, L., Kang, R., Xie, B., Tian, Y., Wu, X., Lv, X., et al. (2018b). Identification of a novel recombinant type 2 porcine reproductive and respiratory syndrome virus in China. *Viruses* 10:151. doi: 10.3390/v10040151

Zhou, L., Kang, R., Yu, J., Xie, B., Chen, C., Li, X., et al. (2018c). Genetic characterization and pathogenicity of a novel recombined porcine reproductive and respiratory syndrome virus 2 among Nadc30-like, Jxa1-like, and mlv-like strains. *Viruses* 10:551. doi: 10.3390/v10100551

Zhou, L., Kang, R., Zhang, Y., Ding, M., Xie, B., Tian, Y., et al. (2018d). Whole genome analysis of two novel type 2 porcine reproductive and respiratory syndrome viruses with complex genome recombination between lineage 8, 3, and 1 strains identified in southwestern China. *Viruses* 10:328. doi: 10.3390/v10060328

Zhou, L., Kang, R., Zhang, Y., Yu, J., Xie, B., Chen, C., et al. (2019). Emergence of two novel recombinant porcine reproductive and respiratory syndrome viruses 2 (lineage 3) in southwestern China. *Vet. Microbiol.* 232, 30–41. doi: 10.1016/j.vetmic.2019.01.026

Zhou, L., Yang, B. N., Xu, L., Jin, H., Ge, X. N., Guo, X., et al. (2017). Efficacy evaluation of three modified-live virus vaccines against a porcine reproductive and respiratory syndrome virus NADC30-like strain. *Vet. Microbiol.* 207, 108–116. doi: 10.1016/j.vetmic.2017.05.031

Zhou, F., Zhao, J., Chen, L., Chang, H. T., Li, Y. T., Liu, H. Y., et al. (2015). Complete genome sequence of a novel porcine reproductive and respiratory syndrome virus that emerged in China. *Genome Announc.* 3, e00702–e00715. doi: 10.1128/genomeA.00702-15

frontiers | Frontiers in Microbiology

TYPE Methods
PUBLISHED 22 September 2023
DOI 10.3389/fmicb.2023.1225587

OPEN ACCESS

EDITED BY
Leyi Wang,
University of Illinois at Urbana-Champaign, United States

REVIEWED BY
Jingfei Wang,
Harbin Veterinary Research Institute (CAAS), China
Vlad Petrovan,
The Pirbright Institute, United Kingdom

*CORRESPONDENCE
Alexey D. Sereda
✉ sereda-56@mail.ru
Irina P. Sindryakova
✉ sindryakova.irina@yandex.ru

RECEIVED 03 July 2023
ACCEPTED 25 August 2023
PUBLISHED 22 September 2023

CITATION
Sereda AD, Namsrayn S, Balyshev VM, Vlasov ME, Sindryakova IP, Koltsova G and Kolbasov DV (2023) Seroimmunotyping of African swine fever virus.
Front. Microbiol. 14:1225587.
doi: 10.3389/fmicb.2023.1225587

Seroimmunotyping of African swine fever virus

Alexey D. Sereda*, Sanzhi Namsrayn, Vladimir M. Balyshev, Mikhail E. Vlasov, Irina P. Sindryakova*, Galina Koltsova and Denis V. Kolbasov

Federal Research Center for Virology and Microbiology (FRCVIM), Vladimir Region, Volginsky, Russia

The extreme genetic and immunobiological heterogeneity exhibited by the African swine fever virus (ASFV) has been a significant impediment in the development of an efficacious vaccine against this disease. Consequently, the lack of internationally accepted protocols for the laboratory evaluation of candidate vaccines has become a major concern within the scientific community. The formulation of such protocols necessitates the establishment of a consensus at the international level on methods for the determination of homologous and heterologous isolates/strains of ASFV. The present article provides a comprehensive description of biological techniques employed in the classification of ASFV by seroimmunotypes. These techniques involve a holistic evaluation of ASFV isolates/strains based on their antigenic properties as determined by the hemadsorption inhibiting test (HAdI) using type-specific sera and an immunological test (IT) conducted on pigs inoculated with attenuated strains. The article outlines the methods for setting up the HAdI test, an IT on pigs, and the processes involved in the acquisition of type-specific serums for the HAdI test. It is pertinent to note that the definitive classification of seroimmunotype can only be ascertained after conducting an IT on pigs. The findings from the HAdI test or the phylogenetic analysis of the EP402R gene should be considered preliminary in nature.

KEYWORDS

African swine fever virus, seroimmunotypes, type-specific pig serum, hemadsorption inhibiting test, immunological test

1. Introduction

African swine fever (ASF) is a contagious septic disease of domestic pigs and wild boars. The course of the disease can be hyperacute, acute, subacute, and chronic (Detray, 1957; Boinas et al., 2004; Blome et al., 2020). The causative agent of ASF is a DNA-containing virus of the *Asfivirus* genus, *Asfarviridae* family (Borca et al., 1998; Viruses IC on T, 2011).

African swine fever is currently having an unprecedented spread globally and one of the reasons for this spread is the lack of a safe and effective registered vaccine against the disease. It is known that pigs that have recovered after infection with the African swine fever virus (ASFV) can be protected from disease and/or death if subsequently infected with related virulent isolates/strains (Plowright, 1986). In addition, pigs inoculated with naturally attenuated or laboratory-selected strains of ASFV, or recombinant viruses, can also be protected from the disease or, if ill, from death after the infection by homologous virulent isolates/strains (Rock, 2017; Gallardo et al., 2019; López et al., 2020).

A widely used ASFV classification system is based on genotyping and determining the phylogenetic relationship of various isolates/strains. Currently, the studied isolates/strains of the

ASFV are distributed into 24 genotypes (Bastos et al., 2003; Nix et al., 2006; Achenbach et al., 2017). Although ASFV genotyping is useful for some purposes, it does not fully correlate with the available data on cross-protection and may have limited value for predicting the effectiveness of vaccine cross-protection (Plowright, 1986; King et al., 2011; Rock, 2017).

In 1960, Malmquist and Hay were the first to document the occurrence of hemadsorption during the replication of ASFV in primary cultures of porcine bone marrow cells (PBMC) and primary peripheral blood leukocytes of swine (PBLS). In addition to the phenomenon of hemadsorption, they found that blood serum obtained from ASFV-infected pigs inhibits hemadsorption in ASFV-infected cultures of PBLS and PBMC cells, but does not affect the cytopathic effect and reproduction of the virus (Malmquist and Hay, 1960). Based on the results of studying the antigenic and protective properties of isolates/strains, a seroimmunotype classification of the ASFV was developed (Malmquist, 1963; Sereda and Balyshev, 2011; Sereda et al., 2020).

In 1968, Coggins reported the isolation of non-hemadsorbing subpopulations of the ASF virus (Coggins, 1968a). Further studies have shown that the loss of the ability to induce hemadsorption for the ASF virus during reproduction in cell culture is a common phenomenon (Pan and Hess, 1985; Jori and Bastos, 2009; Ravaomanana et al., 2010). A number of researchers have noted that non-hemadsorbing strains of the ASF virus isolated in nature or obtained under laboratory conditions have low virulence and the ability to form immune protection against subsequent infection of pigs with homologous virulent hemadsorbing isolates (Pan, 1992; Sánchez-Cordón et al., 2017).

The seroimmunotype classification is based on the results of a comprehensive assessment of ASFV isolates/strains by antigenic properties in the HAdI test with type-specific sera and an IT inoculated with attenuated strains (Sereda et al., 2020). The isolates/strains of the ASFV available in the collection of the FRCVM are divided into nine (I-IX) seroimmunotypes, and three other small groups: isolates whose serological affiliation does not correspond to the results of the immunological test (group X), isolates heterogeneous in seroimmunotype relation (group XI), and yet untyped isolates (group XII; Sereda et al., 2020). Each of the nine seroimmunotypes includes virulent hemadsorbing strains of the ASFV, including reference, and, as a rule, natural or laboratory-attenuated strains/isolates that have low or no virulence and are of hemadsorbing or non-hemadsorbing phenotype. In the classification described above, non-hemadsorbing isolates/strains are differentiated only by the results of an IT.

In our opinion, it is important to establish unified international definitions for homologous and heterologous isolates/strains. Evaluation of candidate vaccines should be based on seroimmunotype classification of isolates/strains established in hemadsorption delay reaction and immunological tests. This article describes methods that are used for ASFV seroimmunotyping.

The following terms will be used with the following meaning: serotype of ASFV is a group of isolates/strains of ASFV formed based on the results of the HAdI test; immunotype of ASFV is a group of isolates/strains of ASFV based on the results of IT; seroimmunotype of ASFV is a group of isolates/strains formed based on the results of grouping by HAdI test and IT.

2. Materials and methods

It is important to ensure that all plasticware used in the experiment is of tissue culture-grade quality. Additionally, all reagents and buffers should be properly sterilized either by autoclaving or filtration methods.

2.1. Preparing PBLS

2.1.1. Materials and equipment

In the experiments, use female or male pigs that are 3 to 4 months old, e.g., 30–40 kg piglets of the Large White Pig breed (Pigs). Place the animals in a BSL 3Ag laboratory. Conduct a 6-day acclimatization period before starting the study. Keep and euthanize pigs according to AVMA guidelines for the care and use of laboratory animals (National Research Council (US), 2011).

2.1.1.1. Hardware

Laminar flow cabinet, CO_2 incubator, refrigerator (4°C), analytical balance, pH meter, inverted microscope, centrifuge (capable of spinning 50 mL conical tubes), and hemocytometer.

2.1.1.2. Consumables

Vacuum blood collection tube, anti-coagulation (EDTA; Chengdu PUTH Medical Plastics Packaging Co., China), polypropylene conical tubes (50 mL), serological pipettes (10 mL), automatic pipettes with a volume of 20–200 µL, 100–1000 µL, aerosol-resistant filter tips, Millex-HV syringe filter unit, and 0.45 µm, PVDF (SLS, England).

2.1.1.3. Chemical reagents

1. Complete blood leukocytes growing media (CBLGM): The Eagle's minimal essential medium (EMEM) containing 10% of fetal bovine serum (FBS), penicillin (100–200 IU/mL), and streptomycin (100–200 mg/mL).
2. Phosphate-buffered saline pH 7.2, divalent cation-free (PBS): Nacl – 8.0 g, KH_2PO_4, – 0.2 g, Na_2HPO_4 ×12 H_2O – 2.9 g, and KCl – 0.2 g. distilled water to 1,000 mL. Check the pH before use. Store at 4°C.
3. Ficoll–Hypaque 1,077 g/cm^3 (GE Healthcare, United States).
4. Distilled water.
5. Red blood cell (RBC) lysis buffer: 155 mM ammonium chloride, 12 mM sodium hydrogen carbonate, and 0.1 mM ethylenediaminetetraacetic acid. Sterilization by filtration.
6. Trypan blue 0.4% (w/v).

2.1.2. Method

African swine fever virus productively infects monocyte/macrophage cells in the domestic pig. Here, we describe the culture of primary peripheral blood leukocytes of swine.

- Collect the required volume of fresh defibrinated pig blood into tubes containing an anticoagulant.
- Add 15 mL of Ficoll–Hypaque solution at 20–22°C to polypropylene conical tubes (50 mL) and overlay it with diluted pig blood in sterile PBS at a 1:1 ratio.

- Centrifuge the tubes at 1000×g for 30 min at 20–22°C with the brake off.
- Carefully aspirate the interphase layer using a serological pipette, transfer it to a new 50 mL tube, and then fill the tube with PBS to the desired volume.
- Centrifuge at 400×g for 10 min at 20–22°C.
- Remove the supernatant by carefully decanting or aspirating it, and then discard it appropriately. Add 5 mL of RBC lysis buffer to each tube, ensuring complete resuspension of the pellet, and incubate the tubes at 20–22°C for 5 min. After the incubation, add 40 mL of PBS and centrifuge the tubes at 400×g for 10 min at 20–22°C.
- Wash cells with PBS twice more. Resuspend cells in CBLGM at a volume 2.0–2.5 times greater than the initial blood volume.
- Mix 100 µL of the resuspended cells with 800 µL of PBS and 100 µL of trypan blue solution. Stir the mixture thoroughly. Proceed to count the number of clear (non-stained) cells using a suitable counting method, such as a hemocytometer. Based on the cell count, calculate the cell concentration using the appropriate formula or software. Adjust the volume of CBLGM cells to a concentration of 3.0–4.0 million cells/mL.

2.2. Preparing washed RBC

2.2.1. Materials and equipment

Pigs (see 2.1.1).

2.2.1.1. Hardware

Laminar flow cabinet, refrigerator (4°C), bench-top centrifuge.

2.2.1.2. Consumables

Vacuum blood collection tube, anti-coagulation (EDTA; Chengdu PUTH Medical Plastics Packaging Co., China), 5 mL centrifuge tube with lid, serological pipettes (5 mL), automatic pipettes with a volume of 100–1000 µL, and aerosol-resistant filter tips.

2.2.1.3. Chemical reagents

1. Complete blood leukocytes growing media: The EMEM containing 10% of FBS, penicillin (100–200 IU/mL), and streptomycin (100–200 mg/mL).
2. Phosphate-buffered saline pH 7.2, divalent cation-free: Nacl – 8.0 g, KH_2PO_4, – 0.2 g, Na_2HPO_4 x12 H_2O – 2.9 g, and KCl – 0.2 g. distilled water to 1000 mL. Check the pH before use. Store at 4°C.

2.2.2. Method

- Centrifuge 1,0 mL of swine whole blood at 400×g for 5 min at 20–22°C.
- Remove plasma and buffy coat layer.
- Resuspend the red cells in 30 mL PBS and invert the tube to mix.
- Centrifuge the sample at 400×g for 5 min at 20–22°C and carefully remove and discard the supernatant. Repeat the washing step two more times using PBS, following the same centrifugation conditions.
- Resuspend RBCs in 1.0 mL of CBLGM, and then dilute the resuspended RBCs in a 1:100 ratio to prepare a 1% solution.

2.3. Obtaining type-specific pig serum for the hemadsorption inhibiting test

2.3.1. Materials and equipment

Pigs (see 2.1.1), PBLS (see 2.1), ASFV strains seroimmunotype III: reference Mozambique-78, and attenuated MK-200.

2.3.1.1. Hardware

Laminar flow cabinet, refrigerator (4°C), freezer (− 40°C), water bath, and thermometer.

2.3.1.2. Consumables

Vacuum blood collection tube, clot activator (Chengdu PUTH Medical Plastics Packaging Co., China), automatic pipettes with a volume of 20–200 µL, 100–1000 µL, aerosol-resistant filter tips, sterile 48-well Nunc cell culture plate with TC treatment, and 1.0 and 10.0 mL syringes.

2.3.1.3. Chemical reagents

1. Complete blood leukocytes growing media: The EMEM containing 10% of FBS, penicillin (100–200 IU/mL), and streptomycin (100–200 mg/mL).
2. 40% solution of phosphonoacetic acid [$HOOCCH_2P(O)(OH)_2$] in sterile water (PAA).

2.3.2. Methods

There are three main methods for obtaining sera that are active in the HAdI test from pigs: (i) survivors of ASF in subacute forms (Malmquist, 1963; Balyshev et al., 2015), (ii) pigs successively inoculated with attenuated and virulent reference strains of ASFV (Balyshev et al., 2015; Imatdinov et al., 2019), and (iii) survivors of acute or subacute forms of ASF as a result of treatment with a chemical – phosphonoacetic acid (PAA; Zubairov et al., 2017).

The infectious activities of ASFV strains were determined by titration in PBLS [four wells for each tenfold dilution; World organization for animal health (2019)]. The results were examined by the presence of hemadsorption phenomenon after 5–7 days. The virus titers were calculated according to the method described by Kerber in Ashmarin's modification and expressed in 50% hemadsorbing units per mL (HAU_{50}/mL; Ashmarin et al., 1975).

2.3.2.1. Serum from subacute ASF survivors

- Infect pigs with a reference strain of ASFV of the selected seroimmunotype. Out of 10 pigs that are kept together, intramuscularly inoculate two pigs with a reference strain Mozambique-78 of ASFV of selected seroimmunotype III at a dose of $10^{2.0}$–$10^{3.0}$ HAU_{50}.
- The remaining eight animals would be infected by contact. When it is 14–21 days post the infection, examine the blood serum of

survivors of the subacute form of ASF for the presence of active antibodies in the HAdI test (See 2.4.1).
- Obtain blood serum from surviving animals on day 42 after infection and test it in HAdI. Typically, their titers range from 1:40 to 1:10240.

2.3.2.2. Serum from pigs successively inoculated with attenuated and virulent reference strains of African swine fever virus

Usually, administration of attenuated ASFV strains into pigs in doses from $10^{2.0}$ to $10^{6.0}$ HAU_{50} does not induce the formation of hemadsorption-inhibiting antibodies. In some cases, natural and laboratory-obtained attenuated hemadsorbing strains that cause a chronic form of ASF induce the formation of HAdI antibodies in pigs with titers no higher than 1:20–1:80. The process of obtaining serums active in the HAdI test by the second method requires taking into account that, on the one hand, after infection with a virulent strain, immunized animals must survive, and on the other hand, they must get sick with the manifestation of characteristic clinical signs of ASF (fever for several days, refusal of feed, and hemorrhages on the skin; Coggins, 1968a).

- Intramuscularly inoculate eight pigs with an attenuated strain MK-200 of ASFV at a dose of $10^{6.0}$–$10^{7.0}$ HAU_{50}.
- After 7–14 days, intramuscularly inoculate animals with a homologous virulent reference strain Mozambique-78 of the ASFV at a dose of $10^{2.0}$–$10^{3.0}$ HAU_{50}.
- In pigs that survived the subacute form of ASF, 14–21 days after the disappearance of clinical signs of the disease, examine blood serum for the presence of antibodies active in the HAdI test (See 2.4.1).

2.3.2.3. Serum from pigs after application of chemicals drugs with therapeutic effects against ASF

The sodium salt of phosphonoacetic acid (phosphonate) inhibits the DNA polymerase of viruses by binding to the pyrophosphate site. Viral polymerase is significantly more sensitive to this drug than swine DNA polymerase. Phosphonoacetic acid, phosphonoacetic acid complex with 7-amino-1,3,5- triazaadamantane, and potassium pyridine salt of phosphonoacetic acid all prevented mortality of more than 80% of infected animals vs. 100% mortality of animals in the control group. The use of phosphonoacetic acid in combination with metisazone under microepizootic conditions prevented mortality of all piglets that had contact with the diseased ones, in comparison to 100% mortality in untreated animals. The possibility of obtaining type-specific sera was established, which removed the step of attenuation of virulent strains. The result allowed to shorten the serum preparation time by 3–12 times, which might be crucial for serotyping the virus since attenuation of individual strains can take up to 6–12 months or more (Zubairov et al., 2017).

- Administer intramuscular injection of the selected seroimmunotype III reference strain, e.g., Mozambique-78, to four pigs. The inoculation should be carried out at a dose ranging from $10^{2.0}$ to $10^{5.0}$ HAU_{50}, with the specific virus dose adjusted based on the virulence of the ASFV strain.
- Monitor the clinical signs and record temperature every day.
- Once the body temperature of the infected pigs starts to rise above 40°C and clinical signs of the disease become evident (usually around 2–3 days after infection), begin administering intramuscular injections of a 40% PAA solution. The recommended dosage is 100–150 mg/kg of body weight. Administer the injections twice a day for the first 3 days, and then switch to once-a-day administration for the subsequent 10 days.
- On day 14, following the last recorded temperature peak, proceed to exsanguinate the animals and collect the blood samples. The collected sera should then be subjected to analysis using the HAdI assay.

In the HAdI assay, the titer of anti-ASFV serum can range from 1:40 to 1: 640. Depending on the virulence of the ASF virus strain, mortality rates in affected animals can range up to 50%.

In all cases, the selected type-specific pig serums are incubated for 30 min at a temperature of 56°C, aliquoted, and stored at −40°C. When selecting type-specific sera, it is assumed that their activity with homologous seroimmunotype reference strains of the ASFV in the HAdI test (see 2.4.1) should be from 1:40 or more (up to 1:10240), and with heterologous ones the inhibition of hemadsorption is not manifested.

2.4. Serotyping of African swine fever virus in the hemadsorption inhibiting test

Serotyping of the ASFV in the HAdI test makes it possible to obtain a preliminary result on the seroimmunotype classification of the studied isolates relatively quickly, which saves money, effort, and time, compared to the conduction of an immunological test on animals. The HAdI test uses reference strains of nine ASFV seroimmunotypes and corresponding type-specific reference pig sera. There are two main modifications of the HAdI test formulation. The first one was proposed by Malmquist (1963). The second one was proposed by Coggins (1968a) in modification Vigario (Vigário et al., 1970; Balyshev et al., 2015). In this article, we present both main modifications.

2.4.1. Determination of working dilutions of type-specific pig sera (working serum dilution, WSD)

In the HAdI test, type-specific pig sera are used in working dilutions corresponding to their doubled titers. The titer of type-specific pig sera is taken as the highest dilution that causes inhibition of hemadsorption, multiplied by the dilution factor of the serum in the culture medium. The HAdI test in micropanel tablets is performed in the working volume, of which 0.90 is a cell suspension, 0.05 is a virus-containing material, and 0.05 is the serum of interest.

2.4.1.1. Materials and equipment

PBLS (see 2.1), RBC (see 2.2), ASFV strain, Mozambique-78, swine anti-ASFV serums (IS1, IS2) to strain Mozambique-78, positive sera III serotype (PS), and normal porcine serum (NS) treated for 30 min at a temperature of 56°C.

2.4.1.1.1. Hardware

Laminar flow cabinet, CO_2 incubator, refrigerator (4°C), freezer (− 40°C), inverted microscope, and water bath.

2.4.1.1.2. Consumables

Multichannel pipettes, automatic pipettes with a volume of 20–200 µL, 100–1000 µL, aerosol-resistant filter tips, and a sterile 48-well Nunc cell culture plate with TC treatment.

2.4.1.1.3. Chemical reagents

1. Complete blood leukocytes growing media: The EMEM containing 10% of FBS, penicillin (100–200 IU/mL), and streptomycin (100–200 mg/mL).
2. Phosphate-buffered saline pH 7.2, divalent cation-free: Nacl – 8.0 g, KH_2PO_4, – 0.2 g, Na_2HPO_4 ×12 H_2O – 2.9 g, and KCl – 0.2 g. distilled water to 1,000 mL. Check the pH before use. Store at 4°C.

2.4.1.2. Method

Determination of working dilutions of investigated type-specific pig serums III serotypes from pigs (IS1 and IS2) in the HAdI test. The HAdI test is performed using 48-well plastic micropanels.

1. On day 0, prepare a suspension of PBLS with a concentration of 3.0–4.0 million cells/mL, and add 10 mL of the suspension to each well of the 48-well plates. Then incubate culture plates in a CO_2 incubator at 37°C for 3 days with 5% CO_2 and 90% relative humidity.
2. On day 3, take the following steps:

a. Calculate the dilution of viral stock required to achieve a concentration of $10^{2.5}$–$10^{3.0}$ HAU_{50}/25 µL for the HAdI test.
b. Dilute the virus in CBLGM.
c. Evaluate the status of adherent cells, specifically monocytes/macrophages, in the culture. Perform a wash by pipetting the medium up and down using an automatic pipette equipped with 1000 µL filter tips. This step aims to remove any non-adherent cells. Carefully discard the medium, and repeat the washing process two additional times to ensure thorough removal of non-adherent cells. Finally, add 450 µL of CBLGM to each well. Leukocyte culture should consist of single flattened, transparent cells uniformly distributed on the surface of the culture tablets with a density of at least 400–500 cells per field of view under low magnification (ocular × 10, lens × 10).
d. Infect cells with ASFV strain, Mozambique-78, $10^{2.0}$–$10^{3.0}$ HAU_{50}/25 µL/well. Leave the «cell culture controls» row not infected (Table 1).
e. Incubate plates overnight at 37°C in CO_2 incubator.

3. On day 4, take the following steps:

a. Prepare a separate 48-well plate, with two-fold serum dilutions (1:2 to 1:256) of IS1, IS2, PS, and NS in CBLGM. Dispense 100 µL of CBLGM into 8 wells, occupying four rows (A-H) of the 48-well plate. In rows 1–4 (Table 1), add 100 µL of swine serum to each well, creating a 1:2 dilution. Ensure duplicates of each sample are included. Additionally, include suitable positive and negative controls in the plate.
b. Add 25 µL of the serum dilutions to the appropriate wells with infected cells.
c. Incubate plates at 37°C for 2 h in a CO_2 incubator.
d. To each well, add 50 µL of 1% swine RBC.
e. Incubate plates overnight at 37°C in a CO_2 incubator.

On day 5, read hemadsorption using an inverted microscope. Note: the maximum dilution of each serum at which HAdI is complete (no rosetting cells) and write down the value. Monocytes/macrophages infected with ASFV with no anti-ASFV serum display a representative hemadsorption pattern. The result interpretation is represented in Table 1. Thus, the WSD of swine blood sera for IS1 and IS2 are 1:320 and 1:160, respectively.

2.4.2. The hemadsorption inhibiting test

The method of setting the HAdI test used at FRCVM differs from the method of Malmquist (1963) in that before setting the reaction, the cultures of the PBLS or PBMC cells are washed with a nutrient media to reduce the number of red blood cells and remove loose cells. The sequence of addition of virus and serum does not play a fundamental role in this modification, since 2–3 days pass before the manifestation of hemadsorption (Vigário et al., 1970; Balyshev et al., 2015). The HAdI test is carried out with a micro method in cultured plastic 48-well micropanels. The HAdI test is performed with the following controls: cell cultures (cell culture to assess the quality of cell culture), type-specific serums (for the absence of non-specific hemadsorption), reference strains of I-IX seroimmunotypes, and test isolates of ASFV (for the presence of characteristic hemadsorption). The test uses type-specific sera, the WSD of which is determined in a preliminary experiment with reference strains of the ASFV.

The HAdI test for determining the serotype of ASFV isolates is carried out using the method described below, using 48-well plastic micropanels.

2.4.2.1. Materials and equipment

PBLS (see 2.1). For serotyping purposes, the following reference strains of ASFV were utilized: I – Lisbon-57, II – Congo-49, III – Mozambique-78, IV – France-32, V – TSP-80, VI – TS-7, VII – Uganda, VIII – Stavropol 01/08, and IX – Davis. These viruses were propagated through 1–2 passages in cultures of PBLS cells, resulting in a viral titer ranging from $10^{6.0}$ to $10^{7.5}$ HAU_{50}/mL. In this study, we investigated the serotype classification of the Katanga-78 and Kaluga-20 isolates. Type-specific pig anti-ASFV serum of serotypes I-IX, with the WSD in the HAdI test not lower than 1:40 (as a rule, 1:80–1:320).

2.4.2.1.1. Hardware

Laminar flow cabinet, CO_2 incubator, refrigerator (4°C), freezer (– 40°C), and inverted microscope.

2.4.2.1.2. Consumables

Multichannel pipettes, automatic pipettes with a volume of 20–200 µL, 100–1000 µL, aerosol-resistant filter tips, and sterile 48-well Nunc cell culture plate with TC treatment.

2.4.2.1.3. Chemical reagents

Complete blood leukocytes growing media: The EMEM containing 10% of FBS, penicillin (100–200 IU/mL), and streptomycin (100–200 mg/mL).

2.4.2.2. Method

1. On day 0, prepare a suspension of PBLS with a concentration of 3.0–4.0 million cells/mL. The working volume, 1.0 mL, of the

10.3389/fmicb.2023.1225587

TABLE 1 Determination of working serum dilution (WSD).

Probes	Serum dilutions								WSD
	A	B	C	D	E	F	G	H	
	1:2	1:4	1:8	1:16	1:32	1:64	1:128	1:256	
	Titers								
	1:40	1:80	1:160	1:320	1:640	1:1280	1:2560	1:5120	
IS1	—*	—	—	—	—	+	+	+**	1:320
IS2	—	—	—	—	+	+	+	+	1:160
PS	—	—	—	—	—	+	+	+	1:320
NS	+	+	+	+	+	+	+	+	No
Virus controls	+	+	+	+	+	+	+	+	
Cell culture controls	—	—	—	—	—	—	—	—	

—*, absence of hemadsorbtion. +**, presence of hemadsorbtion.

TABLE 2 Serotyping scheme of the studied African swine fever virus (ASFV) isolates in the hemadsorption inhibiting test (HAdI).

Strains, isolates, and controls	Serotypes of type-specific pig serum									Virus controls	Serotype of strain/isolate
	1	2	3	4	5	6	7	8	9		
Lisbon-57	—	+	+	+	+	+	+	+	+	+	1
Congo-73	+	—	+	+	+	+	+	+	+	+	2
Mozambique-78	+	+	—	+	+	+	+	+	+	+	3
France-32	+	+	+	—	+	+	+	+	+	+	4
TSP-80	+	+	+	+	—	+	+	+	+	+	5
TS-7	+	+	+	+	+	—	+	+	+	+	6
Uganda	+	+	+	+	+	+	—	+	+	+	7
Stavropol 01/08	+	+	+	+	+	+	+	—	+	+	8
Davis	+	+	+	+	+	+	+	+	—	+	9
Katanga-78	—	+	+	+	+	+	+	+	+	+	1
Kaluga-20	+	+	+	+	+	+	+	—	+	+	8
Serum controls	—	—	—	—	—	—	—	—	—	—	—
Cell culture controls	—	—	—	—	—	—	—	—	—	—	—

(+), presence of 2–5 cells with specific HA in the view field of a microscope, 400×; (—), absence of cells with specific HA.

prepared suspension of cells is introduced into each well of culture plates, and into each well of the 48-well plate. Culture plates in a CO_2 incubator with a CO_2 content of 5% and a relative humidity of 90%, and incubate at a temperature of 37°C for 3 days.

2. On day 3, take the following steps:

a. Calculate the dilution of viral materials I-IX of seroimmunotypes to achieve a concentration of $10^{2.0}$–$10^{3.0}$ HAU_{50}/25 μL for the HAdI test (Table 2).

b. Dilute viruses in CBLGM.

c. Assess the status of adherent cells in each well of the plate. To eliminate non-adherent cells, perform a gentle wash by pipetting up and down in each well using an automatic pipette equipped with 1000 μL and discard the medium from the wells. Finally, add 450 μL of CBLGM to each well.

d. Infect cells with ASFV $10^{2.5}$–$10^{3.0}$ HAU_{50}/25 μL/well.

e. Calculate the dilution of reference sera so that after adding them to the wells in a volume of 25 μL, they reach the working dilutions.

f. Add 25 μL of the serum dilutions to the infected cells according to Table 2.

3. On days 4–7 read hemadsorption using an inverted microscope. Record the results. The results interpretation is represented in Table 2. Thus, the investigated isolate Katanga-78 belongs to the serotype I and isolate Kaluga-20 belongs to the serotype VIII. HAdI is taken into account after 48–72 h in the presence of well-expressed hemadsorption in the virus controls (at least 2–5 cells with specific hemadsorption in the field of view of the microscope, 400×) and its absence in the controls of type-specific sera and cell culture. Type-specific sera should inhibit the hemadsorption of homologous reference strains of ASFV and should not inhibit the hemadsorption of heterologous reference strains. Inhibition of hemadsorption of the studied isolate by one of the nine type-specific reference sera indicates that it belongs to the virus serotype for which this serum was obtained. The scheme of setting the HAdI test with the ASFV is shown in Table 2.

2.4.2.2.1. Note

1. In the absence of inhibition of hemadsorption with reference sera, the test virus should be temporarily assigned to the group of untyped ASFV isolates.
2. When preparing for serotyping in HAdI, it is important to follow the recommendation to use the appropriate reference virulent strains of the ASFV to determine the activity of type-specific sera. The use of attenuated virus strains of the same seroimmunotype for this purpose may distort the result. It was found that the titers of type-specific sera in HAdI with virulent strains were 1.7–2.8 $\log_2$ lower than with the attenuated strains. The highest differences, by 29.5 times, were noted with the attenuated strain FK-32/135 inducing "loose" hemadsorption and with the virulent strain France-32, belonging to the IV seroimmunotype, inducing "dense" hemadsorption (Sereda et al., 2016). These differences could be a consequence of differences between virulent and attenuated strains in the proportion of the circumference of erythrocytes in contact with the plasmalemma of infected macrophages during hemadsorption, or differences in the structure of strain populations based on the number of red blood cells attached to infected macrophages (Sereda et al., 2016).
3. For long-term storage, serums specific to the reference type are lyophilized.
4. To reduce the number of reference strains and sera used in animal seroimmunotyping, geographical isolation sites of the ASFV are preliminarily evaluated. For example, on the Iberian Peninsula, the presence of ASFV I and IV seroimmunotypes is possible, whereas in West Africa, the presence of the following seroimmunotypes is registered: ASFV I, II, and IV (Malogolovkin et al., 2015).

2.5. Immunological test

The seroimmunotype appurtenance of the studied isolates, previously assigned based on the results of the HAdI test to the same group with ASFV strains of the corresponding seroimmunotype, is determined by an immunological test on pigs (Balyshev et al., 2011).

2.5.1. Materials and equipment

Pigs (see 2.1.1), PBLS (see 2.1).

2.5.1.1. Hardware

Laminar flow cabinet, CO_2 incubator, refrigerator (4°C), freezer (− 40°C), analytical balance, inverted microscope, and thermometer.

2.5.1.2. Consumables

Multichannel pipettes, automatic pipettes with a volume of 20–200 µL, 100–1000 µL, aerosol-resistant filter tips, a sterile 48-well Nunc cell culture plate with TC treatment, and 1.0 mL syringes.

2.5.1.3. Chemical reagents

Complete blood leukocytes growing media: The EMEM containing 10% of FBS, penicillin (100–200 IU/mL), and streptomycin (100–200 mg/mL).

2.5.2. Method

- The infectious activity of the tested isolate, as well as the attenuated and virulent reference strains of the ASFV, is determined in the cultures of PBLS (See 2.3.2).
- Pigs (eight heads) are inoculated twice, intramuscularly, with an interval of 14 days with attenuated ASFV strain MK-200 at a dose of $10^{6.0}$–$10^{7.5}$ HAU_{50}.
- Then, after 28 days from the second inoculation, four pigs are intramuscularly infected with a virulent reference strain Mozambique-78 at a dose of $10^{3.0}$ HAU_{50}, and four with the studied isolate at the same dose. To control virulence, an additional two intact pigs each are infected in a similar way with a virulent reference strain of the ASFV and a test isolate at a dose of $10^{3.0}$ HAU_{50}.
- During the experiment all pigs are monitored in terms of body temperature and other clinical signs of ASF. As a rule, during this time, the death of control animals is observed. The specificity of the disease and death from ASF of experimental pigs is confirmed by the isolation of the virus in the culture of PBLS.
- In the absence of death of at least 3/4 of pigs inoculated with an attenuated strain and subsequently infected with a virulent reference strain or a test isolate of the ASFV, they are considered to have an immunological correspondence and belong to the same seroimmunotype.

2.5.2.1. Note

1. In case the pigs inoculated with an attenuated strain and infected with a test isolate die from ASF, then this isolate does not have an immunological correspondence with the attenuated and virulent reference strains taken in the experiment. According to the existing classification, it should be assigned to the group of strains that do not match the results of serotyping in the HAdI test and in the immunological sample.
2. If intact pigs infected with the tested isolate of the virus (virulence control) did not show signs of disease, characteristic symptoms, and did not die from ASF, this indicates its low virulence. After 21 days, these pigs are infected with a virulent reference strain of ASF virus of the presumed serotype. In case of survival of the pigs, the tested isolate of ASF virus is classified as belonging to the same serotype as the reference strain used.

3. Discussion

3.1. Comparative analysis of the genotyping and seroimmunotyping of the African swine fever virus

In 2015, a new approach was proposed that makes it possible to predict with a high degree of probability the seroimmunotype belonging to both hemadsorbing and non-hemadsorbing isolates of the ASFV (Malogolovkin et al., 2015). It is based on sequencing and phylogenetic analysis of the EP402R gene coding the major glycoprotein CD2v of the ASFV, responsible for the phenomenon of hemadsorption during reproduction of the ASFV (Borca et al., 1998; Malogolovkin and Kolbasov, 2019). Now, the method of "serotyping" uses a short fragment of the EP402R gene 90 nucleotides long (Thanh et al., 2021). However, in our opinion, the results of "serotyping" based on the nt sequence of

the EP402R gene should be necessarily confirmed by studies of the antigenic properties of isolates in the HAdI test and IT.

3.2. Determination of the immunotype of non-hemadsorbing African swine fever virus isolates

The HAdI test is not applicable to determine the type of non-hemadsorbing ASFV isolates. Therefore, only an IT is used. If the non-hemadsorbing isolate is virulent, then its type affiliation is determined in an immunological test on pigs previously inoculated with attenuated strains of the ASFV. If the studied non-hemadsorbing isolates of the ASFV are avirulent or weakly virulent, then they are used on vaccinated pigs twice with an interval of 14 days; then, after 28 days pigs are infected with virulent hemadsorbing reference strains of the ASFV of various seroimmunotypes.

3.3. Heterologous seroimmunotype isolates

The seroimmunotype classification has demonstrated its adequacy in studies on obtaining candidate live vaccines based on the selection of attenuated ASFV strains (Sereda et al., 2020). Another result of the application of the seroimmunotype classification was the proof of the heterogeneity of the Kiravira-67 isolate; it is a parent isolate to the four strains that belong to different seroimmunotypes: I, III, V, and VI (Sereda et al., 2014).

It should be noted that the final result of seroimmunotyping is achieved only as a result of setting an immunological test on pigs. Hemadsorption inhibiting test or phylogenetic analysis data on the EP402R gene should be considered preliminary. It was indicated above that the X group according to the seroimmunotype classification includes ASFV strains in which the HAdI results do not coincide with the IT (Sereda et al., 2020). A possible reason for this may be the formation of a mixed ASFV population consisting of isolates/strains of two or more seroimmunotypes. It has been experimentally established that when pigs are infected with mixtures of ASFV strains of two different seroimmunotypes, there is a persistent dominance in the manifestation of hemadsorption of one strain over the other (Sereda et al., 2014).

3.4. Exotic serotyping tests

By utilizing the radioimmunoprecipitation assay, researchers identified a significant virus-specific glycoprotein known as gp110-140 (also referred to as CD2v). This glycoprotein exhibited a molecular weight ranging from 110 to 140 kDa and displayed a characteristic dumbbell-shaped band, which is typical for highly glycosylated proteins (Sereda et al., 1993, 2018). For its detection, two principal conditions were required: (1) use of the metabolically ^{3}H-glycosamine-labeled proteins derived from lysates of PBM naturally susceptible A-cells infected with ASFV hemadsorbing strains as an antigen source; and (2) use of the homologous antisera with high activity in HAdI as an antibody source. Through extensive investigations, the serotype specificity of gp110-140 has been successfully determined (Sereda et al., 2018). While using some homologous components in the radioimmunoprecipitation assay, the dumbbell-like bands of gp 110–140 manifested as the major ones. In the assays using heterologous components, gp 110–140 was not detected in the fluorograms or manifested less intensively as compared to the results of the homologous assay.

A method exists for quantitative assessment of the serological relationship of hemadsorbing ASFV strains. Results of radioimmunoprecipitation are to be recorded not through a visual examination of the fluorogram, but by the number of pulses per minute using a β-counter. ^{3}H-glucosamine labeled gp 110–140 preparations, derived from hemadsorbing ASFV reference strains purified with ion-exchange chromatography on DEAE-Sephacel, were used as antigens for the quantitative version of the radioimmunoprecipitation procedure. The percentage of specific binding obtained with the control sera of intact pigs was not greater than 3%. The serological relationship of gp110-140 with serotype-heterologous antisera varied from 20 to 45% which indicates that the gp110-140 contains both homologous and heterologous epitopes (Sereda et al., 1998, 2018). Thus, the serotype specificity of gp110-140 was confirmed using two versions of radioimmunoprecipitation assay.

In summary, the described seroimmunotyping technique is based on the combination of two immunological tests *in vitro* and *in vivo*. It provides adequate experimental results during the development and evaluation of the protective properties of candidate vaccines against ASF. Knowledge about the seroimmunotype assignment of isolates/strains is useful in monitoring ASF, determining the phylogenetic relationships of virus isolates, and confirming the possible source of virus introduction.

Data availability statement

The original contributions presented in the study are included in the article/supplementary material, further inquiries can be directed to the corresponding authors.

Ethics statement

The manuscript presents research on animals that do not require ethical approval for their study.

Author contributions

AS: writing—original draft preparation. DK: conceptualization, supervision, and project administration. SN and VB: writing—review and editing. MV, IS, and GK contributed to both the conception and design of the work. All authors contributed to the article and approved the submitted version.

Acknowledgments

We are grateful to Galina Glebova for providing animal care.

Conflict of interest

The authors declare that the research was conducted in the absence of any commercial or financial relationships that could be construed as a potential conflict of interest.

Publisher's note

References

Achenbach, J. E., Gallardo, C., Nieto-Pelegrín, E., Rivera-Arroyo, B., Degefa-Negi, T., Arias, M., et al. (2017). Identification of a new genotype of African swine fever virus in domestic pigs from Ethiopia. *Transbound. Emerg. Dis.* 64, 1393–1404. doi: 10.1111/tbed.12511

Alonso, C., Borca, M., Dixon, L., Revilla, Y., Rodriguez, F., Escribano, J. M., et al. (2018). ICTV virus taxonomy profile: Asfarviridae. *J. Gen. Virol.* 99, 613–614. doi: 10.1099/jgv.0.001049

Ashmarin, I., Vasil'yev, I., and Ambrosov, V. (1975) in *Rapid methods of statistical processing and planning experiments*. ed. L. I.-v. Leningr. *2nd* ed (Leningrad, Russia: Leningrad University Press (Gos Univ-ta)), 76.

Balyshev, V. M., Bolgova, M. V., Balysheva, V. I., Knyazeva, N. V., and Zhivoderov, S. P. (2015). Preparation of standard haemadsorption-inhibiting reference sera against African swine fever virus. *Vopr Norm Regul Vet.* 2, 23–25.

Balyshev, V. M., Kalantaenko, Y. F., Bolgova, M. V., and Prodnikova, E. Y. (2011). Seroimmunological affiliation of African swine fever virus isolated in the Russian Federation. *Russ. Agric. Sci.* 37, 427–429. doi: 10.3103/S1068367411050053

Bastos, A. D. S., Penrith, M. L., Crucière, C., Edrich, J. L., Hutchings, G., Roger, F., et al. (2003). Genotyping field strains of African swine fever virus by partial p 72 gene characterisation. *Arch. Virol.* 148, 693–706. doi: 10.1007/s00705-002-0946-8

Blome, S., Franzke, K., and Beer, M. (2020). African swine fever - a review of current knowledge. *Virus Res.* 287:198099. doi: 10.1016/j.virusres.2020.198099

Boinas, F. S., Hutchings, G. H., Dixon, L. K., and Wilkinson, P. J. (2004). Characterization of pathogenic and non-pathogenic African swine fever virus isolates from *Ornithodoros erraticus* inhabiting pig premises in Portugal. *J General Virol. Direct* 85, 2177–2187. doi: 10.1099/vir.0.80058-0

Borca, M. V., Carrillo, C., Zsak, L., Laegreid, W. W., Kutish, G. F., Neilan, J. G., et al. (1998). Deletion of a CD2-like gene, 8-DR, from African swine fever virus affects viral infection in domestic swine. *J. Virol.* 72, 2881–2889. doi: 10.1128/JVI.72.4.2881-2889.1998

Coggins, L. (1968a). Segregation of a nonhemadsorbing African swine fever virus in tissue culture. *Cornell Vet.* 58, 12–20.

Coggins, L. (1968b). A modified hemadsorption-inhibition test for African swine fever virus. *Bull Epizoot Dis Afr Bull Epizoot En Afr.* 16, 61–64.

Detray, D. E. (1957). Persistence of viremia and immunity in African swine fever. *Am. J. Vet. Res.* 18, 811–816.

Gallardo, C., Soler, A., Rodze, I., Nieto, R., Cano-Gómez, C., Fernandez-Pinero, J., et al. (2019). Attenuated and non-haemadsorbing (non-HAD) genotype II African swine fever virus (ASFV) isolated in Europe, Latvia 2017. *Transbound. Emerg. Dis.* 66, 1399–1404. doi: 10.1111/tbed.13132

Imatdinov, A., Kazackova, A. S., Morozova, D. Y., Lyska, V. M., Zhivoderov, S., and Sereda, A. (2019). Experience gained in preparation of hemadsorption inhibiting sera against African swine virus seroimmunotypes III and IV. *Veterinariya* 22, 31–37. doi: 10.30896/0042-4846.2019.22.7.31-37

Jori, F., and Bastos, A. D. S. (2009). Role of wild suids in the epidemiology of African swine fever. *Ecosyst. Health* 6, 296–310. doi: 10.1007/s10393-009-0248-7

King, K., Chapman, D., Argilaguet, J. M., Fishbourne, E., Hutet, E., Cariolet, R., et al. (2011). Protection of European domestic pigs from virulent African isolates of African swine fever virus by experimental immunisation. *Vaccine* 29, 4593–4600. doi: 10.1016/j.vaccine.2011.04.052

López, E., van Heerden, J., Bosch-Camós, L., Accensi, F., Navas, M. J., López-Monteagudo, P., et al. (2020). Live attenuated African swine fever viruses as ideal tools to dissect the mechanisms involved in cross-protection. *Viruses* 12:1474. doi: 10.3390/v12121474

Malmquist, W. A. (1963). Serologic and immunologic studies with African swine fever virus. *Am. J. Vet. Res.* 24, 450–459.

Malmquist, W. A., and Hay, D. (1960). Hemadsorption and cytopathic effect produced by African swine fever virus in swine bone marrow and buffy coat cultures. *Am. J. Vet. Res.* 21, 104–108.

Malogolovkin, A., Burmakina, G., Titov, I., Sereda, A., Gogin, A., Baryshnikova, E., et al. (2015). Comparative analysis of African swine fever virus genotypes and serogroups. *Emerg. Infect. Dis.* 21, 312–315. doi: 10.3201/eid2102.140649

Malogolovkin, A., and Kolbasov, D. (2019). Genetic and antigenic diversity of African swine fever virus. *Virus Res.* 271:197673. doi: 10.1016/j.virusres.2019.197673

National Research Council, (US) (2011). Committee for the Update of the Guide for the Care and Use of Laboratory Animals). *Guide for the Care and Use of Laboratory Animals*. *8th* ed (Washington (DC): National Academies Press (US)).

Nix, R. J., Gallardo, C., Hutchings, G., Blanco, E., and Dixon, L. K. (2006). Molecular epidemiology of African swine fever virus studied by analysis of four variable genome regions. *Arch. Virol.* 151, 2475–2494. doi: 10.1007/s00705-006-0794-z

Pan, I. C. (1992). African swine fever virus: generation of subpopulations with altered immunogenicity and virulence following passage in cell cultures. *J. Vet. Med. Sci.* 54, 43–52. doi: 10.1292/jvms.54.43

Pan, I. C., and Hess, W. R. (1985). Diversity of African swine fever virus. *Am. J. Vet. Res.* 46, 314–320.

Plowright, W. (1986). African swine fever: a retrospective view. *Rev Sci Tech OIE.* 5, 455–468. doi: 10.20506/rst.5.2.246

Ravaomanana, J., Michaud, V., Jori, F., Andriatsimahavandy, A., Roger, F., Albina, E., et al. (2010). First detection of African swine fever virus in *Ornithodoros porcinus* in Madagascar and new insights into tick distribution and taxonomy. *Parasit. Vectors* 3:115. doi: 10.1186/1756-3305-3-115

Rock, D. L. (2017). Challenges for African swine fever vaccine development—"… perhaps the end of the beginning.". *Vet. Microbiol.* 206, 52–58. doi: 10.1016/j.vetmic.2016.10.003

Sánchez-Cordón, P. J., Chapman, D., Jabbar, T., Reis, A. L., Goatley, L., Netherton, C. L., et al. (2017). Different routes and doses influence protection in pigs immunised with the naturally attenuated African swine fever virus isolate OURT88/3. *Antivir. Res.* 138, 1–8. doi: 10.1016/j.antiviral.2016.11.021

Sereda, A., Anokhina, E., Fugina, L., and Makarov, V. (1993). Serological and physical-chemical properties of gp 110-140 of African swine fever virus. *Veterinariya* 1, 26–28.

Sereda, A. D., Anokhina, E. G., Makarov, V. V., and Karpov, G. M. (1998). Method for determining antigen affinity of hemabsorbing isolates of african pig pest viruses. *RU* 2122211:C1.

Sereda, A. D., and Balyshev, V. M. (2011). Antigenic diversity of African swine fever viruses. *Vopr. Virusol.* 56, 38–42.

Sereda, A. D., Balyshev, V. M., Kazakova, A. S., Imatdinov, A. R., and Kolbasov, D. V. (2020). Protective properties of attenuated strains of African swine fever virus belonging to Seroimmunotypes I–VIII. *Pathogens.* 9:274. doi: 10.3390/pathogens9040274

Sereda, A., Balyshev, V. M., Morgunov, Y. P., and Kolbasov, D. (2014). Antigenic characteristics of African swine fever virus in artificial and natural mixed populations. *Selskok. Biol.* 4, 64–69. doi: 10.15389/agrobiology.2014.4.64eng

Sereda, A., Imatdinov, A., and Makarov, V. V. (2016). The haemadsorption at african swine fever (review). *Selskok. Biol.* 51, 763–774. doi: 10.15389/agrobiology.2016.6.763eng

Sereda, A., Kazakova, A., Imatdinov, I., and Kolbasov, D. (2018). Serotype-specific and haemadsorption protein of the african swine fever virus. *Slov. Vet. Res.* 55, 141–151. doi: 10.26873/SVR-454-2018

Thanh, T. H. T., Duc, T. A., Viet, L. D., van, H. T., Thi, N. C., Thi, C. N., et al. (2021). Rapid identification for serotyping of African swine fever virus based on the short fragment of the EP402R gene encoding for CD2-like protein. *Acta Vet. (Beograd)* 71, 98–106. doi: 10.2478/acve-2021-0007

Vigário, J. D., Terrinha, A. M., Bastos, A. L., Moura-Nunes, J. F., Marques, D., and Silva, J. F. (1970). Serological behaviour of isolated African swine fever virus. *Brief report. Arch Gesamte Virusforsch.* 31, 387–389. doi: 10.1007/BF01253773

Viruses IC on T (2011) in *Virus taxonomy: Ninth report of the international committee on taxonomy of viruses*. ed. A. M. King (Netherlands: Elsevier), 1463.

World organization for animal health (2019). "Chapter 3.8.1 African swine fever (infection with African swine fever virus)" in *Manual of diagnostic tests and vaccines for terrestrial animals*. *8th* ed (Paris, France: World Organisation for Animal Health (OIE)). 1–8.

Zubairov, M. M., Selyaninov, Y. O., Roshchin, A. V., and Khokhlov, P. S. (2017). Antiviral activity and therapeutic and preventive effect of phosphonoacetic acid and its derivatives. *Chem Saf Sci.* 1, 146–157. doi: 10.25514/CHS.2017.1.11440

frontiers | Frontiers in Microbiology

TYPE Original Research
PUBLISHED 22 November 2023
DOI 10.3389/fmicb.2023.1280588

OPEN ACCESS

EDITED BY
Gang Wang,
Shandong Agricultural University, China

REVIEWED BY
Roberto M. C. Guedes,
Federal University of Minas Gerais, Brazil
Samah Attia Algharib,
Benha University, Egypt

*CORRESPONDENCE
Abelardo Silva-Júnior
✉ abelardo.junior@icbs.ufal.br

RECEIVED 20 August 2023
ACCEPTED 30 October 2023
PUBLISHED 22 November 2023

CITATION
Toledo LT, de Souza LFL, Pereira CER, Polveiro RC, Bressan GC, Yamatogi RS, Jeong KC, Marks FS, Diamantino CA, de Carvalho VHR, Malcher CS, Petri FAM, de Oliveira LG, Moreira MAS and Silva-Júnior A (2023) A genetic and virulence characterization of Brazilian strains of *Mycoplasma hyopneumoniae*. *Front. Microbiol.* 14:1280588. doi: 10.3389/fmicb.2023.1280588

A genetic and virulence characterization of Brazilian strains of *Mycoplasma hyopneumoniae*

Leonardo Teófilo Toledo[1], Luiz Fernando Lino de Souza[1], Carlos Eduardo Real Pereira[1], Richard Costa Polveiro[1], Gustavo Costa Bressan[2], Ricardo Seiti Yamatogi[1], Kwangcheol Casey Jeong[3], Fernanda Simone Marks[1], Caio Augustus Diamantino[1], Victor Hugo Rabelo de Carvalho[1], Clarisse Sena Malcher[4], Fernando Antônio Moreira Petri[4], Luis Guilherme de Oliveira[4], Maria Aparecida Scatamburlo Moreira[1] and Abelardo Silva-Júnior[5]*

[1]Department of Veterinary Medicine, Federal University of Viçosa, Viçosa, Brazil, [2]Department of Biochemistry and Molecular Biology, Federal University of Viçosa, Viçosa, Brazil, [3]Emerging Pathogens Institute, University of Florida, Gainesville, FL, United States, [4]School of Agricultural and Veterinarian Sciences, São Paulo State University (Unesp), São Paul, Brazil, [5]Institute of Biological and Health Sciences, Federal University of Alagoas, Maceió, Brazil

Mycoplasma hyopneumoniae (*M. hyopneumoniae*) is considered the primary causative agent of porcine enzootic pneumonia (EP), a chronic contagious respiratory disease that causes economic losses. Obtaining new pathogenic isolates and studying the genome and virulence factors are necessary. This study performed a complete sequencing analysis of two Brazilian strains, UFV01 and UFV02, aiming to characterize the isolates in terms of the virulence factors and sequence type. The complete genome analysis revealed the main virulence genes (*mhp385*, *mhp271*, *MHP_RS03455*, *p102*, *p97*, *p216*, *MHP_RS00555*, *mhp107*) and ST-123, the presence of three toxin-related genes (*tlyC*, *PLDc_2* and *hcnC*), and some genetic groups specific to these two isolates. Subsequently, the pathogenicity of the isolates was evaluated via an experimental infection conducted in a swine model. The study was divided into three groups, namely a negative control group ($n = 4$) and two test groups ($n = 8$), totaling 20 animals. They were challenged at 35 days of age with 10^7 CCU (Color Changing Units) *M. hyopneumoniae* via the intratracheal route. The UFV01 group showed earlier and higher seroconversion (IgG) (100%), while only 50% of the UFV02 group seroconverted. The same trend was observed when analyzing the presence of IgA in the bronchoalveolar lavage fluid (BALF) at 35 days post-infection (dpi). The UFV01 group had a mean macroscopic lesion score of 11.75% at 35 dpi, while UFV02 had 3.125%. Microscopic lesions were more severe in the UFV01 group. Based on laryngeal swab samples evaluated by qPCR, and the detection began at 14 days. The UFV01 group showed 75% positivity at 14 dpi. The UFV02 group also started excreting at 14 dpi, with a positivity rate of 37.5%. The results indicate that the UFV01 isolate exhibits higher virulence than UFV02. These findings may aid in developing new vaccines and diagnostic kits and establishing experimental models for testing.

KEYWORDS

UFV01, UFV02, respiratory disease, experimental challenge, Swine. *Mycoplasma hyopneumoniae*, genome, virulence, lesion

1 Introduction

Mycoplasma hyopneumoniae (*M. hyopneumoniae*) is the primary agent of enzootic pneumonia (EP), belonging to the phylum Firmicutes and the class *Mollicutes*. The Mycoplasma genus has genomes ranging from 580 to 2,200 kpb in size, with that of *M. hyopneumoniae* measuring 900 kpb and 300 to 900 nm in diameter. They lack a cell wall, have varied morphology, and are enveloped by a 10 nm thick plasma membrane. Their molecular biology is similar to that of gram-positive bacteria (Kobisch and Friis, 1996; Simionatto et al., 2013). *M. hyopneumoniae* is a globally distributed pathogen specific to domestic pigs (*Sus scrofa domesticus*) and wild boars (*Sus scrofa scrofa*) (Maes et al., 2008). EP is a chronic (Pieters et al., 2009), slowly spreading infectious disease (Roos et al., 2016) characterized by bronchopneumonia. Clinically, it manifests as a dry cough, delayed weight gain, high morbidity, and low mortality (Kuhnert and Overesch, 2014; Maes et al., 2017).

The factors contributing to the severity of EP include management and housing conditions, as well as the virulence of the infecting strain. Variations in virulence have been demonstrated among different field isolates of *M. hyopneumoniae*, leading to a classification of low, medium, and high pathogenicity based on clinical signs and lesions (Vicca et al., 2003; Meyns et al., 2007; dos Santos et al., 2015; Leal Zimmer et al., 2020). *M. hyopneumoniae* employs various mechanisms of pathogenicity such as cell adhesion (Siqueira et al., 2014; Raymond and Djordjevic, 2015; Leal Zimmer et al., 2020), secretion, signaling (Beuckelaere et al., 2022), cytotoxicity, apoptosis, and immunomodulation (Bai et al., 2013; Ni et al., 2015; Deeney et al., 2019; Yu et al., 2020), some of which are not fully understood (Leal Zimmer et al., 2020). Due to the uniqueness of mycoplasmas compared to other studied pathogens, there is limited opportunity to identify known homologous genes in other pathogens (Rycroft, 2020).

Mycoplasma hyopneumoniae adheres to respiratory epithelial cells, induces infiltration of macrophages and lymphocytes, and triggers the accumulation of inflammatory cells, leading to an inflammatory response (Woolley et al., 2012). This process destroys the mucociliary apparatus of the respiratory epithelium, alters the cell architecture, and results in ciliary loss, predisposing individuals to secondary infection (Woolley et al., 2012; Bustamante-Marin and Ostrowski, 2017). Several researchers described and studied mechanisms contribute to *M. hyopneumoniae* ability to colonize the respiratory tract and actively excrete the pathogen over extended periods (Leal Zimmer et al., 2020).

Colonization of the respiratory ciliated epithelium by *M. hyopneumoniae* specifically depends on the expression of two functionally redundant adhesin families, P97 and P102 (Siqueira et al., 2014). Approximately 20–30% of the genes in *M. hyopneumoniae* are responsible for surface protein expression, although many of their functions remain unknown (Felde et al., 2018). Adhesins are crucial, with at least 35 proteins are associated with cell adhesion, including several related to the P97/P102 families (Zhang et al., 1995; Bogema et al., 2012; Siqueira et al., 2014; Raymond and Djordjevic, 2015; Leal Zimmer et al., 2020).

Up to the present moment, 26 genomes deposited at NCBI can be found completely sequenced. The *M. hyopneumoniae* strain J was obtained by Friis in the United Kingdom in 1957 as first isolated (Kobisch and Friis, 1996) and its genome was sequenced in 2005 (Vasconcelos et al., 2005). The other isolates sequenced originate 232 United States (Minion et al., 2004); 7,422 and 7,448 Brazil (Vasconcelos et al., 2005; Siqueira et al., 2013); 168/168-L China (Liu et al., 2011); 11 Netherlands (Kamminga et al., 2017); 98 Netherlands; F7.2C Switzerland (Trueeb et al., 2019); KM014 South Korea (Han et al., 2017); LE China (Xie et al., 2021); TB1 China (Qiu et al., 2019); ES2-L China (Zong et al., 2022) ES2 China; MHP699, MHP650, MHP653, MHP679, MHP682, MHP691, MHP694, MHP709, MHP696 France; NCTC10127 UK and UFV01/UFV02 Brazil.

In Brazil, few studies have reported on the characterization of *M. hyopneumoniae* strains in the country (Yamaguti, 2009; dos Santos et al., 2015; Andrade et al., 2023). Currently, only isolates 7,422 and 7,448 have been completely sequenced and deposited in the NCBI by another research group (Vasconcelos et al., 2005; Siqueira et al., 2013).

Therefore, the objective of this study is to perform a comparative genomic analysis between the UFV01 and UFV02 isolates, as well as with others deposited in the NCBI database. Additionally, the aim is to induce infection in pigs using these two specific *M. hyopneumoniae* isolates to characterize virulence through clinical signs and induced lesions, and to identify variations in antibody levels, DNA load and cytokines.

2 Materials and methods

2.1 Origin and cultivation of the UFV01 and UFV02 isolates

The isolates were obtained through the collection of lungs suspected of EP from slaughtered animals originated from a property located in the Piranga Valley in the state of Minas Gerais, Brazil (Gonzaga et al., 2019). The isolation for obtaining pure cultures was performed following the standardized methodology by Cook et al. (2016).

The isolates were cultured in 1x Friis medium (liquid) and 2.8x Friis medium (solid) and prepared according to Cook et al. (2016). They were reactivated in a liquid medium at a ratio of 1:9 (frozen inoculum to medium). The test tubes were incubated at 37°C and observed daily until a color change occurred. Bacterial growth was evidenced by the alteration of the medium's color. Three passages were performed to reactivate the isolate, and after the fourth passage, the inoculum was aliquoted into individual volumes of 10 mL and frozen at −80°C until the time of inoculation. The isolates were quantified using the Color Changing Units (CCU) technique, performed according to Calus et al. (2010). In parallel, the isolates were cultured

on 2.8x solid Friis medium to visualize the colony morphology. The isolates were incubated for seven days in an oven at 37°C as described by Cook et al. (2016).

2.2 Whole genome sequence analysis of UFV01 and UFV02

The DNA extraction of the isolates (UFV01 and UFV02) was conducted using a Wizard® Genomic DNA Purification Kit (PROMEGA®, United States) following the manufacturer's recommendations. A private company (MicrobesNG/United Kingdom) performed the quantification, library preparation, and sequence steps. The raw data (pair-end 150 bp) were trimmed using the Trimmometics software (Bolger et al., 2014) and quality was analyzed using FastQC (Andrews, 2017). The contigs were assembled by the *De novo* technique, using the SPADES 3.15.3, MIRA 4.9.6, and A5-Miseq software (Chevreux et al., 2004; Tritt et al., 2012; Nurk et al., 2013), and the results were evaluated by with the Quality Assessment Tool for Genome Assemblies – Quast (Gurevich et al., 2013) to choose the best assembly.

The annotation and subsystem classification were made using Prokka 1.14.6 (Seemann, 2014), the Bacterial and Viral Bioinformatics Resource Center (BV-BRC) platform (Olson et al., 2023) and the files built by the Genbank deposit. The virulence factors, toxin gene prediction, resistance genes, and sequence typing (ST) were analyzed using the online platforms Virulence Factors of Pathogenic Bacteria – VFPB,[1] PathoFact version 1.0 (de Nies et al., 2021), the Comprehensive Antibiotic Resistance Database – CARD tools (McArthur et al., 2013), and pubMLST (Jolley et al., 2018) for sequence type determination, considering a cutoff of 70% for the scores of identity and similarity to determine their presence in the genetic system of the bacteria. The genome comparison was performed using BLAST Ring Image Generator (BRIG) (Alikhan et al., 2011) and Anvio-7.1 (Delmont and Eren, 2018; Eren et al., 2020). Orthologue group genes were analyzed and compared using the Orthofinder 2.5.2 software (Emms and Kelly, 2019). The two isolates were compared with 22 assemblies from the NCBI database. The strains used were 98 (Access Number: ASM1341272v1), ES-2 (Access Number: ASM476872v1), ES-2 L (Access Number: ASM1340275v1), F7.2C (Access Number: ASM792398v1), J (Access Number: ASM820v1), KM014 (Access Number: ASM225750v1), MHP650 (Access Number: ASM983217v1), MHP653 (Access Number: ASM983194v1), MHP679 (Access Number: ASM983212v1), MHP691 (Access Number: ASM983208v1), MHP694 (Access Number: ASM983190v1), MHP696 (Access Number: ASM983203v1), MHP699 (Access Number: ASM983185v1), MHP709 (Access Number: ASM983207v1), NCTC10127 (Access Number: 51334_A01-3), LH (Access Number: ASM2138386v1), 168 (Access Number: ASM18318v1), 168 L (Access Number: ASM40085v1), 232 (Access Number: ASM840v1), 7,422 (Access Number: ASM42721v1), 7,448 (Access Number: ASM822v1), and TB1 (Access Number: ASM221348v1) (Supplementary material S1).

1 http://www.mgc.ac.cn/VFs/main.htm

2.3 Experimental design and sample collection

Approximately 23-day-old Landrace x Large White piglets, with an average weight of 7.585 ± 0.591 kg, were acquired from the Agroceres PIC company; all tested negative for *M. hyopneumoniae*. All procedures were performed following the approval of the code of conduct for the use of animals in teaching, research, and extension of the Federal University of Viçosa, regulation 39/2021.

After the arrival of the animals, they underwent a 12-day adaptation period in the facilities. All animals tested negative in the qPCR (Fourour et al., 2018) for agent detection and for the presence of anti- *M. hyopneumoniae* (IgG) antibodies in ELISA *M. hyopneumoniae* Ab test (IDEXX, United States). The study was divided into two test groups ($n = 8$ each) and one negative control group ($n = 4$), totaling 20 animals. One test group was inoculated with the UFV01 isolate, the second group was inoculated with the UFV02 isolate, and the negative control group was inoculated with the Friis medium. The animals were kept in disinfected pens and isolated from the external environment in the isolation unit.

After the 12-day acclimation period, at 35 days of age, the animals in the test groups were intratracheally challenged with 10 mL of inoculum containing 1×10^6 CCU/mL. The negative control group was inoculated with 10 mL of Friis medium. Throughout the entire experimental period, no form of antimicrobial agent was administered through either water or food.

On day 0 (day inoculation), and 7, 14, 21, 28, and 35 days post inoculation, serum and laryngeal swab samples were collected to assess the seroconversion curve and agent excretion. On 35 dpi, all animals were euthanized. Bronchoalveolar lavage fluid (BALF) samples were collected at 35 dpi, immediately after euthanasia.

Duplicate samples of lung lesions for qPCR analysis were collected from portions with suggestive lesions of porcine EP and stored in cryotubes, then kept in liquid nitrogen (−196°C) until DNA extraction.

2.4 Evaluation of the clinical signs

Following the challenge, a daily monitoring routine was implemented in the morning for a duration of 40 min. This monitoring involved observing the animals for 20 min while they were agitated in the stall. Then, the animals were evaluated for 20 min under rest conditions. Incidences of non-productive dry cough episodes occurring during this specified period were systematically quantified and documented by a single observer, who remained blinded to the study's conditions, in accordance with the research conducted by Silva et al. (2022).

2.5 Cytokine evaluation

The tests for cytokine quantification in serum were performed using the Invitrogen IL-10 Porcine ELISA Kit, IFN-gamma Porcine ELISA Kit, and TNF-alpha Porcine ELISA Kit (Thermo Fisher Scientific®, Wilmington, DE, United States). These kits are based on a standard curve within a range of 500 to 7.8 pg./mL for IL-10 and IFN-gamma, and 1,500 to 23.4 pg./mL for TNF-alpha. The samples were tested on two plates. The standard curve was determined by the ELISA reader program and constructed in 4-parameter mode, with

the concentration determined kit provided values and according to the quantification obtained in the tests.

2.6 ELISA for detection of anti-*Mycoplasma hyopneumoniae* IgG and IgA

Blood collection was performed on 0, 7, 14, 21, 28, and 35 dpi from the orbital sinus. The collected samples were centrifuged at 8,000 g for 15 min, and 1 mL of serum was stored and kept at −20°C until use. Anti- *M. hyopneumoniae* IgG antibodies were detected from serum samples using the *M. hyopneumoniae* Ab test (IDEXX, United States), which is a commercial indirect ELISA kit (99.6% specificity and 89.4% sensitivity). The test was conducted following the manufacturer's recommendations. The S/P calculation was also performed according to the manufacturer's instructions. As this was an experimental infection, S/*p* values above 0.3 were considered positive. For the IgA ELISA in BALF, we used the methodology standardized by Mechler-Dreibi et al. (2021). The test is based on the use of reagents and plates from the commercial *M. hyopneumoniae* Ab kit (IDEXX, United States), with some modifications.

2.7 Detection of *Mycoplasma hyopneumoniae* DNA by real time qPCR

The laryngeal swab, lung tissue, and BALF samples had their DNA extracted using the adapted methodology described by Kuramae-Izioka (1997). As endogenous controls for the DNA extractions from the samples, a primer designed by Assao et al. (2019) was used, which amplifies a 107 bp region of the 18S ribosomal gene (GenBank: AY265350.1).

For the detection of the *M. hyopneumoniae* genome in the samples, the set of primers and probes described by Fourour et al. (2018) was used: forward primer: 5' TAAGGGTCAAAGTCAAAGTC-3′, reverse primer: 5′- AAATTAAAAGCTGTTCAAATGC-3′, and hydrolysis probe: 5′- FAM-AACCAGTTTCCACTTCATCGCC-BHQ2-3′. A fragment of *M. hyopneumoniae* DNA was amplified by conventional PCR and cloned using the CloneJET PCR Cloning Kit (Thermo Fisher®) for the construction of the standard curve. All samples were tested in duplicate, and those showing a variation greater than 0.5 Ct were tested again in triplicate.

The reaction consisted of 10 μL of 2X iTaqTM Universal Probes Master Mix (Bio-Rad, California, EUA), 1 μL of each primer at 10 nmol/μl (Invitrogen, USA), 0.6 μL of the hydrolysis probe at 10 nmol/μl (IDT, Iowa City, USA), 5.4 μL of ultrapure water, and 2 μL of DNA per sample, totaling 20 μL of reaction. The qPCR was performed on a CFX-96 real-time thermocycler (Biorad, United States) under the following conditions: an initial denaturation cycle at 95°C for 3 min, followed by 39 cycles of 95°C for 15 s and annealing/extension at 55.7°C for 1 min (Almeida et al., 2020).

2.8 Macroscopic and microscopic lesions

After the euthanasia of the animals at 35 days of infection, lung lesions compatible with swine EP were scored according to the methodology described by Straw et al. (1986). Each of the lung lobes was assessed macroscopically and the percentage of surface area affected by lesions was estimated. The value was multiplied by the weight that each lung lobe represented in relation to the total surface area the lesions can range from 0% (no lesions) to 100% (entire lung affected). The evaluated characteristics included red and firm consolidation in the apical, cardiac, accessory, and diaphragmatic lobes.

Histological slides were prepared for semiquantitative classification of microscopic lesions. The method to mensurate the lesions was adapted from a study published by Hansen et al. (2010). The sections were systematically examined by evaluating the following structures in each section: bronchi, bronchioles, bronchus-associated lymphoid tissue (BALT), alveolar ducts, and alveoli, including alveolar septa, peribronchial, peribronchiolar, and interlobular connective tissues, and pleura. BALT hyperplasia was graded as follows: (−) absent; (1) mild, diffuse infiltration of lymphocytes in peribronchial, peribronchiolar, and perivascular tissues, including the lamina propria of the airways; (2) moderate increase in diffuse lymphocyte infiltration and/or presence of some lymphoid nodules; and (3) with marked the number of lymphoid nodules. Bronchopneumonia and pleuritis lesions were graded in the same way, according to the intensity of the lesions. The pathologists were blinded to assess clinical and lesions data.

2.9 Differential diagnosis

Individual lung swabs were collected from the animals and subjected to total RNA extraction using the commercial RNA extraction kit from Promega United States – ReliaPrep™ RNA Miniprep Systems for the diagnosis of the Influenza A virus using conventional PCR methodology. The primers used in the PCR reactions as a reference were described by Fouchier et al. (2000). For the detection of the bacterial agents (*Glaesserella parasuis*, *Pasteurella multocida*, *Mycoplasma hyorhinis*, *Streptococcus suis*, and *Actinobacillus pleuropneumoniae*), the qPCR technique was used with DNA samples obtained from the BALF, following the methodologies previously described (Bonifait et al., 2014; Fourour et al., 2018; Goecke et al., 2020; Han et al., 2020; Sunaga et al., 2020), respectively (Supplementary material S2).

2.10 Statistical analysis

The quantitative variables were assessed using the Shapiro–Wilk test to check for the normality of errors and the Levene test to assess the homogeneity of variances. Data that did not meet the assumptions of normality and homoscedasticity were subjected to statistical transformations. The degrees of freedom for repeated measures ANOVA were adjusted using the Greenhouse–Geisser correction for the factors of day and the day x treatment interaction. Non-parametric data were subjected to the Wilconxon test with significance of $p < 0.001$.

The data were evaluated using linear models with repeated measures over time, and pairwise comparisons between means were performed using the Tukey's test ($p < 0.05$). Statistical analyzes were conducted using R software, version 4.2.1 (R Core Team, 2022).

3 Results

3.1 WGS analysis

The genomes UFV01 (NCBI: PRJNA542605), and UFV02 (NCBI: PRJNA542605) were previously deposited in the NCBI, with UFV01 presenting 909.816 pair bases, 28.4% G + C content, and 751 CDS; UFV02 presented 959.419 pair bases, 28.5% GC content and 788 CDS. Features such as genome size, number coding system, and GC content were like those of other genomes in the NCBI library. For the CDS and subsystem identification, the protein files obtained from GenBank were used in the BV-BRC platform annotation showed differences in the number of coding sequences and subsystem features (Figure 1), accounting for 58–60% for the CDS identified and 16 predicted subsystems important to classify the genes according to their genes.

UFV01 and UFV02 presented 16 different function classes (Figure 1). Inside of the classes, UFV02 presented 324 annotated genes, and 81 subsystems. In contrast, UFV01 presented 319 annotated genes, thus denoting more genes attributed to the former. Moreover, UFV01 had fewer annotated genes related to protein synthesis (Figure 1-XIII), with four less than UFV02. In addition, it presented two genes less for energy and precursor metabolites generation (Figure 1-VI) and one gene less for RNA Processing (Figure 1-XV). However, it showed two more genes related to Stress Response, Defense, and Virulence (Figure 1-XVI). The smaller number of annotated genes could be related to the larger number of genes with still unidentified characteristics.

The virulence factors identified for both isolates were *mhp385, mhp271, MHP_RS03455, p102, p97, p216, MHP_RS00555,* and *mhp107,* and the characterized toxins were *tlyC* (putative hemolysin), *PLDc_2* (PLD-like domain) and *hcnC* (hydrogen cyanide synthase HcnC). The sequence type for these two isolates characterized using the PubMLST platform was the same and was classified as ST-123. No resistance genes were found in these isolates, except for the isolate UFV02, which presented the gene *KpnF* related to efflux pumps for different compounds (macrolide, aminoglycoside, cephalosporin, tetracycline, peptide antibiotic, rifamycin, disinfecting agents and antiseptics).

The genome comparison is shown in Figure 2. Overall, UFV01 and UFV02 present genomes with few gaps compared to other genomes. Some gaps seem to be present in all genomes when compared to the J strain (analysis reference). Comparing the core-genome analysis (Figure 3), UFV01 presents more exclusive genetic clusters (singletons) that are individual genes without any homologs compared to UFV02. However, the genome of TB1, which is of Chinese origin, had the most compared to all other genomes in this study.

The orthogroup analysis (Figure 4) showed that all genomes share 549 groups. For UFV01 and UFV02 specifically, a total of 03 orthogroups was reported only in these two isolates, and these strains seem to have few more orthogroups compared to the other genomes (Figure 4A). Considering all genomes in this genetics group, the UFV01 and UFV02 seems in the middle of the tree, being um side close of MPH groups strains (French), and the other side close of KM014 (South Korea), F7.2C (Belgium) and 7422/7448 (Brazil) strains (Figure 4B).

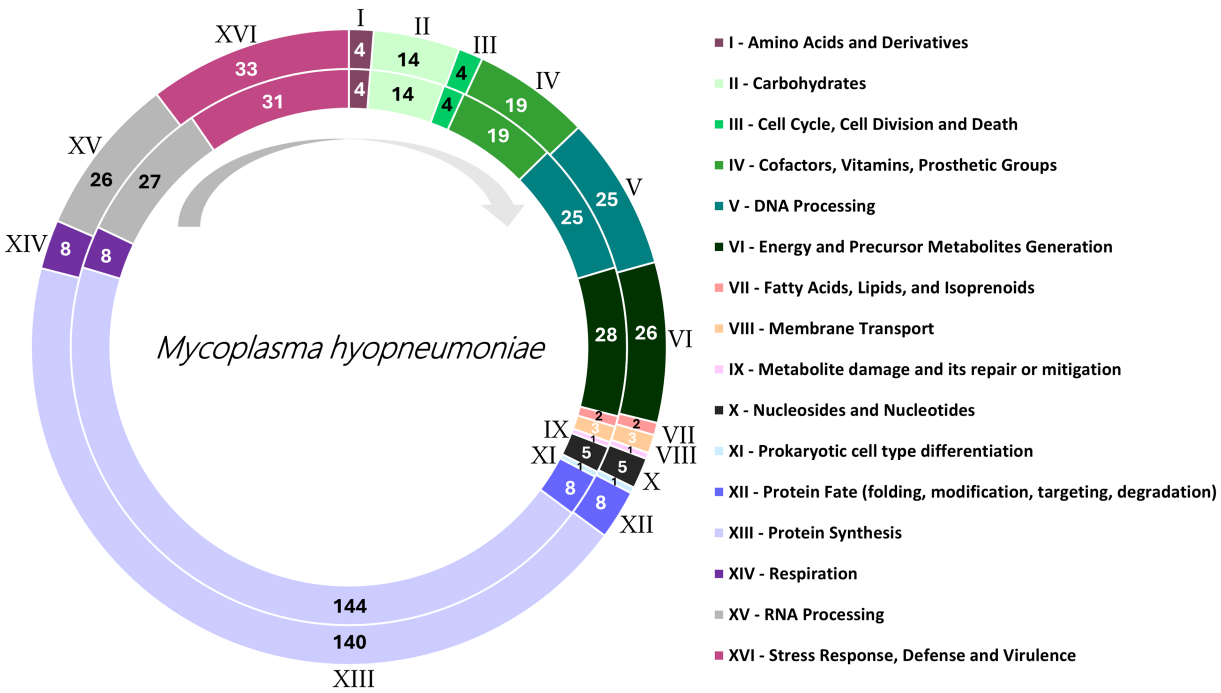

FIGURE 1
Sixteen class category distributions of UFV01 (internal circle) and UFV02 (external circle), annotated by Bacterial and Viral Bioinformatics Resource Center (BV-BRC) using as reference the taxonomy ID: 2099 – *Mesomycoplasma hyopneumoniae*. Each color and Roman numeral identify different function Class, while the numbering inside the circles represents number of genes. The arrow in gray suggests how the caption should be read.

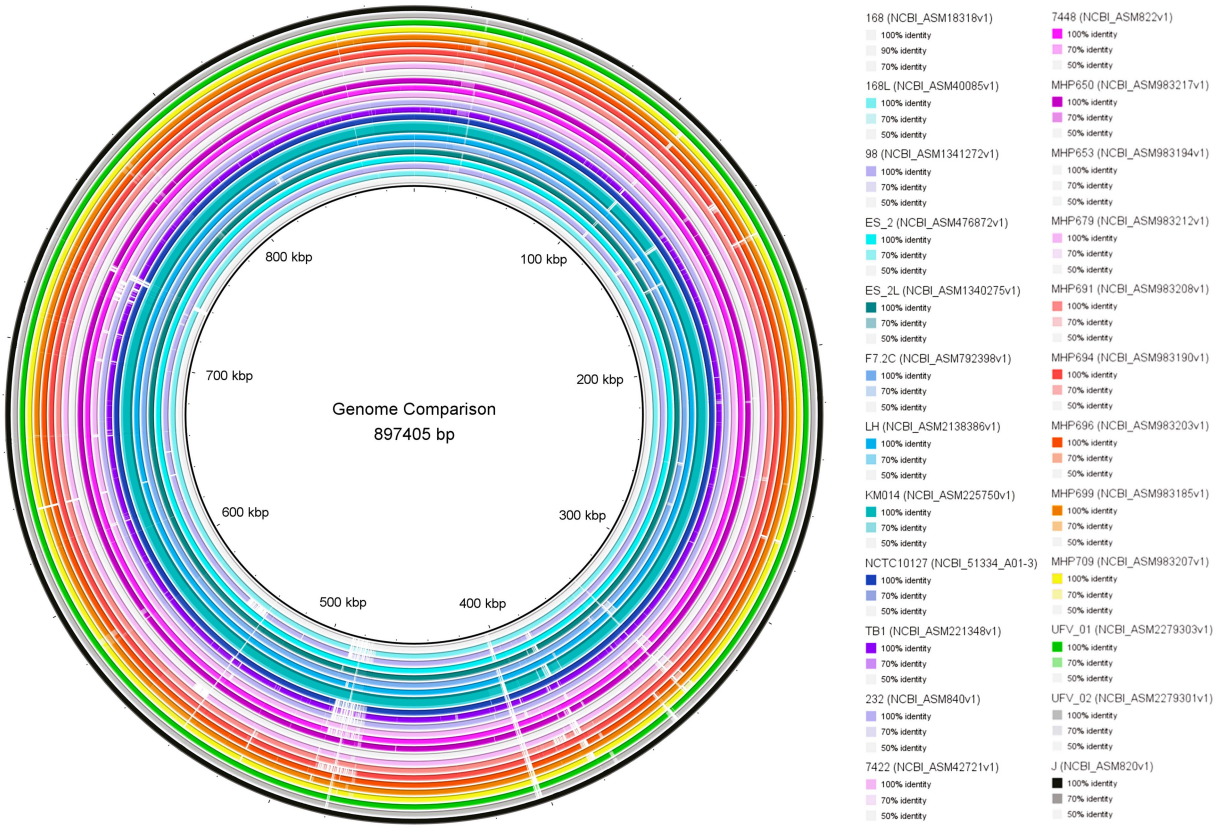

FIGURE 2
Comparison of *Mycoplasma hyopneumoniae* isolates UFV01 and UFV02 with 22 references assemblies from NCBI using the BLAST Ring Image Generator (BRIG) (Alikhan et al., 2011).

3.2 Evaluation of the clinical signs and lung lesions

The cough frequencies of the control, UFV01, and UFV02 groups were observed daily, as described in the methodology. From the first week onwards, animals in the UFV01 and UFV02 groups started to exhibit coughing episodes consistent with EP. The UFV01 group exhibited a higher numerical count of recorded coughs per 40 min in comparison to the UFV02 group at certain intervals (Figure 5A). When evaluating the release media for a duration of 40 min daily, considering the number of animals per group over the entire experimental period, all groups displayed statistically significant differences from one another. Specifically, the UFV01 group showed 0.44 coughs per pig per 40 min, while the UFV02 group exhibited 0.22, and the NC group registered 0.04 (Figure 5B).

Macroscopic lesions characteristic of EP in the lungs were scored from 0 to 100% (indicating the extent of tissue affected). As can be observed in Figure 6, the group inoculated with the UFV01 strain exhibited more severe macroscopic lesions ($p < 0.05$). Specifically, the UFV01 group (Figures 7E–L) presented 11.75% (±6.60) macroscopic lesions at 35 dpi (Figure 6), and the UFV02 group (Figures 7M–T) exhibited 3.125% (±1.55) lesions. The animals in the control group (Figures 7A–D) showed 0% macroscopic lesions.

The microscopic lesions found in the processed fragments consisted of bronchopneumonia, BALT hyperplasia, and pleuritis. They were scored according to Table 1 as absent (−), mild (1), moderate (2), and severe (3). Table 1 presents the frequencies of each respective lesion and its degree of involvement. Animals in the control group (NC) had no lesions. Animals in the UFV01 group had 50% mild bronchopneumonia lesions (4/8), 37.5% moderate lesions (3/8), and 12.5% severe lesions (1/8). Regarding the BALT analysis, 50% had moderate lesions (4/8) and 50% had severe lesions (4/8). In the UFV02 group 62.5% of the pigs had mild bronchopneumonia lesions (5/8) and 37.5% moderate lesions (3/8). The BALT analysis 62.5% mild lesions (5/8) and 25% moderate lesions (2/8) and one animal (1/8) in the UFV02 group showed no lesions. Only the UFV01 group had cases of pleuritis, with 25% mild (2/8) and 12.5% moderate (1/8).

When comparing the mean scores of the lesions according to the scoring described in Table 1, the UFV01 group scored 1.62 for bronchopneumonia, 1.5 for BALT hyperplasia and 0.5 for pleuritis. On the other hand, the UFV02 group scored 1.37, 1.12, and 0.0, respectively, for the three aforementioned lesions (Table 1).

3.3 ELISA IgG and IgA

The animals in the control group remained negative throughout the study. The detection of IgG dynamics of both groups was not uniform. In the UFV01 group, seroconversion began at 21 dpi with 12.5% (1/8) of the animals, increased to 75% (6/8) at 28 dpi and reached 100% (8/8) by 35 dpi. In contrast, in the UFV02 group, only 50% (4/8) had seroconverted at 35 dpi (Figure 8A). The antibody

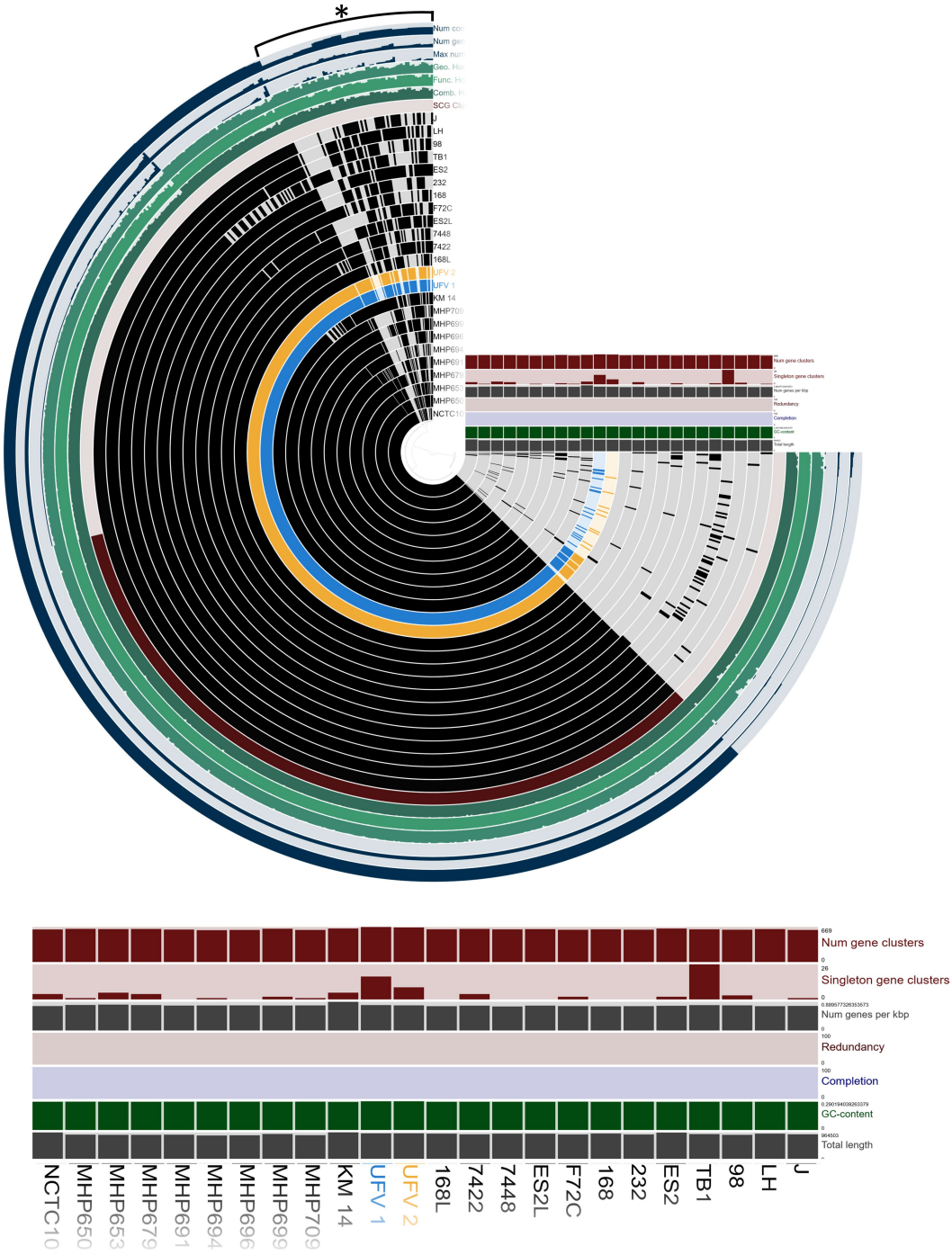

FIGURE 3
Pangenome of 22 reference assemblies downloaded from NCBI and the two isolates, UFV01 (blue) and UFV02 (yellow), using Anvio-7.1 (Delmont and Eren, 2018; Eren et al., 2020). The figure illustrates the core-genome comparison, G + C content, length of genome, number of gene clusters, and singleton gene cluster. *Variable gene cluster.

levels generated by UFV01 were statistically higher than those of UFV02 at 21, 28, and 35 dpi, as observed in Figure 8A.

An analysis was conducted to detect IgA antibodies in the BALF of the three groups. No anti- *M. hyopneumoniae* IgA were detected in the NC group. In the UFV01 group, 100% (8/8) of the individuals tested positive, while only 50% (4/8) tested positive in the UFV02 group, as observed in Figure 8B. The animals that tested positive for IgA in the UFV02 group were the same individuals that tested positive for IgG.

3.4 qPCR of BALF, laryngeal swabs and lung tissue

Laryngeal swabs were collected and subjected to qPCR analysis to evaluate the positivity and bacterial load excreted by the groups. The onset of bacterial shedding occurred at 14 dpi. As observed in Figure 9A and Supplementary material S3, the UFV01 group had a positivity of 75% at 14 dpi (3.76×10^2 copies/μL), 87.5% at 21 dpi

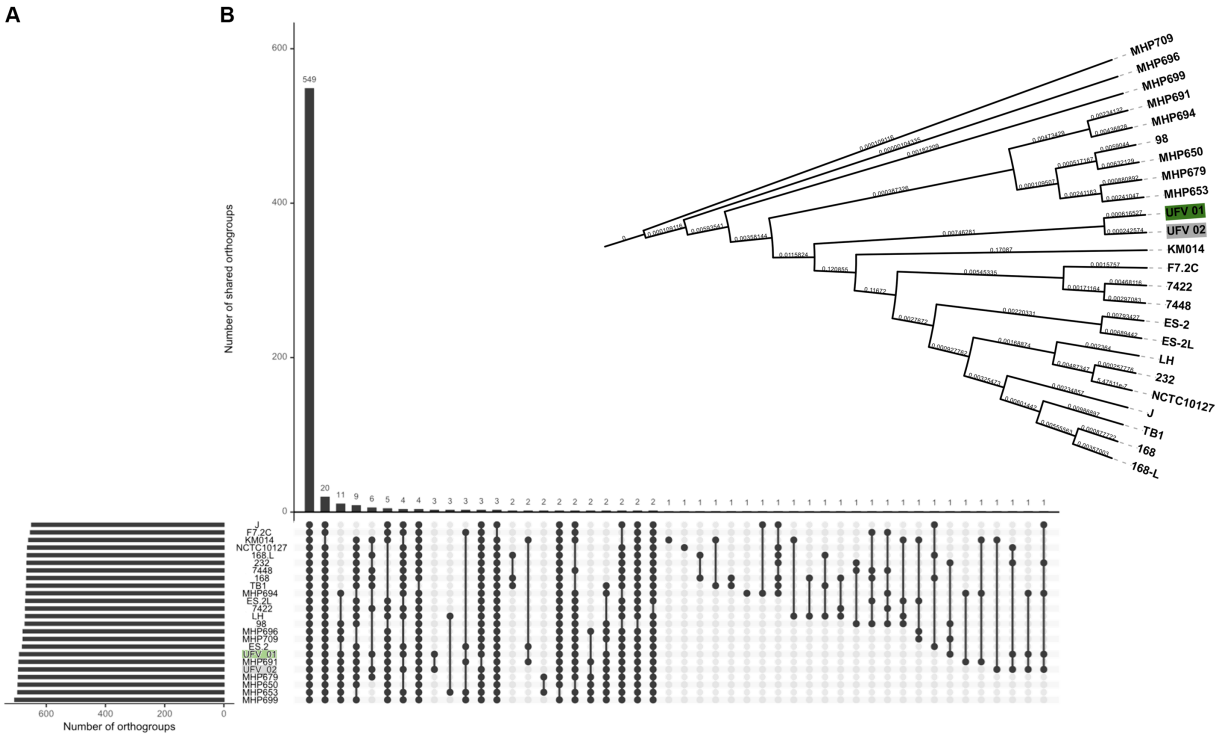

FIGURE 4
Orthogroup comparison of 22 NCBI reference assemblies and the isolates UFV01 (green) and UFV02 (gray), analyzed by the Orthofinder 2.5.2 software (Emms and Kelly, 2019). **(A)** The common and uncommon orthogroups from all genomes **(B)**. Dendogram based on the presence or absence of orthogroups.

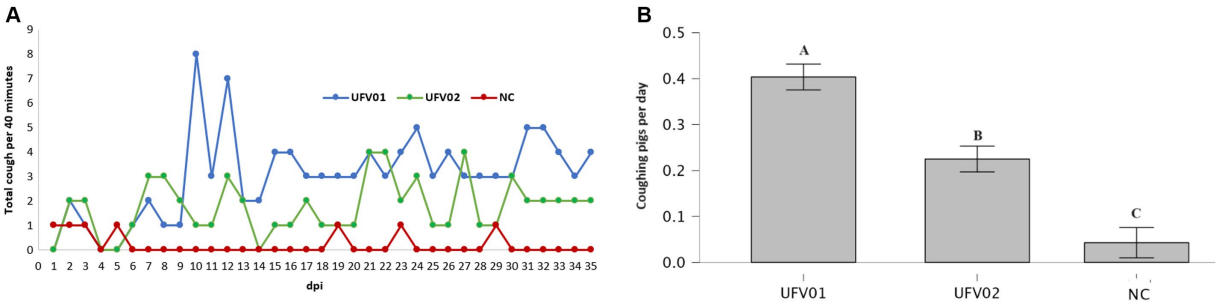

FIGURE 5
(A) Cough frequency assessment graph. Orange line – Control group. Green line – UFV01 group. Blue line – UFV02 group. NC – negative control; dpi – days post inoculation. **(B)** Average daily number of coughs per animal in each experimental group over the 35-day challenge period, measured during 40-min day. Different letters indicate statistical significance based on the Wilcoxon test with a significance level of $p < 0.001$.

(4.36×10^2 copies/μL), 100% at 28 dpi (1.44×10^3 copies/μL), and 87.5% at 35 dpi (1.25×10^4 copies/μL). The UFV02 group also started shedding bacteria at 14 dpi, but with a positivity of 37.5% (1.82×10^2 copies/μL), 75% at 21 dpi (8.33×10^2 copies/μL), 87.5% at 28 dpi (1.44×10^3), and 87.5% at 35 dpi (2.50×10^3 copies/μL). It should be noted that one individual in the UFV02 group (T) tested negative on all days.

Regarding the bacterial loads shed throughout the experimental course, it can be observed in Figure 9A that both challenged groups (UFV01 and UFV02) differed statistically from the negative control group only from 14 to 35 dpi. Both test groups showed a numerical increase in DNA copy excretion from 14 to 35 dpi (Figure 9A; Supplementary material S3), but did not differ statistically from each other.

BALF and lung tissue samples were subjected to qPCR analysis to evaluate the bacterial load present in the respiratory system of the animals at 35 dpi, during euthanasia. As shown in Figure 9B, the NC group tested negative in both analyzes, confirming once again their complete negativity. The UFV01 group showed 100% positivity (8/8) in both the BALF and tissue analyzes, with respective average bacterial loads of 3.57×10^5 copies/μL and 2.63×10^6 copies/μL of DNA. The UFV02 group had 87.5% positivity in both assessments, with an average bacterial load of 6.32×10^6 copies/μL and 3.92×10^6 copies/μL of DNA, respectively. See Supplementary material S3 for more details.

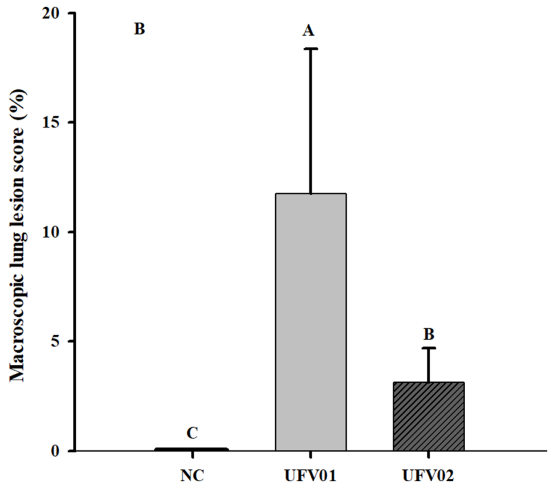

FIGURE 6
Bar graph on a scale of 0% (no lesions) to 100% (entire lung affected). *Different letters indicate significant differences detected in the Tukey's test ($p < 0.05$).

3.5 Cytokines

Cytokines IL-10, IFN-gamma, and TNF-alpha were investigated in serum samples using commercial kits. IFN-gamma was not detected in any of the animal sera at all time points, possibly indicating that its blood concentration was below the test's detection range. Regarding cytokine IL-10, as shown in Figure 10A, there was no significant increase or decrease throughout the experimental dynamics.

TNF-alpha remained higher in the UFV01 and UFV02 groups compared to the NC group at 0, 7, 14, and 21 dpi, but without reaching statistical significance. Only at 28 and 35 dpi did the UFV01 and UFV02 groups show statistically significant differences compared to the NC group (Figure 10B).

3.6 Differential diagnosis

All animals tested negative for Influenza A virus, *Streptococcus suis* and *Glaesserella parasuis*. The UFV01 and UFV02 groups showed 87.5% (7/8) positivity for *Mycoplasma hyorhinis*. As for *Actinobacillus pleuropneumoniae*, the UFV01 group exhibited 25% positivity (animals H and K; 2/8). All three groups tested 100% (8/8 and 4/4) positive for *Pasteurella multocida*.

4 Discussion

The comparative genomic analysis of two strains of *M. hyopneumoniae* and their distinct aspects related to virulence and pathogenicity can be better evaluated when associated with a series of biological processes and characteristics in clinical signs in swine. The UFV01 and UFV02 genomes, isolated in Brazil, had distinct characteristics related to their genomes even though they are genetically related to each other and to other genomes deposited in the NCBI database. The UFV01 strain had fewer annotated genes than strain UFV02, as well as other related yet distinct genetic traits such as nitrogen metabolism, nucleosides and nucleotides, and respiration. It also exclusively presented the *KpnF* gene related to the efflux pump, and had more exclusive genetic clusters (singletons) in its genome. Interestingly, and possibly associated with its genetic characteristics, a higher cough frequency was recorded in the UFV01 group than in the UFV02 group. It also induced more severe macroscopic lung lesions and exclusively presented pleuritis. In addition, seroconversions were higher for both IgG and IgA for UFV01 than for UFV02. On the other hand, TNF-alpha progressively increased for both strains during the post-infection measurements.

The genome analysis of the UFV01 and UFV02 isolates reported genetic features similar to those of other strains of *M. hyopneumoniae*. The predicted virulence factors *mhp385, mhp271, MHP_RS03455, p102, p97, p216, MHP_RS00555,* and *mhp107* have been found in other studies (Zhang et al., 1995; Minion et al., 2004; Seymour et al., 2011; Bogema et al., 2012; Deutscher et al., 2012; Siqueira et al., 2013, 2014; Raymond and Djordjevic, 2015; Kamminga et al., 2020; Leal Zimmer et al., 2020; Pan et al., 2022), with their functions described as adhesin mechanisms allowing the bacteria to establish in the host cell (Zhang et al., 1995; Woolley et al., 2012; Siqueira et al., 2014; Bustamante-Marin and Ostrowski, 2017). The ST-123 assigned to both isolates seems to be an uncommon typing in Brazil, being only reported by Balestrin et al. (2019), which described only two isolates classified as ST-123. Furthermore, the ST-123 strain seems to be evolutionarily close to the ST-124 strain, differing by three pair bases on the *rpoB* gene allele.

Overall, 58–60% of the internal content (CDS) of *M. hyopneumoniae* was classified, standing according with (Tavares et al., 2022). The protein characterized as hypothetical can be attributed to the research timeline, specifically the inherent difficulties in isolating and sequencing these specific bacteria. The first reports of the whole genome sequences of this genus were in 2004–2005 with the 232 (Minion et al., 2004), 7,448 and J strains (Vasconcelos et al., 2005), and thus far only 24 isolates have been reported. Even with new references updating or adding new information on some strains (Darby et al., 1999) the literature provides little information about the genome's features.

The UFV isolates presented the toxins *tlyC* (putative hemolysin), *PLDc_2* (PLD-like domain) and *hcnC* (hydrogen cyanide synthase HcnC). *PLDc_2* (PLD-like domain) was related to *Acinetobacter baumannii* and facilitates the invasion of the host cell (Stahl et al., 2015), and the toxin *hcnC* (hydrogen cyanide synthase) seems to be common in *Pseudomonas* spp., producing cyanide and acting lethally against Drosophila and nematodes (Darby et al., 1999; Broderick et al., 2008). The toxin *tlyC* was reported in other bacteria, such as *Rickettsia typhi* and *Leptospira*, showing no hemolytic action (Radulovic et al., 1999; Carvalho et al., 2009). However, *Brachyspira hyodysenteriae,* a bacterium related to enteric diseases in swine has the *tlyC* gene with hemolytic action (Joerling et al., 2020). In this case, the *tlyC* gene action of the UFV01 and UFV02 isolates needs more study to conclude on the hemolytic features. However, it is hypothesized that the isolates may have obtained the gene from *Brachyspira hyodysenteriae*, an organism of the digestive tract.

The only resistance gene was *KpnF* in UFV02. This gene belongs to the small multidrug resistance family (SMR) efflux pump-related genes, which show resistance to a broad range of drugs including a wide variety of antibiotics, antiseptics and disinfectants (Bay and Turner, 2009). This gene was first reported in *Klebsiella pneumoniae*, promoting antimicrobial resistance (Srinivasan and Rajamohan, 2013)

10.3389/fmicb.2023.1280588

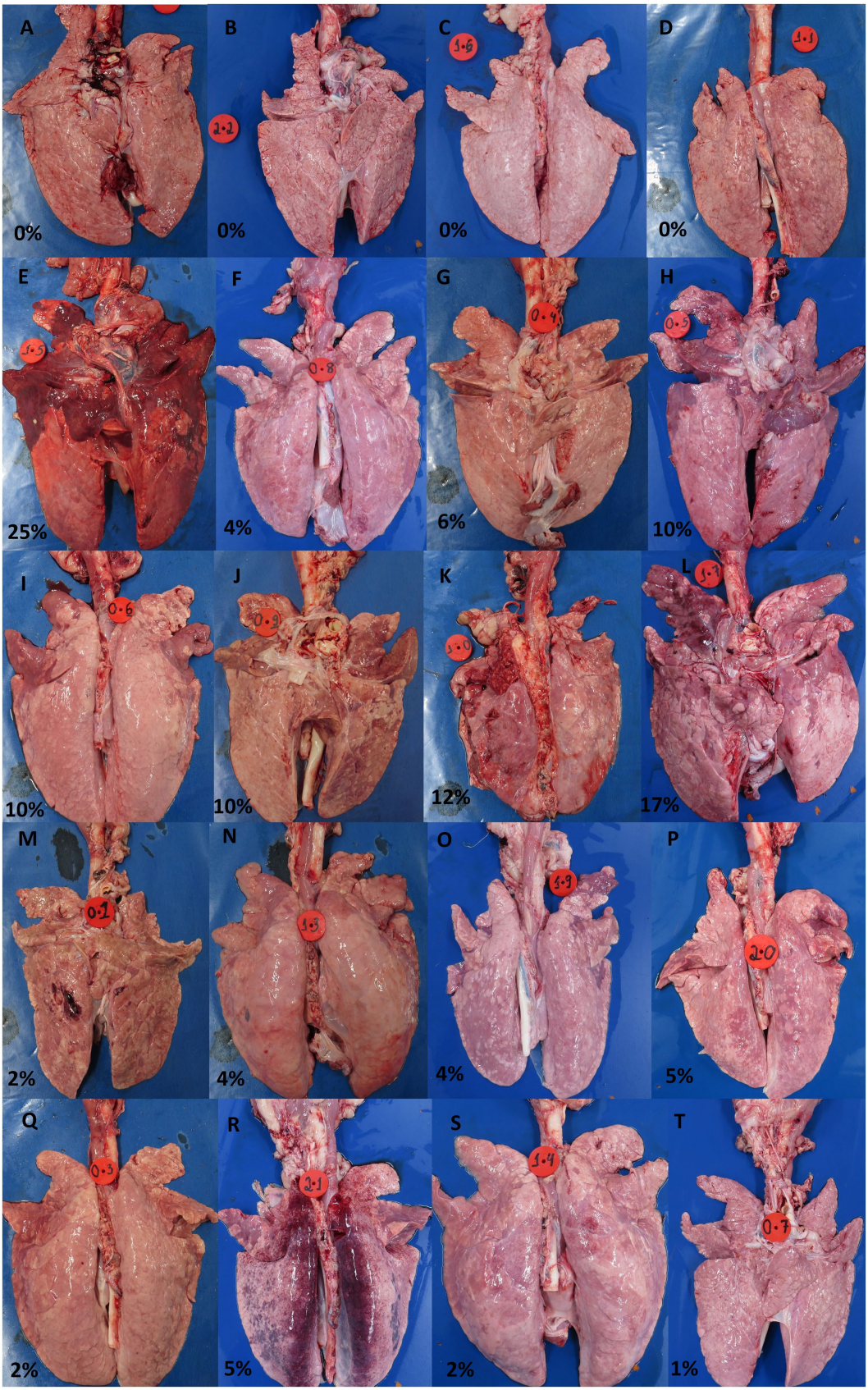

FIGURE 7
Individual photos of the lungs from the control group at 35 dpi **(A–D)**, lungs from the group inoculated with the UFV01 strain at 35 dpi **(E–L)**, and lungs from the UFV02 group at 35 dpi **(M–T)**.

10.3389/fmicb.2023.1280588

TABLE 1 Description of quantified microscopic lesions (bronchopneumonia, BALT hyperplasia, and pleuritis).

Grupo	Animal	Bronchopneumonia	BALT Hyperplasia	Pleuritis
NC	A	–	–	–
	B	–	–	–
	C	–	–	–
	D	–	–	–
Score average		0.00	0.00	0.00
UFV01	E	3	1	2
	F	1	1	-
	G	1	2	-
	H	1	2	1
	I	2	2	-
	J	2	1	-
	K	2	2	-
	L	1	1	1
Score average		1.62	1.5	0.5
UFV02	M	2	1	–
	N	1	2	–
	O	2	1	–
	P	2	1	–
	Q	1	1	–
	R	1	2	–
	S	1	1	–
	T	1	–	–
Score average		1.37	1.12	0.00

Absence of lesions (-), mild lesion (1), moderate lesion (2), and severe lesion (3).

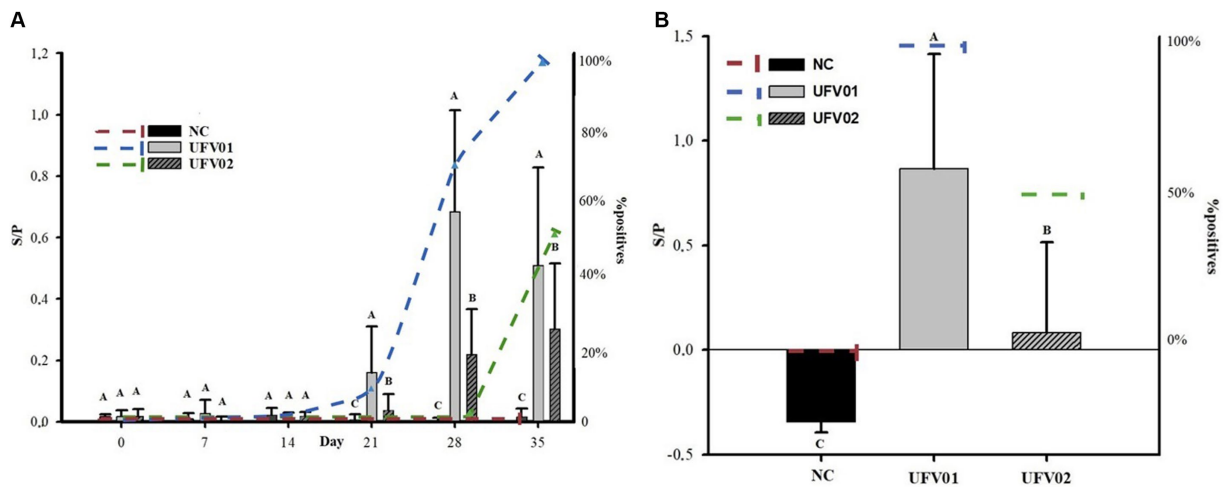

FIGURE 8
(A) Dynamics of IgG antibody detection and the number of positive animals during the experimental course of pigs inoculated with *Mycoplasma hyopneumoniae* using UFV01 and UFV02 isolates. **(B)** Dynamics of IgA antibody detection in BALF and the number of positive animals at 35 days after experimental inoculation with *Mycoplasma hyopneumoniae* using UFV01 and UFV02 isolates. Different letters indicate significant differences detected in the Tukey's test ($p < 0.05$). *The bars indicate antibody levels (S/P) and the dashed lines indicate the percentage (%) of positive animals.

and showing a large spectrum between the β-lactam family (Maurya et al., 2019). This gene was also reported in other *Enterobacteriaceae* such as *Salmonella* (Vilela et al., 2022), but never in *Mycoplasma*.

The genome comparison of the two isolates presented a similar size, with the UFV02 being larger than the others. In the BRIG analysis, the isolates of this study presented fewer gaps in comparison

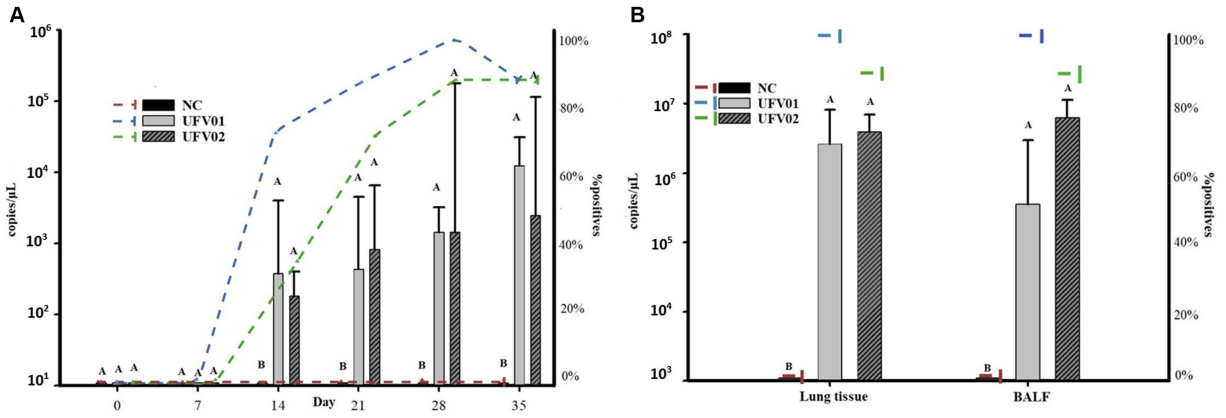

FIGURE 9
(A) Dynamics of the detection of *Mycoplasma hyopneumoniae* P102 gene fragment copies in laryngeal swabs and the number of pigs testing positive after experimental inoculation with the UFV01 and UFV02 isolates. **(B)** Dynamics of the detection of copies of the P102 gene fragment of *Mycoplasma hyopneumoniae* in BALF and lung tissue, and the number of experimentally inoculated pigs testing positive for the UFV01 and UFV02 isolates. Different letters indicate significant differences detected in Tukey's test ($p < 0.05$) for the number of *M. hyopneumoniae* copies. *Bars indicate the number of copies per microliter of DNA detected, and the dashed lines show the percentage (%) of positive animals.

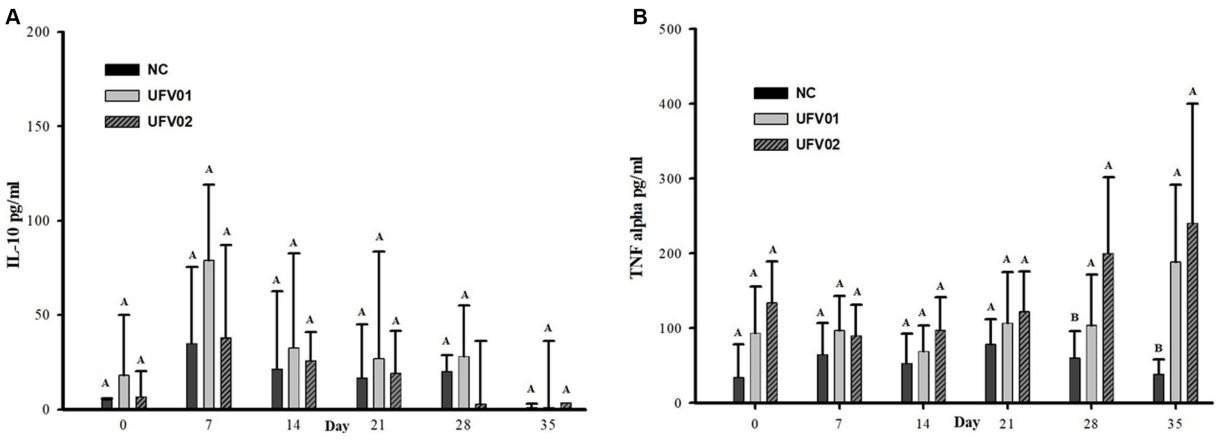

FIGURE 10
Dynamic graph of cytokine detection in the serum of swine experimentally inoculated with *Mycoplasma hyopneumoniae* with the UFV01 and UFV02 isolates. **(A)** IL-10 anti-inflammatory detections in pg./ml. **(B)** TNF-alpha proinflammatory cytokine detection in pg./mL. Different letters indicate a significant difference detected in the Tukey's test ($p < 0.05$).

to the other assemblies, and the pan-genome analysis revealed a robust relationship between the core-genome comparison, except for the TB1 strain. In the region of variable cluster number, UFV01 and UFV02 seem to have the most clusters and singletons, being able to provide more information and explain the phenotypical results observed in the UFV01. In addition, the orthogroup analysis (Figure 3) showed three specific groups belonging only to the UFV isolates and the total separation from the NCBI strains in the dendrogram comparison.

Interestingly, UFV01 and UFV02 showed few differences in the subsystems identified in their genomes, being these differences in the subsystem: Energy and Precursor Metabolites Generation, Protein Synthesis, RNA Processing and Stress Response, Defense and Virulence. Despite the low differences between UFV01 and UFV02, these alterations between the strains, which may corroborate the differences presented in the symptoms and characteristics of the lesions presented. This complex interplay between host and pathogen requires the adaptation of bacterial virulence secretion systems and the innate immune recognition of conserved bacterial molecules (Haraga et al., 2008). Second (Rohmer et al., 2011), under certain circumstances, the metabolic capabilities of a pathogen may undergo changes as a result of functional loss due to mutations, which can confer an advantage within a specific environment. Additionally, it is conceivable that the loss of non-essential metabolic functions could enhance virulence by reducing the metabolic demands on pathways.

The control group did not present clinical signs compatible with enzootic pneumonia. The UFV01 group presented a numerically higher frequency of variation compared to the UFV02 group (Figure 5A). All three groups tested statistically differed from each other using the non-parametric Wilcoxon test $p < 0.001$ (Figure 5B). Garcia-Morante et al. (2022) highlight that the onset of coughing in experimentally infected pigs can be variable and

intermittent, occurring between 1 and 3 weeks after infection. The immunopathological and environmental mechanisms leading to the formation of macroscopic lesions and, consequently, the manifestations of clinical disease are multifactorial. However, in experimental infections with virulent strains, it is described that the peak of the macroscopic lesion occurs at 28 dpi and decreases over time, eventually forming scar tissue (Vicca et al., 2003; Redondo et al., 2009; Garcia-Morante et al., 2017, 2022).

The group inoculated with the UFV01 strain exhibited 11.75% (+6.60) of lungs affected by lesions, the group inoculated with the UFV02 strain showed 3.125% (+1.55), and the negative control group showed 0% lesions at 35 dpi. The three groups differed statistically from each other. Almeida et al. (2020), in an experimental infection using the 232 strain (United States), found that the mean lesion area obtained in the lungs of animals at 28 dpi was 15.84%; this strain is considered to be highly virulent according to several studies (Leal Zimmer et al., 2020; Wu et al., 2022). Vicca et al. (2003), when comparing different isolates in an experimental infection, classified them as high, medium, and low pathogenicity, with the high virulence strains presenting an extent of the lesions in the lungs of inoculated pigs between 13.5% (±7.3) and 15.8% (±7.4), while the low pathogenicity isolates showed this indicator to be between 1.7 (±2.3) and 5.1 (±4.8). Therefore, analyzing the results and parameters from Almeida et al. (2020) and Vicca et al. (2003), the UFV01 isolate demonstrates the ability to cause a higher degree of macroscopic lung lesions than the UFV02 strain. Considering the parameters indicated in the aforementioned works, the UFV01 isolate presented high/medium virulence, while the UFV02 strain exhibited low pathogenicity.

As for the microscopic lesion scoring, the NC group did not present any type of lesion. The UFV01 and UFV02 groups showed bronchopneumonia and BALT, but with different frequencies. Additionally, only the UFV01 group presented cases of pleurisy, indicating secondary involvement. The UFV01 group showed 25% positivity for *Actinobacillus pleuropneumoniae*, 87.5% positivity for *Mycoplasma hyorhinis*, and 100% positivity for *Pasteurella multocida*. In contrast, the UFV02 group was positive for only *Mycoplasma hyorhinis* and *Pasteurella multocida*, without presenting cases of pleurisy. Positive animals for *Actinobacillus pleuropneumoniae* (H and K) in their lungs can be observed in Figure 6. During necropsy in both animals, pleural adhesions to the thoracic cavity can be observed, with more pronounced adhesion in animal K. Some Brazilian studies, such as Baraldi et al. (2019), Galdeano et al. (2019), and Petri et al. (2023), report a high prevalence of this agent in Brazilian production and its close association with *M. hyopneumoniae.* The presence of the *Actinobacillus pleuropneumoniae* together with *M. hyopneumoniae* tends to worsen bronchopneumonia lesions bronchopneumonia. The secondary involvement evidenced by the cases of pleurisy in the UFV01 group potentially occurred due to the fact that this isolate stimulated a higher degree of lesions, opening the door to secondary respiratory agents.

The mean scores of the microscopic lesions in the UFV01 group were 1.62 (bronchopneumonia), 1.5 (BALT hyperplasia) and 0.5 (pleuritis). The UFV02 group showed mean scores of 1.37 (bronchopneumonia), 1.12 (BALT hyperplasia) and 0.0 (pleuritis). Lymphocytic recruitment and its mitotic capacity in lung tissue leads to the described lesion known as BALT hyperplasia (Messier and Ross, 1991), which is considered a typical lesion caused by *M. hyopneumoniae*. On the other hand, bronchopneumonia and pleuritis lesions result from secondary bacterial involvement, including agents such as *Pasteurella multocida*, *Actinobacillus pleuropneumoniae*, *Streptococcus suis* and *Glaesserella parasuis* (De Conti et al., 2021).

Another important point evaluated was the seroconversion of animals through the enzyme-linked immunosorbent assay (ELISA). After the challenge, *M. hyopneumoniae* colonizes the respiratory tract and stimulates humoral immune responses, resulting in the production of IgG and IgA antibodies (Ding et al., 2021). In the study, seroconversion was not uniform. The UFV01 group started seroconversion at 21 dpi and achieved complete seroconversion at 35 dpi (100%), while the UFV02 group had only 50% seroconversion at 35 dpi. This result indicates that the host's immune response against the UFV01 isolate was greater than against the UFV02 isolate, consequently leading to a more pronounced adaptive immune response to *M. hyopneumoniae*. From 21 dpi onwards, the UFV01 group showed statistically significant differences in antibody levels compared to the other groups (Figure 6A). In a study evaluating the seroconversion dynamics of animals challenged with the 232 strain (United States), seroconversion was found to start at 14 dpi, with the peak occurring at 35 dpi (Almeida et al., 2020).

Humoral responses after experimental infection show that specific serum IgG antibodies against *M. hyopneumoniae* are detected 3 to 4 weeks post-infection, reach their peak after 11 to 12 weeks, and then gradually decrease (Kobisch et al., 1993). After a booster infection, serum antibody titers clearly increase and then slowly decrease again (Kobisch et al., 1993). Interestingly, pigs infected with a highly virulent strain seem to seroconvert earlier than those infected with a low virulence strain (Meyns et al., 2004; Villarreal et al., 2011). This fact is confirmed when considering classifying the UFV01 isolate as high or medium virulence and the UFV02 isolate as low virulence, following the classification adopted by Vicca et al. (2003), as the seroconversion in the UFV01 group was higher and earlier compared to the UFV02 group.

IgA plays an important role in mucosal immunity against infectious pathogens. However, the molecular mechanism of IgA secretion in response to infection remains largely unknown, particularly in *Mycoplasma* spp. (Li et al., 2020). We assessed the level of IgA antibodies in the groups from BALF using a standardized method Mechler-dreibi et al. (2021), finding that 100% (8/8) of the animals in the UFV01 group tested positive for IgA detection, compared to only 50% (4/8) of the UFV02 group. The animals positive for serum IgG at 35 dpi were the same pigs that tested positive for IgA in BALF at 35 dpi (Figure 6B). It is believed that *M. hyopneumoniae* induces intense immune responses in mucosa, and long-lasting IgA may provide indispensable local immune protection for the against organism. However, few studies have examined the molecular mechanism by which *M. hyopneumoniae* promotes such strong mucosal immunity characterized by increased IgA levels (Li et al., 2020). The main strategy of respiratory tract mucosal immunity is forming a protective barrier to eliminate invasive respiratory pathogens and prevent active infection and colonization (Mechler-Dreibi et al., 2021). The ability of *M. hyopneumoniae* to adhere and multiply in the porcine respiratory epithelium is dependent on a complex set of adhesins and immunomodulatory strategies that allow *M. hyopneumoniae* to establish itself in the respiratory tract for long periods (Leal Zimmer et al., 2020).

The estimated bacterial quantification in the laryngeal swab increased over time (Figure 7A), although no statistical difference was detected between the UFV01 and UFV02 groups. Animals inoculated with the UFV01 strain showed environmental shedding of the bacteria, as 75% of the animals (6/8) tested positive in the qPCR of nasal swabs at 14 dpi, while the group inoculated with the UFV02 strain showed a detection rate of 37.5% (3/8) at 14 dpi (Figure 7A, Supplementary material S3). The qPCR analyzes for BALF and tissue in the UFV01 group showed 100% (8/8) positivity, while the UFV02 group showed 87.5% positivity (7/8). There was no statistical difference in bacterial load between the groups (Figure 7B; Supplementary material S3).

The production of pro-inflammatory cytokines has been associated with the development of characteristic lesions of EP (Muneta et al., 2008; Okamba et al., 2010; Jorge et al., 2014). TNF-alpha differed statistically between the groups at 28 and 35 dpi, with the animals inoculated with the UFV01 and UFV02 strains showed an increasing trend in this cytokine throughout the experimental period (Figure 8B). TNF-α is an important pro-inflammatory cytokine involved in the secretion of acute-phase proteins and is frequently detected in pigs infected with *M. hyopneumoniae* (Fourour et al., 2019). The consensus among the studies that have analyzed this cytokine is that it plays a role in the accumulation of inflammatory cells in lung tissue, contributing to lesion formation, although the exact timing of its peak expression and decrease has not yet been fully elucidated (Choi et al., 2006; Lorenzo et al., 2006; Redondo et al., 2009; Almeida et al., 2020).

Therefore, UFV01 and UFV02 presented genetic orthology characteristics that differ from the other sequences deposited in international banks, in terms of different ortho groups and similar phylogenomics. In contrast, the functional annotations demonstrate that the two strains are genetically different, as demonstrated in the symptoms presented by the animals. However, the limitations on understanding genetic functions as a whole require further studies. Two important points can be observed between the groups. In the UFV01 group, the animal with the highest degree of lung involvement died. Hence, this group had a mortality rate of 12.5%. On the other hand, the UFV02 group had an animal that, despite being inoculated similarly to the others, did not develop EP and tested negative for the agent throughout the study. Both pieces of information support the presence of differences in virulence between the groups, with UFV01 being more pathogenic. Despite the data presented in our study, further research is needed to deepen our understanding of the genetic differences and their phenotypic presentations.

The UFV01 and UFV02 strains are capable of producing clinical disease. After a thorough analysis of the discussed data, it is possible to infer that the UFV01 strain represents a more pathogenic isolate compared to the UFV02 strain. However, further studies are necessary to elucidate the genetic differences and their phenotypic presentations. New research can stem from our findings, such as the development of vaccines, antimicrobial assessments, diagnostic kits and improvements in control protocols.

Data availability statement

The datasets presented in this study can be found in online repositories. The names of the repository/repositories and accession number(s) can be found in the article/Supplementary material.

Ethics statement

The animal study was approved by Committee on Ethics in the Use of Animals (CEUA). The study was conducted in accordance with the local legislation and institutional requirements.

Author contributions

LT: Writing – original draft, Writing – review & editing, Data curation, Investigation. LS: Investigation, Writing – original draft, Conceptualization, Methodology, Validation. CP: Conceptualization, Methodology, Formal analysis, Writing – original draft, Writing – review & editing. RP: Formal analysis, Methodology, Writing – original draft, Data curation, Writing – review & editing. GB: Methodology, Conceptualization, Resources, Writing – original draft. RY: Methodology, Data curation, Formal analysis, Writing – original draft. KJ: Data curation, Formal analysis, Methodology, Writing – review & editing. FM: Formal analysis, Methodology, Investigation, Writing – review & editing. CD: Formal analysis, Methodology, Writing – original draft. VC: Formal analysis, Methodology, Validation, Writing – original draft. CM: Formal analysis, Methodology, Data curation, Writing – original draft. FP: Formal analysis, Methodology, Writing – original draft. LO: Methodology, Conceptualization, Data curation, Supervision, Writing – original draft. MM: Conceptualization, Supervision, Writing – original draft. AS-J: Conceptualization, Supervision, Writing – original draft, Funding acquisition, Methodology, Project administration, Resources, Writing – review & editing.

Funding

The author(s) declare financial support was received for the research, authorship, and/or publication of this article. This work was supported by Brazilian agencies: Minas Gerais State Agency for Research and Development (FAPEMIG, grant #APQ-01327-14), National Council for Scientific and Technological Development (CNPq, grant #304727/2016-4), Coordination for the Improvement of Higher Education Personnel (CAPES, grant #Finance code 001) and Foundation for Research Support of the State Alagoas (FAPEAL, grant # APQ2022021000101).

Acknowledgments

We would like to thank Agroceres PIC, represented by Veterinary Doctor Ms. Gustavo Simão, for providing the animals used in this study. The MICROVET helped in conducting the necessary analyzes for the research. We are thankful to researcher Natalia Fialho Gonzaga for her valuable contribution to the development of the research. Special thanks to Lukiya Silva Campos Favarato for her assistance in the anesthetic protocol and to Diogo Ribeiro Câmara for performing the statistical analyses.

Conflict of interest

The authors declare that the research was conducted in the absence of any commercial or financial relationships that could be construed as a potential conflict of interest.

The author(s) declared that they were an editorial board member of Frontiers, at the time of submission. This had no impact on the peer review process and the final decision.

Publisher's note

All claims expressed in this article are solely those of the authors and do not necessarily represent those of their affiliated organizations, or those of the publisher, the editors and the reviewers. Any product that may be evaluated in this article, or claim that may be made by its manufacturer, is not guaranteed or endorsed by the publisher.

Supplementary material

The Supplementary material for this article can be found online at: https://www.frontiersin.org/articles/10.3389/fmicb.2023.1280588/full#supplementary-material

References

Alikhan, N. F., Petty, N. K., Ben Zakour, N. L., and Beatson, S. A. (2011). BLAST ring image generator (BRIG): simple prokaryote genome comparisons. *BMC Genomics* 12, 1–10. doi: 10.1186/1471-2164-12-402

Almeida, H. M. S., Mechler-Dreibi, M. L., Sonálio, K., Ferraz, M. E. S., Storino, G. Y., Barbosa, F. O., et al. (2020). Cytokine expression and *Mycoplasma hyopneumoniae* burden in the development of lung lesions in experimentally inoculated pigs. *Vet. Microbiol.* 244:108647. doi: 10.1016/j.vetmic.2020.108647

Andrade, M. R., Daniel, A. G. S., Zarate, J. B., Sato, J. P. H., Santos, L. F., and Guedes, R. M. C. (2023). Genetic diversity of *Mycoplasma hyopneumoniae* in finishing pigs in Minas Gerais. *Pesqui. Vet. Bras.* 43, 1–11. doi: 10.1590/1678-5150-PVB-7155

Andrews, S. (2017). *FastQC: A quality control tool for high throughput sequence data*, 2010.

Assao, V. S., Scatamburlo, T. M., Araujo, E. N., Santos, M. R., Pereira, C. E. R., Guedes, R. M. C., et al. (2019). Correction to: genetic variation of *Mycoplasma hyopneumoniae* from Brazilian field samples. *BMC Microbiol.* 19, 258–212. doi: 10.1186/s12866-019-1637-x

Bai, F., Ni, B., Liu, M., Feng, Z., Xiong, Q., Xiao, S., et al. (2013). *Mycoplasma hyopneumoniae* derived lipid-associated membrane proteins induce apoptosis in porcine alveolar macrophage via increasing nitric oxide production, oxidative stress, and caspase-3 activation. *Vet. Immunol. Immunopathol.* 155, 155–161. doi: 10.1016/j.vetimm.2013.07.004

Balestrin, E., Kuhnert, P., Wolf, J. M., Wolf, L. M., Fonseca, A. S. K., Ikuta, N., et al. (2019). Clonality of *Mycoplasma hyopneumoniae* in swine farms from Brazil. *Vet. Microbiol.* 238:108434. doi: 10.1016/j.vetmic.2019.108434

Baraldi, T. G., Cruz, N. R. N., Pereira, D. A., Galdeano, J. V. B., Gatto, I. R. H., Silva, A. F. D., et al. (2019). Antibodies against *Actinobacillus pleuropneumoniae*, *Mycoplasma hyopneumoniae*, and influenza virus and their relationships with risk factors, clinical signs, and lung lesions in pig farms with one-site production systems in Brazil. *Prev. Vet. Med.* 171:104748. doi: 10.1016/j.prevetmed.2019.104748

Bay, D. C., and Turner, R. J. (2009). Diversity and evolution of the small multidrug resistance protein family. *BMC Evol. Biol.* 9, 140–113. doi: 10.1186/1471-2148-9-140

Beuckelaere, L., Haspeslagh, M., Biebaut, E., Boyen, F., Haesebrouck, F., Krejci, R., et al. (2022). Different local, innate and adaptive immune responses are induced by two commercial *Mycoplasma hyopneumoniae* bacterins and an adjuvant alone. *Front. Immunol.* 13, 1–16. doi: 10.3389/fimmu.2022.1015525

Bogema, D. R., Deutscher, A. T., Woolley, L. K., Seymour, L. M., Raymond, B. B. A., Tacchi, J. L., et al. (2012). Characterization of cleavage events in the multifunctional cilium adhesin Mhp684 (P146) reveals a mechanism by which *Mycoplasma hyopneumoniae* regulates surface topography. *MBio* 3, e00282–e00211. doi: 10.1128/mBio.00282-11

Bolger, A. M., Lohse, M., and Usadel, B. (2014). Trimmomatic: A flexible trimmer for Illumina sequence data. *Bioinformatics* 30, 2114–2120. doi: 10.1093/bioinformatics/btu170

Bonifait, L., Veillette, M., Létourneau, V., Grenier, D., and Duchaine, C. (2014). Detection of *Streptococcus suis* in bioaerosols of swine confinement buildings. *Appl. Environ. Microbiol.* 80, 3296–3304. doi: 10.1128/AEM.04167-13

Broderick, K. E., Chan, A., Balasubramanian, M., Feala, J., Reed, S. L., Panda, M., et al. (2008). Cyanide produced by human isolates of *Pseudomonas aeruginosa* contributes to lethality in *Drosophila melanogaster*. *J. Infect. Dis.* 197, 457–464. doi: 10.1086/525282

Bustamante-Marin, X. M., and Ostrowski, L. E. (2017). Cilia and mucociliary clearance. *Cold Spring Harb. Perspect. Biol.* 9:a028241. doi: 10.1101/cshperspect.a028241

Calus, D., Maes, D., Jannes, G., De Kruif, A., and Butaye, P. (2010). Validation of ATP luminometry for rapid and accurate titration of *Mycoplasma hyopneumoniae* in Friis medium and a comparison with the color changing units assay. *J. Microbiol. Methods* 83, 335–340. doi: 10.1016/j.mimet.2010.09.005

Carvalho, E., Barbosa, A. S., Gómez, R. M., Cianciarullo, A. M., Hauk, P., Abreu, P. A., et al. (2009). Leptospiral TlyC is an extracellular matrix-binding protein and does not present hemolysin activity. *FEBS Lett.* 583, 1381–1385. doi: 10.1016/J.FEBSLET.2009.03.050

Chevreux, B., Pfisterer, T., Drescher, B., Driesel, A. J., Müller, W. E. G., Wetter, T., et al. (2004). Using the miraEST assembler for reliable and automated mRNA transcript assembly and SNP detection in sequenced ESTs. *Genome Res.* 14, 1147–1159. doi: 10.1101/gr.1917404

Choi, C., Kwon, D., Jung, K., Ha, Y., Lee, Y. H., Kim, O., et al. (2006). Expression of inflammatory cytokines in pigs experimentally infected with *Mycoplasma hyopneumoniae*. *J. Comp. Pathol.* 134, 40–46. doi: 10.1016/j.jcpa.2005.06.009

Cook, B. S., Beddow, J. G., Manso-Silván, L., Maglennon, G. A., and Rycroft, A. N. (2016). Selective medium for culture of *Mycoplasma hyopneumoniae*. *Vet. Microbiol.* 195, 158–164. doi: 10.1016/j.vetmic.2016.09.022

Darby, C., Cosma, C. L., Thomas, J. H., and Manoil, C. (1999). Lethal paralysis of *Caenorhabditis elegans* by *Pseudomonas aeruginosa*. *Proc. Natl. Acad. Sci. U. S. A.* 96, 15202–15207. doi: 10.1073/PNAS.96.26.15202

De Conti, E. R., Takeuti, K. L., Schwertz, C. I., Bianchi, R. M., Driemeier, D., and de Barcellos, D. E. S. N. (2021). Agents of pneumonia in slaughtered pigs in southern Brazil. *Pesq. Vet. Bras* 41:e06669. doi: 10.1590/1678-5150-PVB-6669

de Nies, L., Lopes, S., Busi, S. B., Galata, V., Heintz-Buschart, A., Laczny, C. C., et al. (2021). PathoFact: a pipeline for the prediction of virulence factors and antimicrobial resistance genes in metagenomic data. *Microbiome* 9, 49–14. doi: 10.1186/S40168-020-00993-9

Deeney, A. S., Maglennon, G. A., Chapat, L., Crussard, S., Jolivet, E., and Rycroft, A. N. (2019). *Mycoplasma hyopneumoniae* evades phagocytic uptake by porcine alveolar macrophages in vitro. *Vet. Res.* 50, 51–15. doi: 10.1186/s13567-019-0667-6

Delmont, T. O., and Eren, E. M. (2018). Linking pangenomes and metagenomes: the Prochlorococcus metapangenome. *PeerJ* 6:e4320. doi: 10.7717/PEERJ.4320

Deutscher, A. T., Tacchi, J. L., Minion, F. C., Padula, M. P., Crossett, B., Bogema, D. R., et al. (2012). *Mycoplasma hyopneumoniae* surface proteins Mhp385 and Mhp384 bind host cilia and Glycosaminoglycans and are Endoproteolytically processed by proteases that recognize different cleavage motifs. *J. Proteome Res.* 11, 1924–1936. doi: 10.1021/pr200916a

Ding, H., Wen, Y., Xu, Z., Zhou, B., Tlili, C., Tian, Y., et al. (2021). Development of an ELISA for distinguishing convalescent sera with *Mycoplasma hyopneumoniae* infection from hyperimmune sera responses to bacterin vaccination in pigs. *Vet. Med. Sci* 7, 1831–1840. doi: 10.1002/vms3.539

dos Santos, L. F., Sreevatsan, S., Torremorell, M., Moreira, M. A. S., Sibila, M., and Pieters, M. (2015). Genotype distribution of *Mycoplasma hyopneumoniae* in swine herds from different geographical regions. *Vet. Microbiol.* 175, 374–381. doi: 10.1016/j.vetmic.2014.11.018

Emms, D. M., and Kelly, S. (2019). OrthoFinder: phylogenetic orthology inference for comparative genomics. *Genome Biol.* 20:238. doi: 10.1186/s13059-019-1832-y

Eren, A. M., Kiefl, E., Shaiber, A., Veseli, I., Miller, S. E., Schechter, M. S., et al. (2020). Community-led, integrated, reproducible multi-omics with anvi'o. *Nat. Microbiol.* 6, 3–6. doi: 10.1038/s41564-020-00834-3

Felde, O., Kreizinger, Z., Sulyok, K. M., Hrivnák, V., Kiss, K., Jerzsele, Á., et al. (2018). Antibiotic susceptibility testing of *Mycoplasma hyopneumoniae* field isolates from Central Europe for fifteen antibiotics by microbroth dilution method. *PLoS One* 13:e0209030. doi: 10.1371/journal.pone.0209030

Fouchier, R. A. M., Bestebroer, T. M., Herfst, S., Van der Kemp, L., Rimmelzwaan, G. F., and Osterhaus, A. D. M. E. (2000). Detection of influenza a viruses from different species by PCR amplification of conserved sequences in the matrix gene. *J. Clin. Microbiol.* 38, 4096–4101. doi: 10.1128/jcm.38.11.4096-4101.2000

Fourour, S., Fablet, C., Tocqueville, V., Dorenlor, V., Eono, F., Eveno, E., et al. (2018). A new multiplex real-time TaqMan® PCR for quantification of *Mycoplasma hyopneumoniae*, *M. Hyorhinis*, and *M. flocculare*: exploratory epidemiological investigations to research mycoplasmal association in enzootic pneumonia-like lesions in slaughtered pigs. *J. Appl. Microbiol* 125, 345–355. doi: 10.1111/jam.13770

Fourour, S., Marois-Créhan, C., Martelet, L., Fablet, C., Kempf, I., Gottschalk, M., et al. (2019). Intra-species and inter-species differences in cytokine production by porcine antigen-presenting cells stimulated by *Mycoplasma Hyopneumoniae*, *M. Hyorhinis*, and *M. flocculare*. *Pathogens* 8:34. doi: 10.3390/pathogens8010034

Galdeano, J. V. B., Baraldi, T. G., Ferraz, M. E. S., De Souza Almeida, H. M., Mechler-Dreibi, M. L., Costa, W. M. T., et al. (2019). Cross-sectional study of seropositivity, lung lesions, and associated risk factors of the main pathogens of porcine respiratory diseases complex (PRDC) in Goiás, Brazil. *Porc. Health Manag.* 5, 23–10. doi: 10.1186/s40813-019-0130-0

Garcia-Morante, B., Maes, D., Sibila, M., Betlach, A. M., Sponheim, A., Canturri, A., et al. (2022). Improving *Mycoplasma hyopneumoniae* diagnostic capabilities by harnessing the infection dynamics. *Vet. J.* 288:105877. doi: 10.1016/j.tvjl.2022.105877

Garcia-Morante, B., Segalés, J., Fraile, L., Llardén, G., Coll, T., and Sibila, M. (2017). Potential use of local and systemic humoral immune response parameters to forecast *Mycoplasma hyopneumoniae* associated lung lesions. *PLoS One* 12, e0175034–e0175014. doi: 10.1371/journal.pone.0175034

Goecke, N. B., Hjulsager, C. K., Krog, J. S., Skovgaard, K., and Larsen, L. E. (2020). Development of a high-throughput real-time PCR system for detection of enzootic pathogens in pigs. *J. Vet. Diagn. Investig.* 32, 51–64. doi: 10.1177/1040638719890863

Gonzaga, N. F., Souza, L. F. L., Santos, M. R., Assao, V. S., Rycroft, A., Deeney, A. S., et al. (2019). Antimicrobial susceptibility and genetic profile of *Mycoplasma hyopneumoniae* isolates from Brazil. *Braz. J. Microbiol.* 51, 377–384. doi: 10.1007/s42770-019-00185-0

Gurevich, A., Saveliev, V., Vyahhi, N., and Tesler, G. (2013). QUAST: quality assessment tool for genome assemblies. *Bioinformatics* 29, 1072–1075. doi: 10.1093/bioinformatics/btt086

Han, J., Park, B. S., Shin, D. J., Song, S. Y., Jeong, Y. J., and Lee, N. (2017). Complete genome sequence of *Mycoplasma hyopneumoniae* strain KM014, a clinical isolate from South Korea. *Genome Announc.* 5, 16–17. doi: 10.1128/genomeA.01012-17

Han, Q., Wang, J., Li, R., Han, Q., Yuan, W., and Wang, J. (2020). Development of a recombinase polymerase amplification assay for rapid detection of *Haemophilus parasuis* in tissue samples. *Vet. Med. Sci.* 6, 894–900. doi: 10.1002/vms3.287

Hansen, M. S., Pors, S. E., Jensen, H. E., Bille-Hansen, V., Bisgaard, M., Flachs, E. M., et al. (2010). An investigation of the pathology and pathogens associated with porcine respiratory disease complex in Denmark. *J. Comp. Pathol.* 143, 120–131. doi: 10.1016/j.jcpa.2010.01.012

Haraga, A., Ohlson, M. B., and Miller, S. I. (2008). Salmonellae interplay with host cells. *Nat. Rev. Microbiol.* 6, 53–66. doi: 10.1038/nrmicro1788

Joerling, J., Willems, H., Ewers, C., and Herbst, W. (2020). Differential expression of hemolysin genes in weakly and strongly hemolytic *Brachyspira hyodysenteriae* strains. *BMC Vet. Res.* 16:169. doi: 10.1186/S12917-020-02385-5

Jolley, K. A., Bray, J. E., and Maiden, M. C. J. (2018). Open-access bacterial population genomics: BIGSdb software, the PubMLST.org website and their applications. *Wellcome Open Res.* 3:124. doi: 10.12688/WELLCOMEOPENRES.14826.1

Jorge, S., de Oliveira, N. R., Marchioro, S. B., Fisch, A., Gomes, C. K., Hartleben, C. P., et al. (2014). The *Mycoplasma hyopneumoniae* recombinant heat shock protein P42 induces an immune response in pigs under field conditions. *Comp. Immunol. Microbiol. Infect. Dis.* 37, 229–236. doi: 10.1016/j.cimid.2014.07.001

Kamminga, T., Benis, N., Martins dos Santos, V., Bijlsma, J. J. E., and Schaap, P. J. (2020). Combined transcriptome sequencing of *Mycoplasma hyopneumoniae* and infected pig lung tissue reveals up-regulation of bacterial F1-like ATPase and Down-regulation of the P102 cilium Adhesin in vivo. *Front. Microbiol.* 11, 1–14. doi: 10.3389/fmicb.2020.01679

Kamminga, T., Slagman, S. J., Bijlsma, J. J. E., Martins dos Santos, V. A. P., Suarez-Diez, M., and Schaap, P. J. (2017). Metabolic modeling of energy balances in *Mycoplasma hyopneumoniae* shows that pyruvate addition increases growth rate. *Biotechnol. Bioeng.* 114, 2339–2347. doi: 10.1002/bit.26347

Kobisch, M., and Friis, N. F. (1996). Swine mycoplasmoses. *Off. Int. Epizoot.* 15, 1569–1605. doi: 10.20506/rst.15.4.983

Kobisch, M., Gottschalk, M., Lévesque, G., Denicourt, M., and Messier, S. (1993). *Mycoplasma hyopneumoniae* infection in pigs: duration of the disease and resistance to reinfection. *Vet. Res.* 24, 67–77.

Kuhnert, P., and Overesch, G. (2014). Molecular epidemiology of *Mycoplasma hyopneumoniae* from outbreaks of enzootic pneumonia in domestic pig and the role of wild boar. *Vet. Microbiol.* 174, 261–266. doi: 10.1016/j.vetmic.2014.08.022

Kuramae-Izioka, E. E. (1997). A rapid, easy and high yield protocol for total genomic DNA isolation from *Colletotrichum gloeosporioides* and *fusarium oxysporum* for RAPD. *Revista. Unimar.* 19, 683–689.

Leal Zimmer, F. M. A., Paes, J. A., Zaha, A., and Ferreira, H. B. (2020). Pathogenicity & virulence of *Mycoplasma hyopneumoniae*. *Virulence* 11, 1600–1622. doi: 10.1080/21505594.2020.1842659

Li, X., Zhang, Y., Yin, B., Liang, J., Jiang, F., and Wu, W. (2020). Toll-like receptor 2 (TLR2) and TLR4 mediate the IgA immune response induced by *Mycoplasma hyopneumoniae*. *Infect. Immun.* 88, e00697–e00619. doi: 10.1128/IAI.00697-19

Liu, W., Feng, Z., Fang, L., Zhou, Z., Li, Q., Li, S., et al. (2011). Complete genome sequence of *Mycoplasma hyopneumoniae* strain 168. *J. Bacteriol.* 193, 1016–1017. doi: 10.1128/JB.01305-10

Lorenzo, H., Quesada, Ó., Assunção, P., Castro, A., and Rodríguez, F. (2006). Cytokine expression in porcine lungs experimentally infected with *Mycoplasma hyopneumoniae*. *Vet. Immunol. Immunopathol.* 109, 199–207. doi: 10.1016/j.vetimm.2005.07.021

Maes, D., Segales, J., Meyns, T., Sibila, M., Pieters, M., and Haesebrouck, F. (2008). Control of *Mycoplasma hyopneumoniae* infections in pigs. *Vet. Microbiol.* 126, 297–309. doi: 10.1016/j.vetmic.2007.09.008

Maes, D., Sibila, M., Kuhnert, P., Segalés, J., Haesebrouck, F., and Pieters, M. (2017). Update on *Mycoplasma hyopneumoniae* infections in pigs: knowledge gaps for improved disease control. *Transbound. Emerg. Dis.* 65 Suppl 1, 110–124. doi: 10.1111/tbed.12677

Maurya, N., Jangra, M., Tambat, R., and Nandanwar, H. (2019). Alliance of efflux pumps with β-lactamases in multidrug-resistant *Klebsiella pneumoniae* isolates. *Microb. Drug Resist.* 25, 1155–1163. doi: 10.1089/MDR.2018.0414

McArthur, A. G., Waglechner, N., Nizam, F., Yan, A., Azad, M. A., Baylay, A. J., et al. (2013). The comprehensive antibiotic resistance database. Antimicrob. *Agents Chemother.* 57, 3348–3357. doi: 10.1128/AAC.00419-13

Mechler-Dreibi, M. L., Almeida, H. M. S., Sonalio, K., Martines, M. A. C., Petri, F. A. M., Zambotti, B. B., et al. (2021). Oral vaccination of piglets against *Mycoplasma hyopneumoniae* using silica SBA-15 as an adjuvant effectively reduced consolidation lung lesions at slaughter. *Sci. Rep.* 11, 22377–22315. doi: 10.1038/s41598-021-01883-2

Messier, S., and Ross, R. F. (1991). Interactions of *Mycoplasma hyopneumoniae* with porcine lymphocytes. *Am. J. Vet. Res.* 52, 1497–1502.

Meyns, T., Maes, D., Calus, D., Ribbens, S., Dewulf, J., Chiers, K., et al. (2007). Interactions of highly and low virulent *Mycoplasma hyopneumoniae* isolates with the respiratory tract of pigs. *Vet. Microbiol.* 120, 87–95. doi: 10.1016/j.vetmic.2006.10.010

Meyns, T., Maes, D., Dewulf, J., Vicca, J., Haesebrouck, F., and de Kruif, A. (2004). Quantification of the spread of *Mycoplasma hyopneumoniae* in nursery pigs using transmission experiments. *Prev. Vet. Med.* 66, 265–275. doi: 10.1016/j.prevetmed.2004.10.001

Minion, F. C., Lefkowitz, E. J., Madsen, M. L., Cleary, B. J., Swartzell, S. M., and Mahairas, G. G. (2004). The genome sequence of *Mycoplasma hyopneumoniae* strain 232, the agent of swine mycoplasmosis. *J. Bacteriol.* 186, 7123–7133. doi: 10.1128/JB.186.21.7123-7133.2004

Muneta, Y., Minagawa, Y., Shimoji, Y., Ogawa, Y., Hikono, H., and Mori, Y. (2008). Immune response of gnotobiotic piglets against *Mycoplasma hyopneumoniae*. *J. Vet. Med. Sci.* 70, 1065–1070. doi: 10.1292/jvms.70.1065

Ni, B., Bai, F. F., Wei, Y., Liu, M. J., Feng, Z. X., Xiong, Q. Y., et al. (2015). Apoptosis induced by lipid-associated membrane proteins from *Mycoplasma hyopneumoniae* in a porcine lung epithelial cell line with the involvement of caspase 3 and the MAPK pathway. *Genet. Mol. Res.* 14, 15164–15174. doi: 10.4238/2015.150912

Nurk, S., Bankevich, A., Antipov, D., Gurevich, A., Korobeynikov, A., Lapidus, A., et al. (2013). Assembling genomes and mini-metagenomes from highly chimeric reads. *Comput. Mol. Biol.* 7821, 158–170. doi: 10.1007/978-3-642-37195-0_13

Okamba, F. R., Arella, M., Music, N., Jia, J. J., Gottschalk, M., and Gagnon, C. A. (2010). Potential use of a recombinant replication-defective adenovirus vector carrying the C-terminal portion of the P97 adhesin protein as a vaccine against *Mycoplasma hyopneumoniae* in swine. *Vaccine* 28, 4802–4809. doi: 10.1016/j.vaccine.2010.04.089

Olson, R. D., Assaf, R., Brettin, T., Conrad, N., Cucinell, C., Davis, J. J., et al. (2023). Introducing the bacterial and viral bioinformatics resource center (BV-BRC): a resource combining PATRIC, IRD, and ViPR. *Front. Microbiol.* 14:891725. doi: 10.3389/fmicb.2023.891725

Pan, Q., Xu, Q., Liu, T., Zhang, Y., and Xin, J. (2022). *Mycoplasma hyopneumoniae* membrane protein Mhp271 interacts with host UPR protein GRP78 to facilitate infection. *Mol. Microbiol.* 118, 208–222. doi: 10.1111/mmi.14963

Petri, F. A. M., Ferreira, G. C., Arruda, L. P., Malcher, C. S., Storino, G. Y., Almeida, H. M. S., et al. (2023). Associations between pleurisy and the Main bacterial pathogens of the porcine respiratory diseases complex (PRDC). *Animals* 13, 1–15. doi: 10.3390/ani13091493

Pieters, M., Pijoan, C., Fano, E., and Dee, S. (2009). An assessment of the duration of *Mycoplasma hyopneumoniae* infection in an experimentally infected population of pigs. *Vet. Microbiol.* 134, 261–266. doi: 10.1016/j.vetmic.2008.08.016

Qiu, G., Rui, Y., Yi, B., Liu, T., Hao, Z., Li, X., et al. (2019). Identification and genomic analysis of a pathogenic strain of *Mycoplasma hyopneumoniae* (TB1) isolated from Tibetan pigs. *DNA Cell Biol.* 38, 922–932. doi: 10.1089/dna.2018.4560

R Core Team. (2022). *R: A language and environment for statistical computing*. R Foundation for Statistical Computing, Vienna, Austria.

Radulovic, S., Troyer, J. M., Beier, M. S., Lau, A. O. T., and Azad, A. F. (1999). Identification and molecular analysis of the gene encoding *Rickettsia typhi* hemolysin. *Infect. Immun.* 67, 6104–6108. doi: 10.1128/IAI.67.11.6104-6108

Raymond, B. B. A., and Djordjevic, S. (2015). Exploitation of plasminogen by bacterial pathogens of veterinary significance. *Vet. Microbiol.* 178, 1–13. doi: 10.1016/j.vetmic.2015.04.014

Redondo, E., Masot, A. J., Fernández, A., and Gázquez, A. (2009). Histopathological and immunohistochemical findings in the lungs of pigs infected experimentally with *Mycoplasma hyopneumoniae*. *J. Comp. Pathol.* 140, 260–270. doi: 10.1016/j.jcpa.2008.12.008

Rohmer, L., Hocquet, D., and Miller, S. I. (2011). Are pathogenic bacteria just looking for food? Metabolism and microbial pathogenesis. *Trends Microbiol.* 19, 341–348. doi: 10.1016/j.tim.2011.04.003

Roos, L. R., Fano, E., Homwong, N., Payne, B., and Pieters, M. (2016). A model to investigate the optimal seeder-to-naïve ratio for successful natural *Mycoplasma hyopneumoniae* gilt exposure prior to entering the breeding herd. *Vet. Microbiol.* 184, 51–58. doi: 10.1016/j.vetmic.2016.01.008

Rycroft, A. (2020) in *Mycoplasmas in swine*. ed. D. Maes. *1st* ed (Merelbeke, Belgium: Faculty of Veterinary Medicine, Ghent University), 27.

Seemann, T. (2014). Prokka: rapid prokaryotic genome annotation. *Bioinformatics* 30, 2068–2069. doi: 10.1093/bioinformatics/btu153

Seymour, L. M., Falconer, L., Deutscher, A. T., Minion, F. C., Padula, M. P., Dixon, N. E., et al. (2011). Mhp107 is a member of the multifunctional adhesin family of *Mycoplasma hyopneumoniae*. *J. Biol. Chem.* 286, 10097–10104. doi: 10.1074/jbc.M110.208140

Silva, A. P. S. P., Storino, G. Y., Ferreyra, F. S. M., Zhang, M., Fano, E., Polson, D., et al. (2022). Cough associated with the detection of *Mycoplasma hyopneumoniae* DNA in clinical and environmental specimens under controlled conditions. *Porc. Health Manag.* 8, 6–13. doi: 10.1186/s40813-022-00249-y

Simionatto, S., Marchioro, S. B., Maes, D., and Dellagostin, O. A. (2013). *Mycoplasma hyopneumoniae*: from disease to vaccine development. *Vet. Microbiol.* 165, 234–242. doi: 10.1016/j.vetmic.2013.04.019

Siqueira, F. M., Gerber, A. L., Guedes, R. L. M., Almeida, L. G., Schrank, I. S., Vasconcelos, A. T. R., et al. (2014). Unravelling the transcriptome profile of the swine respiratory tract mycoplasmas. *PLoS One* 9:e110327. doi: 10.1371/journal.pone.0110327

Siqueira, F. M., Thompson, C. E., Virginio, V. G., Gonchoroski, T., Reolon, L., Almeida, L. G., et al. (2013). New insights on the biology of swine respiratory tract mycoplasmas from a comparative genome analysis. *BMC Genomics* 14:175. doi: 10.1186/1471-2164-14-175

Srinivasan, V. B., and Rajamohan, G. (2013). KpnEF, a new member of the *Klebsiella pneumoniae* cell envelope stress response regulon, is an SMR-type efflux pump involved in broad-Spectrum antimicrobial resistance. *Antimicrob. Agents Chemother.* 57, 4449–4462. doi: 10.1128/AAC.02284-12

Stahl, J., Bergmann, H., Göttig, S., Ebersberger, I., and Averhoff, B. (2015). *Acinetobacter baumannii* virulence is mediated by the concerted action of three phospholipases D. *PLoS One* 10:e0138360. doi: 10.1371/journal.pone.0138360

Straw, B. E., Dewey, R. D., Morrow, D. J., Bates, R. J., Cornick, R. D., Hurd, M. E., et al. (1986). Examination of swine at slaughter. Part II. Findings at slaughter and their significance. *Compend. Contin. Educ. Pract. Vet.* 8, 106–112.

Sunaga, F., Tsuchiaka, S., Kishimoto, M., Aoki, H., Kakinoki, M., Kure, K., et al. (2020). Development of a one-run real-time PCR detection system for pathogens associated with porcine respiratory diseases. *J. Vet. Med. Sci.* 82, 217–223. doi: 10.1292/jvms.19-0063

Tavares, B. A. R., Paes, J. A., Zaha, A., and Ferreira, H. B. (2022). Reannotation of *Mycoplasma hyopneumoniae* hypothetical proteins revealed novel potential virulence factors. *Microb. Pathog.* 162:105344. doi: 10.1016/j.micpath.2021.105344

Tritt, A., Eisen, J. A., Facciotti, M. T., and Darling, A. E. (2012). An integrated pipeline for de novo assembly of microbial genomes. *PLoS One* 7:e42304. doi: 10.1371/JOURNAL.PONE.0042304

Trueeb, B. S., Gerber, S., Maes, D., Gharib, W. H., and Kuhnert, P. (2019). Tn-sequencing of *Mycoplasma hyopneumoniae* and *Mycoplasma hyorhinis* mutant libraries reveals non-essential genes of porcine mycoplasmas differing in pathogenicity. *Vet. Res.* 50, 55–59. doi: 10.1186/s13567-019-0674-7

Vasconcelos, A. T. R., Ferreira, H. B., Bizarro, C. V., Bonatto, S. L., Carvalho, M. O., Pinto, P. M., et al. (2005). Swine and poultry pathogens: the complete genome sequences of two strains of *Mycoplasma hyopneumoniae* and a strain of *Mycoplasma synoviae*. *J. Bacteriol.* 187, 5568–5577. doi: 10.1128/JB.187.16.5568-5577.2005

Vicca, J., Stakenborg, T., Maes, D., Butaye, P., Peeters, J., De Kruif, A., et al. (2003). Evaluation of virulence of *Mycoplasma hyopneumoniae* field isolates. *Vet. Microbiol.* 97, 177–190. doi: 10.1016/j.vetmic.2003.08.008

Vilela, F. P., dos Prazeres Rodrigues, D., Allard, M. W., and Falcão, J. P. (2022). Prevalence of efflux pump and heavy metal tolerance encoding genes among *Salmonella enterica* serovar Infantis strains from diverse sources in Brazil. *PLoS One* 17:e0277979. doi: 10.1371/JOURNAL.PONE.0277979

Villarreal, I., Maes, D., Vranckx, K., Calus, D., Pasmans, F., and Haesebrouck, F. (2011). Effect of vaccination of pigs against experimental infection with high and low virulence *Mycoplasma hyopneumoniae* strains. *Vaccine* 29, 1731–1735. doi: 10.1016/j.vaccine.2011.01.002

Woolley, L. K., Fell, S., Gonsalves, J. R., Walker, M. J., Djordjevic, S. P., Jenkins, C., et al. (2012). Evaluation of clinical, histological and immunological changes and qPCR detection of *Mycoplasma hyopneumoniae* in tissues during the early stages of *Mycoplasmal pneumonia* in pigs after experimental challenge with two field isolates. *Vet. Microbiol.* 161, 186–195. doi: 10.1016/j.vetmic.2012.07.025

Wu, Y., Yu, Y., Hua, L., Wei, Y., Gan, Y., Chenia, H. Y., et al. (2022). Genotyping and biofilm formation of *Mycoplasma hyopneumoniae* and their association with virulence. *Vet. Res.* 53:95. doi: 10.1186/s13567-022-01109-x

Xie, X., Li, T., Xiong, Q., Feng, Z., Gan, Y., Wang, L., et al. (2021). Nicotinamide adenine dinucleotide-dependent flavin oxidoreductase of *Mycoplasma hyopneumoniae* functions as a potential novel virulence factor and not only as a metabolic enzyme. *Front. Microbiol.* 12:747421. doi: 10.3389/fmicb.2021.747421

Yamaguti, M. (2009). *Isolamento de Mycoplasma de suínos com problemas respiratórios e tipificação dos isolados pela PFGE e sequenciamento do gene 16S rRNA*. Tese de Doutorado, Instituto de Ciências Biomédicas, Universidade de São Paulo, São Paulo-SP, Brasil.

Yu, Y., Wang, J., Han, R., Wang, L., Zhang, L., Zhang, A. Y., et al. (2020). *Mycoplasma hyopneumoniae* evades complement activation by binding to factor H via elongation factor thermo unstable (EF-Tu). *Virulence* 11, 1059–1074. doi: 10.1080/21505594.2020.1806664

Zhang, Q., Young, T. F., and Ross, R. F. (1995). Identification and characterization of a *Mycoplasma hyopneumoniae* adhesin. *Infect. Immun.* 63, 1013–1019. doi: 10.1128/iai.63.3.1013-1019.1995

Zong, B., Zhu, Y., Liu, M., Wang, X., Chen, H., Zhang, Y., et al. (2022). Characteristics of *Mycoplasma hyopneumoniae* strain ES-2 isolated from Chinese native black pig lungs. *Front. Vet. Sci.* 9, 1–13. doi: 10.3389/fvets.2022.883416

frontiers | Frontiers in Microbiology

TYPE Original Research
PUBLISHED 11 January 2024
DOI 10.3389/fmicb.2023.1334968

OPEN ACCESS

EDITED BY
Gang Wang,
Shandong Agricultural University, China

REVIEWED BY
Min Ja Lee,
Animal and Plant Quarantine Agency, Republic of Korea
Hongliang Zhang,
Chinese Academy of Agricultural Sciences, China

*CORRESPONDENCE
Tae-Wook Hahn
✉ twhahn@kangwon.ac.kr

RECEIVED 17 November 2023
ACCEPTED 29 December 2023
PUBLISHED 11 January 2024

CITATION
Kim K, Choi K, Shin M and Hahn T-W (2024) A porcine circovirus type 2d-based virus-like particle vaccine induces humoral and cellular immune responses and effectively protects pigs against PCV2d challenge.
Front. Microbiol. 14:1334968.
doi: 10.3389/fmicb.2023.1334968

A porcine circovirus type 2d-based virus-like particle vaccine induces humoral and cellular immune responses and effectively protects pigs against PCV2d challenge

Kiju Kim[1], Kyusung Choi[1], Minna Shin[1] and Tae-Wook Hahn[1,2]*

[1]INNOVAC, Chuncheon, Republic of Korea, [2]College of Veterinary Medicine and Institute of Veterinary Science, Kangwon National University, Chuncheon, Republic of Korea

The pathogenic porcine circovirus type 2 (PCV2) leads to significant economic losses in pig production. PCV2d is currently the dominant genotype causing porcine circovirus-associated disease (PCVAD) worldwide. Therefore, development of a recombinant PCV2d-based vaccine is required to elicit complete protection against PCV2d infection. In this study, we generated virus-like particles of PCV2d-based capsid protein (Bac-2dCP) using a baculovirus expression system and evaluated its protective efficacy against PCV2d infection in specific pathogen-free (SPF) pigs. Three-week-old SPF miniature pigs were intramuscularly immunized with purified Bac-2dCP and intranasally challenged with PCV2d at 4 weeks post-vaccination. The Bac-2dCP group showed significantly higher IgG levels and neutralizing antibodies against PCV2b and PCV2d genotypes, as well as increased interferon-γ levels, and increased body weight and average daily weight gain compared with positive (challenged) and negative (unchallenged) controls. In particular, the Bac-2dCP group showed almost complete absence of PCV2d DNA in serum, nasal, and rectal swabs and in lung, lymph node, and kidney tissue samples. However, the positive control group exhibited low levels of neutralizing antibody, and high levels of PCV2 DNA in serum, swab, and tissue samples, resulting in PCV2-associated pathological lesions. The results of this study demonstrated that a recombinant Bac-2dCP vaccine conferred complete protection against a PCV2d challenge in SPF miniature pigs.

KEYWORDS

porcine circovirus, virus-like particles, PCV2d-based vaccine, miniature pig, protective immunity

1 Introduction

Porcine circovirus type 2 (PCV2) is primary agent of porcine circovirus-associated disease (PCVAD), which includes post weaning multisystemic wasting syndrome, porcine dermatitis, nephropathy syndrome, and porcine respiratory disease complex (Opriessnig et al., 2007; Lim et al., 2022). PCV2 infection also renders pigs more susceptible to secondary pathogens such as porcine reproductive and respiratory syndrome virus (PRRSV), porcine parvovirus, and *Mycoplasma* spp. by immunosuppression, resulting in increased mortality. PCVAD incurs an

average cost of 3–4 USD (up to 20 USD) per pig in the United States and is therefore recognized as an economically important pathogen in the global swine industry (Gillespie et al., 2009). Because of widespread occurrence of PCV2 on pig farms, vaccination is the only effective method to reduce PCV2 prevalence and thereby control PCVAD (Dvorak et al., 2016).

PCV2 is a small virus approximately 17 nm in diameter, comprising non-enveloped, single-stranded circular DNA of about 1.76 kb in an icosahedral form. PCV2 genotypes are currently classified as PCV2a, PCV2b, PCV2c, PCV2d, and PCV2e by PCV2 open reading frame 2 (ORF2) encoding major capsid protein; PCV2d is currently the most prevalent genotype worldwide (Dupont et al., 2008). The nucleotide sequence similarity of PCV2a ORF2 was 90.8–93.2% with PCV2b and 89.2–92.0% with PCV2d (Zheng et al., 2020). The structural capsid of PCV2 is composed of 60 monomeric capsid proteins that can be self-assembled into PCV2 virus-like particle (VLP) and is known to be an important antigenic determinant that induces neutralizing antibody against PCV2 (Kim et al., 2020). Advantages of PCV2 VLP-based subunit vaccine is very safe, easy preparation, low-cost, high-level of expression and highly effective in PCV2 prevention. Current commercial PCV2 subunit vaccines, Ingelvac CircoFLEX (Boehringer Ingelheim Animal Health), Porcilis PCV (MSD Animal Health) and Circumvent PCV (Merck), are based on PCV2a capsid protein expressed in a baculovirus expression system (Fort et al., 2008; Guo et al., 2022).

After introduction of commercial PCV2a vaccines, a global genotype shift from PCV2a to PCV2b was confirmed in vaccinated herds presenting severe clinical symptoms (Carman et al., 2008). In 2014, a newly emerging PCV2b mutant (PCV2d) was reported in cases of vaccine failure in several countries, including Korea, Brazil, and the United States (Xiao et al., 2012; Salgado et al., 2014; Seo et al., 2014). PCV2d is now the most common genotype causing PCVAD (Opriessnig et al., 2019; Park et al., 2019). This genotype shift is highly likely to occur by persistent PCV2 infection and evasion of the host immune response (Franzo et al., 2016).

It has been proposed that PCV2a-based vaccines cannot provide complete protection against the prevalent PCV2d genotype (Hou et al., 2019; Tseng et al., 2019). In a previous study, pigs immunized with a PCV2b vaccine showed more effective protection against a PCV2a and PCV2b co-challenge than did those immunized with a PCV2a-based vaccine (Opriessnig et al., 2013). In a recent study, we found that a PCV2d-based vaccine significantly reduced PCV2 viremia more than a commercial PCV2a vaccine when applied to pigs naturally infected with PCV2d (Kim and Hahn, 2021). For this reason, the development of a novel PCV2d-based vaccine is required to elicit complete protection against PCV2d infection. Therefore, here, we have evaluated the protective efficacy of a PCV2d-based VLP vaccine in specific pathogen-free (SPF) miniature pigs against an experimental PCV2d challenge.

2 Materials and methods

2.1 PCV2d-based VLP

The recombinant PCV2d capsid protein (Bac-2dCP) was expressed using the ExpiSf Baculovirus Expression System (Kim and Hahn, 2021). Briefly, *Spodoptera frugiperda* (Sf9) cells (ExpiSf9™, Gibco, United States) were cultured in ExpiSf CD medium (Gibco, United States) and infected with the recombinant baculovirus-expressing capsid protein of PCV2d (GenBank Accession No. KY810325). After 7 days, infected cells were centrifuged at 500 × *g* for 10 min and the pellet dissolved in lysis buffer (50 mM NaH_2PO_4 and 300 mM NaCl) containing 1% Igepal CA-630 (Sigma-Aldrich, United States). The supernatant was purified by anion exchange chromatography using Q-Sepharose Fast Flow (GE Healthcare, United States). The purified protein was filtered through a 0.22 μm cellulose acetate membrane (Corning, United States), and protein concentration was measured using a Pierce bicinchoninic acid protein assay kit (Thermo Fisher Scientific, United States). The self-assembled VLPs were observed using a transmission electron microscope (JEM-2100F; JEOL, Tokyo, Japan) at the Chuncheon Center of the Korea Basic Science Institute.

2.2 Immunization and the PCV2d challenge

The procedures for animal handling, care, and experimental protocols were approved by the Institutional Animal Care and Use Committee of Kangwon National University (Permit No. KW-210510-1). The animal experiment was carried out by Optipharm Medipig (Osong, Korea) in its Biosecurity Level 3 facility. Ten 3-week-old SPF Yucatan miniature pigs were randomly divided into three groups. The Bac-2dCP ($n = 5$) group received a 1 mL dose containing 20 μg of purified Bac-2dCP with 50% (v/v) of Montanide IMS 1313 (Seppic, France) by intramuscular administration in the neck region. At 4 weeks post-vaccination (WPV), the Bac-2dCP and positive control (PC; $n = 3$) groups were challenged intranasally with 1 mL of PCV2d ($10^{5.5}$ 50% tissue culture infective dose, $TCID_{50}$/mL) (GenBank Accession No. OP806268) in each nostril. A third group, the negative control (NC; $n = 2$), was unchallenged. Serum, nasal and rectal swab samples were collected at 0, 2, 4, 6, 7, and 8 WPV (Figure 1). At 4 weeks after the challenge, all animals were humanely euthanized by intravenous injection of 2 mmol/kg potassium chloride solution and necropsied to evaluate pathological lesions and viral DNA loads in lung, lymph node, and kidney.

2.3 Clinical signs and average daily weight gain (ADWG)

Following vaccination at 0–7 days, all pigs were monitored daily for rectal temperature and clinical symptoms using a scale ranging from 0 (normal) to 3 (severe). Body weights were measured weekly during the experimental period. ADWG (g/day) was calculated before (0–4 WPV) and after (4–8 WPV) the PCV2 challenge.

2.4 Quantification of PCV2 DNA

Viral DNA from the serum, swab, and tissue samples was extracted using a Viral DNA/RNA Extraction Kit (iNtRON Biotechnology, Korea) according to the manufacturer's protocol.

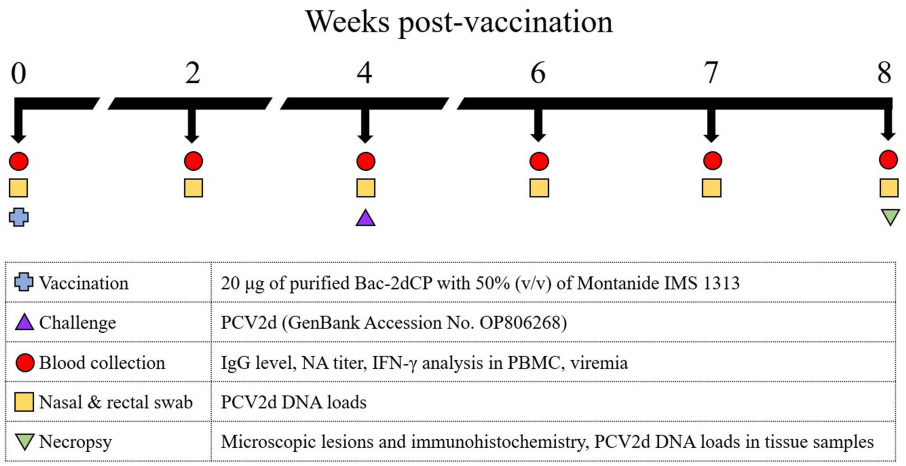

Vaccination	20 μg of purified Bac-2dCP with 50% (v/v) of Montanide IMS 1313
Challenge	PCV2d (GenBank Accession No. OP806268)
Blood collection	IgG level, NA titer, IFN-γ analysis in PBMC, viremia
Nasal & rectal swab	PCV2d DNA loads
Necropsy	Microscopic lesions and immunohistochemistry, PCV2d DNA loads in tissue samples

FIGURE 1
Experimental design. Ten 3-week-old SPF miniature pigs were randomly divided into three groups: The Bac-2dCP ($n = 5$), PC ($n = 3$) and NC ($n = 2$). The Bac-2dCP group was vaccinated intramuscularly once in the neck region. After 4 weeks, Bac-2dCP and PC groups were challenged intranasally with 1 mL of PCV2d ($10^{5.5}$ $TCID_{50}$/mL) in each nostril. The NC group was unchallenged.

Quantitative polymerase chain reaction (qPCR) assays were conducted using a TOPreal™ qPCR 2X PreMIX (SYBR Green High ROX; Enzynomics, Korea) as described previously (Kim and Hahn, 2021).

2.5 Serological assay

All serum samples were tested for PCV2b- and PCV2d-specific IgG antibodies using an indirect enzyme-linked immunosorbent assay (ELISA) (Kim and Hahn, 2021). Microplates (96-well Nunc Maxisorp, Roskilde, Denmark) were coated with 100 ng/well of purified Bac-2bCP or Bac-2dCP. Absorbances were read at 450 nm using a microplate reader (BioTek, United States).

Viral neutralization (VN) titers were determined using an indirect immunofluorescence assay test (Kim et al., 2020). PCV2b supplied by ChoongAng Vaccine Laboratories (Daejeon, Korea) and PCV2d (GenBank Accession No. OP806268) were used in this assay. Briefly, all serum samples from each group were inactivated by heating at 56°C for 30 min. The inactivated samples were serially diluted twofold from 1:4 to 1:16,384 and added to 200 $TCID_{50}$ of PCV2b and PCV2d virus. The serum–virus mixture was incubated at 37°C for 1 h with 5% CO_2 and then applied to a 70–80% confluent monolayer of PK-15 cells at 37°C for 72 h with 5% CO_2. VN titers were determined as the highest serum dilution that exhibited >90% neutralization.

2.6 IFN-γ analysis

Peripheral blood mononuclear cells (PBMCs) were isolated by Ficoll–Hypaque (Choi et al., 2019) density gradient centrifugation at 4, 6, and 8 WPV. PBMCs were stimulated with 10 μg/mL of purified Bac-2dCP for 72 h and the culture supernatants harvested. To determine the PCV2-specific gamma interferon (IFN-γ) level, a Porcine IFN-γ ELISA kit (Invitrogen, United States) was used according to the manufacturer's protocol.

2.7 Microscopic lesions and immunohistochemistry

After euthanasia at 8 WPV, lung, lymph node, and kidney tissues were fixed in 10% buffered formalin, embedded in paraffin, and cut into 4 μm sections. After staining with hematoxylin and eosin, microscopic images were obtained through an Olympus BX53 microscope (Olympus, Japan) and analyzed with Olympus cellSens software. Lesions were scored blind as 0 (no lesions), 1 (minimal), 2 (mild), 3 (moderate), or 4 (severe) (Opriessnig et al., 2004).

PCV2 antigen determination in paraffin-embedded sections was performed by immunohistochemical (IHC) analysis using a rabbit PCV2 capsid polyclonal antibody (Invitrogen) and a VECTASTAIN Elite ABC Universal Kit (Vector Laboratories, United States) (Chianini et al., 2003).

2.8 Statistical analysis

All data are presented as mean ± standard error of the mean (SEM). Statistical data were generated using GraphPad Prism 8.0.1 software (GraphPad Software, La Jolla, CA, United States), and significant differences were determined using one-way analysis of variance followed by Tukey's multiple comparisons test. p values <0.05 were considered statistically significant.

3 Results

3.1 Clinical symptoms and ADWG

After vaccination, all pigs in the Bac-2dCP group maintained normal body temperature like the NC group, and no clinical symptoms of abscesses, inflammation, epilepsy, anorexia, depression, shock, vomiting, or diarrhea were seen. ADWG showed no significant difference between groups before the challenge (0–4 WPV) (Table 1). After the challenge

(4–8 WPV), the highest ADWG was observed in the Bac-2dCP group, while the growth rate was retarded in the PC group.

3.2 PCV2-specific humoral immune responses

PCV2-specific maternally-derived antibody was undetected in all SPF miniature pigs at 0 WPV (Figures 2A,B). After vaccination, the Bac-2dCP group seroconverted to PCV2b- and PCV2d-specific IgG antibodies at 2 WPV. Notably, the PCV2-specific IgG levels rapidly increased in the Bac-2dCP group after the challenge and showed significantly higher ($p < 0.001$) values compared with the PC and NC groups at 6 WPV. In addition, the PC group exhibited PCV2-specific IgG levels similar to those of the Bac-2dCP group at 8 WPV, whereas the NC group remained seronegative throughout the experimental period.

TABLE 1 Body weight and average daily weight gain.

	Weeks post-vaccination	Group		
		Bac-2dCP	PC	NC
Body weight (kg)	0	3.06 ± 0.43	3.33 ± 0.48	3.05 ± 0.05
	4	5.76 ± 0.53	5.87 ± 0.47	6.10 ± 0.10
	8	9.88 ± 0.94	9.05 ± 0.93	9.45 ± 0.05
ADWG (g)	0–4	96.4 ± 15.5	90.5 ± 11.3	108.9 ± 12.5
	4–8	147.1 ± 20.4	113.7 ± 61.0	119.6 ± 8.9
	0–8	121.8 ± 18.0	102.1 ± 36.2	114.3 ± 10.7

Data are presented as group mean values (± standard error of the mean).

3.3 Neutralizing activity

Before vaccination, the serum samples in all groups were negative for VN titers against PCV2. In the Bac-2dCP group, PCV2-specific VN titers were first detected at 2 WPV, then greatly increased at 4 and 6 WPV (Figures 2C,D). At 8 WPV, the PCV2b- and PCV2d-specific VN titers reached maximum mean levels of 10.6 and 10.9 $\log_2$, respectively, which were markedly and significantly higher than those of the NC group ($p < 0.001$). The PC group titers were significantly lower than those of the Bac-2dCP group: $p < 0.001$ for PCV2b and $p < 0.01$ for PCV2d. Nonetheless, their VN titers were substantially higher than those of the NC group.

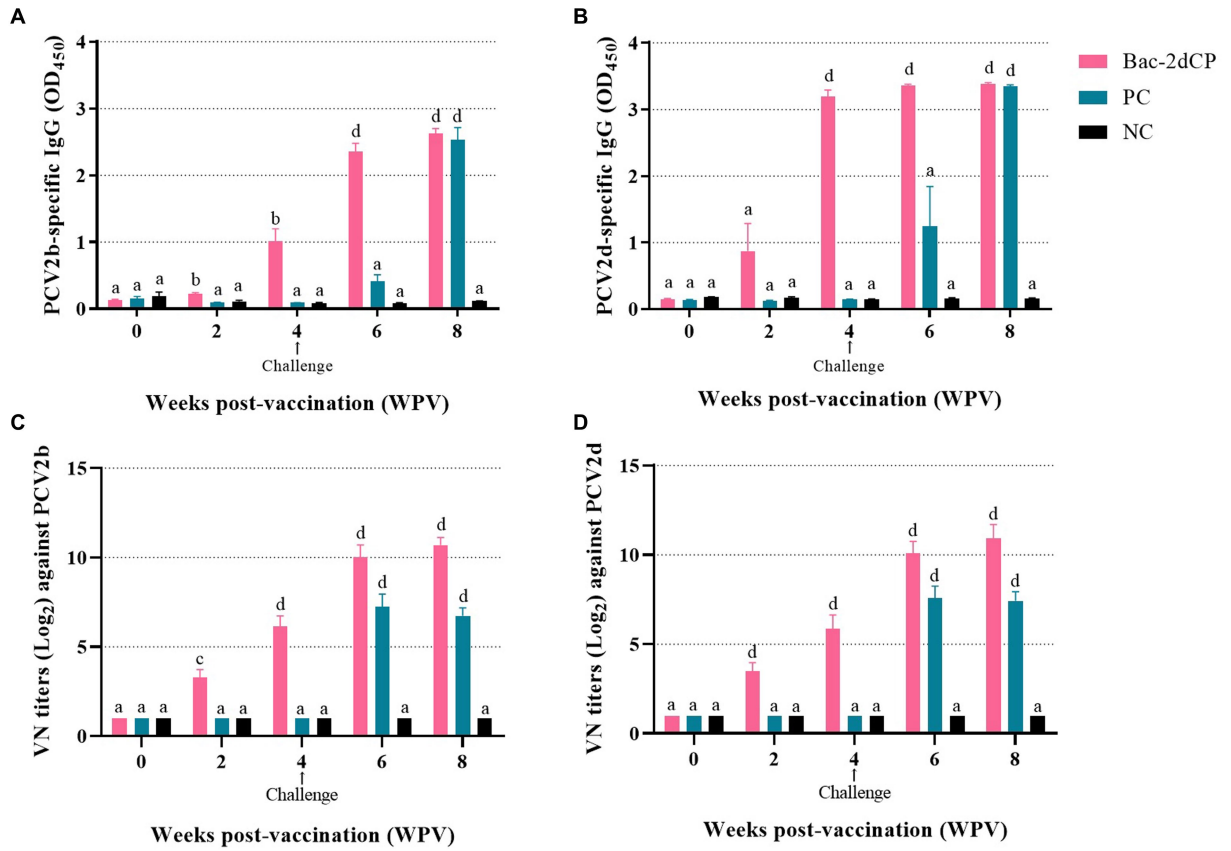

FIGURE 2
Mean values of serum IgG antibody levels and viral neuralization (VN) titers at different weeks post-vaccination **(A)** PCV2b- and **(B)** PCV2d-specific IgG levels were analyzed by indirect ELISA. VN titers (Log_2) against **(C)** PCV2b and **(D)** PCV2d were analyzed by indirect immunofluorescence assay (IFA) test. Data were expressed as mean ± standard error of the mean (SEM). Significant differences compared with NC group are indicated by different superscripts ([a]Not significant, [b]$p < 0.05$, [c]$p < 0.01$ and [d]$p < 0.001$).

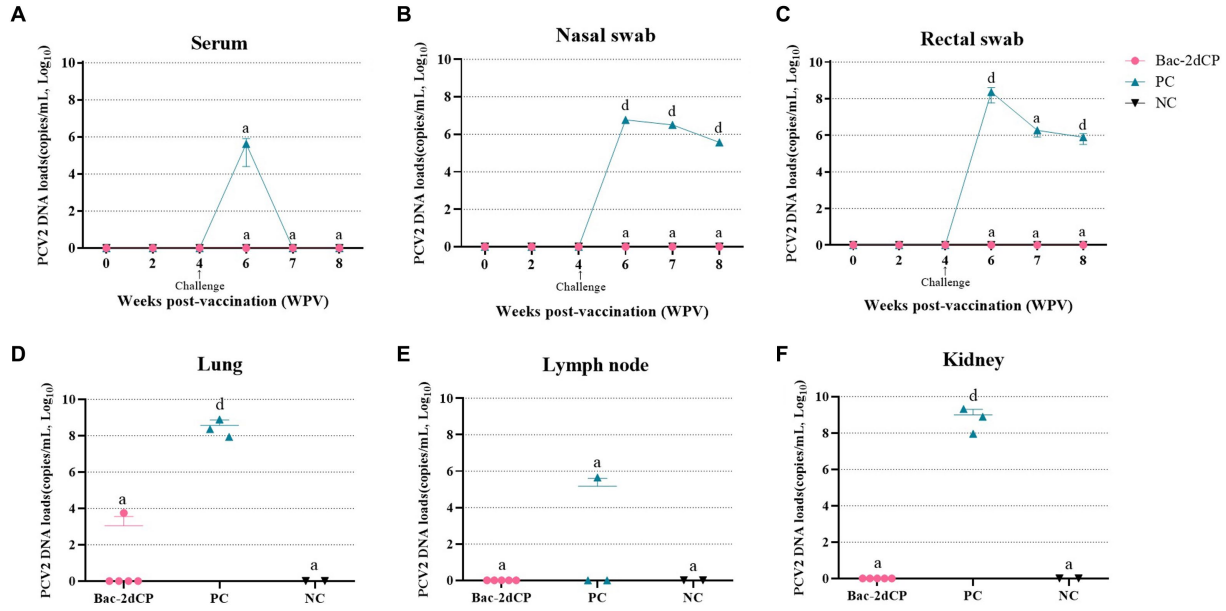

FIGURE 3
Mean values of the PCV2 genomic copy number in **(A)** serum, **(B)** nasal swab, **(C)** rectal swab, **(D)** lung, **(E)** lymph node, and **(F)** kidney tissue samples at different weeks post-vaccination. PCV2 DNA loads were analyzed by quantitative polymerase chain reaction (qPCR) assays. Data were expressed as mean±standard error of the mean (SEM). Significant differences compared with NC group are indicated by different superscripts ([a]Not significant and [d]$p < 0.001$).

3.4 PCV2 DNA loads

In the period from vaccination to challenge, no PCV2d DNA copies were detected in serum, nasal swab, or rectal swab samples from all groups. After 2 weeks post-challenge (6 WPV), a significantly increased level of PCV2d DNA copies in the PC group was observed in the following samples: serum (5.6 $\log_{10}$ copies/mL), nasal swab (6.9 $\log_{10}$ copies/mL, $p < 0.001$), and rectal swab (8.3 $\log_{10}$ copies/mL, $p < 0.001$) (Figures 3A–C, respectively). Importantly, the PC group showed a significant amount of PCV2d DNA in lung (8.5 $\log_{10}$ copies/mL, $p < 0.001$), lymph node (5.1 $\log_{10}$ copies/mL), and kidney tissue samples (8.9 $\log_{10}$ copies/mL, $p < 0.001$) (Figures 3D–F, respectively). By contrast, PCV2d DNA was not detected in any serum, swab, or tissue (except one lung) samples from the Bac-2dCP group, and in this respect, the Bac-2dCP group was closely similar to the NC group.

3.5 IFN-γ levels

At 4 WPV, production of IFN-γ in PBMC stimulated with Bac-2dCP was undetected in the PC and NC groups (Table 2). However, the Bac-2dCP group showed a significantly higher ($p < 0.05$) secretion level of IFN-γ compared with the PC and NC groups. By 2 weeks post-challenge (6 WPV), the PCV2d-specific IFN-γ level of the Bac-2dCP group had decreased, but was still markedly higher than those of the PC and NC groups at 8 WPV.

TABLE 2 Mean group interferon-gamma (IFN-γ) in PBMC.

Group	Weeks post-vaccination		
	4	6	8
Bac-2dCP	128.1 ± 54.7[b]	11.4 ± 6.6[a]	72.9 ± 31.3[a]
PC	0.0[a]	12.8 ± 5.9[a]	22.8 ± 22.3[a]
NC	0.0[a]	3.6 ± 3.6[a]	7.3 ± 7.3[a]

The data are presented as group mean values (pg/mL ± standard error). Significant differences ($p < 0.05$) compared with NC group are indicated by different superscripts.

3.6 Histopathological and immunohistochemical results

Mild perivascular and peribronchiolar cuffing were observed in lesions that were found in all groups (Table 3 and Figure 4A). Some pigs in the Bac-2dCP and PC groups showed bronchus-associated lymphoid tissue (BALT) hyperplasia. Notably, the PC group showed PCV2-associated lung lesions of suppurative bronchointerstitial pneumonia, peribronchiolar fibroplasia with bronchiolar segmentation, and pulmonary edema. In addition, lymphoid depletion in lymph node and interstitial inflammatory cell infiltration in kidney were observed only in the PC group. However, the Bac-2dCP group did not display PCV2-associated lesions in lung, lymph node, or kidney, a result identical to that of the NC group. Interestingly, lung and kidney lesion scores in the Bac-2dCP group were significantly ($p < 0.01$) lower than those in the PC group (Figure 5).

TABLE 3 Histopathologic and IHC findings in lung, lymph node, and kidney.

Findings	No. of pigs (positive/total)		
	Bac-2dCP	PC	NC
Lung			
Perivascular and peribronchiolar cuffing	5/5	3/3	2/2
BALT hyperplasia	2/5	1/3	0/2
Suppurative bronchointerstitial pneumonia	0/5	1/3	0/2
Peribronchiolar fibroplasia with bronchiolar segmentation	0/5	1/3	0/2
Pulmonary edema	0/5	2/3	0/2
PCV2 detection (IHC)	1/5	1/3	0/2
Lymph node			
Lymphoid depletion	0/5	1/3	0/2
PCV2 detection (IHC)	0/5	2/3	0/2
Kidney			
Interstitial inflammatory cell infiltration	0/5	3/3	0/2
PCV2 detection (IHC)	0/5	3/3	0/2

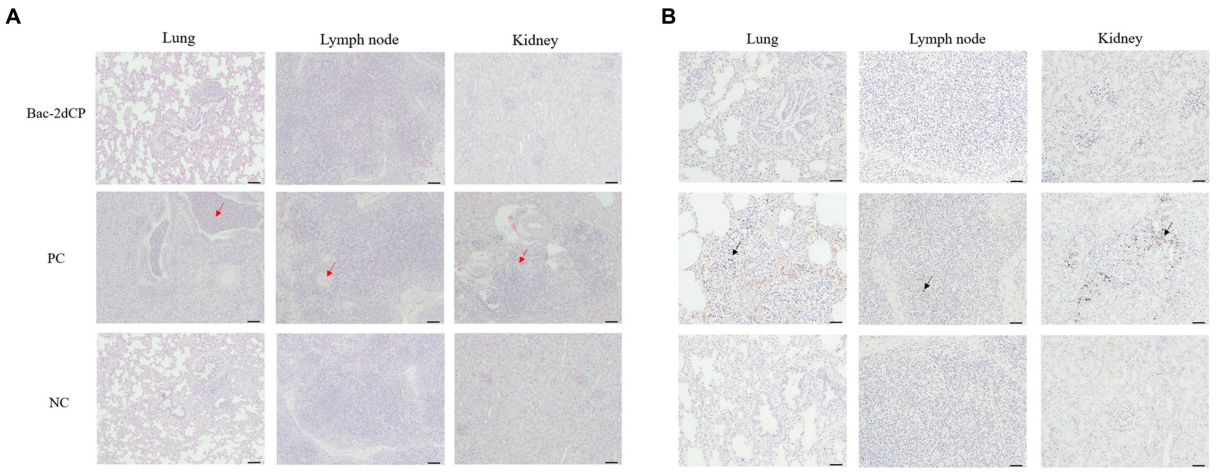

FIGURE 4
Histopathological evaluation and detection of PCV2 antigen in tissues at 4 weeks post-challenge. **(A)** Hematoxylin and eosin staining and **(B)** immunohistochemistry in lung, lymph node, and kidney tissues. The red arrows indicate pulmonary edema, lymphoid depletion and interstitial inflammatory cell infiltration in the lung, lymph node and kidney tissues of PC group, respectively. PCV2 antigens were shown by black arrows. Scale bars indicate **(A)** 100 μm and **(B)** 50 μm.

For the IHC examination, PCV2 antigen was undetected in almost all lung, lymph node, and kidney tissue samples in the Bac-2dCP and NC groups (Figure 4B). However, the PC group showed high amounts of PCV2 antigen in tissue samples.

4 Discussion

Following the introduction of commercial PCV2a-based vaccines, new genotypes have emerged by viral evolution (Ilha et al., 2020). To alleviate these concerns, cross-protective ability is an important quality of PCV2 vaccines. Our previous study demonstrated that our Bac-2dCP VLP vaccine provides not only effective protection against the homologous PCV2d genotype (the most dominant genotype), but also cross-immunization protection against the heterologous PCV2b genotype in pigs naturally infected with PCV2d (Kim and Hahn, 2021). Arising from this result, the objective of the present study was to evaluate the protective efficacy of Bac-2dCP VLP vaccine in an SPF miniature pig model against an experimental PCV2d challenge. The SPF miniature pig provides the advantages of no maternal antibodies, genetic stability, susceptibility to infection, ease of rearing, and higher statistical power in vaccination and challenge experiments (Khan, 1984; Klinkenberg et al., 2002; Gan et al., 2020).

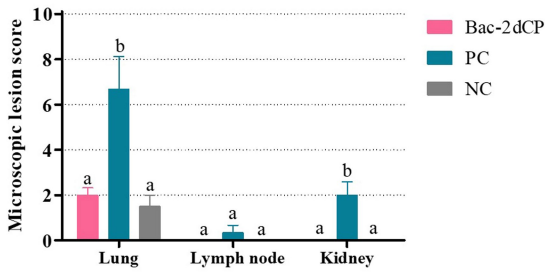

FIGURE 5
Microscopic lesion scores in lung, lymph node, and kidney at 4 weeks post-challenge. Histopathological lesions were scored blind as 0 (no lesions), 1 (minimal), 2 (mild), 3 (moderate), or 4 (severe). Data were expressed as mean ± standard error of the mean (SEM). Significant differences compared with NC group are indicated by different superscripts ([a]Not significant and [b]$p < 0.05$).

The presence of neutralizing antibody against PCV2 is an important mechanism to control PCVAD and has a pivotal role in viral clearance (Chae, 2012; Dvorak et al., 2018). A previous study reported that a PCV2a-based commercial vaccine induced neutralizing antibody titers of 8.0 $\log_2$ at 7 WPV in conventional pigs, and that PCV2 DNA was detected at low levels in blood after PCV2a, PCV2b, and PCV2d challenges (Park et al., 2019). In addition, commercial PCV2a-vaccinated herds showed a reduction of PCV2 viremia, shedding, and transmission against a PCV2d challenge under experimental conditions (Opriessnig et al., 2017). However, low levels of PCV2 viremia mean that the virus has not completely cleared, resulting in chronic subclinical infection with PCV2. Therefore, these commercial PCV2 vaccines appear to provide incomplete cross-protection against the current dominant PCV2d genotype (Peswani et al., 2022). Consequently, it is important that next-generation PCV2 vaccines induce sufficient immune protection against PCV2d. A recent study demonstrated that vaccination with PCV2d VLP in pigs induced high levels of PCV2d-specific neutralizing antibodies, and that PCV2 DNA loads in blood and nasal swab against PCV2d and PRRSV dual-challenge were similar to those of the unchallenged group (Kang et al., 2021). In the present study, miniature pigs vaccinated with Bac-2dCP VLP elicited a sufficient immune response in PCV2b and PCV2d VN titers. Interestingly, the vaccinated group was confirmed to be almost devoid of PCV2, unlike the significantly higher viral loads from serum, swab, and tissue samples in the PC group after the PCV2d challenge. Further, the vaccinated group exhibited almost complete protection against PCV2-associated microscopic lesions in lung, lymph node, and kidney, similar to the results in the NC group. These data suggest that sufficient neutralizing antibodies produced by vaccination contributed to effective protection against PCV2d infection, reduced PCV2-associated pathological lesions. Meanwhile, histopathologic difference against PCV2d challenge in PC group seems to be dependent on the susceptibility or innate immunity between the individual pig.

Cell-mediated immunity is also known to be a key factor in PCV2 clearance and long-term protection against PCV2 infection (Venegas-Vargas et al., 2021). PCV2-specific IFN-γ production is related to reductions in viremia, shedding, and PCV2-associated lesions (Ferrari et al., 2014; Park et al., 2014). A previous study reported that the maximum PCV2-specific IFN-γ level in PBMC was 74.4 pg/mL in pigs vaccinated with Ingelvac CircoFLEX at 3 WPV (Li et al., 2020). In the present study, a high level of IFN-γ response was observed in the vaccinated group (128.1 pg/mL) at 4 WPV, and was significantly different ($p < 0.05$) from the two control groups. After challenge, the IFN-γ of vaccinated group was again elevated at 8 WPV, it could be inferred that PCV2-specific IFN-γ was secreted by memory T cells to protect against PCV2d shedding from nasal and rectal of PC group. This enhanced IFN-γ secretion by vaccination appears to regulate the protective immune response and to contribute to viral clearance in serum, swab, and tissue samples after a PCV2d challenge.

5 Conclusion

The present study demonstrated that recombinant Bac-2dCP VLP vaccine can effectively induce PCV2-specific humoral and cell-mediated immune responses and provide complete protection from PCV2 viremia, nasal, and rectal shedding. It can also significantly reduce viral loads in lung, lymph node, and kidney tissues against a PCV2d challenge in SPF miniature pigs. Therefore, the Bac-2dCP vaccine is an attractive candidate to control the PCVAD caused by the currently prevalent PCV2d genotype. However, further studies are needed to evaluate the comparative efficacy and immune persistence of Bac-2dCP vaccine in conventional pigs.

Data availability statement

The original contributions presented in the study are included in the article/Supplementary material, further inquiries can be directed to the corresponding author.

Ethics statement

The animal studies were approved by Institutional Animal Care and Use Committee of Kangwon National University. The studies were conducted in accordance with the local legislation and institutional requirements. Written informed consent was obtained from the owners for the participation of their animals in this study.

Author contributions

KK: Writing – original draft, Writing – review & editing. KC: Writing – review & editing. MS: Writing – review & editing. T-WH: Writing – review & editing.

Funding

The author(s) declare financial support was received for the research, authorship, and/or publication of this article. This research was supported by the TIPS Program (10422697) from Ministry of SMEs and Startups and by the Gangwon Promising Bio Company Growth Package Program from Chuncheon Bioindustry Foundation.

Acknowledgments

We would like to thank Mrs. Eunjin Hong (Innovac) for technical assistance.

Conflict of interest

KK, KC, MS, and T-WH were employed by INNOVAC.

Publisher's note

All claims expressed in this article are solely those of the authors and do not necessarily represent those of their affiliated organizations, or those of the publisher, the editors and the reviewers. Any product that may be evaluated in this article, or claim that may be made by its manufacturer, is not guaranteed or endorsed by the publisher.

References

Carman, S., Cai, H. Y., DeLay, J., Youssef, S. A., McEwen, B. J., Gagnon, C. A., et al. (2008). The emergence of a new strain of porcine circovirus-2 in Ontario and Quebec swine and its association with severe porcine circovirus associated disease—2004–2006. *Can. J. Vet. Res.* 72, 259–268.

Chae, C. (2012). Commercial porcine circovirus type 2 vaccines: efficacy and clinical application. *Vet. J.* 194, 151–157. doi: 10.1016/j.tvjl.2012.06.031

Chianini, F., Majo, N., Segalés, J., Domınguez, J., and Domingo, M. (2003). Immunohistochemical characterisation of PCV2 associate lesions in lymphoid and non-lymphoid tissues of pigs with natural postweaning multisystemic wasting syndrome (PMWS). *Vet. Immunol. Immunopathol.* 94, 63–75. doi: 10.1016/S0165-2427(03)00079-5

Choi, J. Y., Lyoo, K. S., Kim, K., Lee, K. W., and Hahn, T. W. (2019). A pilot comparative study of recombinant protein and whole-virus inactivated vaccines against porcine circovirus type 2 in conventionally reared pigs. *Res. Vet. Sci.* 123, 192–194. doi: 10.1016/j.rvsc.2019.01.002

Dupont, K., Nielsen, E. O., Baekbo, P., and Larsen, L. E. (2008). Genomic analysis of PCV2 isolates from Danish archives and a current PMWS case–control study supports a shift in genotypes with time. *Vet. Microbiol.* 128, 56–64. doi: 10.1016/j.vetmic.2007.09.016

Dvorak, C. M., Payne, B. J., Seate, J. L., and Murtaugh, M. P. (2018). Effect of maternal antibody transfer on antibody dynamics and control of porcine circovirus type 2 infection in offspring. *Viral Immunol.* 31, 40–46. doi: 10.1089/vim.2017.0058

Dvorak, C. M., Yang, Y., Haley, C., Sharma, N., and Murtaugh, M. P. (2016). National reduction in porcine circovirus type 2 prevalence following introduction of vaccination. *Vet. Microbiol.* 189, 86–90. doi: 10.1016/j.vetmic.2016.05.002

Ferrari, L., Borghetti, P., De Angelis, E., and Martelli, P. (2014). Memory T cell proliferative responses and IFN-γ productivity sustain long-lasting efficacy of a cap-based PCV2 vaccine upon PCV2 natural infection and associated disease. *Vet. Res.* 45, 44–16. doi: 10.1186/1297-9716-45-44

Fort, M., Sibila, M., Allepuz, A., Mateu, E., Roerink, F., and Segalés, J. (2008). Porcine circovirus type 2 (PCV2) vaccination of conventional pigs prevents viremia against PCV2 isolates of different genotypes and geographic origins. *Vaccine* 26, 1063–1071. doi: 10.1016/j.vaccine.2007.12.019

Franzo, G., Cortey, M., Segalés, J., Hughes, J., and Drigo, M. (2016). Phylodynamic analysis of porcine circovirus type 2 reveals global waves of emerging genotypes and the circulation of recombinant forms. *Mol. Phylogenet. Evol.* 100, 269–280. doi: 10.1016/j.ympev.2016.04.028

Gan, Y., Xie, X., Zhang, L., Xiong, Q., Shao, G., and Feng, Z. (2020). Establishment of a model of *Mycoplasma hyopneumoniae* infection using Bama miniature pigs. *Food Prod. Process. Nutr.* 2, 1–13. doi: 10.1186/s43014-020-00034-w

Gillespie, J., Opriessnig, T., Meng, X. J., Pelzer, K., and Buechner-Maxwell, V. (2009). Porcine circovirus type 2 and porcine circovirus-associated disease. *J. Vet. Int. Med.* 23, 1151–1163. doi: 10.1111/j.1939-1676.2009.0389.x

Guo, J., Hou, L., Zhou, J., Wang, D., Cui, Y., Feng, X., et al. (2022). Porcine circovirus type 2 vaccines: commercial application and research advances. *Viruses* 14:2005. doi: 10.3390/v14092005

Hou, Z., Wang, H., Feng, Y., Li, Q., and Li, J. (2019). A candidate DNA vaccine encoding a fusion protein of porcine complement C3d-P28 and ORF2 of porcine circovirus type 2 induces cross-protective immunity against PCV2b and PCV2d in pigs. *Virol. J.* 16, 57–58. doi: 10.1186/s12985-019-1156-2

Ilha, M., Nara, P., and Ramamoorthy, S. (2020). Early antibody responses map to non-protective, PCV2 capsid protein epitopes. *Virology* 540, 23–29. doi: 10.1016/j.virol.2019.11.008

Kang, S., Bae, S., Lee, H., Jeong, Y., Lee, M., You, S., et al. (2021). Porcine circovirus (PCV) genotype 2d-based virus-like particles (VLPs) induced broad cross-neutralizing antibodies against diverse genotypes and provided protection in dual-challenge infection of a PCV2d virus and a type 1 porcine reproductive and respiratory syndrome virus (PRRSV). *Pathogens* 10:1145. doi: 10.3390/pathogens10091145

Khan, M. A. (1984). Minipig: advantages and disadvantages as a model in toxicity testing. *J. Am. Coll. Toxicol.* 3, 337–342. doi: 10.3109/1091581840910439

Kim, K., and Hahn, T. (2021). Evaluation of novel recombinant porcine circovirus type 2d (PCV2d) vaccine in pigs naturally infected with PCV2d. *Vaccine* 39, 529–535. doi: 10.1016/j.vaccine.2020.12.013

Kim, K., Shin, M., and Hahn, T. (2020). Deletion of a decoy epitope in porcine circovirus 2 (PCV2) capsid protein affects the protective immune response in mice. *Arch. Virol.* 165, 2829–2835. doi: 10.1007/s00705-020-04831-z

Klinkenberg, D., Moormann, R., De Smit, A. J., Bouma, A., and De Jong, M. (2002). Influence of maternal antibodies on efficacy of a subunit vaccine: transmission of classical swine fever virus between pigs vaccinated at 2 weeks of age. *Vaccine* 20, 3005–3013. doi: 10.1016/S0042-207X(02)00283-X

Li, Y., Lin, Y., Xin, G., Zhou, X., Lu, H., Zhang, X., et al. (2020). Comparative evaluation of ELPylated virus-like particle vaccine with two commercial PCV2 vaccines by experimental challenge. *Vaccine* 38, 3952–3959. doi: 10.1016/j.vaccine.2020.03.060

Lim, J., Jin, M., Yoon, I., and Yoo, H. S. (2022). Efficacy of bivalent vaccines of porcine circovirus type 2 and *Mycoplasma hyopneumoniae* in specific pathogen-free pigs challenged with porcine circovirus type 2d. *J. Vet. Sci.* 23:e49. doi: 10.4142/jvs.21287

Opriessnig, T., Castro, A. M., Karuppanan, A. K., Gauger, P. C., Halbur, P. G., Matzinger, S. R., et al. (2019). A porcine circovirus type 2b (PCV2b)-based experimental vaccine is effective in the PCV2b-*Mycoplasma hyopneumoniae* coinfection pig model. *Vaccine* 37, 6688–6695. doi: 10.1016/j.vaccine.2019.09.029

Opriessnig, T., Meng, X., and Halbur, P. G. (2007). Porcine circovirus type 2–associated disease: update on current terminology, clinical manifestations, pathogenesis, diagnosis, and intervention strategies. *J. Vet. Diagn. Investig.* 19, 591–615. doi: 10.1177/10406387070190060

Opriessnig, T., O'Neill, K., Gerber, P. F., de Castro, A. M., Gimenéz-Lirola, L. G., Beach, N. M., et al. (2013). A PCV2 vaccine based on genotype 2b is more effective than a 2a-based vaccine to protect against PCV2b or combined PCV2a/2b viremia in pigs with concurrent PCV2, PRRSV and PPV infection. *Vaccine* 31, 487–494. doi: 10.1016/j.vaccine.2012.11.030

Opriessnig, T., Thacker, E. L., Yu, S., Fenaux, M., Meng, X., and Halbur, P. G. (2004). Experimental reproduction of postweaning multisystemic wasting syndrome in pigs by dual infection with *Mycoplasma hyopneumoniae* and porcine circovirus type 2. *Vet. Pathol.* 41, 624–640. doi: 10.1354/vp.41-6-62

Opriessnig, T., Xiao, C., Halbur, P. G., Gerber, P. F., Matzinger, S. R., and Meng, X. (2017). A commercial porcine circovirus (PCV) type 2a-based vaccine reduces PCV2d viremia and shedding and prevents PCV2d transmission to naive pigs under experimental conditions. *Vaccine* 35, 248–254. doi: 10.1016/j.vaccine.2016.11.085

Park, K. H., Oh, T., Yang, S., Cho, H., Kang, I., and Chae, C. (2019). Evaluation of a porcine circovirus type 2a (PCV2a) vaccine efficacy against experimental PCV2a, PCV2b, and PCV2d challenge. *Vet. Microbiol.* 231, 87–92. doi: 10.1016/j.vetmic.2019.03.002

Park, C., Seo, H. W., Han, K., and Chae, C. (2014). Comparison of four commercial one-dose porcine circovirus type 2 (PCV2) vaccines administered to pigs challenged with PCV2 and porcine reproductive and respiratory syndrome virus at 17 weeks postvaccination to control porcine respiratory disease complex under Korean field conditions. *Clin. Vaccine Immunol.* 21, 399–406. doi: 10.1128/CVI.00768-13

Peswani, A. R., Narkpuk, J., Krueger, A., Bracewell, D. G., Lekcharoensuk, P., Haslam, S. M., et al. (2022). Novel constructs and 1-step chromatography protocols for the production of porcine circovirus 2d (PCV2d) and circovirus 3 (PCV3) subunit vaccine candidates. *Food Bioprod. Process.* 131, 125–135. doi: 10.1016/j.fbp.2021.10.001

Salgado, R. L., Vidigal, P. M., de Souza, L. F., Onofre, T. S., Gonzaga, N. F., Eller, M. R., et al. (2014). Identification of an emergent porcine circovirus-2 in vaccinated pigs from a Brazilian farm during a postweaning multisystemic wasting syndrome outbreak. *Genome Announc.* 2:163. doi: 10.1128/genomea.00163-14

Seo, H. W., Park, C., Kang, I., Choi, K., Jeong, J., Park, S., et al. (2014). Genetic and antigenic characterization of a newly emerging porcine circovirus type 2b mutant first isolated in cases of vaccine failure in Korea. *Arch. Virol.* 159, 3107–3111. doi: 10.1007/s00705-014-2164-6

Tseng, Y., Hsieh, C., Kuo, T., Liu, J., Hsu, T., and Hsieh, S. (2019). Construction of a *Lactobacillus plantarum* strain expressing the capsid protein of porcine circovirus type 2d (PCV2d) as an oral vaccine. *Indian J. Microbiol.* 59, 490–499. doi: 10.1007/s12088-019-00827-9

Venegas-Vargas, C., Taylor, L. P., Foss, D. L., Godbee, T. K., Philip, R., and Bandrick, M. (2021). Cellular and humoral immunity following vaccination with two different PCV2 vaccines (containing PCV2a or PCV2a/PCV2b) and challenge with virulent PCV2d. *Vaccine* 39, 5615–5625. doi: 10.1016/j.vaccine.2021.08.013

Xiao, C., Halbur, P. G., and Opriessnig, T. (2012). Complete genome sequence of a novel porcine circovirus type 2b variant present in cases of vaccine failures in the United States. *J. Virol.* 86:12469. doi: 10.1128/jvi.02345-12

Zheng, G., Lu, Q., Wang, F., Xing, G., Feng, H., Jin, Q., et al. (2020). Phylogenetic analysis of porcine circovirus type 2 (PCV2) between 2015 and 2018 in Henan Province, China. *BMC Vet. Res.* 16, 1–10. doi: 10.1186/s12917-019-2193-1

frontiers | Frontiers in Microbiology

TYPE Original Research
PUBLISHED 23 January 2024
DOI 10.3389/fmicb.2024.1326696

OPEN ACCESS

EDITED BY
Taofeng Du,
Northwest A&F University, China

REVIEWED BY
Yani Sun,
Northwest A&F University, China
Ming Zhou,
Huazhong Agricultural University, China

*CORRESPONDENCE
Sheela Ramamoorthy
✉ sheela.ramamoorthy@ndsu.edu

RECEIVED 23 October 2023
ACCEPTED 10 January 2024
PUBLISHED 23 January 2024

CITATION
Ssemadaali M, Islam M-T, Fang W, Aboezz Z, Webb B and Ramamoorthy S (2024) Trans-replicase helper activity of porcine circoviruses promotes the synergistic replication of torque teno virus. *Front. Microbiol.* 15:1326696. doi: 10.3389/fmicb.2024.1326696

Trans-replicase helper activity of porcine circoviruses promotes the synergistic replication of torque teno virus

Marvin Ssemadaali[1], Md-Tariqul Islam[1,2], Wenjuan Fang[1], Zeinab Aboezz[1,3], Brett Webb[4] and Sheela Ramamoorthy[1]*

[1]Department of Microbiological Sciences, North Dakota State University, Fargo, ND, United States, [2]Department of Microbiology and Immunology, Faculty of Veterinary, Animal, and Biomedical Sciences, Sylhet Agricultural University, Sylhet, Bangladesh, [3]Department of Virology, Faculty of Veterinary Medicine, Benha University, Banha, Egypt, [4]Veterinary Diagnostic Laboratory, North Dakota State University, Fargo, ND, United States

While the primary pathogenic potential of torque teno viruses (TTVs) is yet to be defined, TTVs are often co-detected with other pathogens and are suspected of exacerbating clinical disease in coinfections. Swine TTVs (TTSuVs) enhance clinical signs of porcine circovirus type 2 (PCV2) in a gnotobiotic pig model. However, the mechanisms involved are unknown. In this study, we observed that co-culture of TTSuV1 and PCV1, and specifically supplementing TTSuV1 cultures with the PCV replicase protein in trans consistently resulted in higher levels of replication of TTSuV1 when compared to TTSuV1 cultured alone. Therefore, the hypothesis that the PCV replicase (rep) protein has trans-replicase helper activity for TTSuV1 was examined. Based on EMSA and reporter gene assays, it was determined that the PCV1 rep directly interacted with the TTSuV1 UTR. The TTSuV1 rep trans-complemented a PCV rep null mutant virus, indicating that the TTSuV1 and PCV1 replicase proteins supported the replication of both viruses. In mice, the administration of plasmids encoding the PCV1 rep and a TTSuV1 infectious clone resulted in the production of higher TTSuV1 genome copies in dually exposed mice when compared to singly exposed mice. Higher sero-conversion and lymphoid hyperplasia were also observed in the dually exposed experimental mice. Thus, this study provides evidence for trans-replicase activity of PCVs and TTVs as a novel mechanism of explaining enhanced viral replication in coinfections involving both viruses.

KEYWORDS

torque teno virus (TTV), co-infection, porcine circovirus (PCV), replicase, mice, EMSA, complementation, ELISA

1 Introduction

Torque teno viruses (TTVs) are diverse and ubiquitous commensals which colonize a wide range of mammalian species. While they were previously classified as a genus within the Circoviridae family, they were reassigned to a separate family called Anelloviridae in 2009 (Biagini, 2009; Lefkowitz et al., 2018). Whether TTVs act as primary pathogens is a topic of scientific debate. However, numerous epidemiological studies document a correlation between TTVs and a wide range of infectious and non-infectious disease conditions such as chronic

hepatitis C (Kawanaka et al., 2002), autoimmunity (Rezahosseini et al., 2019), cancer (Pan et al., 2018) and respiratory disease (Bal et al., 2022). In these studies, higher TTV loads were linked to more severe diseases and immunosuppression. TTVs also contaminate blood transfusion products and are a marker for tissue rejection in organ transplantation (Karimi et al., 2013).

Among the members of the Anelloviridae family, swine TTVs (TTSuVs) are the only members with demonstrated pathogenic potential in an experimental animal models (Krakowka and Ellis, 2008). In gnotobiotic pigs, coinfection of TTSuV1 with porcine circovirus type 2 (PCV2), the cause of post-weaning multi-systemic wasting disease syndrome in piglets, or porcine reproductive and respiratory disease syndrome virus (PRRSV) resulted in enhanced clinical signs due to PCV2 and PRRSV, respectively (Ellis et al., 2008; Krakowka et al., 2008). In previous studies we found that TTSuV1 is 85% more likely to be detected in morbid pigs than healthy pigs (Rammohan et al., 2012). Given TTSuVs possible zoonotic potential (Ssemadaali et al., 2016), the detection of TTVs in pork products and their role in exacerbating coinfections (Kekarainen et al., 2009, Karimi et al., 2013, Webb et al., 2020), understanding the molecular mechanisms by which TTVs can potentially enhance other infections or disease conditions becomes important.

Like circoviruses cloned, re-circularized viral genomic DNA or dimerized infectious clones (Fenaux et al., 2002) produce TTV specific signals in cell culture and pig models. However, sustained, or robust viral replication is not achieved (Kamahora et al., 2000; Kakkola et al., 2007; Huang et al., 2012). TTVs can be readily detected by PCR in naturally infected hosts, efficient laboratory culture has been a long-standing challenge. This observation supports the premise that efficient TTV replication is supported by factors acting in trans in natural infections. These factors could originate either from the host or coinfecting agents. As an analogous model linear, single stranded adeno-associated viruses (AAV's) are capable of independently replicating their own DNA. However, they require helper viruses such as adenovirus, herpes simplex virus and cytomegalovirus for efficient and productive replication. Promiscuous trans-replicase activity (Zhang et al., 2016) is one among several known molecular mechanisms involved in the interactions between dependoviruses and their helper viruses (Meier et al., 2020). Similarly, the replicase (rep) proteins of the non-pathogenic PCV1 and pathogenic PCV2 are highly conserved and are known to function interchangeably (Mankertz et al., 2003). Rep proteins of divergent ssDNA viral families share conserved structural features such as a nonanucleotide loop, endonuclease domains, and RCR motifs which are required for rolling circle replication of the viral genome (Mankertz et al., 2004). They even share commonalities with prokaryotic plasmid DNA replication machinery (Tarasova and Khayat, 2021). The largest TTV ORF, ORF1, encodes a multi-functional protein that serves as the capsid and also contains replicase related domains such as the rolling circle replication (RCR) motifs (Webb et al., 2020). To better understand the mechanisms by which TTSuV1 exacerbates clinical signs in pigs coinfected with TTSuV1 and PCV2 (Ellis et al., 2008; Krakowka et al., 2008), we herein explore hypothesis that the PCV rep protein has trans-replicase activity for TTSuV1 and promotes TTSuV1 replication. The findings described provide a possible mechanistic explanation for the observed increase in viral titers and pathogenicity in coinfections involving pathogenic PCVs and TTVs.

2 Materials and methods

2.1 Cells, viruses, and recombinant proteins

Porcine kidney cell line (PK15N, 005-TDV, National Veterinary Services Laboratory, Ames, IA, United States) (designated as PK15N throughout the document), PK-15 cells persistently infected with porcine circovirus type 1 (PCV1) (PK-15, CCL3-ATCC, Manassas, VA) (designated as PCV1 + PK15 cells throughout the document), and swine testicular cells (ST, ATCC, Manassas, VA) were used in the below described experiments. All reagents and PK15N and ST cells used were previously tested and found to be negative for TTSuVs and PCVs. Recombinant TTSuV1 (Gen Bank KT037083) and PCV2b 41513 (Gen Bank ALD62452) were rescued by transfection as previously described (Singh and Ramamoorthy, 2016a,b; Rakibuzzaman et al., 2021), with the exception that the genomes were dimerized to enable direct transfection and rescue without the need for excision and recircularization of the viral genome. In addition, a V5 tag encoding the amino acid sequence GKPIPNPLLGLDST was inserted into the 3′ end of the TTSuV1 ORF1 by overlap extension PCR and directional cloning to serve as a genetic and antigenic marker for the cloned TTSuV1 genomic DNA. The TTSuV1 ORF1 gene was cloned and expressed as described before (Singh and Ramamoorthy, 2016a,b). The PCV1 rep was amplified using forward primer 5′-CTGAggatgcGCCACCATGCCCAGCAAGAAGAATG-3′ and reverse primer 5′-AGCTctcgagGTAATTTATTTCATATGGAAA-3′ from the PCV1 + PK15 cell cultures. The amplified fragment was directionally cloned into a pcDNAV5-HisA mammalian expression vector (Thermo Fisher, Grand Island, NY), using the BamHI and XhoI restriction sites. The integrity of all the recombinant plasmid constructs was verified by restriction digestion and sequencing. All expressed proteins had a C-term V5 tag. Protein expression for the individual constructs was verified by transfection in PK15 and ST cells, using the TransIT-2020 (Mirus Bio, Madison, WI), following the manufacturer's instructions and immunofluorescence assays (IFAs), using specific antibodies.

2.2 Virus culture

To culture TTSuV1, PK15N or ST cells were cultured to 50% confluence in 6 well tissue culture plates in the presence of DMEM containing 10% FBS and 1% penicillin streptomycin and transfected or infected as previously described (Singh and Ramamoorthy, 2016a,b; Rakibuzzaman et al., 2021). To rescue recombinant TTSuV1, the dimerized genomic TTSuV1 DNA construct was used for transfection. The PCV1 + PK-15 cells were used to prepare PCV1 cultures. Virus cultures were quantified by the $TCID_{50}$ method and stored in aliquots at −80°C for further use. For flow cytometry cells were collected from duplicates of treatment and fixed with 4%PFA and stored at 4°C.

2.3 Viral detection by an immunofluorescence assay

As TTSuV1 and PCV1 are non-cytolytic, the presence of replicating virus or the expression of viral proteins was assessed by IFAs. Briefly, 50% confluent PK-15 or ST cells were infected or

transfected as previously described (Singh and Ramamoorthy, 2016a,b, Rakibuzzaman et al., 2021). After 48 h of incubation, the cells were washed in Hank's balanced salt solution (HBSS) (Corning, Manassas, VA) and fixed in ice cold acetone: methanol (1:1). Detection of the recombinant TTSuV1 virus or TTSuV1 ORF1 protein was achieved with a rabbit polyclonal hyperimmune serum collected from rabbits administered a synthetic peptide from the TTSuV1 ORF1 (RWRRRLGRRRRRYRK, position 6–20) (ProMab Biotechnologies, Richmond, CA). The specificity of the antibody was independently verified using previously a validated rabbit polyclonal anti-TTSuV1 ORF1 antibody (Huang et al., 2012) or a commercial mouse derived anti-V5 tag antibody (Thermo Fisher, Grand Island, NY). The rabbit polyclonal antibodies were used at a 1:200 dilution, and the monoclonal V5 antibody at a 1:500 dilution. The PCV1 ORF1 protein was detected using the V5 monoclonal antibody at 1:500 or polyclonal PCV1-specific swine serum at 1:200. Anti-rabbit, mouse or swine IgG conjugated to FITC (KPL, Gaithersburg, MD) was used as the secondary antibody at a 1:100 dilution for 45 min and slides were visualized in a fluorescent microscope.

2.4 Transfection of TTSuV1 infectious clone in PCV1 + PK15 cells

To determine if the presence of PCV1 enhances TTSuV1 replication, the dimerized TTSuV1 genome was transfected into PCV1 + PK15 cells as described above. PCV1 free PK15N cells transfected with the dimerized TTSuV1 genome were used as a control. The rescued TTSuV1 was serially passaged in PCV1 + PK15 and PK15N cells six times. The difference in viral replication between treatments was assessed by the $TCID_{50}$ method using the Reed and Muench (1938) formula (Figure 1(left)), by qPCR (Figure 1(middle)) and by flow cytometry (Figure 1(right)).

2.5 Replication patterns of TTSuV1 and PCV1 during coinfection *in vitro*

To determine the effects of coinfection with pre-titrated amounts of TTSuV1 and PCV1, PK15N and ST cells were separately cultured in 6-well plates to a confluence of 50%. Cultured cells were infected with 1 mL of PCV1 culture at 1×10^3 $TCID_{50}$/mL. The plates were incubated for 6 h at 37°C in a CO_2 incubator. The cells were then washed 5 times to remove non-adsorbed PCV1 and then overlaid with 1 mL of TTSuV1 culture which had been resuspended to 1×10^3 $TCID_{50}$/mL. After 24 h, the cells were washed 5× to remove non-adsorbed TTSuV1 and 2 mL of 2% FBS containing DMEM media was added to the cells. The coinfected cells were incubated for 72 h at 37°C in a CO_2 incubator. Cells infected with TTSuV1 only or PCV1 only and uninfected cells were included as controls. After the 72 h incubation, the plates were frozen, and viral cultures were collected as described above. The difference in viral replication between treatments was assessed by the $TCID_{50}$ method using the Reed and Muench (1938) formula (Figure 2A), by qPCR (Figure 2B) and by flow cytometry (Figure 2C).

2.6 Role of PCV1 rep protein in TTSuV1 replication *in vitro*

To assess whether the PCV1 rep protein played a role increasing TTSuV1 titers in co-cultures, the procedures described above were repeated with modification. Briefly, PK15N and ST cell-lines were grown to 50% confluence in $25cm^3$ flask. The cultured cells were co-transfected with 2 μg of circularized TTSuV1 genome and 1 μg of plasmid DNA expressing PCV1 replicase, using TransIT-2020 (Mirus Bio, Madison, WI), following the manufacturer's instructions. Cells transfected with the individual constructs and untransfected cells were used as controls. Effective transfection was assessed by IFA using virus or protein specific antibodies. After a 72 h incubation, the flasks were frozen, and viral cultures were collected as described above. he difference in viral replication between treatments was assessed by the $TCID_{50}$ method using the Reed and Muench (1938) formula (Figure 3A), by qPCR (Figure 3B) and by flow cytometry (Figure 3C).

2.7 TTSuV1-specific qPCR

Samples obtained from the experiments described above were tested by a TTSuV1-specific qPCR in duplicate. The qPCR targets a unique region within the ORF1 gene (GenBank accession KT037083, position 1,563–1,565 bps). Briefly, DNA was extracted with the

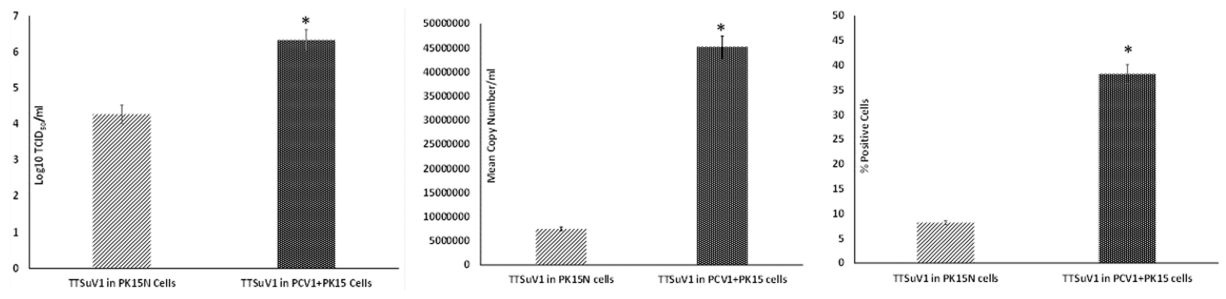

FIGURE 1
Enhanced replication of TTSuV1 in PCV1 + PK15 cells: PK15N or PCV1 + PK15 cells were transfected with the TTSuV1 dimerized infectious clone. TTSuV1 replication was measured as $log_{10}TCID_{50}$ (left), by qPCR (middle) and by flow cytometry (right). Light slanted lines—TTSuV1 dimerized infectious clone transfected in PK15N cells, dark bar—TTSuV1 dimerized infectious clone transfected in PCV1 + PK15N cells. *Significantly different from the PK15N control, $p \leq 0.05$ (student *t*-test).

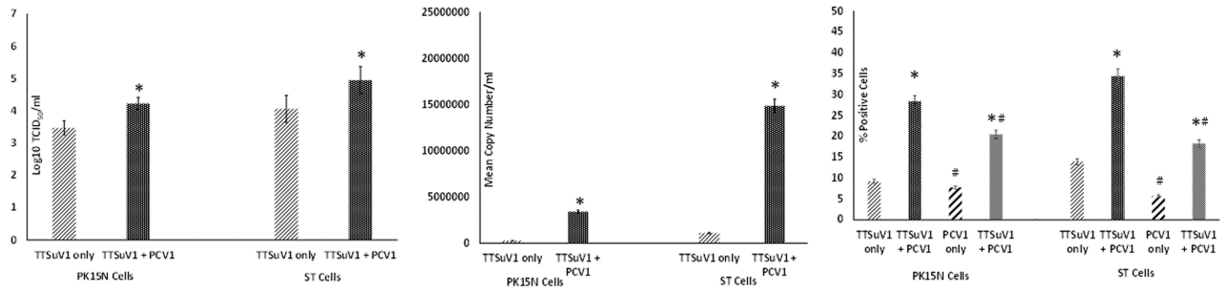

FIGURE 2
Enhanced replication of TTSuV1 and PCV1 during coinfection *in vitro*: PK15N or ST cells were infected with 1×10^3 $TCID_{50}$ of TTSuV1 only or coinfected with 1×10^3 $TCID_{50}$ TTSuV1 and PCV1 each. TTSuV1 replication was measured as $log_{10}TCID_{50}$ (left), by qPCR (middle) and by flow cytometry (right). Light slanted lines—cells infected with TTSuV1 only, dark bar—cells coinfected with TTSuV1 and PCV1, right panel. #Stained with an anti-PCV1 antibody, dark slanted lines—cells infected with PCV1 only, grey dotted bar—cells coinfected with TTSuV1 and PCV1. *Significantly different from the PK15N control, $p \leq 0.05$ (student *t*-test).

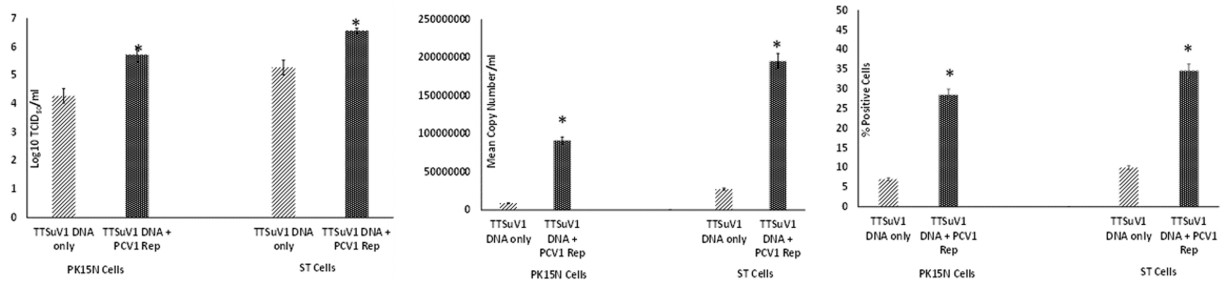

FIGURE 3
Enhanced replication of TTSuV1 by over-expressed supplementation of PCV1 rep *in vitro*: PK15N or ST cells were transfected with the TTSuV1 infectious clone alone or in combination with a plasmid encoding the PCV1 rep. TTSuV1 replication was measured as $log_{10}TCID_{50}$ (left), by qPCR (middle) and by flow cytometry (right). Light slanted lines—cells transfected with the TTSuV1 infectious clone only, dark bar—cells transfected with the TTSuV1 infectious clone and plasmid encoding the PCV1 rep, *Significantly different from the PK15N control, $p \leq 0.05$ (student *t*-test).

QIAamp DNA Mini Kit (Qiagen, Valencia, CA, United States) following manufacturer's instructions and eluted into a 50 µL volume. Twenty-five nanogram of template DNA was tested using the QuantiFast Probe PCR Mix (Qiagen United States) with 0.2 µM probe (56 FAM/CACACAACACAGCAGGAA/3IABkFQ) and 0.4 µM primers (5′-TACCCGGCTTTGCTTCGACAGTG-3′ and 5′GCCATAGATTTCTAGCGATCCCAATTGCG-3′). The qPCR program consisted of 95°C for 5 min, followed by 35 cycles of denaturation at 95°C for 15 s, annealing for 57°C for 30 s and extension for 72°C for 30 s, and 5 min holding in a thermocycler (CFX96 Touch, Bio-Rad, Hercules, CA, United States). Each qPCR run included a no template control, plasmid positive control and appropriate standard curve to convert Ct values to copy numbers. The qPCR was optimized to a lowest detection limit of 200 copies/mL (Figures 1B, 2B, 3B).

2.8 Flow cytometry

Cells harvested from the above-described experiments were fixed and permeabilized (fixation/permeabilization solution™ BD bioscience, Franklin lakes, NJ). Primary antibody working concentrations were optimized by titration. To detect TTSuV1 antigen, intracellular staining was carried out for 45 min at room temperature with rabbit polyclonal TTSuV1 Ab anti-peptide antibody at a 1:200 dilution. Detection was achieved with FITC conjugated anti-rabbit IgG (KPL, Gaithersburg, MD) at a 1:100 dilution in 2% BSA^+ permeabilization/wash buffer (BD Perm/Wash™, BD bioscience, United States) for 30 min at RT. For the coinfection experiment, cells were also stained with a PCV1-specific polyclonal swine antibody and detected using anti-swine IgG conjugated to FITC (KPL, Gaithersburg, MD) at 1:100 dilution. Stained cells were analyzed in a Cytoflex S flow cytometer (Beckman Coulter, Brea, CA). Single stained and rabbit IgG isotype controls were included in all assays. A high-speed cell sorter was used to count 100,000 events with an appropriate gating strategy. Dead cells, debris and doublets were excluded from analysis. TTSuV1 infected cells were identified by plotting the counts of TTSuV1 antigen positive cells detected by FITC staining against the forward scatter (FSC) height, resulting in an upward shift in fluorescent intensity distribution in dot plots or a lateral shift from the uninfected control cells in a histogram (Figure 4). Data was analyzed using the CytExpert 1.2 software (Beckman Coulter) to determine differences in intracellular fluorescent signal between treatments (Figures 1C, 2C, 3C).

2.9 Transmission electron microscopy

To confirm the successful assembly and production of recombinant TTSuV1 particles, 50 µL of rescued virus was used to coat a 300-mesh carbon coated palladium grid for 10 min. The coated

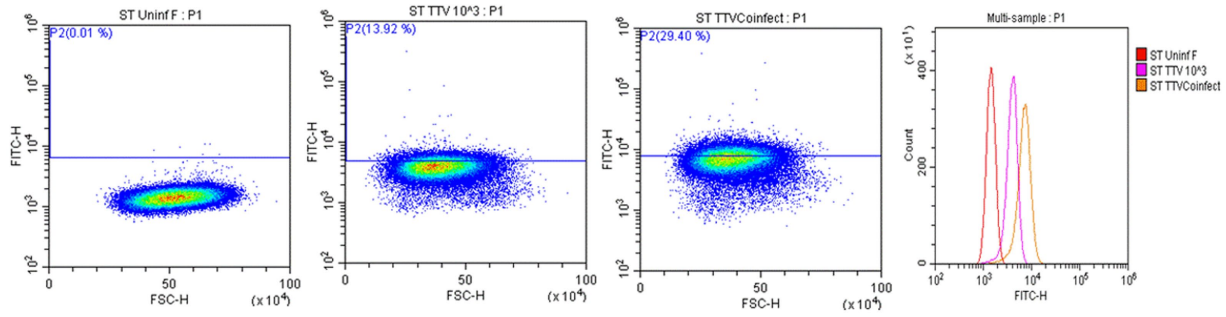

FIGURE 4
Flow cytometry for the detection of TTSuV1 antigen. Representative images of TTSuV1 infected ST cells stained with TTSuV1-specific anti-peptide rabbit polyclonal antibody. Dot plots—*X* axis—FSC-H, *Y* axis—FITC-H or fluorescent signal due to intracellular TTSuV1 antigen. The horizontal line indicates the gate, numbers in parenthesis indicate the percentage of cells within the gated area. Left dot plot—untreated ST cells, Middle dot plot—ST cells infected with 1×10^3 $TCID_{50}$/mL of TTSuV, right dot plot—ST cells coinfected with 1×10^3 $TCID_{50}$/mL of PCV1 and TTSuV1. On the dot plots, an increase in detection of intracellular antigen is indicated by an upward shift on the *Y* axis. Far right image—overlay histogram depicting the effect of coinfection. *X* axis—FITC H, *Y* axis—counts. Red peak—uninfected ST cells, pink peak—ST cells infected with TTSuV1 only, yellow peak—ST cells coinfected with PCV1 and TTSuV1. On the overlay histogram, an increase in detection of intracellular FITC stained TTSuV1 antigen is indicated by a lateral shift on the *X* axis.

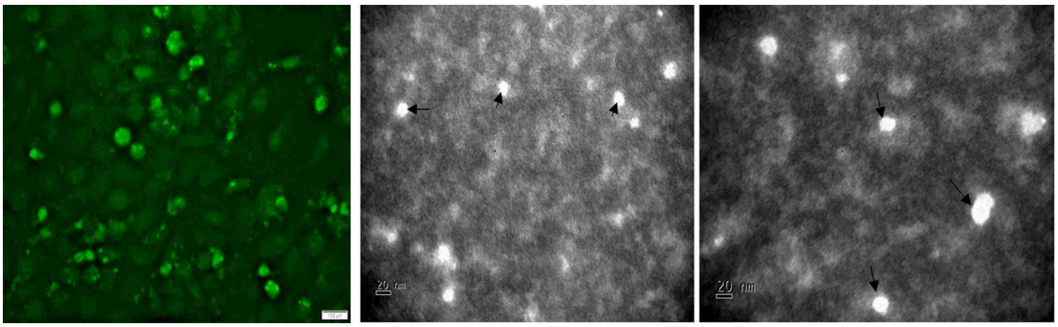

FIGURE 5
Detection of TTSuV1 virions and PCV1 replicase protein. Left—TTSuV1-specific, intranuclear fluorescence detected by an anti-peptide rabbit polyclonal antibody in an immunofluorescence assay (20× magnification). Middle and right—electron micrographs of TTSuV1 virions after the first passage in ST cells (scale bar = 20 nm).

grid was then negatively stained with 2% phosphotungstic acid (PTA) (Brenner and Horne, 1959) and examined by a JEOL JEM-100CX II transmission electron microscope (Figure 5).

2.10 Electrophoretic mobility shift assay

The physical interaction between the PCV1 Rep protein and the TTSuV1 intergenic region untranslated region (UTR) (Figure 6 left) was examined by an electrophoretic mobility shift assay (EMSA). Either a biotin-labelling (Pierce 3′ End DNA labelling kit, Thermo Fisher Scientific, Grand Island, NY) or a SYBR based kit (Electrophoretic Mobility-Shift Assay Kit, with SYBR™ Green & SYPRO™ Ruby EMSA stains, Thermo Fisher Scientific, Grand Island, NY) was used, following manufacturer's instructions. Briefly, a 210 bp fragment of the TTSuV1 UTR, containing the origin of replication (−76 to +130) and a putative stem-loop signal (Figure 6 left) was amplified by PCR (forward primer: TGATTGGAC GGGAGCTCAAGTC and reverse primer: TCCGCTCAGC TGCTCCTGC). The PCV1 and TTSuV1 replicase proteins were expressed by transfection of HEK cells with plasmids encoding the respective proteins. Concentrated nuclear protein was harvested as previously described (Luo et al., 2014). Protein concentration was measured by the BCA method. Extracted protein was immediately aliquoted and stored at −80°C until use.

For hybridization of the DNA to proteins, varying concentrations of DNA were mixed with 5 µL of protein extracts of TTSuV1 or PCV1 replicase protein, in the presence the respective kit hybridization buffers, following manufacturer's instructions. Poly (d*A*·d*T*) and Poly(d*I*·d*C*) were used as binding competitors in the reaction since the UTR amplicon has high GC content. The reaction was then incubated at room temperature for 20 min. All EMSA reaction products were separated on a 6% Native polyacrylamide gel at 100 V for 1.5 h. TTSuV1 UTR DNA only or untransfected cell extracts incubated with DNA were included as a negative control, while TTSuV1 DNA and TTSuV1 replicase proteins were included as a positive control. The test group included the PCV1 replicase protein and TTSuV1 UTR DNA. The resolved complexes in the gel were immediately transferred onto a nylon membrane, using a semi-dry transfer system with an ice cooling system at 380 mA for 35 min. The membrane was cross-linked

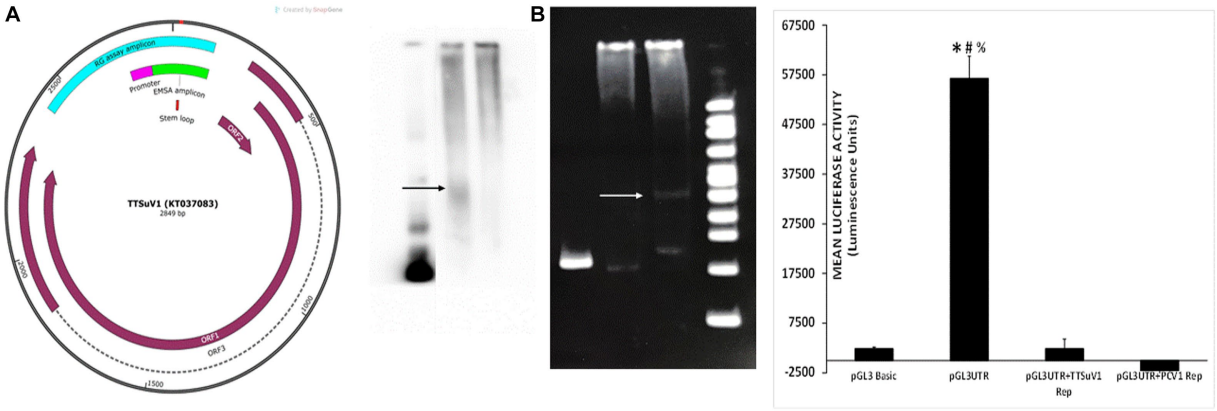

FIGURE 6
Physical interaction of PCV1 rep with the TTSuV1 untranslated region. Left—genome map of TTSuV1 (Gen Bank accession—KT037083). Brown arrows—identified open reading frames (ORFs), dashed lines—exons, green—amplicon for the EMSA, pink—putative promoter region, teal—amplicon for the reporter gene assay, red—stem loop. Middle panel—electrophoretic mobility shift assay (EMSA). **(A)** Interaction of the biotin labelled TTSuV1 UTR DNA with the PCV1 rep protein detected by chemiluminescence. Arrow shows the upward shift compared to TTSuV1 UTR DNA alone. Lane 1—TTSuV1 UTR DNA only, Lane 2—TTSuV1 UTR DNA hybridized to PCV1 rep, Lane 3—Untransfected negative control cell extract. **(B)** Interaction of the TTSuV1 UTR DNA with the putative replicase protein encoded by TTSuV1 ORF1 as detected by a SYBR green EMSA kit. Arrow shows the upward shift compared to TTSuV1 UTR DNA alone. Lane 4—TTSuV1 UTR DNA only, Lane 5—Untransfected negative control cell extract, Lane 6—TTSuV1 UTR DNA hybridized to TTSuV1 rep. Lane 7—100 bp DNA ladder. Right—reporter gene assay: activity of PCV1 rep and TTSuV1 rep in binding to a promoter located in the TTV UTR. Cells were transfected with either the empty pGL3 basic plasmid, or TTSuV1 UTR region cloned in pGL3 basic (pGL3UTR), or pGL3UTR and TTSuV1 rep expression plasmid or pGL3UTR and PCV1 rep expression plasmid. *X* axis—treatments, *Y* axis—luciferase activity in luminescence units. *Significantly different from pGL3UTR + TTSuV1 rep, $p \leq 0.05$ (student *t*-test). #Significantly different from pGL3UTR + PCV1 rep, $p \leq 0.05$ (student *t*-test). #Significantly different from pGL3 basic, $p \leq 0.05$ (student *t*-test).

before staining. The protein: DNA interaction was detected by either chemiluminescence (Light Shift Chemiluminescence EMSA kit, Thermo Fisher Scientific, Grand Island, NY) or SYBR following the manufacturer's instructions (Figure 6 middle) and images obtained (FluorChem FC2 Imaging system, Alpha Innotech, San Leandro, CA).

2.11 Reporter gene assay

To test the hypothesis that the viral rep proteins can potentially influence viral gene expression by interacting with a TTSuV1 promoter located in the TTSuV1 UTR, a 566 bp segment (Figure 6 right) including the TTSuV1 UTR and the putative promoter which was identified based on published literature (Suzuki et al., 2004; Liu et al., 2016), was cloned into a promoter-less reporter gene system (pGL3 basic, Promega, Madison, WI). The primers used for cloning included CGATgctagcAATCTATGGCCGAGCATGGG and ATGCaagcttTCCGCTCAGCTGCTCCTGC. The cloned region covered −432 to +130 bps adjacent to the TATA box (Figure 6 left). The construct was designated pGL3UTR (pGL3 basic containing TTSuV1 UTR) and validated by sequencing. Vero cells were co-transfected (TransIT-2020, Mirus Bio, Madison, WI), following the manufacturer's instructions, as described above. The treatments consisted of pGL3UTR + TTSuV1 ORF1, pGL3UTR + PCV1 ORF1. The controls included the pGL3 basic alone (no promoter) as negative control, pGL3UTR as a baseline control, and pGL3UTR^{+} empty V5His plasmid as a background control for the plasmid backbone in which the TTSuV1 and PCV1 rep were expressed. Five replicates of each treatment were tested. After 72 h of incubation at 37°C, luciferase activity was assessed (Bright-Glo kit system, Promega, Madison, WI), following manufacturer's instructions, and the luminescence readings recorded (Synergy luminometer, Agilent Technologies, Santa Clara, CA). The baseline luciferase activity values for the empty V5HisA backbone of the mammalian expression vector were deducted from the experimental treatments before data analysis (Figure 6 right).

2.12 Trans-complementation of PCV2 rep by TTSuV1 rep

The start codon of the PCV2 replicase protein was deleted by site directed mutagenesis (*Q5 Site-Directed Mutagenesis Kit*, Thermo Fisher Scientific, Grand Island, NY), in the backbone of a cloned monomeric genomic copy of PCV2b strain 41,513 (Gen Bank KR816332) (Constans et al., 2015). The deletion was confirmed by sequencing and the functional absence of viral replication was confirmed by IFA by transfecting PK15 cells with the re-circularized mutated PCV2b genomic DNA (Figure 7, top middle). To determine if the mutation could be trans-complemented by the TTSuV1 rep, the mutated PCV2b genomic DNA was co-transfected with either the TTSuV1 ORF1 expression plasmid or the dimerized copy of the TTSuV1 genome, as described above. As PCV1 and PCV2 reps are interchangeable, co-transfection with the PCV1 rep expression plasmid served as a positive control for complementation. Effective rescue and replication of PCV2 due to complementation was assessed by an IFA, using a PCV2 specific antibody (Figure 7). Transfection controls for the TTSuV1 ORF1 and dimerized TTSuV1 genome were checked by IFA using a TTSuV1 specific antibody. Untreated cells were used as a negative control.

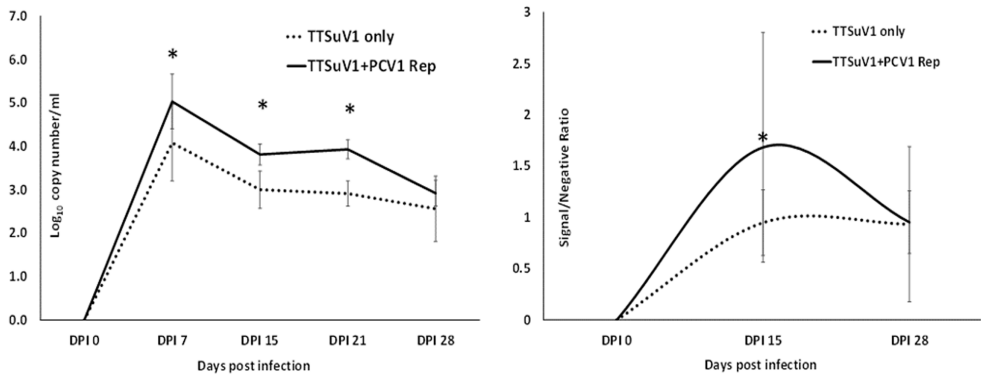

FIGURE 7
Trans-complementation of the PCV2 replicase protein: immunofluorescence assay (IFA) to detect PCV2 using a PCV2-specific antibody. Effective PCV2 rescue and replication is indicated by apple green, nuclear fluorescence. Blue—DAPI stained nuclei. Top left—uninfected cell control, top middle—cells transfected with the PCV2b ORF1 null mutant, top right—cells transfected with the PCV1 ORF1 (rep) expressing plasmid, bottom left—cells co-transfected with the PCV2b ORF1 null mutant and TTSuV1 dimerized infectious clone, bottom middle—cells co-transfected with the PCV2b ORF1 null mutant and plasmid expressing PCV1 ORF1, bottom right—cells co-transfected with the PCV2b ORF1 null mutant and plasmid expressing TTSuV1 ORF1.

2.13 Effect of PCV1 replicase on TTSuV1 replication in mice

All animal experimentation was carried out in compliance with the N. Dakota State University IACUC regulations. To determine if the presence of PCV1 rep will enhance TTSuV1 replication *in vivo*, 24 2 weeks-old, male and female C57/BL6 mice were administered treatments as follows: Group I—300 μL PBS, 50 μL i/n and 250 μL i/m, $N = 4$, Group II—50 μg of plasmid DNA encoding the PCV1 rep in a 300 μL volume, 50 μL i/n and 250 μL i/m, $N = 4$, Group III—50 μg of plasmid DNA encoding the TTSuV1 dimerized genome in a 300 μL volume, 50 μL i/n and 250 μL i/m, $N = 8$, Group IV—50 μg of plasmid DNA encoding the PCV1 rep and TTSuV1 dimerized genome each in a total of 300 μL volume at 50 μL i/n and 250 μL i/m, $N = 8$. Group III and Group IV mice were administered the TTSuV1 dimerized plasmid 24 h after administration of the PCV1 rep plasmid. The mice were observed daily for any signs of physical abnormalities. Whole blood was collected on day 0, 7, 15, 21 and 28 post inoculation to assess TTSuV1 genome copy numbers by qPCR. Serum was collected on day 0, 15, 28 post infection to assess antibody responses to TTSuV1 by ELISA. Samples were assessed in duplicate by qPCR using DNA extracted with the QIAamp DNA blood mini-Kit (Qiagen, Valencia, CA, United States), essentially as described above (Figure 8—left). Half the number of mice in each group were euthanized on day 15 and the remaining mice on day 30 post exposure. Liver, kidney, spleen, heart, lungs, large intestine, and ileum were fixed in 10% formaldehyde for histopathological analysis.

2.14 TTSuV1 ELISA

The measurement of antibody responses to TTSuV1 was carried out essentially as described previously (Ssemadaali et al., 2016). Briefly, 96 well ELISA plates (High bind microplates, Corning®, NY) were coated with 50 μL of purified recombinant TTSuV1 ORF2 antigen (1:100,000 dilution) in carbonate coating buffer (pH 9.6), overnight at room temperature. The coated plates were washed with PBST and blocked with a commercial block (General block, ImmunoChemistry Technologies, Bloomington, MN) containing 2% BSA and 2% normal goat serum for 2 h at 37°C. The experimental mouse sera were diluted to 1:10 in PBST containing 2% BSA dilution and 50 μL volumes were added to the plate. The plates were incubated for 1 h at 37°C. Detection was achieved using a goat anti-mouse HRPO-conjugate (KPL, Gaithersburg, MD) at a 1:2500 dilution for 45 min at 37°C following incubation with the TMB substrate (KPL, Gaithersburg, MD). The reaction was stopped after 5 min by adding 1 M HCl solution. Plates were read at 450 nm using ELISA plate reader (Elx800 reader, BioTek Instruments, Inc., Winooski, VT). Samples were assessed in three independent assays in duplicate (minimum 4 values each as some samples were exhausted). Day 0 samples were used to obtain the mean baseline for negative samples. Data across each independent assay was normalized using the negative control. The optical density values were expressed as a signal to negative ratio after reduction of the background (Figure 8—right).

2.15 Assessment of histopathological lesions

The mice were examined for any gross changes to organs during necropsy. Sections of lung, liver, spleen, pancreas, kidney, and intestines were stained by hematoxylin and eosin following the standard operating procedures of the *N*. Dakota State University Veterinary Diagnostic Laboratory. The sections were scored for microscopic lesions in a blinded fashion by a board-certified pathologist. Lymphoid hyperplasia and extramedullary hematopoiesis in the spleen were assessed. The scoring system used to grade lymphoid hyperplasia was as follows: Marked decrease =2, moderate decrease =2, mild decrease =3, normal =4, mild increase =5, moderate increase =6, marked increase =7. Extramedullary hematopoiesis was scored as follows: normal =1, mild =2, moderate =3, marked =4 (Figure 9).

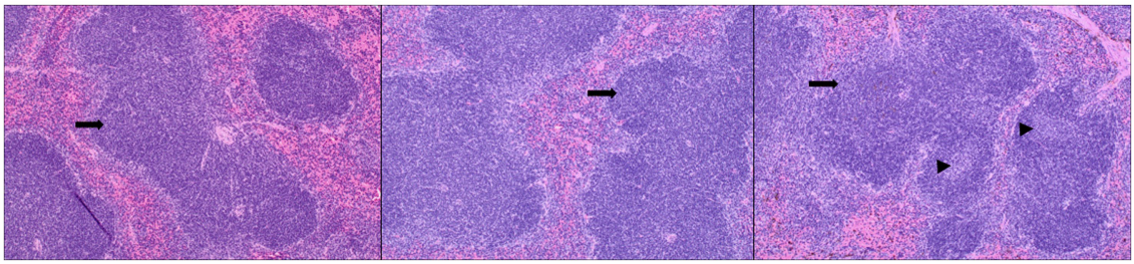

FIGURE 8
Replication of TTSuV1 in mice. Left—copy numbers of TTSuV1 DNA as detected in whole blood by a TTSuV1-specific qPCR assay. *X* axis—days post infection, *Y* axis—$\log_{10}$ copy number/mL. Solid line—mean values for mice administered TTSuV1 infectious clone and plasmid encoding the PCV1 replicase. Dotted line—mean values for mice administered TTSuV1 infectious clone alone. Right—antibody responses in mice. TTSuV1-specific IgG responses measured by an ELISA. Solid line—mean values for mice administered TTSuV1 infectious clone and plasmid encoding the PCV1 replicase. Dotted line—mean values for mice administered the TTSuV1 infectious clone alone. *X* axis—days post infection, *Y* axis—signal/negative ratio. *Significantly different from the single infection group, $p \leq 0.05$ (student *t*-test).

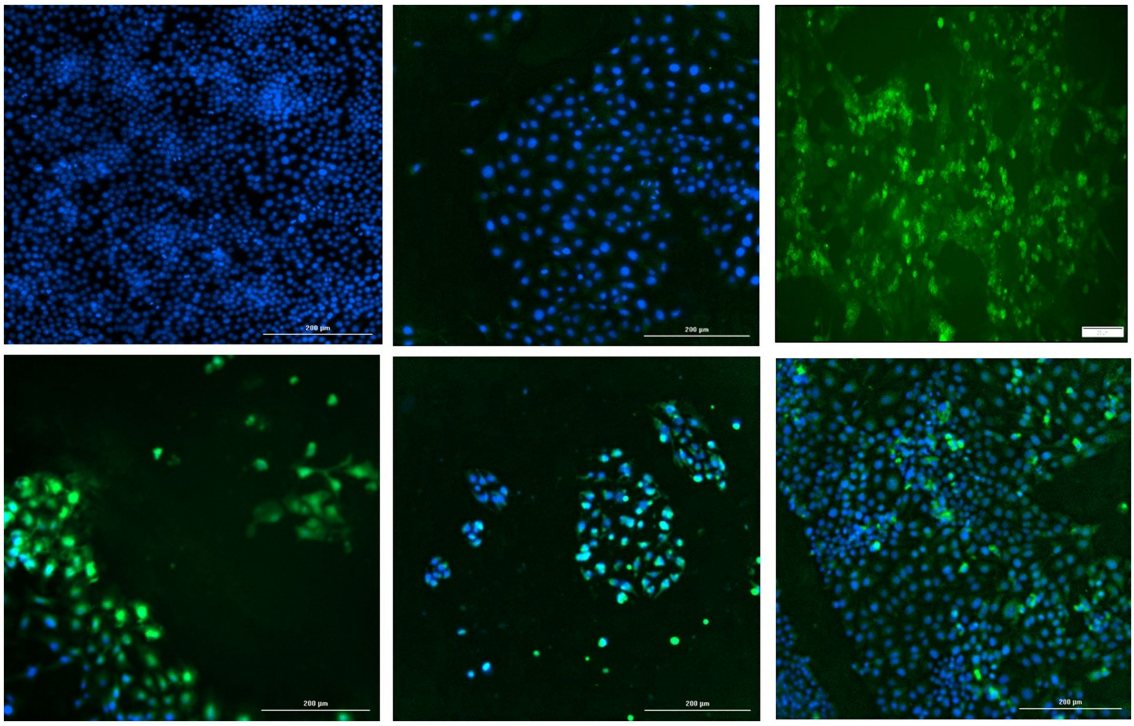

FIGURE 9
Splenic lesions in infected mice: representative images of H&E-stained sections of mouse spleen. Left—untreated mice, middle—mice administered the TTSuV1 infectious clone alone demonstrating mild lymphoid hyperplasia, right—mice administered both the TTSuV1 infectious clone and PCV1 rep encoding plasmid DNA demonstrating moderate lymphoid hyperplasia. No differences in extramedullary hematopoiesis were detected. Arrows—white pulp, arrowheads—germinal center development. magnification-100×.

2.16 Statistical analysis

Data analysis was carried out using Microsoft excel or Minitab 19 (Minitab, State College, PA). Following assessment for normal distribution, significance levels were set at $p < 0.05$ for all tests. The ELISA, qPCR, luminescence and histology data were analyzed by the student's *t*-test. The figures and graphs included depict average or consolidated values with standard deviations and statistical significance for differences between test groups.

3 Results

3.1 The presence of PCV1 or PCV1 rep protein enhances TTSuV1 replication

To determine whether PCV1, or specifically the PCV1 rep protein, can increase TTSuV1 titers in cell culture, PK15N or ST cells were either co-infected with PCV1 and TTSuV1 or co-transfected with a recombinant TTSuV1 infectious clone and plasmid expressing the PCV1 rep. Three different quantification techniques were used to

quantify virus; $log_{10}TCID_{50}$ to measure replicative TTSuV1 (Figure 1 left, Figure 2 left, and Figure 3 left), a TTSuV1-specific qPCR to measure viral genome copy numbers (Figure 1 middle, Figure 2 middle, and Figure 3 middle) and flow cytometry to measure intracellular TTSuV1 antigen (Figure 1 right, Figure 2 right, and Figure 3 right).

Transfection of the dimerized TTSuV1 genome in PCV1 + PK15 cells resulted in a significantly higher replication of TTSuV1 compared to transfection in PK15N cells, indicating that the presence of PCV1 supported the replication of TTSuV1 (Figure 1). Further, the viability of the rescued TTSuV1 was sustained without a loss of titer for 10 serial passages in PCV1 + PK-15 cells but not in the PCV1 negative PK15 N cells (data not shown), as previously observed by others (Huang et al., 2012). To further confirm the results, PK15N and swine testicular (ST) cells were coinfected with pre-titrated and equal amounts of PCV1 and TTSuV1. The coinfected cells had significantly higher TTSuV1 titers compared to singly infected cells (Figure 2). To specifically determine if the PCV1 rep played a role in enhanced TTSuV1 replication in coinfections, possibly via trans-replicase activity, the PCV1 replicase protein was transiently over-expressed in PK15N and ST cells, in combination with the dimerized TTSuV1 genome. Consistent with previous observations, higher levels of TTSuV1 replication were detected in cells co-transfected with the PCV1 rep and TTSuV1 infectious clone compared to cells singly transfected with the TTSuV1 infectious clone alone (Figure 3). The observed results were consistent across the three different quantification techniques, i.e., $log_{10}TCID_{50}$, qPCR and flow cytometry. Overall, ST cells supported higher levels of TTSuV1 replication than PK-15 cells across the treatment conditions. Reciprocally, measurement of PCV1 intracellular antigen by flow cytometry showed that PCV1 antigen detection was also significantly higher in the presence of TTSuV1 (Figure 2 right, treatments indicated by a #). Untransfected or uninfected cells remained clear of specific signals for all experiments. Representative images for data acquisition by flow cytometry are provided in Figure 4. The specificity of the TTSuV1 anti-peptide rabbit antibodies used was independently verified with previously validated antibodies (Huang et al., 2011) (Figure 5 left). The rescue of structurally intact TTSuV1 was further confirmed by the presence of approximately 20-25 nm sized icosahedral particles by electron microscopy (Figure 5 middle and right).

3.2 The PCV1 replicase protein interacts with the TTSuV1 UTR region

Exploration of the physical interaction of the PCV1 replicase protein with the intergenic TTSuV1 UTR region (Figure 6 left) by an electrophoretic mobility shift assay (EMSA), showed that the PCV1 rep colocalized with the TTSuV1 UTR, as indicated by an upward shift in the sample containing both the TTSuV1 UTR DNA and PCV1 rep protein when compared to the sample with the TTSuV1 UTR DNA alone (Figure 6A middle). As expected, the TTSuV1 rep positive control and was found to bind to the TTSuV1 UTR DNA, as indicated by an upward shift (Figure 6B middle) compared to the TTSuV1 DNA only control.

As the TTSuV1 UTR is believed to contain a putative promoter (Figure 6 left), the possible interaction of the PCV1 and TTSuV1 rep proteins with the promoter was explored using a luciferase-based reporter gene assay. When the cloned reporter gene constructed containing the UTR fragment (pGL3UTR) was transfected into Vero cells, strong promoter activity was detected luciferase activity (Figure 6 right), while transfection of the empty control pGL3 basic plasmid did not. However, when a mammalian protein expression plasmid, encoding either the PCV1 rep or TTSuV1 ORF1 proteins was co-transfected along with the pGL3UTR plasmid, the promoter activity was completely abrogated, indicating that both TTSuV1 and PCV1 rep proteins bound with very high affinity to the UTR DNA, out competing the binding of the cellular transcription factors that stimulated the reporter gene expression (Figure 6 right).

3.3 The TTSuV1 ORF1 product trans-complements a PCV2 replicase null mutant

To determine if the TTSuV1 and PCV reps can function interchangeably, the start codon of the rep gene was deleted in a PCV2b infectious clone by site directed mutagenesis. As expected, deletion of the ATG of the rep gene resulted in abrogation of viral replication in cells transfected with the mutated PCV2b infectious clone, as assessed absence of green, fluorescent signals by an IFA (Figure 7 top middle). However, co-transfection of the mutated PCV2b infectious clone with either the dimerized TTSuV1 infectious clone (Figure 7 bottom left), or a plasmid encoding the PCV2 ORF1 (Figure 7 bottom middle) or a plasmid encoding the TTSuV1 ORF1 (Figure 7 bottom right) trans-complemented the silenced PCV2b rep and resulted in successful rescue of PCV2b as evidenced by apple green nuclear fluorescence in IFAs.

3.4 PCV1 replicase increases TTSuV1 genome copy numbers in mice

To determine if the presence of PCV1 rep will enhance TTV replication *in vivo*, mice were administered the TTSuV1 infectious clone alone or in combination with the PCV rep encoding plasmid. A comparison of the TTSuV1 genome copy numbers by qPCR showed that mice in the dually exposed group had higher copy numbers of TTSuV1 DNA in all the time points tested. The difference was statistically significant at days post exposure 7, 15 and 21 but not at day 28. TTSuV1 DNA was not detected in the control mice administered PBS or DNA encoding the PCV1 replicase alone (Figure 8 left). When antibody responses against TTSuV1 were measured by ELISA the rate and magnitude of seroconversion was greater at 15 days post-exposure in the dually exposed mice when compared to the mice inoculated with TTSuV1 DNA alone (Figure 8 right). Antibody levels in both experimental groups were similar by 28 days, correlating with the kinetics of viral replication observed by qPCR (Figure 8). The expression of the PCV1 rep protein in mice was verified by the detection of antibody responses against the PCV1 rep using an immunofluorescence assay (data not shown).

The primary observable microscopic lesions in the experimental mice consisted of splenic lymphoid hyperplasia (Figure 9). The mean scores were slightly higher in the co-inoculated group (DPI 15–5.5 ± 0.58, DPI 30–5.67 ± 0.58) compared to the singly inoculated group (DPI 15–5.25 ± 0.50, DPI 30–5.25 ± 0.50). However, the

differences were not statistically significant. Consistent microscopic lesions or significant gross changes were not observed in other major organs.

4 Discussion

While the extensive epidemiological association of TTVs with a variety of infectious and non-infectious disease conditions is well documented in published literature, current understanding of the mechanisms involved is limited, likely due to the difficulty in culturing TTVs in the laboratory and a lack of standardized animal models (Kekarainen and Segales, 2012, Spandole et al., 2015, Webb et al., 2020). We and others have observed that transfection of TTSuV genomic DNA in cells results in viral protein production and infection, but there is progressive loss of viability of the rescued virus (Huang et al., 2012; Singh and Ramamoorthy, 2016a,b). The serendipitous observation that high TTSuV1 titers were produced when a dimerized TTSuV1 infectious clone was accidentally transfected into PCV1 + PK15 cells instead of the PCV1 negative PK15N cells, prompted the exploration of synergies in the mechanisms of replication of PCVs and TTSuV1 in this study.

Coinfection of adeno associated virus (AAV), a dependovirus, with its helper viruses is reported to reduce the helper virus's replication (Meyers et al., 2001). However, in this study, the positive effect on replication appeared to be reciprocal for PCVs and TTSuV1 as increased PCV1 signals were observed in coinfected cells by flow cytometry (Figure 2C). The intracellular TTSuV1 or PCV1 antigen measured by flow cytometry very likely represented viable virus and similar flow cytometry-based strategies have been used to measure viral replication for other viruses (Shen et al., 2002). The trend of observations being consistent between the 3 different quantification methods used (Figures 1–3) provides robust validation for the conclusion that PCV1, and specifically PCV1 rep, positively influences TTSuV1 replication.

Similar to our findings that the PCV1 replicase protein interacts physically with the TTSuV1 UTR (Figure 6), the helicase primase complex and ssDNA binding proteins of helper herpes simplex viruses bind to the AAV inverted terminal repeats (ITRs) to promote AAV DNA replication (Weindler and Heilbronn, 1991). Further, a human herpes virus 6 (HHV6) protein is reported to act as a homolog to the AAV rep protein (Thomson et al., 1994). Rolling circle amplification (RCR) of circular DNA genomes is achieved via the nicking, helicase, ATPase and endonuclease activity of replicase proteins (Wawrzyniak et al., 2017). While we demonstrate that the PCV1 rep physically interacts with to the TTSuV1 UTR DNA (Figure 6), performing mutation and complementation analysis to determine which of these functions is executed or facilitated by the non-cognate rep protein or the understand the exact mechanistic nature of the interaction is not within the scope of this study.

Transcriptional regulation is another recognized mechanism by which coinfecting viruses can influence each other's replication and pathogenesis. For example, adenoviral proteins are known to bind to an AAV promoter upregulating the transcription of the AAV rep proteins (Chang et al., 1989). The full-length PCV1 rep represses its own transcription initiation, whereas the spliced *Rep′* protein does not (Mankertz et al., 2003). While the transcriptome of TTVs is yet to be fully understood, a TTV minimal promoter has been previously mapped to the intergenic UTR region in human TTVs (Figure 6 left) (Suzuki et al., 2004; Liu et al., 2016). While described data confirms the presence of the promoter in TTSuV1 (Figure 6 right), the exact TTSuV1 UTR residues involved in binding to the rep proteins are not known and were not identified in this study. As the putative promoter region was present in both the EMSA and reporter gene amplicons (Figure 6 middle and right), it is reasonable to infer that PCV or TTSuV1 rep proteins may not have transcription factor like functions but rather bind to the UTR region with very high affinity to promote viral DNA replication. Based on other studies showing that the TTSuV1 UTR region also contains regulatory and binding sequences for NF-kB, SP-1, AP-2, ATF/CREB and that the TTV ORF2 product downregulates the NF-kB (Zheng et al., 2007), IFN-β and IL-13 (Singh and Ramamoorthy, 2016a,b). It is possible that other indirect mechanisms may also be involved in TTVs and PCVs promoting each other's replication.

As the TTSuV1 ORF1 is believed to encode a bifunctional protein that serves both as the capsid and has replicase activity, deletion of the start codon of the TTSuV1 ORF1 would result loss of both capsid and rep functions. Hence, this approach could not be used to assess trans-complementation functions. Hence, a rep deficient PCV2b mutant which could potentially be trans-complemented by the TTSuV1 ORF1 product was developed (Figure 7). Besides sharing conserved rep proteins, circoviruses share a conserved nonanucleotide sequence required for RCR with other CRESS viruses and even related plant viruses from the *Geminiviridae* and *Nanoviridae* families. Some monopartite begomoviruses which belong to *Geminivirdae* require beta satellite nanoviruses to induce overt disease. The beta satellite viruses are promiscuous in rep binding or ATPase interactions as they associate with several cognate and non-cognate helper *geminiviruses* via their trans-acting rep binding sites (Zhang et al., 2016). Given the genetic relatedness of ssDNA viruses, it is highly likely that relaxed specificity of the rep binding motifs for TTVs and PCVs can allow for similar trans-acting binding with structurally related replicases from other viruses.

Rodent TTVs have been previously described in rats. Administration of TTV positive human blood resulted in the detection of TTV DNA in the blood and tissues of the exposed mice for several days (Isaeva and Viazov, 2002; Xiong et al., 2018). As TTVs are not usually pathogenic, overt clinical signs or severe lesions were not expected or observed in the experimental mice in this study (Figure 9). As active viral DNA replication occurs early in infection, it is likely that the maximum load of TTSuV1 DNA was observed at day 7 post-exposure (Figure 8 left). Although the detection of TTSuV1 DNA by itself may not mean that productive viral infection occurred, the observation that seroconversion occurred between days 0–15 post-exposure (Figure 8 right) in a pattern consistent with the qPCR data and moderate splenic lesions were observed in dually exposed mice is suggestive of productive TTSuV1 infection. A more detailed characterization of TTV infection in mice was not undertaken and is the focus of future studies. While published epidemiological and experimental studies show that TTVs exacerbate PCV2 clinical signs, the primary hypothesis tested in this study is that the replicase protein of PCVs has trans-replicase activity for TTVSuV1. The replicase proteins of PCV1 and PCV2 are highly conserved and exchangeable. Using the PCV1 system enabled us to study the effects of the rep on TTSuV1 without any possible confounding pathogenic effects due to PCV2 in the mouse model.

In conclusion, data from this study suggests that an overlap in viral DNA replication pathways can lead to increased viral replication and possibly disease manifestations, thus providing novel insight into the complex molecular interactions between TTVs and PCVs in coinfections. The current study also has implications for developing better laboratory culture methods and *in vivo* models for TTV's. With the current explosion in the discovery of small DNA viruses due to metagenomic sequencing and emphasis on understanding how the microbiome and virome contribute to health and disease, improved knowledge regarding how viruses interact in coinfections can be critical to developing better tools for prevention.

Data availability statement

The datasets presented in this study can be found in online repositories. The names of the repository/repositories and accession number(s) can be found in the article/supplementary material.

Ethics statement

The animal study was approved by North Dakota State University Institutional Animal Care and Ethics Committee. The study was conducted in accordance with the local legislation and institutional requirements.

Author contributions

MS: Data curation, Investigation, Methodology, Writing – review & editing. M-TI: Data curation, Investigation, Methodology, Writing – original draft, Writing – review & editing. WF: Investigation, Methodology, Writing – review & editing. ZA: Data curation, Formal analysis, Investigation, Methodology, Writing – review & editing. BW: Data curation, Formal analysis, Investigation, Methodology, Writing – review & editing. SR: Conceptualization, Funding acquisition, Investigation, Methodology, Resources, Supervision, Writing – original draft, Writing – review & editing.

Funding

The author(s) declare financial support was received for the research, authorship, and/or publication of this article. SR was supported by a NIH-NIAID grant (number 1R21AI137963), and in part, by the National Institute of Food and Agriculture, U.S. Department of Agriculture, under Project No. ND02427.

Acknowledgments

The authors thank X. J. Meng, Virginia Tech for the TTSuV-specific rabbit antisera. The authors acknowledge the valuable technical assistance provided by previous laboratory alumni including A. G. M. Rakibuzzaman, Pankaj Singh, Hong Dong, Anuradha Vegi, Karl Effertz, Olexander Kolyvushko, and Sarjana Safain. The authors thank Scott Hoselton for assistance with the flow cytometry.

Conflict of interest

The authors declare that the research was conducted in the absence of any commercial or financial relationships that could be construed as a potential conflict of interest.

Publisher's note

References

Bal, A., Destras, G., Sabatier, M., Pichon, M., Regue, H., Oriol, G., et al. (2022). Metagenomic analysis reveals high abundance of torque teno mini virus in the respiratory tract of children with acute respiratory illness. *Viruses* 14:955. doi: 10.3390/v14050955

Biagini, P. (2009). Classification of TTV and related viruses (anelloviruses). *Curr. Top. Microbiol. Immunol.* 331, 21–33. doi: 10.1007/978-3-540-70972-5_2

Brenner, S., and Horne, R. W. (1959). A negative staining method for high resolution electron microscopy of viruses. *Biochim. Biophys. Acta* 34, 103–110. doi: 10.1016/0006-3002(59)90237-9

Chang, L. S., Shi, Y., and Shenk, T. (1989). Adeno-associated virus P5 promoter contains an adenovirus E1A-inducible element and a binding site for the major late transcription factor. *J. Virol.* 63, 3479–3488. doi: 10.1128/jvi.63.8.3479-3488.1989

Constans, M., Ssemadaali, M., Kolyvushko, O., and Ramamoorthy, S. (2015). Antigenic determinants of possible vaccine escape by porcine circovirus subtype 2b viruses. *Bioinform. Biol. Insights* 9, 1–12. doi: 10.4137/BBI.S30226

Ellis, J. A., Allan, G., and Krakowka, S. (2008). Effect of coinfection with genogroup 1 porcine torque teno virus on porcine circovirus type 2-associated postweaning multisystemic wasting syndrome in gnotobiotic pigs. *Am. J. Vet. Res.* 69, 1608–1614. doi: 10.2460/ajvr.69.12.1608

Fenaux, M., Halbur, P. G., Haqshenas, G., Royer, R., Thomas, P., Nawagitgul, P., et al. (2002). Cloned genomic DNA of type 2 porcine circovirus is infectious when injected directly into the liver and lymph nodes of pigs: characterization of clinical disease, virus distribution, and pathologic lesions. *J. Virol.* 76, 541–551. doi: 10.1128/JVI.76.2.541-551.2002

Huang, Y. W., Harrall, K. K., Dryman, B. A., Beach, N. M., Kenney, S. P., Opriessnig, T., et al. (2011). Expression of the putative ORF1 capsid protein of torque teno sus virus 2 (TTSuV2) and development of western blot and ELISA serodiagnostic assays: correlation between TTSuV2 viral load and IgG antibody level in pigs. *Virus Res.* 158, 79–88. doi: 10.1016/j.virusres.2011.03.013

Huang, Y. W., Harrall, K. K., Dryman, B. A., Opriessnig, T., Vaughn, E. M., Roof, M. B., et al. (2012). Serological profile of torque teno Sus virus species 1 (TTSuV1) in pigs and antigenic relationships between two TTSuV1 genotypes (1a and 1b), between two species (TTSuV1 and-2), and between porcine and human anelloviruses. *J. Virol.* 86, 10628–10639. doi: 10.1128/JVI.00176-12

Huang, Y. W., Patterson, A. R., Opriessnig, T., Dryman, B. A., Gallei, A., Harrall, K. K., et al. (2012). Rescue of a porcine anellovirus (torque teno sus virus 2) from cloned genomic DNA in pigs. *J. Virol.* 86, 6042–6054. doi: 10.1128/JVI.00175-12

Isaeva, E. I., and Viazov, S. O. (2002). Infection of mice with TT virus. *Vopr. Virusol.* 47, 36–38.

Kakkola, L., Tommiska, J., Boele, L. C., Miettinen, S., Blom, T., Kekarainen, T., et al. (2007). Construction and biological activity of a full-length molecular clone of human torque teno virus (TTV) genotype 6. *FEBS J.* 274, 4719–4730. doi: 10.1111/j.1742-4658.2007.06020.x

Kamahora, T., Hino, S., and Miyata, H. (2000). Three spliced mRNAs of TT virus transcribed from a plasmid containing the entire genome in COS1 cells. *J. Virol.* 74, 9980–9986. doi: 10.1128/JVI.74.21.9980-9986.2000

Karimi, G., Gharehbaghian, A., Tafti, M. F., and Vafaiyan, V. (2013). Emerging infectious threats to the blood supply: seroepidemiological studies in Iran—a review. *Transfus. Med. Hemother.* 40, 210–217. doi: 10.1159/000351540

Kawanaka, M., Niiyama, G., Mahmood, S., Ifukube, S., Yoshida, N., Onishi, H., et al. (2002). Effect of TT virus co-infection on interferon response in chronic hepatitis C patients. *Liver* 22, 351–355. doi: 10.1034/j.1600-0676.2002.01560.x

Kekarainen, T., Martinez-Guino, L., and Segales, J. (2009). Swine torque Teno virus detection in pig commercial vaccines, enzymes for laboratory use and human drugs containing components of porcine origin. *J. Gen. Virol.* 90, 648–653. doi: 10.1099/vir.0.006841-0

Kekarainen, T., and Segales, J. (2012). Torque teno sus virus in pigs: an emerging pathogen? *Transbound. Emerg. Dis.* 59, 103–108. doi: 10.1111/j.1865-1682.2011.01289.x

Krakowka, S., and Ellis, J. A. (2008). Evaluation of the effects of porcine genogroup 1 torque teno virus in gnotobiotic swine. *Am. J. Vet. Res.* 69, 1623–1629. doi: 10.2460/ajvr.69.12.1623

Krakowka, S., Hartunian, C., Hamberg, A., Shoup, D., Rings, M., Zhang, Y., et al. (2008). Evaluation of induction of porcine dermatitis and nephropathy syndrome in gnotobiotic pigs with negative results for porcine circovirus type 2. *Am. J. Vet. Res.* 69, 1615–1622. doi: 10.2460/ajvr.69.12.1615

Lefkowitz, E. J., Dempsey, D. M., Hendrickson, R. C., Orton, R. J., Siddell, S. G., and Smith, D. B. (2018). Virus taxonomy: the database of the International Committee on Taxonomy of Viruses (ICTV). *Nucleic Acids Res.* 46, D708–D717. doi: 10.1093/nar/gkx932

Liu, J., Wei, Y., Huang, L., Wang, Y., Chen, D., Wu, H., et al. (2016). Functional characterization of a new promoter isolated from torque teno sus virus 1. *Arch. Virol.* 161, 303–306. doi: 10.1007/s00705-015-2656-z

Luo, Y., Hara, T., Ishido, Y., Yoshihara, A., Oda, K., Makino, M., et al. (2014). Rapid preparation of high-purity nuclear proteins from a small number of cultured cells for use in electrophoretic mobility shift assays. *BMC Immunol.* 15:586. doi: 10.1186/s12865-014-0062-z

Mankertz, A., Caliskan, R., Hattermann, K., Hillenbrand, B., Kurzendoerfer, P., Mueller, B., et al. (2004). Molecular biology of porcine circovirus: analyses of gene expression and viral replication. *Vet. Microbiol.* 98, 81–88. doi: 10.1016/j.vetmic.2003.10.014

Mankertz, A., Mueller, B., Steinfeldt, T., Schmitt, C., and Finsterbusch, T. (2003). New reporter gene-based replication assay reveals exchangeability of replication factors of porcine circovirus types 1 and 2. *J. Virol.* 77, 9885–9893. doi: 10.1128/JVI.77.18.9885-9893.2003

Meier, A. F., Fraefel, C., and Seyffert, M. (2020). The interplay between adeno-associated virus and its helper viruses. *Viruses* 12:662. doi: 10.3390/v12060662

Meyers, C., Alam, S., Mane, M., and Hermonat, P. L. (2001). Altered biology of adeno-associated virus type 2 and human papillomavirus during dual infection of natural host tissue. *Virology* 287, 30–39. doi: 10.1006/viro.2001.0968

Pan, S., Yu, T., Wang, Y., Lu, R., Wang, H., Xie, Y., et al. (2018). Identification of a torque teno mini virus (TTMV) in Hodgkin's lymphoma patients. *Front. Microbiol.* 9:1680. doi: 10.3389/fmicb.2018.01680

Rakibuzzaman, A., Pineyro, P., Pillatzki, A., and Ramamoorthy, S. (2021). Harnessing the genetic plasticity of porcine circovirus type 2 to target suicidal replication. *Viruses* 13:1676. doi: 10.3390/v13091676

Rammohan, L., Xue, L., Wang, C., Chittick, W., Ganesan, S., and Ramamoorthy, S. (2012). Increased prevalence of torque teno viruses in porcine respiratory disease complex affected pigs. *Vet. Microbiol.* 157, 61–68. doi: 10.1016/j.vetmic.2011.12.013

Reed, L. J., and Muench, H. (1938). A simple method of estimating 50 percent end points. *Am. J. Epidemiol.* 27, 493–497. doi: 10.1093/oxfordjournals.aje.a118408

Rezahosseini, O., Drabe, C. H., Sorensen, S. S., Rasmussen, A., Perch, M., Ostrowski, S. R., et al. (2019). Torque-teno virus viral load as a potential endogenous marker of immune function in solid organ transplantation. *Transplant. Rev.* 33, 137–144. doi: 10.1016/j.trre.2019.03.004

Shen, C. F., Meghrous, J., and Kamen, A. (2002). Quantitation of baculovirus particles by flow cytometry. *J. Virol. Methods* 105, 321–330. doi: 10.1016/S0166-0934(02)00128-3

Singh, P., and Ramamoorthy, S. (2016a). Immune gene expression in swine macrophages expressing the torque teno sus virus1 (TTSuV1) ORF-1 and 2 proteins. *Virus Res.* 220, 33–38. doi: 10.1016/j.virusres.2016.04.004

Singh, P., and Ramamoorthy, S. (2016b). Lack of strong anti-viral immune gene stimulation in torque teno sus virus1 infected macrophage cells. *Virology* 495, 63–70. doi: 10.1016/j.virol.2016.04.028

Spandole, S., Cimponeriu, D., Berca, L. M., and Mihaescu, G. (2015). Human anelloviruses: an update of molecular, epidemiological and clinical aspects. *Arch. Virol.* 160, 893–908. doi: 10.1007/s00705-015-2363-9

Ssemadaali, M. A., Effertz, K., Singh, P., Kolyvushko, O., and Ramamoorthy, S. (2016). Identification of heterologous torque teno viruses in humans and swine. *Sci. Rep.* 6:26655. doi: 10.1038/srep26655

Suzuki, T., Suzuki, R., Li, J., Hijikata, M., Matsuda, M., Li, T. C., et al. (2004). Identification of basal promoter and enhancer elements in an untranslated region of the TT virus genome. *J. Virol.* 78, 10820–10824. doi: 10.1128/JVI.78.19.10820-10824.2004

Tarasova, E., and Khayat, R. (2021). A structural perspective of reps from CRESS-DNA viruses and their bacterial plasmid homologues. *Viruses* 14:37. doi: 10.3390/v14010037

Thomson, B. J., Weindler, F. W., Gray, D., Schwaab, V., and Heilbronn, R. (1994). Human herpesvirus 6 (HHV-6) is a helper virus for adeno-associated virus type 2 (AAV-2) and the AAV-2 rep gene homologue in HHV-6 can mediate AAV-2 DNA replication and regulate gene expression. *Virology* 204, 304–311. doi: 10.1006/viro.1994.1535

Wawrzyniak, P., Plucienniczak, G., and Bartosik, D. (2017). The different faces of rolling-circle replication and its multifunctional initiator proteins. *Front. Microbiol.* 8:2353. doi: 10.3389/fmicb.2017.02353

Webb, B., Rakibuzzaman, A., and Ramamoorthy, S. (2020). Torque teno viruses in health and disease. *Virus Res.* 285:198013. doi: 10.1016/j.virusres.2020.198013

Weindler, F. W., and Heilbronn, R. (1991). A subset of herpes simplex virus replication genes provides helper functions for productive adeno-associated virus replication. *J. Virol.* 65, 2476–2483. doi: 10.1128/jvi.65.5.2476-2483.1991

Xiong, Y. Q., Mo, Y., Chen, M. J., Cai, W., He, W. Q., and Chen, Q. (2018). Detection and phylogenetic analysis of torque teno virus (TTV) carried by murine rodents and house shrews in China. *Virology* 516, 189–195. doi: 10.1016/j.virol.2018.01.017

Zhang, T., Xu, X., Huang, C., Qian, Y., Li, Z., and Zhou, X. (2016). A novel DNA motif contributes to selective replication of a geminivirus-associated betasatellite by a helper virus-encoded replication-related protein. *J. Virol.* 90, 2077–2089. doi: 10.1128/JVI.02290-15

Zheng, H., Ye, L., Fang, X., Li, B., Wang, Y., Xiang, X., et al. (2007). Torque teno virus (SANBAN isolate) ORF2 protein suppresses NF-kappaB pathways via interaction with IkappaB kinases. *J. Virol.* 81, 11917–11924. doi: 10.1128/JVI.01101-07

frontiers | Frontiers in Microbiology

TYPE Original Research
PUBLISHED 05 February 2024
DOI 10.3389/fmicb.2024.1332175

OPEN ACCESS

EDITED BY
Gustaf E. Rydell,
University of Gothenburg, Sweden

REVIEWED BY
Xiaorong Zhang,
Yangzhou University, China
Colleen Mayberry,
Jackson Laboratory, United States

*CORRESPONDENCE
José Antonio López-Guerrero
ja.lopez@uam.es
Sabina Andreu
sandreu@cbm.csic.es

†These authors have contributed equally to this work

RECEIVED 02 November 2023
ACCEPTED 15 January 2024
PUBLISHED 05 February 2024

CITATION
Andreu S, Agúndez C, Ripa I, López-Guerrero JA and Bello-Morales R (2024) Pseudorabies virus uses clathrin mediated endocytosis to enter PK15 swine cell line.
Front. Microbiol. 15:1332175.
doi: 10.3389/fmicb.2024.1332175

Pseudorabies virus uses clathrin mediated endocytosis to enter PK15 swine cell line

Sabina Andreu[1,2]*, Carmen Agúndez[1], Inés Ripa[1,2], José Antonio López-Guerrero[1,2]*† and Raquel Bello-Morales[1,2]†

[1]Departamento de Biología Molecular, Universidad Autónoma de Madrid, Madrid, Spain, [2]Centro de Biología Molecular Severo Ochoa (Consejo Superior de Investigaciones Científicas), Madrid, Spain

Pseudorabies virus (PRV), a herpesvirus responsible for Aujeszky's disease, causes high mortality in swine populations. To develop effective and novel antiviral strategies, it is essential to understand the mechanism of entry used by PRV to infect its host. Viruses have different ways of entering host cells. Among others, they can use endocytosis, a fundamental cellular process by which substances from the external environment are internalized into the cell. This process is classified into clathrin-mediated endocytosis (CME) and clathrin-independent endocytosis (CIE), depending on the role of clathrin. Although the involvement of cholesterol-rich lipid rafts in the entry of PRV has already been described, the importance of other endocytic pathways involving clathrin remains unexplored to date. Here, we characterize the role of CME in PRV entry into the PK15 swine cell line. By using CME inhibitory drugs, we report a decrease in PRV infection when the CME pathway is blocked. We also perform the shRNA knockdown of the μ-subunit of the adaptor protein AP-2 (AP2M1), which plays an important role in the maturation of clathrin-coated vesicles, and the infection is greatly reduced when this subunit is knocked down. Furthermore, transmission electron microscopy images report PRV virions inside clathrin-coated vesicles. Overall, this study suggests for the first time that CME is a mechanism used by PRV to enter PK15 cells and provides valuable insights into its possible routes of entry.

KEYWORDS

pseudorabies virus, herpesvirus, clathrin, viral entry, PK15 cell line

1 Introduction

Viruses may be simple in composition, but they have evolved to present a wide variety of complex mechanisms to interact with and infect host cells. Some viruses can enter the cell directly through fusion with the plasma membrane, but other routes based on endocytosis are preferred (Yamauchi and Helenius, 2013; Cossart and Helenius, 2014). Endocytosis is a fundamental mechanism described in eukaryotic cells, by which substances from the external environment (including solutes, fluids, components of the plasma membrane, and pathogens) are internalized into the cytoplasm through invagination of the cell membrane (Kaksonen and Roux, 2018). This process contributes to nutrient and ligand uptake, cell signaling, and adhesion, among others (Le Roy and Wrana, 2005).

Endocytosis can be classified into two main groups focusing on the role of clathrin, namely clathrin-mediated endocytosis (CME) or clathrin-independent endocytosis (CIE). The latter group includes caveolae-mediated endocytosis, lipid raft-dependent endocytosis, macropinocytosis and other lesser-known processes (Mercer et al., 2010; Hemalatha and Mayor, 2019). Although viruses primarily use CME as their route of entry, they can enter through more than one single pathway (Kaksonen and Roux, 2018; Ripa et al., 2021). Typically, the CME pathway begins with the stimulation by ligands of specific receptors on the cell membrane. This triggers the recruitment of triskelia-shaped clathrin to the plasma membrane forming clathrin-coated pits (CCPs) of 100 triskelia on average (Mettlen et al., 2018). Clathrin is anchored to the plasma membrane via protein adaptor complexes (such as adaptor protein 2 or AP-2), giving rise to clathrin-coated vesicles (CCVs) (McMahon and Boucrot, 2011; Brodsky, 2012; Mettlen et al., 2018). Finally, the GTPase activity of dynamin is responsible for the budding of clathrin vesicles by self-assembling into rings that form a collar around the neck of the vesicles (Mettlen et al., 2009; Prichard et al., 2022). Once the cargo has been internalized, not only the clathrin, but also the cytoplasmic complexes and membrane receptors involved in this process can be recycled and reused (Le Roy and Wrana, 2005; Barrow et al., 2013).

Pseudorabies virus (PRV) belongs to the family *Herpesviridae* and is the pathogenic agent of Aujeszky's disease, which causes severe symptoms and high mortality in swine populations, its natural host (Andreu et al., 2020). Previous studies have demonstrated the entry of several herpesviruses through CME in different cell lines (Sobhy, 2017); for example, herpes simplex virus type 1 (HSV-1) (Nicola, 2016; Praena et al., 2020; Tebaldi et al., 2020), Epstein-Barr virus (EBV) (Millert and Hutt-Fletcher, 1992), bovine herpesvirus 1 (BoHV-1) (Pastenkos et al., 2018), and Kaposi's sarcoma-associated virus (KSHV/HHV-8) (Kerur et al., 2010). In addition, the relevance of cholesterol-rich lipid rafts in PRV entry has already been characterized (Desplanques et al., 2008; Ren et al., 2011), but so far, the importance of other endocytic pathways that the virus hijacks to enter the cell has not been explored.

In the present study, we characterize the role of CME in the entry of PRV into the established swine cell line PK15. To this end, a set of studies with CME inhibitory drugs were performed, revealing a decrease in the infection when blocking this pathway by this method. The importance of clathrin in PRV infection was also determined by silencing the μ subunit of the adaptor AP-2, by a knockdown approach. Furthermore, transmission microscopy images also elucidate the interaction of PRV virions with clathrin vesicles. Our results provide the first evidence that the absence of CME reduces PRV infection and that this endocytic process is critical for PRV entry in PK15 cell line.

2 Materials and methods

2.1 Cell cultures

PK15 is an established cell line that originated from kidney epithelial cells of an adult pig (*Sus scrofa domestica*) (Todaro et al., 1974), and was generously provided by Dr. Yolanda Revilla (CBMSO, Madrid, Spain). Cells were maintained in low-glucose Dulbecco's modified Eagle medium (DMEM) (Life Technologies, Paisley, UK) supplemented with 5% fetal bovine serum (FBS), glutamine (2 mM), penicillin (50 U/mL) and streptomycin (50 μg/mL) (Gibco, CA, USA), at 37 °C in a humidified atmosphere of 5% CO_2. The absence of mycoplasma was confirmed by using the PCR Mycoplasma Detection kit (Takara Bio, San José, CA, USA).

2.2 Viruses

Recombinant strain PRV-XGF-N (Viejo-Borbolla et al., 2010) was kindly provided by Dr. Enrique Tabarés (UAM, Madrid, Spain). PRV-XGF-N was obtained by replacing the gene encoding the PRV gG glycoprotein (glycoprotein that is not part of the virion as it is secreted into the medium by infected cells, being not essential for virulence) with the *EGFP* gene in NIA-3 wild type PRV strain. PRV-XGF-N was propagated and titrated with a 50% tissue culture infective dose ($TCID_{50}$) assay in PK15 cells as previously described (Andreu et al., 2021).

2.3 Antibodies and reagents

Chlorpromazine (C8138), dynasore (D7693), and pitstop 2 (SML1169) were purchased from Sigma-Aldrich (St. Louis, MO, USA). Mowiol was obtained from Calbiochem (Merck Chemicals, Darmstadt, Germany), To-Pro-3 from Thermo fisher (Waltham, MA, USA) and human transferrin (Tf) CF®543 and CF® 555-Labeled Dye Dextran 10,000 MW conjugates were purchased from Biotium (Fremont, CA, USA). X-tremeGENE 360 Transfection Reagent (XTG360-RO) was obtained from Roche (Basel, Switzerland). All drugs in this study were dissolved in 0.1% v/v dimethyl sulfoxide (DMSO), except for chlorpromazine and Tf which were dissolved in sterile distilled water.

Primary antibodies used were mouse monoclonal anti-GFP (11814460001, Roche), mouse monoclonal anti-β-actin peroxidase antibody (A3854, Sigma), rabbit monoclonal anti-AP2M1 (ab75995, abcam, Cambridge, UK), and rabbit anti-IE180 (Gómez-Sebastián and Tabarés, 2004) (kindly provided by Dr. Enrique Tabarés). Horseradish peroxidase conjugate (HRP) secondary anti-IgG antibodies were purchased from Millipore (Darmstadt, Germany).

2.4 Cell viability assay

The potential cytotoxic effect of chlorpromazine, dynasore, and pitstop 2 in PK15 cells was analyzed by the MTT [3-(4,5-dimethylthiazol-2-yl)-2,5-diphenyltetrazolium bromide] assay (Promega, Cell Titer 96® Non-Radioactive Cell Proliferation Assay). Non-confluent monolayers of PK15 cells plated in 96-well tissue culture dishes and cultured in DMEM supplemented with 5% FBS were incubated for 24 h with different concentrations between 0 and 100 μM of each compound. Four replicates were carried out for each concentration. Then, cells were incubated with a final concentration of 0.5 mg/mL of MTT in a humidified atmosphere for 4 h, and formazan crystals were solubilized in 0.01 M HCl with 10% SDS. The resulting-colored solution was quantified using the scanning multiwell spectrophotometer iMarkTM Microplate

Reader (BioRad, Hercules, CA, USA), measuring the absorbance of formazan at 595 nm. The readouts obtained from MTT assay were further normalized to the value of untreated cells where the viability value was set to 100%.

The effect of the antibiotic puromycin on PK15 cells was also tested by this method. Cells were incubated for 48 h with puromycin ranging from 0 to 10 μM, and results were obtained following the same protocol as before.

2.5 Endocytosis assay

Cells grown on 24-well plates on round coverslips were treated for 1 h with either 20 μM chlorpromazine, 100 μM dynasore, or 50 μM pitstop 2 at 37°C and then maintained for 30 min on ice with human transferrin conjugate Tf CF®543 (5 μg/mL) or CF® 555 Labeled Dye Dextran 10,000 MW (5 μg/mL). All cells were incubated again for 5 or 10 min, respectively, at 37°C in a humidified 5% CO_2 atmosphere to allow internalization of Tf or dextran conjugate. Finally, cells were washed with PBS followed by fixation for immunofluorescence microscopy.

2.6 Immunofluorescence microscopy

Cells grown on 24-well plates on round coverslips were fixed in 4% paraformaldehyde (PFA) for 15 min and rinsed with PBS. Cells were then permeabilized with 0.2% Triton X-100, rinsed and incubated for 30 min at room temperature (RT) with 3% bovine serum albumin in PBS (blocking buffer). For a labeled immunofluorescence analysis, coverslips were incubated in a wet chamber and nuclei were stained with To-Pro-3 for 10 min. After thorough washing, coverslips were mounted on a slide using mounting media (Mowiol). Images were obtained using a LSM 710 Inverted Confocal Microscope (Zeiss, Vienna, Austria), equipped with an Argon laser and a He/Ne 633 nm laser, using 40x/1.4 NA Oil lens. Pinhole size was set to 1 AU. Processing of confocal images was performed using the Fiji-ImageJ software (version Image J 1.53c) (Schindelin et al., 2012).

2.7 Flow cytometry

To perform fluorescence activated cell sorting (FACS) analysis, cells were dissociated by 2 min incubation with 0.05% trypsin/0.1% EDTA (Invitrogen, Waltham, MA, USA) at RT and washed and incubated for 20 min with Ghost Dye Red 780 (1:1000 in PBS, CYTEK). After centrifugation, the pellet was washed with PBS and fixed with 1%-PFA-1% FBS in PBS for 15 min. Finally, cells were rinsed and resuspended in PBS. Cells were analyzed using a FACSCalibur Flow Cytometer from BD (Franklin Lakes, NJ, USA). Data were processed with FlowJo software (BD, version 10.6.2).

2.8 Western blot analysis

Cells were lysed using the radioimmunoprecipitation assay (RIPA) buffer mixed with a protease inhibitor cocktail from Roche (Basel, Switzerland), and the total protein load was quantified by Bradford assay (Bio-Rad Laboratories, Inc. Hercules, CA, USA). Equalized protein samples were separated by SDS-PAGE in 10% acrylamide gels under non-reducing conditions and later transferred onto Merck Millipore Immobilon-P membranes. Membranes were blocked for 30 min in 5% non-fat dry milk at RT, incubated overnight at 4°C with the appropriate primary antibodies (anti-GFP 1:1000, anti-IE180 1:200), washed with 0.05% Tween 20 in PBS, and incubated with HRP-conjugated secondary antibodies for 1 h at RT. Anti-β-actin-peroxidase antibody (1:50,000) was directly incubated for 1 h at RT. After extensive washing, the membranes were finally incubated with an enhanced chemiluminescence Western blotting kit, ECL Western Blotting Detection Reagent (GE. Healthcare, Chicago, IL, USA) to visualize the protein band. The intensity of immunoblot bands was analyzed using Fiji-ImageJ software (version Image J 1.53c).

2.9 shRNA knockdown

To knockdown (KD) the gene expression of AP2M1 in PK15 cells, the RNA interference strategy was used. Five commercial shRNA oligonucleotides designed to target against different regions of the AP2M1 gene were purchased (Table 1). Control cells were transfected with pLKO.1-puro non-target shRNA control plasmid DNA (Sigma-Aldrich).

PK15 cells were seeded in 96-well tissue culture plates at an approximate confluency of 70%. At least 1 h after cell transfection, the culture medium was replaced for fresh DMEM medium supplemented with 5% FBS. shRNA plasmid DNAs were diluted in DMEM to reach a concentration of 1 μg/μl. A total of 100 μl of this shRNA was mixed with the XtremeGENE transfection agent (3 μl of reagent for every 100 μg of shRNA; ratio 3:1) and this mixture was incubated for 20 min at RT. Subsequently, 10 μl of said mix was added in the form of drops to 10 wells per condition and the plate was shaken vigorously to ensure distribution over the entire surface.

TABLE 1 ID and specific sequence of commercial shRNA plasmid DNAs (Sigma-Aldrich) used for the KD of AP2M1 gene in PK15 cell line.

ID of shRNA plasmid DNA	Code name	Specific sequence
TRCN0000060238	A	5′-GTGGTCATCAAGTCCAACTTT-3′
TRCN0000060239	B	5′-CACCAGCTTCTTCCACGTTAA-3′
TRCN0000060241	C	5′-GCTGGATGAGATTCTAGACTT-3′
TRCN0000333063	D	5′-GTGGTCATCAAGTCCAACTTT-3′
TRCN0000381904	E	5′-GGCGAGAGGGTATCAAGTATC-3′
SHC016-1A	Non-target	5′-GCGCGATAGCGCTAATAATTT-3′

After 48 h of incubation at 37°C in a humidified atmosphere of 5% CO_2, the transfection mix was replaced with DMEM supplemented with 5% FBS and 5 μg/ml puromycin to select transfected cells. Two days later, cells growing in medium with puromycin were isolated, grown on 24-well plates, and processed for immunoblot or RT-qPCR to determine the efficacy of shRNA silencing. A previous cytotoxicity assay (MTT) was performed to elucidate the concentration of puromycin that was able to kill wild type PK15 cells which had not incorporated the plasmid, as described in the "cell viability assay" section.

2.10 RT-qPCR

To characterize the success in silencing *AP2M1* gene in PK15 cells, transfected cells A6, B3 and C1 were cultured in 24-well plates for 24 h. Later, cells were treated with 0.25 trypsin and 0.03% EDTA in PBS and the total RNA from six different samples per condition was extracted using a RNeasy mini kit (Qiagen, Venlo, Netherlands). RNA integrity was evaluated on an Agilent 2100 bioanalyzer (Agilent Technologies, Santa Clara, CA, USA), and quantification of RNA was performed on a Nanodrop ND-1000 spectrophotometer (Thermo Fisher). RNA integrity number (RIN) values were between 9 and 10, corresponding to samples with high integrity. Genomic DNA contamination was assessed by amplification of representative samples without retrotranscriptase. RT reactions were performed using SsoFast™ EvaGreen® Supermix (Bio-Rad, #1725204) and qPCR using Power SYBR® Green PCR Master Mix (ThermoFisher, #4367659). Briefly, 1 μg of total RNA from each sample was combined with master mix containing a mixture of random primers and oligo-dT for priming. The No-RT master mix included in the pack was used as RTcontrol. The reaction volume was completed up to 20 μL (RT reactions) and 10 μL (qPCR) with DNAse/RNAse free distilled water following manufacturer's instructions. Amplification conditions of qPCR followed these steps: (30 s × 95°C, 5 s × 60°C) × 40 cycles and melting curve from 60 to 95°C (incrementing 0.5°C/s). Amplifications of the representative samples were either negative or delayed more than 5 cycles compared to the corresponding RT + reactions. Primers were designed by the Genomics Core Facility at the Centro de Biología Molecular Severo Ochoa (CBMSO) using Primer Blast, following an intron-spanning strategy. To guarantee silencing efficacy, *AP2M1* primer sets were designed to overlap the site targeted by the shRNAs on the mRNA. The NormFinder algorithm was used to identify β-actin (*ATCB*) as the most suitable gene for the normalization due to its high stability. Primer sequences were as follows (**Table 2**).

2.11 Transmission electron microscopy (TEM)

Cells were seeded in 24-well tissue culture plates and maintained in DMEM supplemented in 5% FBS for 24 h. Then, they were pretreated or not with 100 μM dynasore, 20 μM chlorpromazine or 50 μM pitstop 2 for 1 h before infection, and then infected or mock-infected with PRV-XGF-N at an m.o.i of 30 for 1 h at 4°C, to allow viral attachment to the cellular surface without yet entering the cell. After this time, cells were incubated at 37°C for 20 min. Finally, cells were fixed with 2% PFA+ 2.5% glutaraldehyde in 0.1 M phosphate buffer, pH 7.4 and processed for transmission electron microscopy. Fixed monolayers were washed once with PBS and once with distilled water. Cells post-fixation was as follows: 45 min at RT with 1% osmium tetroxide (TAAB Laboratories Equipment Ltd.) in PBS, washed with distilled water, 45 min incubation ay RT with 1% aqueous uranyl acetate (Electron Microscopy Sciences, Hatfield, PA, USA) and after dehydration with increasing concentrations of ethanol absolute, cells were embedded in epoxy resin EML-812 (TAAB Laboratories Equipment Ltd., 2 days, RT). Resin-containing gelatin capsules (TAAB Laboratories Equipment Ltd.) were placed on the coverslips and polymerized (2 days, 60°C). Resin blocks were detached from coverslips by successive immersion in liquid nitrogen and hot water. Ultrathin 70 nm-thick sections, parallel to the monolayer, were obtained with a Leica ultramicrotome (Leica Microsystems GmbH, Wetzlar, Germany), transferred to Formvar-coated EM GS2x1-N3 nickel buttonhole grids, and stained with 5 % aqueous uranyl acetate (10 min, RT) and lead citrate (3 min, RT). Sections were visualized on a JEOL 1400 electron microscope equipped with a LaB6 filament and operated at 100 kV. Images were recorded with a GATAN One View digital camera at various magnifications and processed by Fiji-ImageJ software (version Image J 1.53c).

2.12 Statistical analysis and quantification of fluorescence

Results obtained from the experiments were analyzed using Prism software v8.0.1 (GraphPad software, Inc., San Diego, CA, USA). Data were subjected to Mann-Whitney *U*-tests to determine significant differences between groups, and a *P*-value of < 0.05 was considered statistically significant. For fluorescence intensity quantifications, various regions of interest (ROIs) were measured from groups of 30 cells with 3 areas of each image to normalize for the cell number and background intensity. The software Fiji-ImageJ (version Image J 1.53c) was used to quantify fluorescence intensity

TABLE 2 ID and specific sequence of customized primers used for qPCR.

Primer set	Forward	Reverse
A6	5′-TCCGAGTGATCCCGCTAGT-3′	5′-TTCTCGCTGGCCTTGTACTT-3′
B3	5′-CGGGTCTACCGAGATGACA-3′	5′-TCGAAGACCATGGCAGCATT -3′
C1	5′-GTGTGATGTAATGGCTGCCT-3′	5′-CTTCTTTCGTCTGATGCTGGCT-3′
WT	5′-GGCATCAAAAGCCAGCATC-3′	5′-GGAGGTTCACACTCTCCAGC-3′
ACTB	5′-CCTCCTTCCTGGGCATGG-3′	5′-GGATGCTCCATCCAACCGAC-3′

for the 555 channel. Images were transformed to 8-bit gray scale and fluorescence intensity was analyzed using the particle analysis function, after correcting the background, as previously described (Shihan et al., 2021).

3 Results

3.1 Endocytosis assays with CME chemical inhibitors and its cytotoxic effect in PK15 cell line

First, CME chemical inhibitors chlorpromazine, dynasore and pitstop 2 were tested to determine the concentrations that did not exhibit harmful cytotoxic effects in PK15 cells. After 24 h of drug addition, cells maintained their viability above 70% when treated with either 100 μM dynasore, 20 μM chlorpromazine, or 50 μM pitstop 2 (**Figure 1A**). This was the threshold chosen for the rest of the assays, as recommended by the ISO 10993-5:2009 (E) standard (ISO 10993-5:2009, Under Review). The absence of cytotoxicity of the solvent at the concentrations used to make the pertinent dilutions of the drugs (DMSO) was also demonstrated (results not shown).

It is well-known that human transferrin uses the CME pathway to enter the cells (Cossart and Helenius, 2014). In this term, human transferrin conjugate Tf CF® 543 was used in this study to establish a suitable method to monitor CME endocytosis in PK15 cells and to demonstrate that the compounds dynasore, chlorpromazine and pitstop 2 did block this pathway. These three drugs are known for blocking CME by using different strategies: dynasore blocks the GTPase dynamin that leads to the fission of CCPs from the plasma membrane (Macia et al., 2006); pitstop 2 prevents clathrin-heavy-chain (CHC) from interacting with adaptor proteins necessary for the formation of CCPs (Bayati et al., 2021), and chlorpromazine dissociates clathrin networks in the inner leaflet of the plasma membrane during CCPs assembly (Vercauteren et al., 2010), all blocking the uptake of Tf.

Cells were pretreated for 1 h with dynasore, chlorpromazine or pitstop 2 at 37°C and then incubated for 30 min on ice with Tf conjugate (5 μg/mL). Subsequently, cells were incubated again for 5 min at 37°C in a humidified 5% CO_2 atmosphere to allow internalization of Tf (still in the presence of the inhibitors), and finally cells were processed for confocal microscopy. Fluorescence microscopy images after treatment with the drugs showed a decrease in Tf uptake, in comparison to the non-treated control (**Figure 1B**). Quantification of Tf uptake is also performed (**Figure 1C**). These drugs reduced the internalization of Tf, suggesting that CME was partially blocked or inhibited. Furthermore, no appreciable amounts of Tf were observed in dynasore-treated cells, but a small amount of Tf is noticeable in the case of chlorpromazine and even more in pitstop 2-treated cells. However, the simulated CME is insignificant compared to non-treated cells, in which there is a marked accumulation of Tf in a perinuclear region, corresponding to the endosomal recycling compartment (**Figure 1B**, marked with arrows). In addition, CME drugs showed a dose-dependent effect on the inhibition of Tf uptake, with the highest non-cytotoxic concentrations inhibiting the most (results not shown).

Furthermore, to confirm that the drugs used in this study did not interfere with other endocytic pathways at the concentrations tested, the effect on the uptake of fluorescently labeled dextran, which is internalized following a clathrin-independent route, was analyzed (**Figure 1D**). All drugs blocked internalization of Tf, a process that requires formation of CCPs and is dynamin dependent (Cossart and Helenius, 2014), while maintaining internalization of dextran, whose internalization was also quantified (Figure E).

3.2 Effect of CME inhibitory drugs in PRV infection

Once the efficacy of the drugs in blocking CME in PK15 cell line was determined, the next step was to study whether this inhibition of the route affected PRV infection. For this, the internalization of PRV-XGF-N was examined in the presence of dynasore, chlorpromazine, and pitstop 2. Briefly, PK15 cells were pre-treated for 1 h with these drugs and then infected with PRV-XGF-N at an m.o.i of 0.5 for another hour. Cells were maintained in culture medium after infection and samples were collected at 4 or 24 h p.i for flow cytometry, Western blot, and confocal fluorescence microscopy. A significant decrease in viral infection was noticed in all cells pretreated with CME-blocking drugs, in comparison to non-treated and DMSO-treated cells. This decrease in viral GFP was detected not only in flow cytometry analysis (**Figure 2A**), but also in Western blot (**Figure 2B**), where no band corresponding to viral GFP is revealed in the mentioned conditions. For samples collected at 4 h p.i., the expression of immediate protein IE180 was evaluated (**Figure 2B**), to ensure that the decrease in infection was due solely to clathrin blockade during the entry phase. It is when PRV has already entered, and the genome arrives to the nucleus when IE genes are transcribed. As in the case of GFP, no band corresponding to viral IE180 is observed in the drug-treated samples. The same decrease in viral GFP is reported in fluorescence microscopy images (**Figure 2C**). These results suggest that CME could be a possible route of entry of PRV.

3.3 Effect of AP2M1 knockdown silencing in PRV infection

A loss-of-function analysis was performed to inhibit CME by knocking down the gene encoding the subunit μ of the AP-2 (AP2M1) adaptor with a previously defined shRNA pool. This could best demonstrate the role of clathrin in PRV entry, as the AP-2 complex plays an essential role in CME (Rappoport, 2008). PK15 cells were transfected with various shRNA plasmid DNAs targeting different sites located on the CDS of AP2M1 and were selected at 48 h post-transfection in a media supplemented with 5 μg/ml puromycin. From 5 different shRNA initially used, only three shRNAs A, B, and C (see **Table 2**, "2 Materials and methods") kept viable, and the efficacy of shRNA silencing was evaluated in these samples. Multiple shRNA for the same target were used to verify that the correct phenotype caused by the KD is observed. Transfection of PK15 cells with AP2M1 shRNAs led to a decrease in the expression of AP2M1 protein levels in three of the samples (A6, B3, C1) when compared to cells transfected with non-target shRNA,

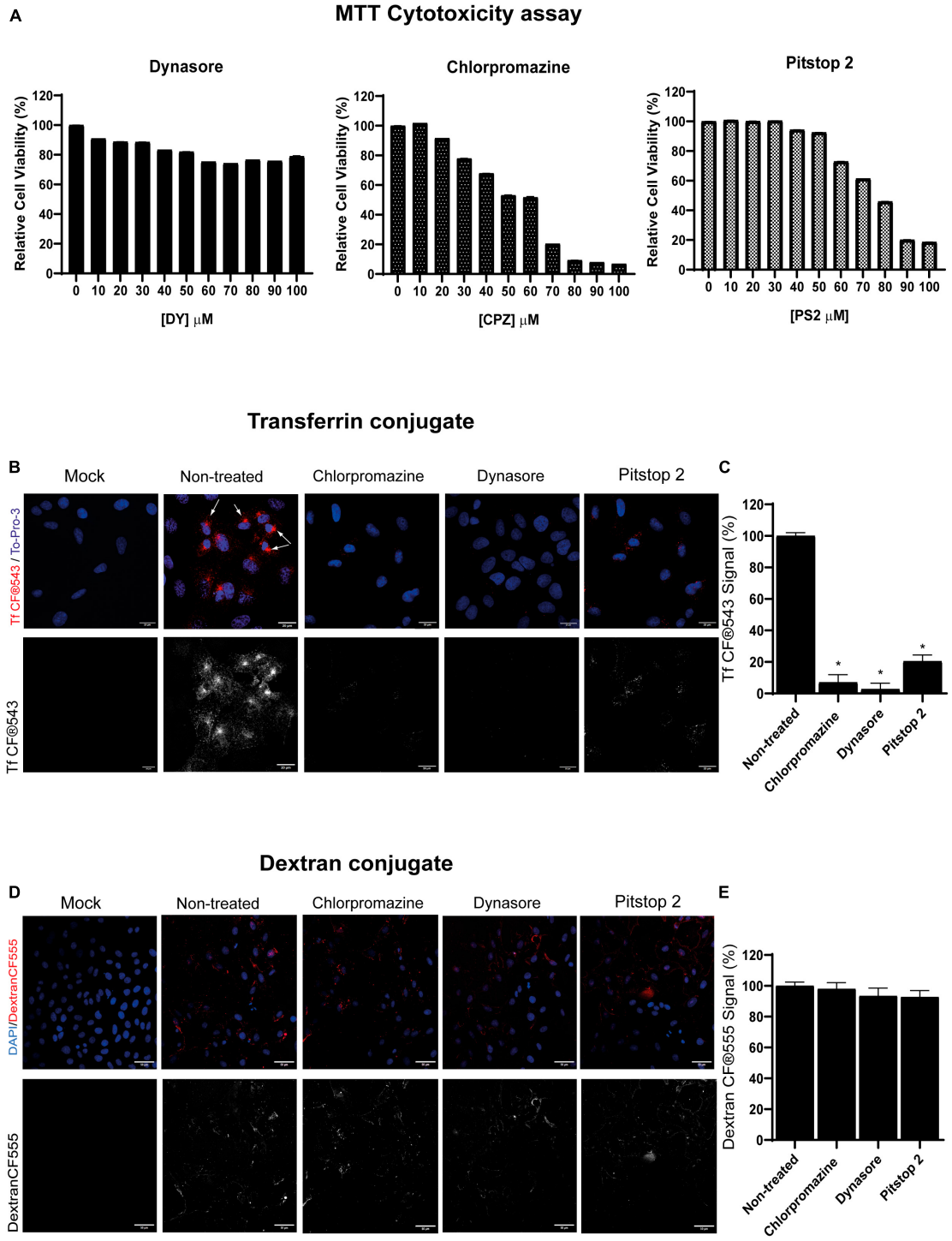

FIGURE 1
Clathrin-mediated endocytosis (CME) chemical inhibitors dynasore, chlorpromazine, and pitstop 2 disrupt transferrin but no dextran uptake at non-cytotoxic doses. **(A)** Cellular viability of PK15 cells exposed to dynasore, chlorpromazine, and pitstop 2 for 24 h. Cell viability was measured by MTT tetrazolium salt assay and calculated as the percentage of cell viability compared to untreated cells; columns represent the mean percentage of relative cellular viability ± S.D. (n = 4) after exposure to the drugs. **(B)** Transferrin uptake in PK15 cells is blocked by CME chemical inhibitors. PK15 cells were mock-treated or treated with either 20 μM chlorpromazine, 100 μM dynasore, or 50 μM pitstop 2 for 1 h and then incubated for 30 min on ice with Tf CF®543 (5 μg/ml). Finally, cells were fixed after 5 min of incubation at 37°C. Fluorescence microscopy images are shown, with Tf in red and cellular nuclei stained with To-Pro-3 in blue. Arrows point to the accumulation of Tf in the endosomal recycling compartments. **(C)** Quantification of Tf CF®543. Cells were acquired and analyzed as in **(B,D)**; ROIs from groups of 30 cells and 3 areas of each image were measured. Mean percentage of fluorescence ± S.D. is shown. **(D)** Dextran-CF®555 uptake is not altered in PK15 cells treated with CME-inhibitory drugs. PK15 cells were incubated or mock-incubated as described in **(B)** but instead of Tf, they were incubated with CF®555 Labeled Dye Dextran 10,000 MW (5 μg/mL) for 15 min at 4°C. Cells were then transferred to 37°C for 10 min, washed, and then fixed with 4% PFA and stained as before. **(E)** Quantification of CF®555 Dextran. Cells were acquired and analyzed as previously described. Measurement of mean fluorescence intensity from 555 channel in a ROI was performed. Mean percentage of fluorescence ± S.D. is shown.

10.3389/fmicb.2024.1332175

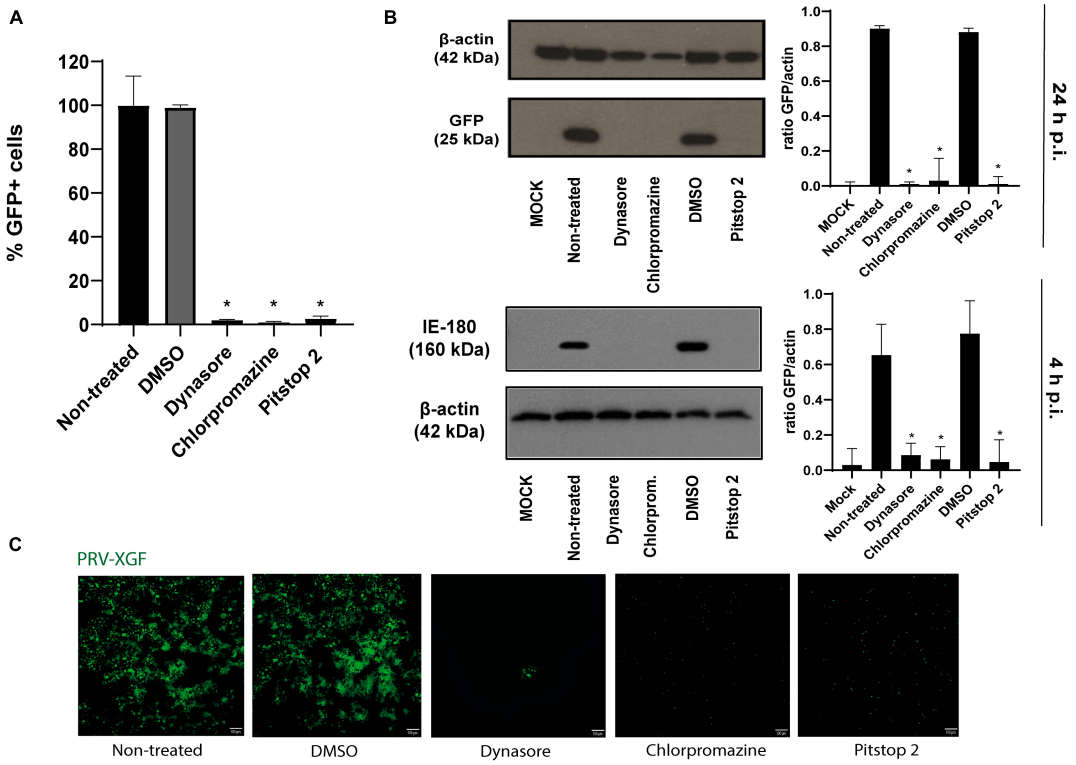

FIGURE 2
Pseudorabies virus (PRV)-XGF-N infection is blocked by CME chemical inhibitors. PK15 cells were pre-treated with either 0.1% (v/v) DMSO, 100 μM dynasore, 20 μM chlorpromazine, or 50 μM pitstop 2 for 1 h and then infected with PRV-XGF-N at an m.o.i of 0.5 (collected at 24 h p.i.) or moi 5 (collected at 4 h p.i.). Cells were maintained until they were collected in the presence of the drugs. **(A)** Flow cytometry data show the percentage of normalized infection 24 h p.i. (% GFP+ cells) ± S.D. for each condition. Triplicate experiments were performed for each data point ($n = 3$). *$p < 0.05$. **(B)** Western blot analysis of total cell lysates showing viral GFP and IE180 for each condition. β-actin was used as protein loading control. Values of Western blot quantification are reported as the mean ± S.D. ($n = 3$), *$p < 0.05$. **(C)** Fluorescence microscopy images show GFP+ signal corresponding to viral infection 24 h p.i. ($n = 3$).

as demonstrated by Western blot analysis (Figure 3A). RT-qPCR analysis was also made to amplify the target mRNA (Figure 3B), using flanking primer sets that encompassed the region containing the shRNA target. Successful KD of AP2M1 in samples A6 and B3 was achieved, as seen by the reduced levels of mRNA, so this pair of transfected cells were the ones selected for further studies. However, the KD of AP2M1 in C1 PK15 cells was not significantly achieved; the decrease in AP2M1 mRNA relative levels was approximately 30%, and a band of little intensity referring to AP2M1 is shown in Western blot analysis (protein expression levels). Furthermore, no differences either in shape or size (Supplementary Figure 1A) or in viability (Supplementary Figure 1B), were observed between wild-type PK15 and PK15 AP2M1-KD cells (which supports that cells might also use CIE routes to maintain a normal surface/volume ratio). To further confirm that the CME pathway was effectively blocked in KD cells, A6, B3, and C1 were incubated with Tf conjugate, revealing a decrease in the internalization of this compound in successfully KD-samples compared to wild-type PK15 cells (Supplementary Figure 2).

After verifying the specific KD of AP2M1 in PK15 cells, successfully KD samples were infected with PRV-XGF-N to study whether the lack of the μ subunit of AP-2 affects the entry of this virus. As it was shown above, A6 was the sample showing the lowest expression of AP-2, followed by B3 and finally C1. Flow cytometry analysis (Figure 4A) reported that GFP corresponding to viral infection decreased the most in A6 cells, followed by B3 and C1, the latter reaching the same infection levels as non-target cells. These results were corroborated by immunoblot (Figure 4B), and fluorescence microscopy (Figure 4C). The expression of IE180 at short times after infection was also performed (Figure 4B), following the same pattern of expression as GFP at 24 h p.i.. Furthermore, the decrease in infection rates tended to follow a directly proportional relation with the expression of AP2M1; the lower the AP2M1 expression, the lower the viral infection rate. This experiment was also performed with PRV wild-type strain NIA-3, following the same methodology as with PRV-XGF-N (Supplementary Figure 3), to ensure that the recombinant strain used during all experiments behaved the same way than the wild-type one. According to the results, AP2M1 knockdown reduces PRV-XGF-N endocytosis into PK15 cells.

3.4 Visualization of clathrin-coated vesicles and their interaction with PRV by transmission electron microscopy

Transmission electron microscopy (TEM) assays were performed to ultra-structurally analyze how PRV entered

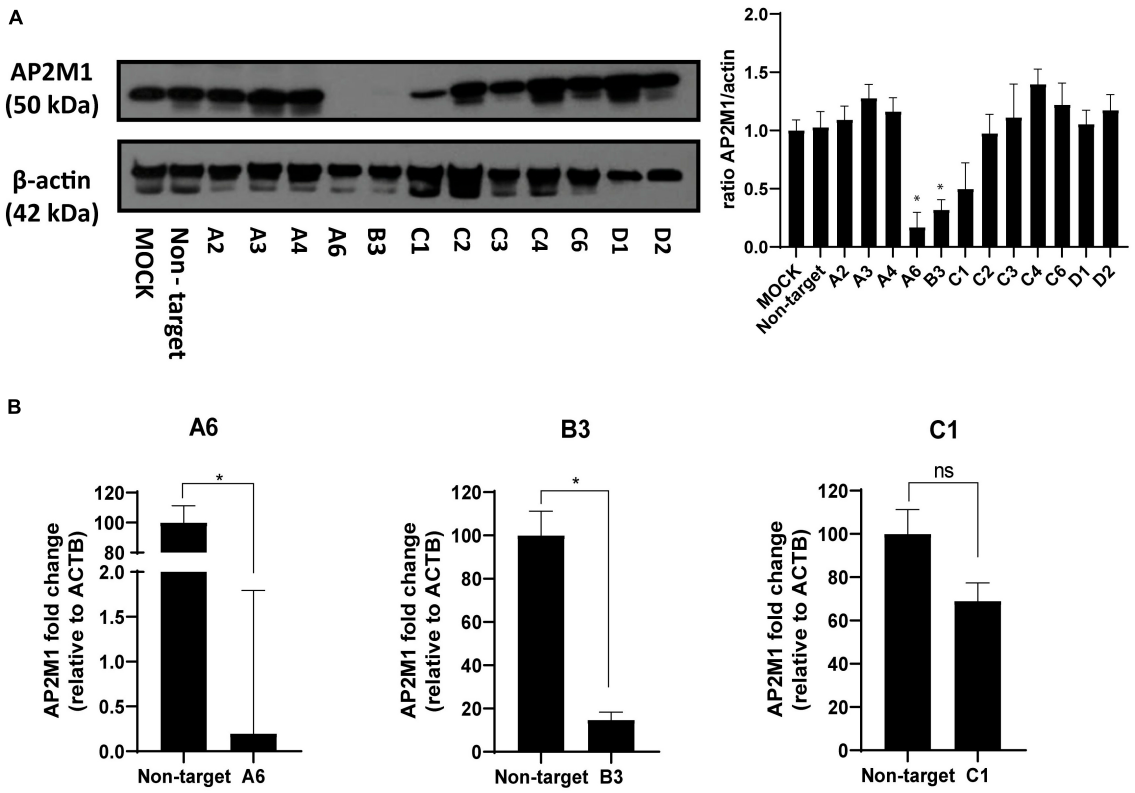

FIGURE 3
Determination of AP2M1 shRNA knockdown efficiency in PK15 cells. PK15 cells were transfected with a pool of shRNA to KD the expression of AP2M1. KD efficiency was checked by both Western blot and RT-qPCR. **(A)** Western blot analysis of total cell lysates subjected to SDS-PAGE showing AP2M1 for each condition. β-actin was chosen as protein loading control. Values of immunoblot quantification are reported as the mean ± S.D. (n = 3); *$p < 0.05$. **(B)** qPCR amplification of AP2M1 mRNA from AP2M1 A6, B3, and C1 shRNA-treated PK15 cells in comparison to the non-targeted control. mRNA level is relative to β-actin (*ACTB*) control (n = 6, mean ± S.D.). *$p < 0.05$ was considered as statistically significant compared to the non-targeting shRNA-transfected cells.

PK15 cells in a CME-dependent pathway. Fortunately, clathrin is naturally electrodense and can be directly seen without immunolabeling. TEM images revealed PRV-XGF-N virions internalized in CCVs (**Figures 5A–C**), directly being surrounded by clathrin anchored to the cell membrane (**Figure 5D**) or surrounded by clathrin (**Figure 5E**). Clathrin vesicles are characterized for showing its characteristic "bristle-like" pattern. Quantification of the number of virions internalized through CME was also assessed (**Figure 5F**), revealing that in all samples treated with CME-blocking drugs, the number of internalized virions was lower, and from those that managed to enter the cell, no viruses were detected using CCVs to enter. These results in concordance with the above strongly suggest that CME is clearly involved in the entry of PRV in PK15 cell line.

4 Discussion

Based on the available evidence, PRV can enter different cell types by using distinct mechanisms. Previous studies have reported non-endocytic pathways for PRV entry in RK13 cells (Granzow et al., 2005) and CHO cell lines (Nixdorf et al., 1999), and fusion under low pH conditions in PK15, Vero, MDBK and SK-N-SH cell lines (Miller et al., 2019). In addition, hypertonic treatment in PK15 infected cells (to inhibit viral entry via endocytosis in a general way) revealed a decrease in PRV infectivity, suggesting that this virus might use endocytic-related pathways to enter this cell line (Miller et al., 2019). Another recent study in which researchers inhibit CME with an inhibitor of Niemann-Pick C2 (NPC1) results in defects in CCP dynamics, which acutely interfere with Tf endocytosis, and PRV entry (Li et al., 2022). Nevertheless, no further research on whether PRV uses CME to enter PK15 cells has been done to date.

Depletion of essential proteins that mediate CME derive into indirect effects on cellular function and/or morphogenesis (Dutta et al., 2012). For this reason, selective inhibitory drugs have been used in this study, as a first pharmacological approach, revealing a decrease in the infection with PRV-XGF-N when blocking CME. On the one hand, dynasore is a reversible inhibitor of the GTPase activity of dynamin, preventing the fission of CCPs (Kirchhausen et al., 2008), and pitstop 2 prevents the interaction between CHC and adaptor proteins related with formation of CCPs (Bayati et al., 2021). Nonetheless, the pleiotropic and off-target effects of these drugs have been described, as dynasore also presents dynamin-independent effects such us the disruption of lipid rafts, and pitstop 2 was reported to have additional cellular targets besides CHC (Macia et al., 2006; Dutta et al., 2012; Preta et al., 2015). On the other hand, chlorpromazine specifically inhibits CME by dissociating clathrin networks in the inner leaflet of the plasma

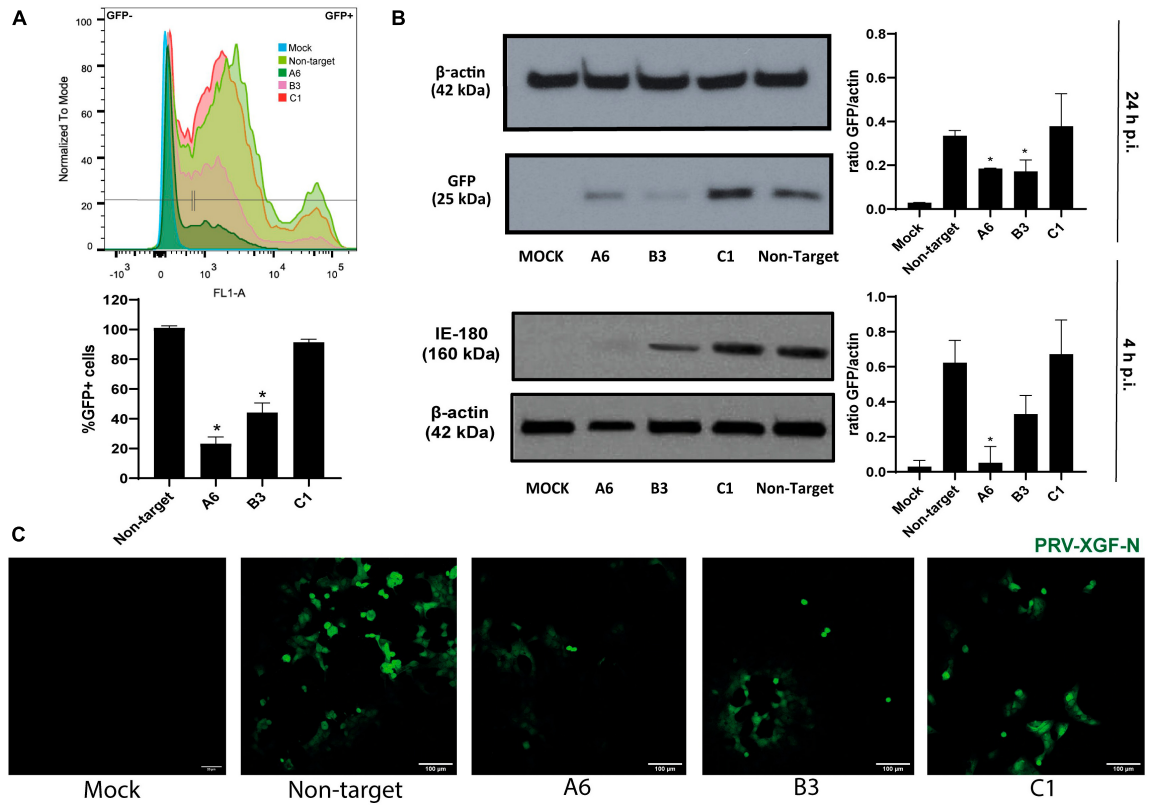

FIGURE 4
The knockdown of *AP2M1* in PK15 cells reduces PRV infection. KD PK15 cells A6, B3, and C1, and non-target cells were subjected to infection with PRV-XGF-N at an m.o.i of 0.5 (collected at 24 h p.i.) or moi 5 (collected at 4 h p.i.). After the corresponding time, samples were processed for the following experiments. **(A)** Flow cytometry analysis show the mean of the percentage of normalized infection 24 h p.i. (%GFP+ cells) ± S.D. (n = 4). Plots represent the histograms of GFP-positive (+) and GFP-negative (-) cells; *$p < 0.05$. **(B)** Western blot analysis of total cell lysates subjected to SDS-PAGE showing viral GFP or IE180 for each condition. β-actin was chosen as protein loading control. Values of immunoblot quantification are reported as the mean ± S.D. (n = 3); *$p < 0.05$. **(C)** Fluorescence microscopy images show GFP+ signal corresponding to viral infection 24 h p.i.

membrane during CCPs formation (Vercauteren et al., 2010). To validate the endocytosis assay performed with these drugs, we monitored the entry of dextran sulfate, a compound that is internalized by a clathrin-independent route. As a result, at the concentrations and cell system used here, while all CME inhibitory drugs altered Tf uptake, there were no differences in dextran uptake.

To confirm the results obtained in the experiments performed in the presence of the drugs, silencing of the μ subunit of AP-2 (AP2M1) with shRNAs was additionally performed. AP-2 is the second most abundant component of clathrin vesicles. This adaptor plays an important role in the maturation of CCPs so, when it is not present, the clathrin is not recruited and mature vesicles do not form (McMahon and Boucrot, 2011). AP-2 is an heterotetramer formed by four subunits (α, β, σ, and μ) and the phosphorylation of μ subunit by the kinase enzyme AP-2 associated protein kinase 1 (AAK1) stimulates clathrin and supports the cell surface receptor incorporation (Robinson, 2015; Tongmuang et al., 2020). As no chemical inhibitors of the whole AP-2 adaptor are commercially available, we used shRNA-based KD of the subunit μ, achieving approximately 90% depletion. AP-2 is structured into two heterodimers α/σ and ß/μ, so the lack of μ inhibits the assembly of heterodimer ß/μ and then leads to degradation of the ß subunit. As not enough ß/μ heterodimer is available, the full assembly is stopped and degradation of the other dimer α/σ is induced (Tobys et al., 2021). Several studies report that AP-2 complex acts, through its μ subunit, as a physical linker between clathrin triskelions and internalization sequences in receptors on the cell membrane in the first step of CCVs formation (Van Minnebruggen et al., 2004), so the absence of μ disrupts this process. A previous study also revealed the colocalization of glycoprotein gB (glycoprotein that contains internalization motifs) of PRV with AP-2 complex, demonstrating that during the early steps of the infection, PRV glycoprotein colocalize with clathrin triskelions (Van Minnebruggen et al., 2004).

In addition, no observable differences in shape or size between PK15 and AP2M1-KD were noticed, so cells might use CIE routes to maintain a normal surface/volume ratio. It must be considered that internalization through CME represents a major, albeit not exclusive pathway of entry into cells, as CIE pathways remain active to maintain internalization. That explains that PRV-XGF-N internalization is not completely stopped when blocking CME, taking into account that this pathway is not 100% blocked. In addition, several studies have postulated that clathrin not only plays an important role in the entry of numerous viruses into the host cell, but may also be involved, together with the protein dynamin, in endomembrane vesicular transport and envelope protein delivery to assembly sites, especially in the case of HSV-1 (Albecka et al., 2016). To make sure that in our experiments the decrease of

10.3389/fmicb.2024.1332175

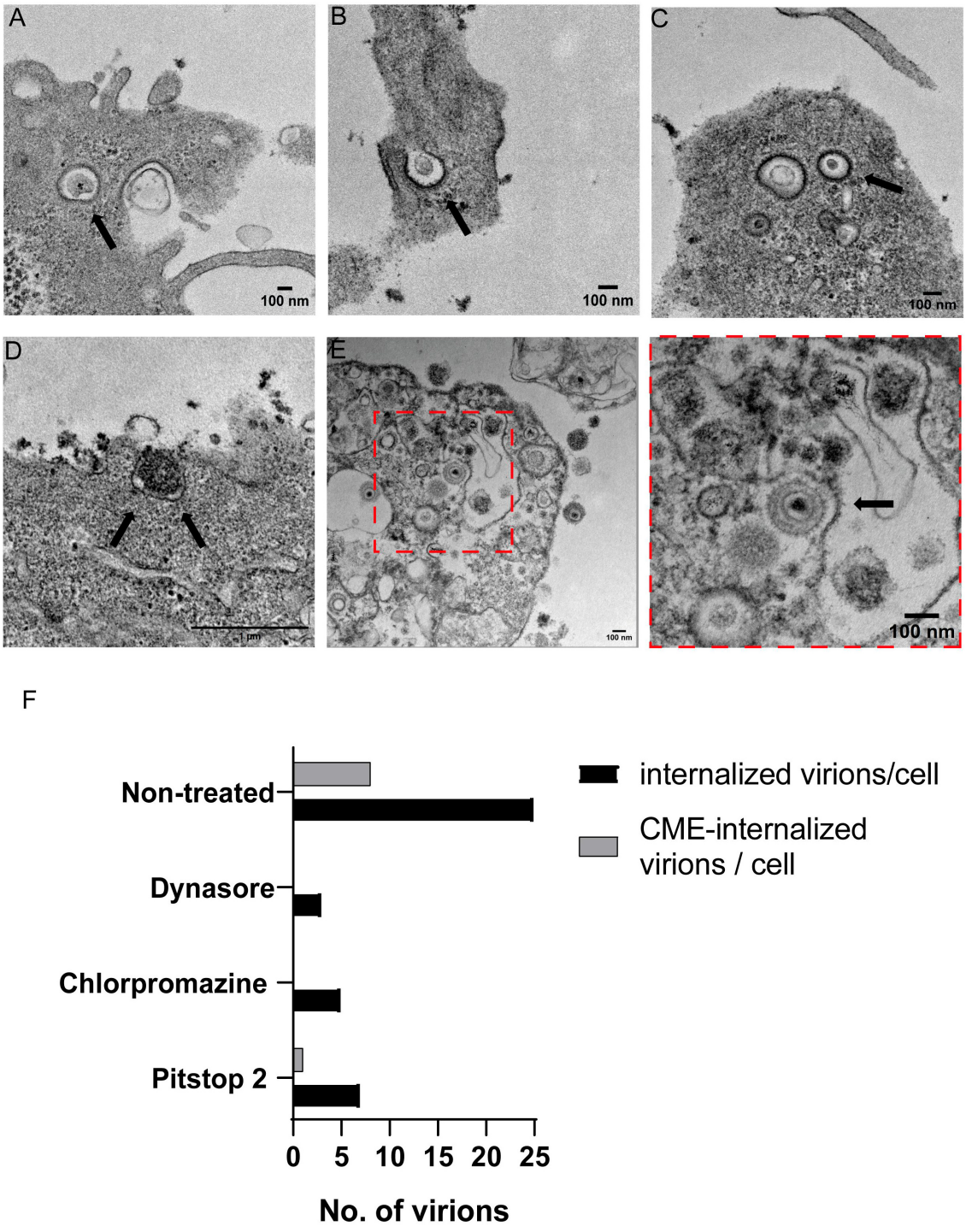

FIGURE 5
Transmission electron microscopy analysis of PRV-XGF-N virions inside clathrin vesicles in PK15 cells. Cells were infected with PRV-XGF-N at an m.o.i of 30 for 1 h at 4°C. Then they were maintained for 20 min at 37°C and processed for TEM. Arrows point to in **(A–C)** PRV-XGF-N virions inside clathrin vesicles, **(D)** virion entering a forming clathrin vesicle anchored in the cell membrane, and **(E)** overview of PRV-XGF-N surrounded by clathrin. **(F)** Quantification of the number of internalized virions per cell (*n* = 20 cells analyzed) in cells non-treated or treated with 100 μM dynasore, 20 μM chlorpromazine or 50 μM pitstop 2 for 1 h before infection, and during the 20 min of infection. The graph shows the number of virions inside the cell and from those, the virions entering via CME or internalized into CCVs.

infection when CME is inhibited is only due to blocked entry, infection experiments at short times were performed, evaluating the expression of IE180. Stopping the infection at such short times in experiments from the Figures 2, 4, 5 ensures that the virus has just entered and is performing its first infection cycle; therefore, it has not yet reached the assembly phase where clathrin possibly also plays a transporter role, although potentially to a lesser extent than during entry.

For best visualization of PRV-XGF-N using CME to enter PK15 cells, TEM was chosen as it currently is the unique imaging technique that allows direct visualization of viral particles at a nanometer-scale resolution (Roingeard et al., 2019). The images show virions internalized as cargo in CCVs, and virions surrounded by clathrin, as expected because viruses can produce signals for clathrin recruitment when internalization (Praena et al., 2020). It should be noted that the recombinant PRV-XGF-N strain used in the study lacks the gene encoding the gG glycoprotein. However, this is not of concern for clathrin entry studies, since gG is not essential for virulence and is not part of the virion structure, as it is secreted into the medium by the infected cells (Viejo-Borbolla et al., 2010). Having a GFP-expressing PRV strain that mimics the entry of wild-type PRV certainly speeds up and facilitates experimental work.

Understanding the mechanisms of PRV viral entry into host cells is crucial to contribute to the design of antiviral drugs or strategies that target this early step of infection. Various studies are already proposing antiviral agents against PRV which act early in its viral cycle, such as valpromide (Andreu et al., 2021), valnoctamide (Praena et al., 2019), U18666A (Li et al., 2022), or quercetin (Sun et al., 2021).

Together, our data enrich previous information about PRV viral cycle, focusing on the characterization of viral entry by using CME. We suggest that clathrin plays a relevant role in the endocytic entry of PRV-XGF-N into PK15 swine cell line, as demonstrated in AP2M1-KD cells and in the treatment with CME-inhibitory drugs. Both approaches led to a decrease in PRV-XGF-N infection. Further research not only *in vitro* but in models closer to the clinic is needed to unravel the intracellular trafficking route and the degree of involvement of clathrin and AP-2 in the route of entry of PRV.

Data availability statement

The original contributions presented in the study are included in the article/**Supplementary material**, further inquiries can be directed to the corresponding authors.

Ethics statement

Ethical approval was not required for the studies on animals in accordance with the local legislation and institutional requirements because only commercially available established cell lines were used.

Author contributions

SA: Data curation, Formal analysis, Investigation, Methodology, Writing – original draft, Writing – review and editing, Conceptualization. CA: Data curation, Investigation, Methodology, Writing – review and editing. IR: Writing – review and editing. JL-G: Conceptualization, Funding acquisition, Project administration, Supervision, Writing – review and editing. RB-M: Conceptualization, Data curation, Formal analysis, Funding acquisition, Investigation, Methodology, Supervision, Writing – original draft, Writing – review and editing.

Funding

The author(s) declare financial support was received for the research, authorship, and/or publication of this article. This work was supported by the Spanish Ministry of Science and Innovation (Ministerio de Ciencia e Innovación, grant number PID2022-140632NB-I00). The funders had no role in study design, data collection, analysis, publishing decisions, or manuscript preparation.

Conflict of interest

The authors declare that the research was conducted in the absence of any commercial or financial relationships that could be construed as a potential conflict of interest.

Publisher's note

Supplementary material

The Supplementary Material for this article can be found online at: https://www.frontiersin.org/articles/10.3389/fmicb.2024.1332175/full#supplementary-material

References

Albecka, A., Laine, R. F., Janssen, A. F. J., Kaminski, C. F., and Crump, C. M. (2016). HSV-1 glycoproteins are delivered to virus assembly sites through dynamin-dependent endocytosis. *Traffic* 17, 21–39. doi: 10.1111/tra.12340

Andreu, S., Ripa, I., Bello-Morales, R., and López-Guerrero, J. A. (2020). Valproic acid and its amidic derivatives as new antivirals against alphaherpesviruses. *Viruses* 12:1356. doi: 10.3390/v12121356

Andreu, S., Ripa, I., Praena, B., López-guerrero, J. A., and Bello-Morales, R. (2021). The valproic acid derivative valpromide inhibits pseudorabies virus infection in swine epithelial and mouse neuroblastoma cell lines. *Viruses* 13:2522. doi: 10.3390/v13122522

Barrow, E., Nicola, A. V., and Liu, J. (2013). Multiscale perspectives of virus entry via endocytosis. *Virol. J.* 10:177. doi: 10.1186/1743-422X-10-177

Bayati, A., Kumar, R., Francis, V., and McPherson, P. S. (2021). SARS-CoV-2 infects cells after viral entry via clathrin-mediated endocytosis. *J. Biol. Chem.* 296:100306.

Brodsky, F. M. (2012). Diversity of clathrin function: new tricks for an old protein. *Annu. Rev. Cell Dev. Biol.* 28, 309–336. doi: 10.1146/annurev-cellbio-101011-155716

Cossart, P., and Helenius, A. (2014). Endocytosis of viruses and bacteria. *Cold Spring Harb. Perspect. Biol.* 6:a016972.

Desplanques, A. S., Nauwynck, H. J., Vercauteren, D., Geens, T., and Favoreel, H. W. (2008). Plasma membrane cholesterol is required for efficient pseudorabies virus entry. *Virology* 376:339. doi: 10.1016/j.virol.2008.03.039

Dutta, D., Williamson, C. D., Cole, N. B., and Donaldson, J. G. (2012). Pitstop 2 is a potent inhibitor of clathrin-independent endocytosis. *PLoS One* 7:45799. doi: 10.1371/JOURNAL.PONE.0045799

Gómez-Sebastián, S., and Tabarés, E. (2004). Negative regulation of herpes simplex virus type 1 ICP4 promoter by IE180 protein of pseudorabies virus. *J. General Virol.* 85, 2125–2130. doi: 10.1099/vir.0.80119-0

Granzow, H., Klupp, B. G., and Mettenleiter, T. C. (2005). Entry of pseudorabies virus: an immunogold-labeling study. *J. Virol.* 79, 3200–3205.

Hemalatha, A., and Mayor, S. (2019). Recent advances in clathrin-independent endocytosis. *F1000Res* 8:F1000 Faculty Rev-138.

ISO 10993-5:2009 (Under Review). *Biological Evaluation of Medical Devices — Part 5: Tests for in Vitro Cytotoxicity*. Available online at: https://www.iso.org/standard/36406.html/ (accessed 19 September, 2023).

Kaksonen, M., and Roux, A. (2018). Mechanisms of clathrin-mediated endocytosis. *Nat. Rev. Mol. Cell Biol.* 19, 313–326.

Kerur, N., Veettil, M. V., Sharma-Walia, N., Sadagopan, S., Bottero, V., Paul, A. G., et al. (2010). Characterization of entry and infection of Monocytic THP-1 cells by Kaposi's Sarcoma Associated Herpesvirus (KSHV): role of heparan sulfate, DC-SIGN, integrins and signaling. *Virology* 406, 103–116. doi: 10.1016/j.virol.2010.07.012

Kirchhausen, T., Macia, E., and Pelish, H. E. (2008). Use of dynasore, the small molecule inhibitor of dynamin, in the regulation of endocytosis. *Methods Enzymol.* 438, 77–93.

Le Roy, C., and Wrana, J. L. (2005). Clathrin and non-clathrin-mediated endocytic regulation of cell signalling. *Nat. Rev. Mol. Cell Biol.* 6, 112–126. doi: 10.1038/nrm1571

Li, G., Su, B., Fu, P., Bai, Y., Ding, G., Li, D., et al. (2022). NPC1-regulated dynamic of clathrin-coated pits is essential for viral entry. *Sci. China Life Sci.* 65, 341–361. doi: 10.1007/s11427-021-1929-y

Macia, E., Ehrlich, M., Massol, R., Boucrot, E., Brunner, C., and Kirchhausen, T. (2006). Dynasore, a cell-permeable inhibitor of dynamin. *Dev. Cell* 10, 839–850.

McMahon, H. T., and Boucrot, E. (2011). Molecular mechanism and physiological functions of clathrin-mediated endocytosis. *Nat. Rev. Mol. Cell Biol.* 12, 517–533.

Mercer, J., Schelhaas, M., and Helenius, A. (2010). Virus entry by endocytosis. *Annu. Rev. Biochem.* 79, 803–833.

Mettlen, M., Chen, P. H., Srinivasan, S., Danuser, G., and Schmid, S. L. (2018). Regulation of clathrin-mediated endocytosis. *Annu. Rev. Biochem.* 87:871.

Mettlen, M., Pucadyil, T., Ramachandran, R., and Schmid, S. L. (2009). Dissecting Dynamin's role in clathrin-mediated endocytosis. *Biochem. Soc. Trans.* 37:1022.

Miller, J. L., Weed, D. J., Lee, B. H., Pritchard, S. M., and Nicola, A. V. (2019). Low-PH endocytic entry of the porcine alphaherpesvirus pseudorabies virus. *J. Virol.* 93:e01849-18. doi: 10.1128/JVI.01849-18

Millert, N., and Hutt-Fletcher, L. M. (1992). Epstein-barr virus enters b cells and epithelial cells by different routes. *J. Virol.* 66:3409.

Nicola, A. V. (2016). Herpesvirus entry into host cells mediated by endosomal low PH. *Traffic* 17, 965–975. doi: 10.1111/tra.12408

Nixdorf, R., Schmidt, J., Karger, A., and Mettenleiter, T. C. (1999). Infection of Chinese hamster ovary cells by Pseudorabies virus. *J. Virol.* 73, 8019–8026.

Pastenkos, G., Lee, B., Pritchard, S. M., and Nicola, A. V. (2018). Bovine herpesvirus 1 entry by a low-PH endosomal pathway. *J. Virol.* 92:e00839-18. doi: 10.1128/JVI.00839-18

Praena, B., Bello-Morales, R., de Castro, F., and López-Guerrero, J. A. (2019). Amidic derivatives of Valproic acid, Valpromide and Valnoctamide, inhibit HSV-1 infection in oligodendrocytes. *Antiviral Res.* 168, 91–99. doi: 10.1016/j.antiviral.2019.05.006

Praena, B., Bello-Morales, R., and López-Guerrero, J. A. (2020). Hsv-1 endocytic entry into a human oligodendrocytic cell line is mediated by clathrin and dynamin but not caveolin. *Viruses* 12:734. doi: 10.3390/v12070734

Preta, G., Cronin, J. G., and Sheldon, I. M. (2015). Dynasore - not just a Dynamin inhibitor. *Cell Commun. Signal.* 13:24.

Prichard, K. L., O'Brien, N. S., Murcia, S. R., Baker, J. R., and McCluskey, A. (2022). Role of clathrin and dynamin in clathrin mediated endocytosis/synaptic vesicle recycling and implications in neurological diseases. *Front. Cell Neurosci.* 15:549. doi: 10.3389/FNCEL.2021.754110/BIBTEX

Rappoport, J. Z. (2008). Focusing on clathrin-mediated endocytosis. *Biochem. J.* 412, 415–423.

Ren, X., Yin, J., Li, G., and Herrler, G. (2011). Cholesterol dependence of pseudorabies herpesvirus entry. *Curr. Microbiol.* 62, 261–266. doi: 10.1007/s00284-010-9700-8

Ripa, I., Andreu, S., López-Guerrero, J. A., and Bello-Morales, R. (2021). Membrane rafts: portals for viral entry. *Front. Microbiol.* 12:631274. doi: 10.3389/FMICB.2021.631274

Robinson, M. S. (2015). Forty years of clathrin-coated vesicles. *Traffic* 16, 1210–1238.

Roingeard, P., Raynal, P. I., Eymieux, S., and Blanchard, E. (2019). Virus detection by transmission electron microscopy: still useful for diagnosis and a plus for biosafety. *Rev. Med. Virol.* 29:e2019. doi: 10.1002/rmv.2019

Schindelin, J., Arganda-Carreras, I., Frise, E., Kaynig, V., Longair, M., Pietzsch, T., et al. (2012). Fiji: an open-source platform for biological-image analysis. *Nat. Methods* 9, 676–682. doi: 10.1038/nmeth.2019

Shihan, M. H., Novo, S. G., Le Marchand, S. J., Wang, Y., and Duncan, M. K. (2021). A simple method for quantitating confocal fluorescent images. *Biochem. Biophys. Rep.* 25:100916.

Sobhy, H. (2017). A comparative review of viral entry and attachment during large and giant DsDNA virus infections. *Archives Virol.* 162, 3567–3585. doi: 10.1007/s00705-017-3497-8

Sun, Y., Li, C., Li, Z., Shangguan, A., Jiang, J., Zeng, W., et al. (2021). Quercetin as an antiviral agent inhibits the Pseudorabies virus in vitro and in vivo. *Virus Res.* 305:198556. doi: 10.1016/j.virusres.2021.198556

Tebaldi, G., Pritchard, S. M., and Nicola, A. V. (2020). Herpes simplex virus entry by a nonconventional endocytic pathway. *J. Virol.* 94:e01910-20 doi: 10.1128/JVI.01910-20

Tobys, D., Kowalski, L. M., Cziudaj, E., Müller, S., Zentis, P., Pach, E., et al. (2021). Inhibition of clathrin-mediated endocytosis by knockdown of AP-2 leads to alterations in the plasma membrane proteome. *Traffic* 22, 6–22. doi: 10.1111/tra.12770

Todaro, G. J., Benveniste, R. E., Lieber, M. M., and Sherr, C. J. (1974). Characterization of a type C virus released from the porcine cell Line PK(15). *Virology* 58, 65–74. doi: 10.1016/0042-6822(74)90141-x

Tongmuang, N., Yasamut, U., Noisakran, S., Sreekanth, G. P., and Yenchitsomanus, P. (2020). thai; Limjindaporn, T. suppression of M1 subunit of the adaptor protein complex 2 reduces dengue virus release. *Virus Genes* 56, 27–36. doi: 10.1007/s11262-019-01710-x

Van Minnebruggen, G., Favoreel, H. W., and Nauwynck, H. J. (2004). Internalization of Pseudorabies virus Glycoprotein B is mediated by an interaction between the YQRL motif in its cytoplasmic domain and the clathrin-associated AP-2 adaptor complex. *J. Virol.* 78, 8852–8859. doi: 10.1128/JVI.78.16.8852-8859.2004

Vercauteren, D., Vandenbroucke, R. E., Jones, A. T., Rejman, J., Demeester, J., De Smedt, S. C., et al. (2010). The use of inhibitors to study endocytic pathways of gene carriers: optimization and pitfalls. *Mol. Ther.* 18, 561–569. doi: 10.1038/mt.2009.281

Viejo-Borbolla, A., Muñoz, A., Tabarés, E., and Alcamí, A. (2010). Glycoprotein G from pseudorabies virus binds to chemokines with high affinity and inhibits their function. *J. General Virol.* 91, 23–31. doi: 10.1099/vir.0.011940-0

Yamauchi, Y., and Helenius, A. (2013). Virus entry at a glance. *J. Cell Sci.* 126, 1289–1295. doi: 10.1242/jcs.119685

frontiers | Frontiers in Microbiology

TYPE Original Research
PUBLISHED 08 February 2024
DOI 10.3389/fmicb.2024.1352315

OPEN ACCESS

EDITED BY
Leyi Wang,
University of Illinois at Urbana-Champaign, United States

REVIEWED BY
Xiuqing Wang,
South Dakota State University, United States
Michael Rahe,
North Carolina State University, United States

*CORRESPONDENCE
J. A. Pasternak
jpastern@purdue.edu

RECEIVED 07 December 2023
ACCEPTED 26 January 2024
PUBLISHED 08 February 2024

CITATION
Rudy K, Jeon D, Smith AA, Harding JCS and Pasternak JA (2024) PRRSV-2 viral load in critical non-lymphoid tissues is associated with late gestation fetal compromise. *Front. Microbiol.* 15:1352315. doi: 10.3389/fmicb.2024.1352315

PRRSV-2 viral load in critical non-lymphoid tissues is associated with late gestation fetal compromise

K. Rudy[1], D. Jeon[1], A. A. Smith[1], J. C. S. Harding[2] and J. A. Pasternak[1]*

[1]Department of Animal Sciences, Purdue University, West Lafayette, IN, United States, [2]Department of Large Animal Clinical Sciences, Western College of Veterinary Medicine, University of Saskatchewan, Saskatoon, SK, Canada

The impact of late gestation PRRSV-2 infection is highly variable within a litter, with a subset of fetuses displaying varying degrees of compromise following infection while others remain viable despite significant systemic viral load. To understand the underlying cause of this variation, we examined the susceptibility, distribution and impact of viral infection within non-lymphoid tissues. Samples of brain, heart, kidney, liver, lung, and skeletal muscle were obtained from fetuses of pregnant gilts at gestation day 86, and the presence and distribution of CD163+ cells within each tissue evaluated via immunohistofluorescence. Equivalent samples were collected from phenotypic extremes representing resistant, resilient and susceptible fetuses at 21 days following infection of pregnant gilts with PRRSV-2 at day 86 of gestation. Viral load and its impact in each tissue was evaluated by a combination of qPCR, *in vitro* viral recovery, and local expression of IFNG and CD163. Resting populations of CD163+ cells were observed in all six non-lymphoid tissues from healthy day 86 fetuses, though the apparent density and the morphology of positive cells varied between tissue. Viral RNA was detected in all six tissues derived from fetuses previously classified as highly infected, and infectious viral particles successfully recovered. Significantly more viral RNA was detected in heart, brain, lung and skeletal muscle of susceptible fetuses, relative to their viable counterparts. Infection was associated with an increase in the expression of CD163 in brain, kidney and lung. In addition, the presence of virus in each tissue coincided with a significant upregulation in the expression of IFNG, but the scale of this response was not associated with fetal susceptibility. Thus, PRRSV-2 is widely distributed across these susceptible non-lymphoid fetal tissues, and fetal outcome is associated with local viral load in critical fetal organs.

KEYWORDS

PRRSV, fetal, immune response, non-lymphoid, *in utero* infection, Nidovirus, meconium staining

1 Introduction

Porcine reproductive and respiratory syndrome virus (PRRSV) is a highly transmissible, single-stranded RNA virus, originally associated with its reproductive consequences in the early 1990's (Terpstra et al., 1991). Though initially detected in specific geographic regions, the virus now has near global distribution, with endemic and emerging strains found in nearly

every major pork producing country. Within the American swine herd, PRRSV was last estimated to cause annual losses in excess of $660 million, 45% of which is incurred by the breeding herd (Holtkamp et al., 2013). Unlike postnatally infected pigs which experience respiratory symptoms and reduced growth performance (Van Reeth et al., 2001; Pasternak et al., 2021), most strains cause limited respiratory symptoms in the infected dams (Ladinig et al., 2015). Thus, the primary economic impact of PRRSV within the breeding herd results from reproductive consequences including an increase in stillbirths, *in utero* death, and abortions. The fetal outcomes following maternal PRRSV infection vary substantially within a litter, with the most susceptible population found dead or autolyzed *in utero* (Benson et al., 2002). An additional portion of the live fetal population is found meconium stained, which is recognized as an initial marker of severe fetal stress and is the first indicator of fetal compromise (Harding et al., 2017). Those pigs that do survive to term are born weak, often congenitally infected and more susceptible to other pathogens (Feng et al., 2001).

PRRSV is able to cross the late gestation porcine placenta, via an as yet unidentified mechanism, and thereby productively infect a subset of fetuses (Kranker et al., 1998). A pair of early studies surveyed viral load across a range of fetal tissues including heart, liver, lung, spleen, tonsils, thymus and umbilical cord, following late gestation maternal challenge (Benson et al., 2002; Rowland, 2010). Virus was, at minimum, sporadically detected in all these tissues, however, the relative frequency of viral recovery led to the conclusion that the fetal thymus was the primary site of viral infection (Rowland, 2010). Since this seminal finding, thymic viral load has been used in conjunction with serum and placenta to categorize infection status in studies designed to elucidate the physiological impact and mechanism of fetal compromise. Serial studies following infection at a fixed time point have shown an orderly progression of infection beginning with the placenta, followed by fetal serum, and then finally the fetal thymus (Malgarin et al., 2019). However, subsequent studies demonstrated that a fetal immune response is only initiated after significant virus has accumulated within the thymus (Van Goor et al., 2020). It was initially hypothesized that the fetal immune response may represent a double-edged sword, combating viral progression, while at the same time compromising fetal development and survival (Rowland, 2010). However, there is limited evidence that the scale of this inflammatory cytokine response plays a role in fetal compromise (Pasternak et al., 2020a). PRRSV infection has also been associated with alteration in the structure and physiology of the maternal fetal interface, however, it is not known whether such effects are the cause or consequence of fetal death (Barrera-Zarate et al., 2022; Guidoni et al., 2022). Thus, the fundamental mechanism by which transplacental infection results in fetal compromise has yet to be identified, potentially hampering the development of beneficial treatments.

To better understand viral load as it relates to fetal compromise, we first evaluated PRRSV susceptibility of late gestation fetal tissues by assessing the presence of cells expressing the virus's obligate receptor CD163. We then quantified PRRSV viral RNA in tissues from fetuses classified using an established model of phenotypic extremes in serum and thymic viral load and verified the presence of infectious particles using *in vitro* culture. Finally, we evaluated the impact of viral infection on the local immune response by quantifying IFNG and CD163 expression.

2 Materials and methods

2.1 Fetal tissues

For assessment of healthy fetal tissues, three Landrace x Large White gilts were selected and housed at the Animal Sciences Research and Education Center (ASREC) at Purdue University in compliance with Institutional Animal Care and Use Committee regulations and approved by the Purdue Animal Care and Use Committee (Protocol #2103002122). The gilts were estrus synchronized using oral progestogen [15 mg/day Altrenogest] and bred via artificial insemination at the first standing estrus post withdraw, and every 24 h after until the end of standing estrus. Pregnancy was verified by ultrasound between days 25 and 30 and gestation and allowed to progress until day 86 relative to the first insemination. Gilts were stunned with a penetrating captive bolt followed by rapid exsanguination to allow for sampling of fetal tissues including the brain (BRN), heart (HRT), liver (LVR), lung (LNG), kidney (KID), and longissimus dorsi muscle (MUS) from healthy viable fetuses. To investigate the distribution of virus in fetal tissues, archived samples were selected from a previously described PRRSV challenge trial (Ko et al., 2022), carried out in strict accordance with the guidelines of the Canadian Council of Animal Care and with approval of the University of Saskatchewan's Animal Research Ethics Board (Protocol #20180071). In short, N = 22 pregnant gilts (Fast Genetics, Spiritwood, Canada) were inoculated with 1×10^5 TCID50 PRRSV species 2 (PRRSV-2) strain NVSL 97-7895 on gestation day 86, delivered via a combination of intramuscular injection and intranasal atomization. An additional $N = 5$ gilts were sham inoculated to produce gestationally age matched controls (CON). At 21 days post inoculation (DPI), all animals were humanely euthanized by cranial captive bolt and intravenous barbiturate overdose. The gravid uterus was extracted and the fetal preservation (viable, meconium stained, dead, autolyzed and mummified) and phenotypes, including body weight and crown rump length, assessed as previously described (Ko et al., 2022). Tissue samples were then collected from all fetuses with visible pulsations within the umbilical cord (fetal preservation of viable or meconium stained). Developmentally normal fetuses were further subdivided by degree of fetal preservation, based on the presence and severity of meconium staining. In the absence of meconium staining, fetuses were classified as viable (VIA), while those exhibiting severe meconium staining (head and body) were classified as non-viable (MEC). Fetuses were rapidly exsanguinated post-mortem by severing the axillary artery, and blood samples collected for the isolation of serum. Fetal tissues including the BRN, HRT, LVR, LNG, KID and MUS, along with a combination of cervical and thoracic thymus, were collected from each fetus and individually snap frozen in liquid nitrogen. All samples were stored at-80°C for later analysis. Viral load in fetal serum and thymus was quantified by qPCR as previously described (Malgarin et al., 2021) and used in combination with meconium staining status to identify fetuses in three biologically extreme groups (Table 1). Viable fetuses with no detectable viral load in either serum or thymus were classified as uninfected (UNIF). Fetuses with >5 $\log_{10}$ of virus in serum and thymus were considered highly infected, and further subdivided into high viral load viable (HV-VIA), or high viral load meconium stained (HV-MEC). A fourth control group (CON) of viable fetuses was selected from sham inoculated and gestationally age matched gilts. From each of these

TABLE 1 Phenotypes of fetal groups representing biological extremes in resistance in response to maternal PRRSV infection.

				Viral load*	
Group	*N*	Fetal weight (g)	Crown rump length (cm)	Serum	Thymus
CON	10	990.77 ± 218.76	35.7 ± 2.5	0 (0–0)	0 (0–0)
UNIF	10	956.13 ± 217.78	36.5 2.8	0 (0–0)	0 (0–0)
HV-VIA	10	907.40 ± 216.55	35.9 ± 2.9	7.79 (5.93–9.22)	6.73 (5.51–7.89)
HV-MEC	10	1044.7 ± 249.78	35.7 ± 3.1	8.22 (7.41–9.09)	6.74 (5.01–8.09)

Fetal weight and crown rump length are reported as mean ± standard deviation.
*serum and thymic viral load in the form of log 10 RNA copies per mg (thymus) or mL (serum) and reported as mean (range).

groups, $N = 10$ fetuses with the lowest z-scores for serum T4 were selected as previously described, such that no significant differences in other phenotypic parameters such as fetal weight or crown rump length existed between groups (Mulligan et al., 2022).

2.2 Immunohistofluorescence

Samples of BRN, HRT, LVR, LNG, KID, and MUS from healthy fetuses, derived from unchallenged gilts at day 86 of gestation were suspended in optimal cutting temperature media (OCT) and frozen on the surface of a dry ice block. Sequential 10 µm thick cross-sections of each tissue were cut on a Leica CM1950 cryotome at −20°C, affixed to Superfrost Plus slides (Thermo Fisher Scientific, Waltham, MA, United States) and air-dried for 30 min at room temperature. Slides were rehydrated in phosphate buffered saline (PBS) before fixing in ice-cold acetone for 10 min. Tissue sections were blocked against non-specific binding for 2 h with 0.1% w/v BSA and 10% horse serum in PBS. Sections were then incubated over night at 4°C with 10 µg/mL mouse anti-bovine CD163 [Clone LND68A, Washington State Monoclonal Antibody Center], previously shown to cross-react with both isoforms of the porcine target (Pasternak et al., 2019), or the equivalent concentration of mouse IgG1 isotype control. Sections were then washed three times in PBS before incubating with 1 µg/mL Alexa Fluor 555 conjugated F(ab')2-goat anti-mouse IgG, secondary antibody for 2 h at room temperature. Slides were again washed three times before counter staining with 0.5 µg/mL DAPI in methanol for 10 min at room temperature and cover slipping with Mowiol. Fluorescent evaluation and imaging were carried out in triplicate using an Echo Revolution microscope equipped with 10× and 20× objectives.

2.3 Viral load and host gene expression in non-lymphoid tissues

Samples of BRN, HRT, LVR, LNG, KID and MUS from each selected fetus were cryogenically homogenized using a pre-chilled mortar and pestle. Trizol (Thermofisher, Waltham, MA, United States) was then used to extract total RNA from a subsample of each tissue homogenate using a double precipitation protocol (Oliver et al., 2011). DNA contamination was removed using the Turbo DNA-free Kit (Invitrogen) as per the manufacturer's instructions, but with the addition of 5 U of RNase Inhibitor (ThermoFisher). Concentration and purity of the RNA was assessed using a Nanodrop ND-1000 spectrophotometer (ThermoFisher), and integrity was evaluated using denaturing gel electrophoresis (Kent-Dennis et al., 2019). Reverse transcription with 2 µg total RNA was carried out using the High-Capacity cDNA Reverse Transcription Kit (Applied Biosystems, Foster City, CA, United States). Absolute quantification of PRRSV-2 was carried out using virus specific primers (5′-TAATGGG CTGGCATTCCT-3′ and 5′-ACACGGTCGCCCTAATTG-3′) and a corresponding Taqman probe (5′-FAM-TGTGGTGAATG GCACTGATTG-BHQ-3′), with a seven-point standard curve starting at 10^7 copies/µL of the target amplicon cloned into TOPO vector (Invitrogen, Carlsbad, CA, United States). Host gene expression was measured using previously validated gene specific primers (Table 2). All qPCR assays were carried out in duplicate using 20 ng cDNA per reaction on a CFX Connect Real-Time System (Bio-Rad) using SsoAdvanced Universal SYBR Green SuperMix (Bio-Rad). Absolute quantification for viral load is expressed in the form of copy number (CN) per 20 ng equivalent cDNA as previously established (Ison et al., 2022). For relative quantification, the stability of eight housekeeping genes was evaluated, and the geometric mean of two or three stable genes in each tissue was used to normalize expression of each gene of interest, and fold change was then calculated relative to the mean expression in the control group using the $2^{-\Delta\Delta CT}$ method.

2.4 Viral recovery from tissue

MARC-145 cells were cultured in high glucose minimal essential media supplemented with 10% fetal bovine serum, 100 units/mL of penicillin, 100 µg/mL of streptomycin, and 0.225 µg/mL of amphotericin B. Where sufficient sample of fetal tissue were available, 70–100 mg aliquots, previously ground to a fine powder under liquid nitrogen, were mixed with culture media at a ratio of 1 mg/mL. Zirconia beads (1 mm, biospec) were added, and the mixture further homogenized for two 1 min periods at 60 Hz. The mixture was then centrifuged at 10,000 × g for 10 min and the resulting lysate collected. MARC-145 cells in 96 well plates were inoculated in triplicate with 100 µL of tissue lysate and cultured for 72 h at 37°C and 5% CO_2. Media was aspirated and the cells washed twice with PBS, followed by subsequent fixation with 80% acetone for 10 min. The acetone was then removed and the plates dried for 1 h at room temperature. Cells were then blocked with 1% BSA in PBS, before incubating with a 1:1000 dilution of mouse anti-PRRSV antibody (SDOW-17, RTI, Brookings, SD) for 30 min at 37°C. Cells were then washed twice with PBS before incubating with 2 µg/mL Alexa488 conjugated goat anti mouse IgG1 (A-21121, Thermofisher scientific) for 15 min at room temperature. Monolayers were then washed twice with PBS and counter stained with 1 µg/mL DAPI for 5 min at room

TABLE 2 Porcine specific qPCR primer sequences.

Target	NCBI Gene ID	Forward primer	Reverse primer	Tm (°C)	Length (bp)	Target sequence or Reference
ACTB	414,396	5′-CCAGCACGATGAAGATCAAG-3′	5′-AGTCCGCCTAGAAGCATTTG-3′	60	171	Ison et al. (2023)
CD163	397,031	5′-ATTACCTGCTCAGCCCACAG-3′	5′-CGCCTCCAGAGAGAAGTCAG-3′	61	126	NM_213976.1
HMBS	396,581	5′-AGGATGGGCAACTCTACCTG-3′	5′-GATGGTGGCCTGCATAGTCT-3′	61	83	Pasternak et al. (2016)
IFNG	396,991	5′-GCTCTGGGAAACTGAATGAC-3′	5′-TCTCTGGCCTTGGAACATAG-3′	61	167	Pasternak et al. (2020a)
PPIA	397,637	5′-CACTGCCAAGACTGAGTGGT-3′	5′-TGTCCACAGTCAGCAATGGT-3′	61	144	Pasternak et al. (2020b)
RPL19	396,989	5′-AACTCCCGTCAGCAGATCC-3′	5′-AGTACCCTTCCGCTTACCG-3′	60	147	Pasternak et al. (2015)
SDHA	780,433	5′-CTACAAGGGGCAGGTTCTGA-3′	5′-AAGACAACGAGGTCCAGGAG-3′	61	141	Pasternak et al. (2016)
STX5	100,628,048	5′-TGCAGAGTCGTCAGAATGGA-3′	5′-CCAGGATTGTCAGCTTCTCC-3′	60	144	Pasternak et al. (2020a)
TBP	110,259,740	5′-CTGAATGCTGAGGCGATTTC-3′	5′-GCTGTGGAGTCAGTCCTGTG-3′	61	186	Pasternak et al. (2020b)
YWHAZ	780,440	5′-TGATGATAAGAAAGGGATTGTGG-3′	5′-GTTCAGCAATGGCTTCATCA-3′	62	203	Pasternak et al. (2020a,b)

temperature, washed with PBS, and then examined for PRRSV infection on an inverted fluorescent scope. Virus was deemed recovered from a given sample if positive PRRSV staining was observed in one or more wells.

2.5 Data analysis

All data processing and statistical analyses were performed in R 4.2.3 (R Core Team, 2019). Viral load and host tissue gene expression data were assessed for normality using a combination of graphical assessment and Shapiro-Wilks test and found to be non-normal. Data was subsequently evaluated within tissue using a non-parametric approach consisting of Kruskal-Wallis followed by a pairwise Wilcox test with Benjamini-Hochberg correction for multiple group testing. Numerical data was visualized using the ggplot2 package (Wickham, 2016) with statistically significant differences ($p < 0.05$), where present, marked with unique superscripts.

3 Results

3.1 CD163 in late gestation fetal tissues

To determine the capacity for PRRSV-2 infection in late gestation non-lymphoid fetal tissues, we assessed the availability of the obligate receptor, CD163, by immunohistoflourescence and carried out a qualitative assessment of morphology and distribution. Positive staining for CD163 was observed on the surface of cells in all six non-lymphoid tissues from healthy day 86 fetuses, though the relative density, morphology and spatial localization of positive cells varied between tissue (Figure 1). In the brain, staining for CD163 found positive cells to be spatially restricted to the pia matter (outer most surface of the BRN sections evaluated). In the HRT, clusters of positive cells were observed throughout the ventricular myocardium and epicardium. Positive cells were observed throughout the KID but appeared to be enriched within the collecting ducts and renal capsule relative to the cortex. In the LNG, positive staining was observed within the interstitial compartment and alveolar spaces. In the LVR, positive CD163 staining of small cells were found to be evenly distributed throughout the hepatic lobule. Positive staining of satellite cells, closely associated with the surface of muscle fibers were observed throughout the cross section of MUS.

3.2 Viral load in non-lymphoid tissues

To evaluate the broader distribution of PRRSV-2 RNA, we initially assessed viral load in six non-lymphoid tissues including BRN, HRT, KID, LNG, LVR and MUS (Figure 2) in fetuses from PRRSV-2 infected gilts. No significant viral load was observed in any of the six tissues in fetuses previously categorized at UNIF based on prior assessment of serum and thymus. In contrast, significant quantities of viral RNA were detected in all six tissues derived from high infected fetuses. Overall, the median viral load for HV fetuses was greatest in the HRT. The highest viral load in non-lymphoid tissues was also detected in the HRT ($\tilde{x}$ = 26,734 CN/20 ng cDNA), and significantly greater ($p = 0.021$) virus concentration was found in HRT tissue from HV-MEC ($\tilde{x}$ = 42,798 CN/20 ng cDNA) relative to HV-VIA ($\tilde{x}$ = 13,233 CN/20 ng cDNA). A similar median viral load was detected in KID and LNG from HV fetuses ($\tilde{x}$ = 7,445 and $\tilde{x}$ = 7,779 CN/20 ng cDNA respectively). While a significant difference ($p = 0.037$) was identified in the LNG of HV-VIA ($\tilde{x}$ = 6,207 CN/20 ng cDNA) compared to HV-MEC ($\tilde{x}$ = 36,534 CN/20 ng cDNA), no significant difference ($p = 0.41$) between HV-VIA ($\tilde{x}$ = 6,426 CN/20 ng cDNA) and HV-MEC ($\tilde{x}$ = 18,444 CN/20 ng cDNA) was observed in KID. Equivalent median viral loads were also observed in BRN and LVR ($\tilde{x}$ = 1,774 and $\tilde{x}$ = 1,900 CN/20 ng cDNA respectively). Viral load was significantly ($p = 0.045$) greater in BRN tissues from HV-MEC ($\tilde{x}$ = 6,486 CN/20 ng cDNA) than HV-VIA ($\tilde{x}$ = 743 CN/20 ng cDNA), but equivalent in LVR of HV-VIA ($\tilde{x}$ = 950 CN/20 ng cDNA) and HV-MEC ($\tilde{x}$ = 3,658 CN/20 ng cDNA) fetuses. The lowest viral load in tissues from HV fetuses was detected in MUS ($\tilde{x}$ = 548 CN/20 ng cDNA), with significantly ($p = 0.02$) greater virus observed in MUS from HV-MEC ($\tilde{x}$ = 1,704 CN/20 ng cDNA) relative to HV-VIA ($\tilde{x}$ = 256 CN/20 ng cDNA) fetuses.

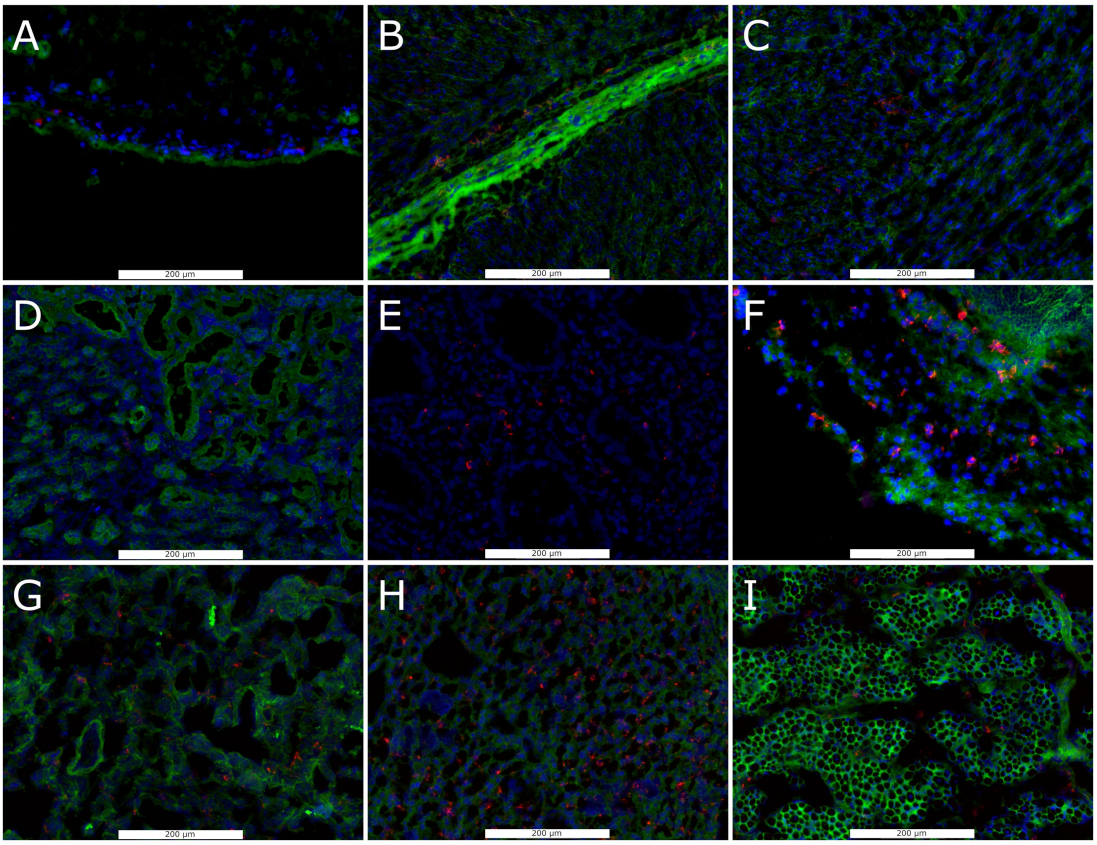

FIGURE 1
Representative florescent images of CD163+ cell staining in frozen sections of non-lymphoid fetal tissues collected at day 86 of gestation, including brain **(A)**, heart including epicardium **(B)**, and myocardium **(C)**, kidney including cortex **(D)**, collecting duct **(E)**, and capsule **(F)**, lung **(G)**, liver **(H)** and loin muscle **(I)**. Sections were stained with antibodies against anti-CD163 (Red), with DAPI (blue) and wheat germ agglutinin (Green) as a counter stains.

3.3 Viral recovery

To confirm the presence of infectious viral particles, we inoculated MARC-145 cells with fetal tissue lysates and evaluated viral recovery via immunofluorescent staining with a PRRSV specific monoclonal antibody (Table 3). No virus was recovered from lysates prepared from any of the six tissues isolated from control fetuses. In contrast, virus was successfully recovered in over 90% in HRT, LNG and MUS samples originating from highly infected (HV-VIA & HV-MEC) fetuses. Overall viral recovery rates were lower in KID, LVR and BRN, at 70, 42 and 30%, respectively. No significant difference in the recovery rate was observed between HV-VIA and HV-MEC fetuses for any of the tissues evaluated.

3.4 Impact of local infection

To determine if viral infection status impacts the local population of susceptible cells, we evaluated the gene expression of CD163 across six non-lymphoid fetal tissues from PRRSV infected gilts (Figure 3). Median expression of CD163 was significantly increased by 2.3 fold in the BRN ($p < 0.001$), 2.7 fold in the LNG ($p = 0.005$) and 2.2 fold in the KID ($p = 0.19$) of HV-MEC fetuses relative to UNIF. Increased expression of CD163 in MUS from HV-MEC fetuses showed a trend toward significance ($p = 0.052$) relative to both CON and UNIF groups. In contrast, gene expression of CD163 in the LVR of HV-VIA fetuses was decreased by 15 fold relative to CON ($p = 0.002$). No significant change in CD163 was observed in the HRT. Finally, to understand the local inflammatory response following infection of non-lymphoid tissues, we evaluated gene expression of IFNG (Figure 4). No significant difference in IFNG expression was observed any of the six tissues from UNIF fetuses relative to CON. Expression was significantly increased relative to CON in all six tissues from HV-VIA and HV-MEC fetuses, but no significant difference between these two highly infected groups was observed. The largest increases in median IFNG gene expression among highly infected fetuses were found in the HRT ($\tilde{x} = 18.1$ fold), KID ($\tilde{x} = 15.0$ fold), LNG ($\tilde{x} = 27.9$ fold) and LVR ($\tilde{x} = 19.2$ fold), while upregulation in the MUS ($\tilde{x} = 10.2$ fold) and BRN ($\tilde{x} = 6.6$ fold) were comparatively lower.

4 Discussion

PRRSV is capable of crossing the late gestation porcine placenta and productively infecting the fetus. Unlike postnatal animals, where the primary site of infection is the lung, the thymus has historically been recognized as the primary site of viral replication in the fetus (Rowland, 2010). Assessment of viral load in additional samples including blood and placenta have been used in conjunction with thymus to categorize fetal infection status and evaluate progressive severity in infection (Van

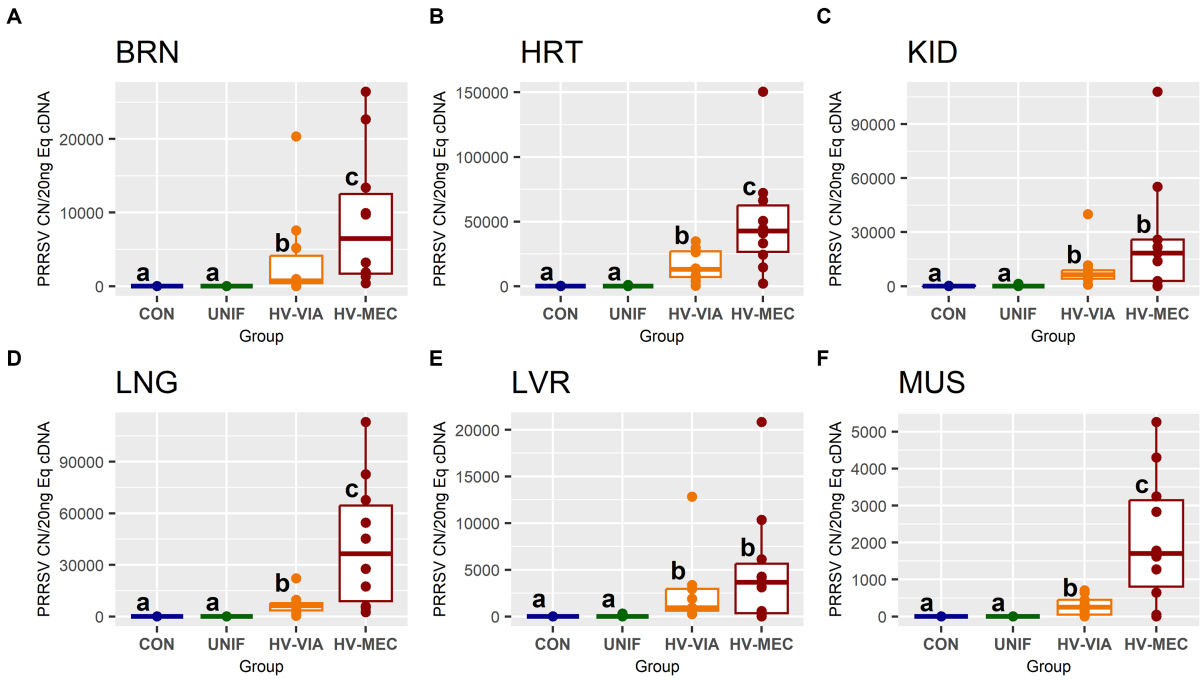

FIGURE 2
Viral RNA, as measured by PRRSV-2 strain specific absolute quantification qPCR, in fetal brain (BRN), heart (HRT), kidney (KID), lung (LNG), liver (LVR) and skeletal muscle (MUS) in fetuses uninfected (UNIF), high viral load viable (HV-VIA) and high viral load meconium stained (HV-MEC), 21 days after maternal PRRSV2 challenge, along with equivalent tissues from control (CON) fetuses derived from gestationally age matched and sham inoculated dams. Viral load is expressed as copy number (CN) per 20 ng equivalent cDNA, with unique superscripts indicating statistically significant differences ($p < 0.05$).

TABLE 3 Rate of viral recovery using cell lysates from 6 non-lymphoid tissues derived from high viral load viable (HV-VIA) and meconium stained (HV-MEC) fetuses.

	Fetal classification			
Tissue	Control	HV-VIA	HV-MEC	Fisher's *p*-value*
Brain	0/3 (0%)	4/10 (40%)	2/10 (20%)	0.629
Heart	0/3 (0%)	8/9 (88.89%)	17/17 (100%)	0.346
Kidney	0/3 (0%)	11/16 (68.75%)	13/18 (72.22%)	1
Liver	0/4 (0%)	4/10 (40%)	4/9 (44.44%)	1
Lung	0/3 (0%)	8/9 (88.89%)	10/10 (100%)	0.474
Muscle	0/4 (0%)	9/10 (90%)	8/8 (100%)	1

*p-value for Fisher exact test for recovery rate between HV-VIA and HV-MEC groups.

Goor et al., 2020). While such studies have evaluated the physiological impact of fetal systems logically associated with viability such as immune regulation (Pasternak et al., 2020b), cardiovascular stress (Pasternak et al., 2020a; Malgarin et al., 2021), and placental function (Guidoni et al., 2021; Barrera-Zarate et al., 2022), no definitive explanation for virus-induced fetal compromise has been identified. However, a number of studies have found evidence to suggest infection of other fetal organs does occur (Cheon and Chae, 2000; Cheon and Chae, 2001; Rowland, 2010), although sporadically within the larger fetal population. Thus, the objective of the present study was to evaluate the capacity for PRRSV infection in non-lymphoid organs, their response to infection and the association with fetal viability.

Cellular infection by PRRSV is dependent on the presence of its obligate receptor CD163 (Van Gorp et al., 2008), which under normal circumstances functions in the clearance of hemoglobin (Kristiansen et al., 2001). This cell surface protein is primarily found on monocytes, macrophages (Buechler et al., 2000) and specific subsets of dendritic cells (Maniecki et al., 2006). The majority of postnatal tissues contain a resident population of macrophages which are established during early embryonic development, though the equivalent population in a subset of tissues is known to be generated postnatally from blood derived macrophages (Davies et al., 2020). Regardless of their source, most subpopulations of mature tissue macrophages express the hemoglobin-haptoglobin scavenger CD163 (Fabriek et al., 2005). Previous work in fetal pigs has demonstrated the presence of hepatic, splenic and pulmonary CD163 positive cells throughout gestation (Karniychuk and Nauwynck, 2009), but the presence of such cells in other fetal tissues has not been previously established. Using a similar Immunohistofluorescence approach, we have demonstrated the presence of CD163 positive cells in four additional fetal organs including HRT, KID, BRN and MUS at day 86 of gestation, indicating widespread capacity for PRRSV infection across non-lymphoid tissues.

Interestingly, the apparent abundance, spatial distribution and morphology of CD163 cells varied substantially between tissues. In the LVR, CD163 staining was associated with relatively small cells with even distribution throughout the tissue, which would be consistent with Kupffer cells. As with previous reports in both humans (Naito et al., 1997) and swine (Karniychuk and Nauwynck, 2009), a large number of such cells were observed evenly distributed throughout the fetal LVR. Also consistent with previous reports

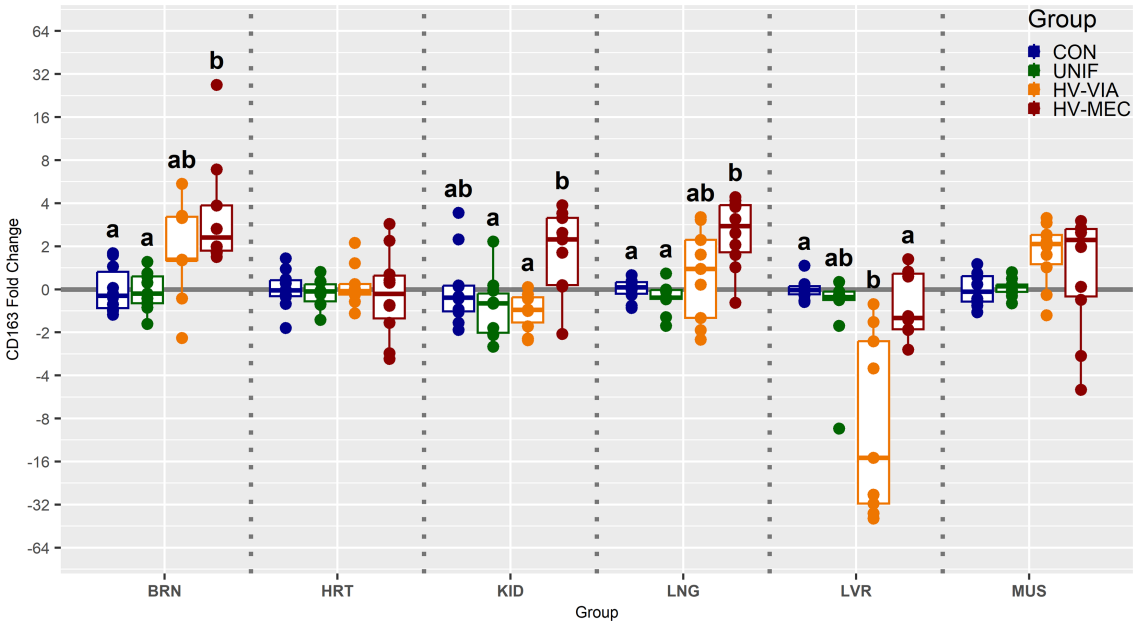

FIGURE 3
Expression of cluster of differentiation marker 163 (CD163) as measured by qPCR in fetal brain (BRN), heart (HRT), kidney (KID), lung (LNG), liver (LVR) and skeletal muscle (MUS) in fetuses uninfected (UNIF), high viral load viable (HV-VIA) and high viral load meconium stained (HV-MEC), 21 days after maternal PRRSV2 challenge, along with equivalent tissues from control (CON) fetuses derived from gestationally age matched and sham inoculated dams. Fold changes are calculated within tissue relative to the average expression of in the control group with unique superscripts indicating statistically significant differences ($p < 0.05$).

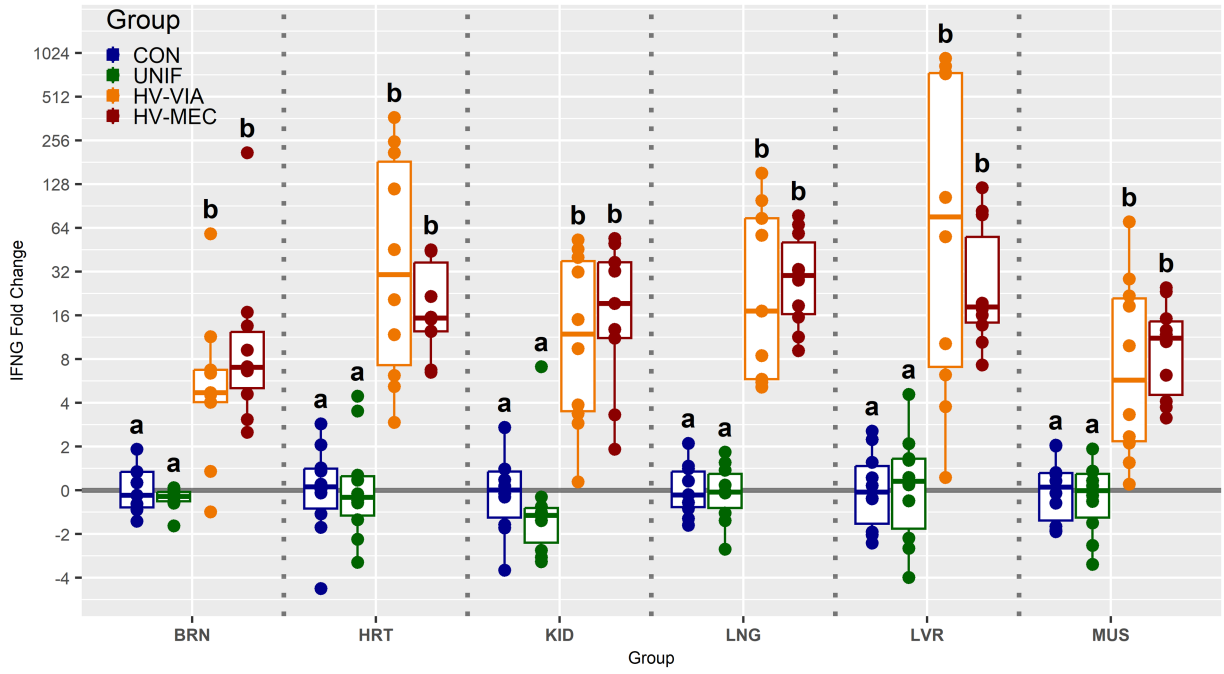

FIGURE 4
Expression of interferon gamma (IFNG) as measured by qPCR in fetal brain (BRN), heart (HRT), kidney (KID), lung (LNG), liver (LVR) and skeletal muscle (MUS) in fetuses uninfected (UNIF), high viral load viable (HV-VIA) and high viral load meconium stained (HV-MEC), 21 days after maternal PRRSV2 challenge, along with equivalent tissues from control (CON) fetuses derived from gestationally age matched and sham inoculated dams. Fold changes are calculated within tissue relative to the average expression of in the control group with unique superscripts indicating statistically significant differences ($p < 0.05$).

(Karniychuk and Nauwynck, 2009), the abundance of cells positively stained for CD163 was comparatively low in pulmonary tissues. Macrophages are the most abundant immune cell within the heart, a population which is established during early embryonic development by yolk sac derived progenitors (Epelman et al., 2014). It is thus unsurprising that a substantial population of CD163 positive staining was observed in cardiac tissue from the late gestation fetal pig, where it was associated with relatively large cells within the tissue of the ventricle. Cells with similar morphology were found throughout the fetal pig KID, though a substantial enrichment was observed in remnants of the renal capsule. Staining in the skeletal muscle was associated with small cells on the surface of muscle fibers, consistent with muscle resident macrophages known to express high levels of CD163 and originate from both embryonic yolk sac and liver, as well as postnatally from blood monocytes (Wang et al., 2020). In the brain, positive staining for CD163 was largely restricted to the pia mater, which is known to contain border associated macrophages (Taketomi and Tsuruta, 2023). The apparent lack of staining in the neural parenchyma is consistent with prior observations which show an absence of macrophages in the cerebrum and cerebellum during late gestation (Matsumoto and Ikuta, 1985).

Given these resting populations of PRRSV susceptible resident cells during late gestation, it is perhaps unsurprising that viral RNA was detected in samples of all six non-lymphoid tissues from fetuses previously classified as high viral load based on serum and thymus alone. The presence of infectious viral particles in these tissues is further supported by high success rates for *in vitro* recovery from the corresponding tissue lysates. Comparatively high viral load in the HRT relative to the LNG is consistent with prior work by other labs investigating late gestation fetal infection (Rowland, 2010). By definition, serum from HV-VIA and HV-MEC fetuses contained greater than 10^5 copies of viral RNA per μl, and thus the contribution of virus from circulation to the present observations in tissues cannot be ruled out. Fetuses in the present trial were exsanguinated via the axillary artery, and while the efficacy of this approach in reducing blood volume in various fetal organs has not been established, when employed postnatally for the purpose of slaughter, total blood volume is only reduced by 40%–60%, but residual content in lean meat reduced to just 2–9 mL/kg (Warriss, 1984). In addition, studies investigating the presence of virus in stillborn PRRSV infected piglets using immunohistochemistry have shown positive viral staining in both cardiac and renal tissue (Cheon and Chae, 2000; Cheon and Chae, 2001).

More critically, while fetuses identified as HV-VIA and HV-MEC have equivalent viral load in serum and thymus (Table 1), the viral load measured by qPCR in BRN, HRT, LNG and MUS was significantly elevated in HV-MEC fetuses compared to HV-VIA. This result may indicate that increased infection of critical non-lymphoid organs may be a causative factor differentiating between resilient and susceptible fetuses. Elevated viral load in the heart is of specific interest with regards to explaining fetal compromise. In humans, *in utero* infection with viral pathogens such as rubella has been associated with altered cardiac developmental processes and structural defects (Singampalli et al., 2021). Elevated viral load in the brain is of similar interest, given prior observations with Zika virus, which has been show to infect the fetal brain (Retallack et al., 2016) and result in abnormalities including microcephaly and, in some cases, fetal death (Leisher et al., 2021).

In conjunction with infection, we observed elevated expression of CD163 in the BRN, KID and LNG of HV-MEC fetuses which could be explained by three distinct hypotheses. The first of which is transcriptional upregulation in the tissue resident macrophages, which occurs during the establishment of an activated phenotype (Etzerodt and Moestrup, 2013). Second is that tissue resident macrophages are able to re-enter the cell cycle despite being terminally differentiated (Kulle et al., 2022), so the apparent upregulation could indicate proliferation resulting in a proportional increase of CD163+ cells relative to other constituents. Finally, increased transcription of CD163 could be associated with recruitment of blood monocytes or macrophages from other tissues. As the liver is the original source from which other tissue resident macrophage pools are created (Hoeffel and Ginhoux, 2015), this latter hypothesis may be supported by the decrease in hepatic CD163. The fact that this change in hepatic expression occurs in the HV-VIA rather than HV-MEC may simply indicate an early stage in the migration process. The observed stability of cardiac CD163 expression across phenotypic groups, in conjunction with significant viral load in the highly infected fetuses, suggests that the population of susceptible cells was present prior to infection and is not the product of macrophage infiltration.

Even in the absence of standard clinical signs, maternal infection with PRRSV produces a robust immune response characterized by increases in circulating IFNα and IFNγ (Ladinig et al., 2015). Following vertical transmission, the fetus displays a similar increase in serum type 1 and 2 interferons (Pasternak et al., 2020b). This is largely consistent with the local immune responses within fetal lymphoid organs such as the spleen and thymus, where there is a robust upregulation in expression of IFNB, IFNG and an array of other cytokines and chemokines (Pasternak et al., 2020a,b). The observed increase in IFNG expression in the fetal brain and lung observed in the present study are consistent with prior work from other investigators (Rowland, 2010; Antonson et al., 2018). The present study is, however, the first to demonstrate a local immune response, in the form of upregulated IFNG, within cardiac, hepatic, renal and musculoskeletal tissues. Due to the timing of sample collection relative to maternal challenge, it is not possible to differentiate between IFNG produced by resident cells present in the tissues prior to infection and those with which may have infiltrated following infection, however, regardless of the cellular source, the increased IFNG expression following infection indicates a localized inflammatory response. The observed upregulation in IFNG within these six non-lymphoid tissues was entirely restricted to highly infected fetuses, further supporting local viral infection. Interestingly, there was no difference in immune response between HV-VIA and HV-MEC groups, indicating the local immune interferon response is not associated with loss of fetal viability.

5 Conclusion

Collectively, our results show that non-lymphoid fetal organs not only contain a population of PRRSV susceptible cells, but harbor infectious viral particles following vertical PRRSV transmission. Most critically, the concentration of viral RNA within fetal HRT, BRN, LNG and MUS was elevated in compromised, meconium-stained fetuses compared to infected viable fetuses. Both local infection and interferon expression were found to be coincident in all tissues,

though the latter was not associated with loss of fetal viability. Further evaluation of the acute physiological effects of infection and inflammation in these non-lymphoid tissues will be critical in understanding the mechanism by which *in utero* PRRSV infection compromises fetal viability. In addition, fetal PRRSV infection may represent a high value biomedical model to study the long term developmental effects of *in utero* inflammation.

Data availability statement

The datasets presented in this study can be found in online repositories. The names of the repository/repositories and accession number(s) can be found at: https://github.com/JAlexPasternak/Fetal-_PRRSV_Distribution.

Ethics statement

The animal study was approved by Purdue University Institutional Animal Care and Use Committee and University of Saskatchewan's Animal Research Ethics Board. The study was conducted in accordance with the local legislation and institutional requirements.

Author contributions

KR: Investigation, Methodology, Validation, Writing – review & editing. DJ: Investigation, Methodology, Validation, Writing – review & editing. AS: Investigation, Methodology, Validation, Writing – review & editing. JH: Conceptualization, Funding acquisition, Methodology, Project administration, Writing – review & editing. JP: Conceptualization, Data curation, Formal Analysis, Funding acquisition, Investigation, Methodology, Project administration, Resources, Software, Supervision, Validation, Visualization, Writing – original draft, Writing – review & editing.

Funding

The author(s) declare financial support was received for the research, authorship, and/or publication of this article. Collection of healthy fetal samples was funded by Purdue University as part of AgSEED Crossroads funding to support Indiana's Agriculture and Rural Development. Funding for the challenge experiments was provided by Genome Alberta through the A3GP program (Project ALGP47) with in-kind contributions and support from Fast Genetics.

Acknowledgments

The samples used in this experiment were derived from a large scale, multi-institutional challenge experiment conducted at the University of Saskatchewan in collaboration with Fast Genetics and funded by Genome Alberta. Additional assistance was provided Margaret Mulligan, Devon Anderson, Jocelyn Kleiman, Andrew Caldemeyer, and Leah Jenkins.

Conflict of interest

The authors declare that the research was conducted in the absence of any commercial or financial relationships that could be construed as a potential conflict of interest.

Publisher's note

References

Antonson, A. M., Balakrishnan, B., Radlowski, E. C., Petr, G., and Johnson, R. W. (2018). Altered hippocampal gene expression and morphology in fetal piglets following maternal respiratory viral infection. *Dev. Neurosci.* 40, 104–119. doi: 10.1159/000486850

Barrera-Zarate, J. A., Detmer, S. E., Pasternak, J. A., Hamonic, G., Mac Phee, D. J., and Harding, J. C. S. (2022). Effect of porcine reproductive and respiratory syndrome virus 2 on angiogenesis and cell proliferation at the maternal-fetal Interface. *Vet. Pathol.* 59, 940–949. doi: 10.1177/03009858221105053

Benson, J. E., Yaeger, M. J., Christopher-Hennings, J., Lager, K., and Yoon, K.-J. (2002). A comparison of virus isolation, immunohistochemistry, fetal serology, and reverse-transcription polymerase chain reaction assay for the identification of porcine reproductive and respiratory syndrome virus Transplacental infection in the fetus. *J. Vet. Diagn. Invest.* 14, 8–14. doi: 10.1177/104063870201400103

Buechler, C., Ritter, M., Orsó, E., Langmann, T., Klucken, J., and Schmitz, G. (2000). Regulation of scavenger receptor CD163 expression in human monocytes and macrophages by pro-and Antiinflammatory stimuli. *J. Leukoc. Biol.* 67, 97–103. doi: 10.1002/jlb.67.1.97

Cheon, D. S., and Chae, C. (2000). Comparison of virus isolation, reverse transcription-polymerase chain reaction, immunohistochemistry, and in situ hybridization for the detection of porcine reproductive and respiratory syndrome virus from naturally aborted fetuses and stillborn piglets. *J. Vet. Diagn. Invest.* 12, 582–587. doi: 10.1177/104063870001200619

Cheon, D.-S., and Chae, C. (2001). Distribution of porcine reproductive and respiratory syndrome virus in stillborn and Liveborn piglets from experimentally infected sows. *J. Comp. Pathol.* 124, 231–237. doi: 10.1053/jcpa.2000.0457

Davies, K. L., Camm, E. J., Atkinson, E. V., Lopez, T., Forhead, A. J., Murray, A. J., et al. (2020). Development and thyroid hormone dependence of skeletal muscle mitochondrial function towards birth. *J. Physiol.* 598, 2453–2468. doi: 10.1113/JP279194

Epelman, S., Lavine, K. J., Beaudin, A. E., Sojka, D. K., Carrero, J. A., Calderon, B., et al. (2014). Embryonic and adult-derived resident cardiac macrophages are maintained through distinct mechanisms at steady state and during inflammation. *Immunity* 40, 91–104. doi: 10.1016/j.immuni.2013.11.019

Etzerodt, A., and Moestrup, S. K. (2013). CD163 and inflammation: biological, diagnostic, and therapeutic aspects. *Antioxid. Redox Signal.* 18, 2352–2363. doi: 10.1089/ars.2012.4834

Fabriek, B. O., Dijkstra, C. D., and Van Den Berg, T. K. (2005). The macrophage scavenger receptor CD163. *Immunobiology* 210, 153–160. doi: 10.1016/j.imbio.2005.05.010

Feng, W., Laster, S. M., Tompkins, M., Brown, T., Xu, J. S., Altier, C., et al. (2001). In utero infection by porcine reproductive and respiratory syndrome virus is sufficient to increase susceptibility of piglets to challenge by *Streptococcus Suis* type II. *J. Virol.* 75, 4889–4895. doi: 10.1128/JVI.75.10.4889-4895.2001

Guidoni, P. B., Alex Pasternak, J., Hamonic, G., Mac Phee, D. J., and Harding, J. C. S. (2022). Effect of porcine reproductive and respiratory syndrome virus 2 on tight junction gene expression at the maternal-fetal Interface. *Theriogenology* 184, 162–170. doi: 10.1016/j.theriogenology.2022.03.011

Guidoni, P. B., Pasternak, J. A., Hamonic, G., Mac Phee, D. J., and Harding, J. C. S. (2021). Decreased tight junction protein intensity in the placenta of porcine reproductive

and respiratory syndrome Virus-2 infected fetuses. *Placenta* 112, 153–161. doi: 10.1016/j.placenta.2021.07.300

Harding, J. C. S., Ladinig, A., Novakovic, P., Detmer, S. E., Wilkinson, J. M., Yang, T., et al. (2017). Novel insights into host responses and reproductive pathophysiology of porcine reproductive and respiratory syndrome caused by PRRSV-2. *Vet. Microbiol.* 209, 114–123. doi: 10.1016/j.vetmic.2017.02.019

Hoeffel, G., and Ginhoux, F. (2015). Ontogeny of tissue-resident macrophages. *Front. Immunol.* 6:486. doi: 10.3389/fimmu.2015.00486

Holtkamp, D., Kliebenstein, J. B., Neumann, E. J., Zimmerman, J. J., Rotto, H. F., Yoder, T. K., et al. (2013). Assessment of the economic impact of porcine reproductive and respiratory syndrome virus on United States pork producers. *J Swine Health Product* 21, 72–84. doi: 10.2460/javma.2005.227.385

Ison, E. K., Hopf-Jannasch, A. S., Harding, J. C. S., and Alex Pasternak, J. (2022). Effects of porcine reproductive and respiratory syndrome virus (PRRSV) on thyroid hormone metabolism in the late gestation fetus. *Vet. Res.* 53:74. doi: 10.1186/s13567-022-01092-3

Ison, E. K., Kent-Dennis, C. E., Fazioli, J., Mulligan, M. K., Pham, A., Alex, J., et al. (2023). Compensatory mechanisms in response to induced hypothyroidism in the late gestation pig fetus. *Biol. Reprod.* 108, 731–743. doi: 10.1093/biolre/ioad024

Karniychuk, U. U., and Nauwynck, H. J. (2009). Quantitative changes of Sialoadhesin and CD163 positive macrophages in the implantation sites and organs of porcine embryos/fetuses during gestation. *Placenta* 30, 497–500. doi: 10.1016/j.placenta.2009.03.016

Kent-Dennis, C., Pasternak, A., Plaizier, J. C., and Penner, G. B. (2019). Potential for a localized immune response by the ruminal epithelium in nonpregnant heifers following a short-term subacute ruminal acidosis challenge. *J. Dairy Sci.* 102, 7556–7569. doi: 10.3168/jds.2019-16294

Ko, H., Jourdyn Sammons, J., Pasternak, A., Hamonic, G., Starrak, G., MacPhee, D. J., et al. (2022). Phenotypic effect of a single nucleotide polymorphism on SSC7 on fetal outcomes in PRRSV-2 infected gilts. *Livest. Sci.* 255:104800. doi: 10.1016/j.livsci.2021.104800

Kranker, S., Nielsen, J., Bille-Hansen, V., and Bøtner, A. (1998). Experimental inoculation of swine at various stages of gestation with a Danish isolate of porcine reproductive and respiratory syndrome virus (PRRSV). *Vet. Microbiol.* 61, 21–31. doi: 10.1016/s0378-1135(98)00176-x

Kristiansen, M., Graversen, J. H., Jacobsen, C., Sonne, O., Hans-Jürgen Hoffman, S. K., Law, A., et al. (2001). Identification of the Haemoglobin scavenger receptor. *Nature* 409, 198–201. doi: 10.1038/35051594

Kulle, A., Thanabalasuriar, A., Cohen, T. S., and Szydlowska, M. (2022). Resident macrophages of the lung and liver: the guardians of our tissues. *Front. Immunol.* 13:1029085. doi: 10.3389/fimmu.2022.1029085

Ladinig, A., Detmer, S. E., Clarke, K., Ashley, C., Rowland, R. R. R., Lunney, J. K., et al. (2015). Pathogenicity of three type 2 porcine reproductive and respiratory syndrome virus strains in experimentally inoculated pregnant gilts. *Virus Res.* 203, 24–35. doi: 10.1016/j.virusres.2015.03.005

Leisher, S. H., Balalian, A. A., Reinebrant, H., Shiau, S., Flenady, V., Kuhn, L., et al. (2021). Systematic review: fetal death reporting and risk in Zika-affected pregnancies. *Trop. Med. Int. Health* 26, 133–145. doi: 10.1111/tmi.13522

Malgarin, C. M., Fiona Moser, J., Pasternak, A., Hamonic, G., Detmer, S. E., MacPhee, D. J., et al. (2021). Fetal hypoxia and apoptosis following maternal porcine reproductive and respiratory syndrome virus (PRRSV) infection. *BMC Vet. Res.* 17:182. doi: 10.1186/S12917-021-02883-0

Malgarin, C. M., Nosach, R., Novakovic, P., Suleman, M., Ladinig, A., Detmer, S. E., et al. (2019). Classification of fetal resilience to porcine reproductive and respiratory syndrome (PRRS) based on temporal viral load in late gestation maternal tissues and fetuses. *Virus Res.* 260, 151–162. doi: 10.1016/j.virusres.2018.12.002

Maniecki, M. B., Møller, H. J., Moestrup, S. K., and Møller, B. K. (2006). CD163 positive subsets of blood dendritic cells: the scavenging macrophage receptors CD163 and CD91 are Coexpressed on human dendritic cells and monocytes. *Immunobiology* 211, 407–417. doi: 10.1016/j.imbio.2006.05.019

Matsumoto, Y., and Ikuta, F. (1985). Appearance and distribution of fetal brain macrophages in mice: Immunohistochemical study with a monoclonal antibody. *Cell Tissue Res.* 239, 271–278. doi: 10.1007/BF00218004

Mulligan, M. K., Kleiman, J. E., Caldemeyer, A. C., Harding, J. C. S., and Alex Pasternak, J. (2022). Porcine reproductive and respiratory virus 2 infection of the fetus results in multi-organ cell cycle suppression. *Vet. Res.* 53:13. doi: 10.1186/s13567-022-01030-3

Naito, M., Hasegawa, G., and Takahashi, K. (1997). Development, differentiation, and maturation of Kupffer cells. *Microsc. Res. Tech.* 39, 350–364. doi: 10.1002/(SICI)1097-0029(19971115)39:4<350::AID-JEMT5>3.0.CO;2-L

Oliver, G., Novak, S., Patterson, J. L., Pasternak, J. A., Paradis, F., Norrby, M., et al. (2011). Restricted feed intake in lactating Primiparous sows. II. Effects on subsequent litter sex ratio and embryonic gene expression. *Reprod. Fertil. Dev.* 23, 899–911. doi: 10.1071/RD11013

Pasternak, A. J., Hamonic, G. M., Van Kessel, A., and Wilson, H. L. (2016). Postnatal regulation of MAMDC 4 in the porcine intestinal epithelium is influenced by bacterial colonization. *Physiol. Rep.* 4:e13018. doi: 10.14814/phy2.13018

Pasternak, J. A., Kent-Dennis, C., Van Kessel, A. G., and Wilson, H. L. (2015). Claudin-4 undergoes age-dependent change in cellular localization on pig Jejunal villous epithelial cells, independent of bacterial colonization. *Mediators Inflamm.* 2015, 1–14. doi: 10.1155/2015/263629

Pasternak, J. A., MacPhee, D. J., and Harding, J. C. S. (2019). Development and application of a porcine specific ELISA for the quantification of soluble CD163. *Vet. Immunol. Immunopathol.* 210, 60–67. doi: 10.1016/j.vetimm.2019.03.011

Pasternak, J. A., MacPhee, D. J., and Harding, J. C. S. (2020a). Maternal and fetal thyroid dysfunction following porcine reproductive and respiratory syndrome Virus2 infection. *Vet. Res.* 51:47. doi: 10.1186/s13567-020-00772-2

Pasternak, J. A., MacPhee, D. J., and Harding, J. C. S. (2020b). Fetal cytokine response to porcine reproductive and respiratory syndrome Virus-2 infection. *Cytokine* 126:154883. doi: 10.1016/j.cyto.2019.154883

Pasternak, J. A., MacPhee, D. J., Lunney, J. K., Rowland, R. R. R., Dyck, M. K., Fortin, F., et al. (2021). Thyroid hormone suppression in feeder pigs following Polymicrobial or porcine reproductive and respiratory syndrome Virus-2 challenge. *J. Anim. Sci.* 99:skab325. doi: 10.1093/jas/skab325

R Core Team. (2019). "*R: A language and environment for statistical computing*." Vienna, Austria.

Retallack, H., Di Lullo, E., Arias, C., Knopp, K. A., Laurie, M. T., Sandoval-Espinosa, C., et al. (2016). Zika virus cell tropism in the developing human brain and inhibition by azithromycin. *Proc. Natl. Acad. Sci.* 113, 14408–14413. doi: 10.1073/pnas.1618029113

Rowland, R. R. R. (2010). The interaction between PRRSV and the late gestation pig fetus. *Virus Res.* 154, 114–122. doi: 10.1016/j.virusres.2010.09.001

Singampalli, K. L., Jui, E., Shani, K., Ning, Y., Connell, J. P., Birla, R. K., et al. (2021). Congenital heart disease: an immunological perspective. *Front Cardiovasc Med* 8:701375. doi: 10.3389/fcvm.2021.701375

Taketomi, T., and Tsuruta, F. (2023). Towards an understanding of microglia and border-associated macrophages. *Biology* 12:1091. doi: 10.3390/biology12081091

Terpstra, C., Wensvoort, G., and Pol, J. M. A. (1991). Experimental reproduction of porcine epidemic abortion and respiratory syndrome (mystery swine disease) by infection with Lelystad vims: Koch's postulates fulfilled. *Vet. Q.* 13, 131–136. doi: 10.1080/01652176.1991.9694297

Van Reeth, K., Nauwynck, H., and Pensaert, M. (2001). Clinical effects of experimental dual infections with porcine reproductive and respiratory syndrome virus followed by swine influenza virus in conventional and colostrum-deprived pigs. *J. Vet. Med. B.* 48, 283–292. doi: 10.1046/j.1439-0450.2001.00438.x

Van Gorp, H., Van Breedam, W., Delputte, P. L., and Nauwynck, H. J. (2008). Sialoadhesin and CD163 join forces during entry of the porcine reproductive and respiratory syndrome virus. *J. Gen. Virol.* 89, 2943–2953. doi: 10.1099/vir.0.2008/005009-0

Van Goor, A., Pasternak, A., Walker, K., Hong, L., Malgarin, C., MacPhee, D. J., et al. (2020). Differential responses in placenta and fetal Thymus at 12 days post infection elucidate mechanisms of viral level and fetal compromise following PRRSV2 infection. *BMC Genomics* 21:763. doi: 10.1186/s12864-020-07154-0

Wang, X., Sathe, A. A., Smith, G. R., Ruf-Zamojski, F., Nair, V., Lavine, K. J., et al. (2020). Heterogeneous origins and functions of mouse skeletal muscle-resident macrophages. *Proc. Natl. Acad. Sci.* 117, 20729–20740. doi: 10.1073/pnas.1915950117

Warriss, P. (1984). Exsanguination of animals at slaughter and the residual blood content of meat. *Vet. Rec.* 115, 292–295. doi: 10.1136/vr.115.12.292

Wickham, H. (2016). *Ggplot2: Elegant graphics for data analysis*. Springer-Verlag New York.

frontiers | Frontiers in Microbiology

TYPE Original Research
PUBLISHED 14 February 2024
DOI 10.3389/fmicb.2024.1328177

OPEN ACCESS

EDITED BY
Gang Wang,
Shandong Agricultural University, China

REVIEWED BY
Qin Zhao,
Northwest A&F University, China
Youhui Si,
Huazhong Agricultural University, China

*CORRESPONDENCE
Shaobin Shang
✉ shaobinshang@yzu.edu.cn
Jiajun Wu
✉ wujiajun82@126.com

†These authors have contributed equally to this work

RECEIVED 26 October 2023
ACCEPTED 23 January 2024
PUBLISHED 14 February 2024

CITATION
Tian Y, Wang D, He S, Cao Z, Li W, Jiang F, Shi Y, Hao Y, Wei X, Wang Q, Qie S, Wang J, Li T, Hao X, Zhu J, Wu J, Shang S and Zhai X (2024) Immune cell early activation, apoptotic kinetic, and T-cell functional impairment in domestic pigs after ASFV CADC_HN09 strain infection.
Front. Microbiol. 15:1328177.
doi: 10.3389/fmicb.2024.1328177

Immune cell early activation, apoptotic kinetic, and T-cell functional impairment in domestic pigs after ASFV CADC_HN09 strain infection

Yunfei Tian[1†], Dongyue Wang[2†], Shicheng He[3], Zhen Cao[2], Wencai Li[2], Fei Jiang[2], Yifan Shi[2], Yuxin Hao[2], Xinhao Wei[2], Qingqing Wang[2], Shuai Qie[2], Jiangtao Wang[2], Ting Li[2], Xiaoli Hao[1], Jianzhong Zhu[1,4], Jiajun Wu[2]*, Shaobin Shang[1,4]* and Xinyan Zhai[2]

[1]College of Veterinary Medicine, Institute of Comparative Medicine, Yangzhou University, Yangzhou, China, [2]The Biosafety High-Level Laboratory Management Office, China Animal Disease Control Center, Beijing, China, [3]Animal Disease Control Center of Hunan Province, Changsha, China, [4]Jiangsu Co-Innovation Center for Prevention and Control of Important Animal Infectious Diseases and Zoonosis, Yangzhou University, Yangzhou, China

African swine fever (ASF) caused by the African swine fever virus (ASFV) is a fatal and highly contagious disease of domestic pigs characterized by rapid disease progression and death within 2 weeks. How the immune cells respond to acute ASFV infection and contribute to the immunopathogenesis of ASFV has not been completely understood. In this study, we examined the activation, apoptosis, and functional changes of distinct immune cells in domestic pigs following acute infection with the ASFV CADC_HN09 strain using multicolor flow cytometry. We found that ASFV infection induced broad apoptosis of DCs, monocytes, neutrophils, and lymphocytes in the peripheral blood of pigs over time. The expression of MHC class II molecule (SLA-DR/DQ) on monocytes and conventional DCs as well as CD21 expression on B cells were downregulated after ASFV infection, implying a potential impairment of antigen presentation and humoral response. Further examination of CD69 and *ex vivo* expression of IFN-γ on immune cells showed that T cells were transiently activated and expressed IFN-γ as early as 5 days post-infection. However, the capability of T cells to produce cytokines was significantly impaired in the infected pigs when stimulated with mitogen. These results suggest that the adaptive cellular immunity to ASFV might be initiated but later overridden by ASFV-induced immunosuppression. Our study clarified the cell types that were affected by ASFV infection and contributed to lymphopenia, improving our understanding of the immunopathogenesis of ASFV.

KEYWORDS

ASFV, apoptotic, T cell early activation, cytokine, immunopathogenesis

Introduction

African swine fever (ASF) caused by the African swine fever virus (ASFV) is a fatal and highly contagious disease of domestic pigs and wild boars, with a mortality rate of up to 100% (Galindo and Alonso, 2017). Since its first identification in Kenya in 1921 (Cwynar et al., 2019), this disease has spread from Africa to Europe and Asia, affecting many countries. In August 2018, the first case of ASF was documented in Shenyang, China, and since then, ASF has caused tremendous economic losses and has been the most devastating disease affecting the swine industry in China (Ge et al., 2018; Zhou et al., 2018; Zhao et al., 2019). ASFV is a double-stranded DNA virus and the only member of the Asfarviridae family. The ASFV genome has 170–190 kb nucleotides and contains 151–167 open reading frames (ORFs), depending on the virus strain (Dixon et al., 2013), which encode 54 structural proteins and more than 100 non-structural proteins (Alejo et al., 2018) involved in viral replication and assembly as well as in modulating host cellular functions and immune evasion (Galindo and Alonso, 2017).

Virulent ASFV infection generally leads to an acute/peracute hemorrhagic disease in domestic pigs, and the infected pigs usually die within 2 weeks (6–9 days for experimental inoculation, and 13–14 days post-contact) (Zhao et al., 2019). However, the detailed mechanism underlying rapid disease progression and death has not been completely understood (Takamatsu et al., 2013; Pikalo et al., 2019). It was known that ASFV mainly infects myeloid lineage cells, including monocytes, neutrophils, macrophages (Carrasco et al., 1996a; Gomez-Villamandos et al., 2013), and dendritic cells (DCs) (Franzoni et al., 2018). Severe leucopenia or lymphopenia was evident in the periphery blood and lymphoid organs of ASFV-infected pigs due to apoptosis (Oura et al., 1998; Karalyan et al., 2012), accompanied by the emergence of immature cells and atypical lymphocytes (Karalyan et al., 2012). However, the cell types that were affected by ASFV infection and contributed to lymphopenia have not been well defined, though *in situ* apoptotic immune cells were primarily examined by the terminal deoxynucleotidyl transferase (TdT) dUTP Nick-end labeling (TUNEL) technique (Oura et al., 1998).

In addition, ASFV infection also results in an exacerbated inflammatory cytokine storm, which is characterized by sustained elevation of serum pro-inflammatory interleukins, tumor necrosis factor (TNF), and chemokines (Wang et al., 2020; Franzoni et al., 2023), and TNF-α is required for cell apoptosis in porcine alveolar macrophages (PAMs) after ASFV infection (Zheng et al., 2022). There was no direct evidence showing that T cells were activated or IFN-γ was released by specific cell types, though the transient increase of IFN-γ was observed from day 4–6 post-inoculation (Karalyan et al., 2012). Recent studies showed that an infection of the highly virulent ASFV strain led to the reduction of distinct T-cell subsets to some degree, except for $CD4^+CD8^+$ T cells in domestic pigs (Huhr et al., 2020), whereas the moderate virulent ASFV strain induced an increase in $CD8\alpha^+$ and $CD4^+CD8\alpha^+$ αβ T cells and delayed the proliferation of $CD8\alpha^+$ T cells in domestic pigs (Schafer et al., 2021). However, whether T cells are activated or functionally impaired during rapid disease progression and death caused by virulent ASFV infection is still lacking in evidence. The dynamics of distinct immune cell activation and apoptosis as well as functional changes of T cells during ASFV infection remain to be clarified, in order to better understand the immunopathogenesis of ASFV.

In this study, we examined the activation, apoptosis, and functional changes of distinct immune cells in domestic pigs following acute infection with the ASFV CADC_HN09 strain using multicolor flow cytometry, in combination with an anti-pig CD69 antibody we developed previously (Tian et al., 2022) and *ex vivo* staining of IFN-γ-producing cells. Our results showed that there was transient T-cell activation and functional impairment as well as broad apoptosis on distinct immune cells after virulent ASFV infection.

Materials and methods

Ethics statement

All experiments involving ASFV were approved by the Institutional Biosafety Committee of the Ministry of Agriculture and Rural Affairs of China (07140020210615–1) and performed in animal biosafety level 3 (ABSL-3) facilities, in accordance with the institutional biosafety manual of China Animal Disease Control Center. All the protocols for animal studies complied with the guidelines of the Animal Welfare and Ethics of China Animal Disease Control Center.

Animals and virus

Piglets for the ASFV infection experiment were purchased from Beijing Qingquanwan Pig Breeding Co. LTD, were unvaccinated with vaccines, and were routinely pre-detected for ASFV, PRRSV, PRV, PCV, and PEDV by RT-qPCR. The ASFV CADC_HN09 strain was isolated and sequenced (GenBank accession number: MZ614662) in 2021, belongs to genotype II, and is kept in China Animal Disease Control Center.

Infection experiments with ASFV

In experiment 1, eight 2-month-old ASFV-free healthy piglets were randomly divided into two groups. One group (five pigs) was intramuscularly infected with 10 hemadsorbing doses (HAD_{50}) of ASFV CADC_HN09 strain per piglet while a control group (three pigs) was uninfected (see Table 1). Periphery blood of each pig was collected at 0, 3, 5, and 7 days post-infection (dpi) for the isolation of PBMCs and immunophenotyping by flow cytometry (FCM).

In experiment 2, 18 2-month-old healthy piglets were randomly divided into two groups (nine pigs in each group). One group was intramuscularly infected with 10 HAD_{50} of ASFV CADC_HN09 strain per piglet, and the other group was left uninfected and served as

TABLE 1 Infection experiments and sample collection.

Days post-infection		0	3	5	7
Experiment 1 (blood)	Uninfected	3	3	3	3
	Infected	5	5	5	3
Experiment 2 (organs)	Uninfected		3	3	3
	Infected		3	3	3

control at 3, 5, and 7 dpi. Pigs were euthanized at each time-point, and the lung, spleen, and mandibular lymph node (mLN) were collected for single-cell suspension, serum preparation, and immunophenotyping by flow cytometry.

Clinical signs and rectal temperatures of the piglets were recorded daily over the course of the experiment. The clinical score was evaluated as previously described (Petrov et al., 2018), which comprised the parameters of liveliness, bearing, breathing, gait, skin, and feed uptake.

Single-cell preparation

Single-cell suspension from peripheral blood and organs was prepared according to a previous study (Hao et al., 2020; Tian et al., 2022). Briefly, PBMCs were isolated from the heparinized periphery blood of pigs by gradient density centrifugation with a Porcine PBMC Isolation Kit (Tianjin Haoyang Co. Ltd., China). Single-cell suspensions from mLN and spleen were prepared by grinding the tissues through 70-μm cell strainers (BD, United States) in 2% fetal bovine serum (FBS) RPMI-1640 medium. Lung samples were predigested with collagenase IV and DNase I (Sigma, Germany) for 30 min at 37°C in a water bath and then ground, followed by isolation with a Porcine Lymphocyte Isolation Kit (Tianjin Haoyang Co. Ltd., China). Red blood cells in samples were lysed with red blood cell lysis buffer (Solarbio, China). Live cells were counted using a hemocytometer, and the cell concentration was adjusted to 2×10^7 cells/mL.

Flow cytometry

Single-cell suspensions from blood and organs were seeded in 96-well V-bottom plates, with 2×10^6 cells in each well. After centrifugation, cells were incubated for 30 min at RT in the dark with a cocktail of fluorescence-conjugated antibodies or biotinylated antibodies and/or followed by a secondary antibody staining, as previously reported (Maisonnasse et al., 2016; Lagumdzic et al., 2023). Antibodies used in the FCM are summarized in Table 2. The early apoptosis of myeloid lineage cells and lymphocytes was detected using an Annexin V detection kit (Biolegend, United States), cytokine secretion of lymphocytes was detected by intracellular cytokine staining (ICS), and the proliferation of lymphocytes was examined by intranuclear transcriptional factor staining, with different staining panels. After each staining, a washing step was performed with FCM buffer (0.5% BSA PBS) by centrifuging at 400 g for 5 min at 4°C. A minimal number of 300,000 cells was acquired for FCM analysis. Live singlets in PBMCs were gated based on their forward scatter (FSC) and side scatter (SSC) properties, together with a negative fixable viability dye eFluor® 780 (FVD780, Thermo Scientific, United States) signal. FCM was performed with FACS LSRFortessa (BD Biosciences, Franklin Lakes, NJ, United States), and the data were analyzed by FlowJo software v10.6.2 (Tree Star Inc., Ashland, OR, United States).

Apoptosis detection

PBMCs were seeded in 96-well V-bottom plates, with 2×10^6 cells in each well and stained first with FVD780 in pre-cold PBS for 10 min at 4°C. Then, the cells were stained with antibody cocktails containing fluorescein-conjugated antibodies to CD172, CD163, SLA-II DR/DQ, or CD21, γδTCR, CD3, CD4, and CD8α, followed by a second antibody staining in FCM buffer at RT for 30 min. Thereafter, cells were washed with FCM buffer, and stained with fluorescein-labeled Annexin V diluted in Annexin V binding buffer (Biolegend, United States) for 15 min at 4°C. Cells were washed and resuspended with Annexin V binding buffer and immediately analyzed by FCM.

Intracellular cytokine staining

For *in vitro* activation of lymphocyte, 2×10^6 PBMCs per sample were seeded in 96-well U-bottom plates kept in a 200-μL RPMI-1640 complete medium containing 10% FBS, 100 U/mL penicillin, and 100 mg/mL streptomycin (Gibco, United Kingdom) and stimulated for 6 h with 50 ng/mL PMA and 500 ng/mL ionomycin in the presence of 10 μg/mL Brefeldin A (Biolegend, United States).

After incubation, cells were stained for cell surface markers for 30 min at RT, washed with FCM buffer, and fixed with 4% paraformaldehyde for 10 min; then, the cells were permeabilized with Perm/wash buffer (BD, United States) for 20 min, and stained with Alexa Fluor® 647 Mouse Anti-Pig IFN-γ (BD, United States), Brilliant Violet 421™ anti-human TNF-α (BioLegend), and FITC-conjugated anti-IL-2 mAbs (Thermo Fisher, United States) diluted in Perm/wash buffer for 30 min in dark at RT. After washing with Perm/wash buffer, the cells were resuspended with 0.5% PFA PBS buffer and examined by FCM. For *ex vivo* detection of IFN-γ production by T cells, freshly isolated PBMCs were directly stained with cell surface markers and then subjected to the intracellular staining protocol.

Intranuclear transcriptional factor staining

Intranuclear Ki67 and Foxp3 factors were stained as below. Briefly, cells were first stained with antibodies against surface markers CD21, γδTCR, CD3, CD4, and CD8α. Then, the cells were fixed and permeabilized with fixation/permeabilization buffer (Invitrogen, United States) for 45 min and stained with mouse anti-Ki67 (BD Horizon™, United States) and/or anti-Foxp3 (Invitrogen, United States) diluted in permeabilization buffer (Invitrogen, United States) for another 45 min. After final washing with the permeabilization buffer, cells were resuspended with 0.5% PFA PBS buffer and examined by FCM.

ELISA

Pig sera were isolated at 5 dpi for the detection of IL-1β and IL-18 using a commercial ELISA kit (Thermo Fisher, United States). The test was carried out according to the manufacturer's protocol.

Statistical analysis

Statistical analysis was performed with GraphPad Prism software (GraphPad, La Jolla, CA). When comparing experimental values from two groups, Student's t-tests were routinely used. Statistical significance is noted ($^*p < 0.05$; $^{**}p < 0.01$; $^{***}p < 0.001$).

TABLE 2 Antibodies used in this study.

Antigen	Clone	Isotype	Fluorochrome	Source
CD3ε	BB23-8E6-8C8	Mouse IgG2a, κ	PerCP-Cy™5.5	BD
CD4a	74–12-4	Mouse IgG2b, κ	PE-Cy™7	BD Pharmingen
CD8a	76–2-11	Mouse IgG2a, κ	Biotin	Southernbiotech
CD21	BB6-11C9.6	Mouse IgG1, κ	AlexaFluor®488	Southernbiotech
γδTCR	MAC320	Rat PVG IgG2a	PE	BD
CD69	5F12	Mouse IgG1, κ	Dylight755	in-house
CD163	2A10/11	Mouse IgG1	RPE	Bio-rad
CD172a	74–22-15	Mouse IgG1, κ	FITC	Southernbiotech
SLA II DR	2E9/13	IgG2b	APC	Bio-rad
SLA II DQ	K274.3G8	IgG1	APC	Bio-rad
IL-2	A150D3F1	Mouse IgG2a	FITC	Invitrogen
IFN-γ	P2G10	Mouse IgG1, κ	Alexa Fluor® 647	BD
TNF-α	MAB11	Mouse IgG1, κ	BV 421™	BioLegend
Ki67	B56	Mouse IgG1, κ	BV 421™	BD Horizon™
Foxp3	FJK-16s	Rat IgG2a, κ	PE	Invitrogen
Biotin	–		BV 510™	BioLegend

Results

Clinical manifestations

After inoculation of ASFV CADC_HN09, the piglets showed a loss of appetite, depression, lethargy, skin cyanosis, and dyspnea. Most of the infected piglets showed high fever (over 41°C) that started from 5 dpi and lasted until the end (Supplementary Figure S1), consistent with a previous report (Zhao et al., 2019). Two piglets were euthanized at 6 dpi due to severe clinical signs.

Virulent ASFV infection led to the predominant reduction of B cells, CD4 T cells, monocytes, and dendritic cells in periphery blood

As lymphopenia was previously evident in the tissues of the infected pigs, but the cell types were not completely identified, we intended to identify the changes of distinct immune cells in the periphery blood of ASFV-infected pigs. We first defined different immune cell subsets from myeloid lineage by multicolor flow cytometry according to a previous report (Maisonnasse et al., 2016). As shown in Figure 1 and Supplementary Figure S2A, in terms of numbers, MHC II$^+$CD172a$^+$CD163$^+$ monocytes and MHC II$^+$CD172a$^-$CD163$^-$ conventional dendritic cells type I (cDC1) gradually decreased over the course of infection (Figures 1A,B), while MHC II$^+$CD172a$^+$CD163$^-$ conventional dendritic cell type II (cDC2) and neutrophils (MHC II$^-$CD163$^-$CD172$^+$) significantly increased after infection (Figures 1C,D). As the PBMC isolation kit we used could not completely remove granulocytes, neutrophil was also analyzed in this study. Further analyzing the changes in lymphocyte subsets showed that total lymphocytes, total T cells (CD3$^+$), and γδ T cells slowly decreased (Figures 1E–G; Supplementary Figure S2B) over the course of the disease, while CD21$^+$ B cells and CD4$^+$ T cells (CD3$^+$CD8$^-$CD4$^+$) decreased more drastically from 5 dpi in terms of numbers (Figures 1H,I). The numbers of CD4$^+$CD8$^+$ T cells and CD8$^+$ T cells were relatively stable until 7 dpi, after which they decreased, whereas the number of NK cells (CD3$^-$CD8$^+$ T) showed a slight increase and then decreased (Figures 1J–L). In contrast, the corresponding cell populations in the uninfected pigs were not much changed, suggesting that technical and experimental variations at each timepoint were minimized.

Virulent ASFV infection caused different levels of apoptosis on distinct immune cells

Although apoptosis was detected in porcine macrophage during *in vitro* infection with high and low virulent ASFV isolates (Ramiro-Ibanez et al., 1996; Portugal et al., 2009) and in lymphocytes in the liver, kidney tissues, and lymphoid organs of the infected pigs (Gomez-Villamandos et al., 1995; Ramiro-Ibanez et al., 1996; Carrasco et al., 1996b), *in vivo* apoptotic kinetics of distinct immune cells in PBMCs after virulent ASFV infection have not been examined. We first examined the expression of Annexin V on the cell surface for measuring the early apoptosis of myeloid lineage subsets including DCs, monocytes, and neutrophils using multicolor flow cytometry. The results showed that early apoptosis (Annexin V-positive cells) occurred as early as 3 dpi in DCs, monocytes, and neutrophils in PBMCs to various extents (Figure 2). The kinetics of apoptosis in these cells peaked at 7 dpi, in which the percentages of apoptotic cDC1 (Figure 2A), cDC2 (Figure 2B), monocytes (Figure 2C), and neutrophils (Figure 2D) reached an average of 26.71 ± 18.42%, 31.03 ± 25.49%, 33.23 ± 10.97%, and 20.78 ± 16.64%, respectively.

Similarly, we simultaneously examined the apoptosis of several subsets of lymphocytes in terms of Annexin V expression. As shown

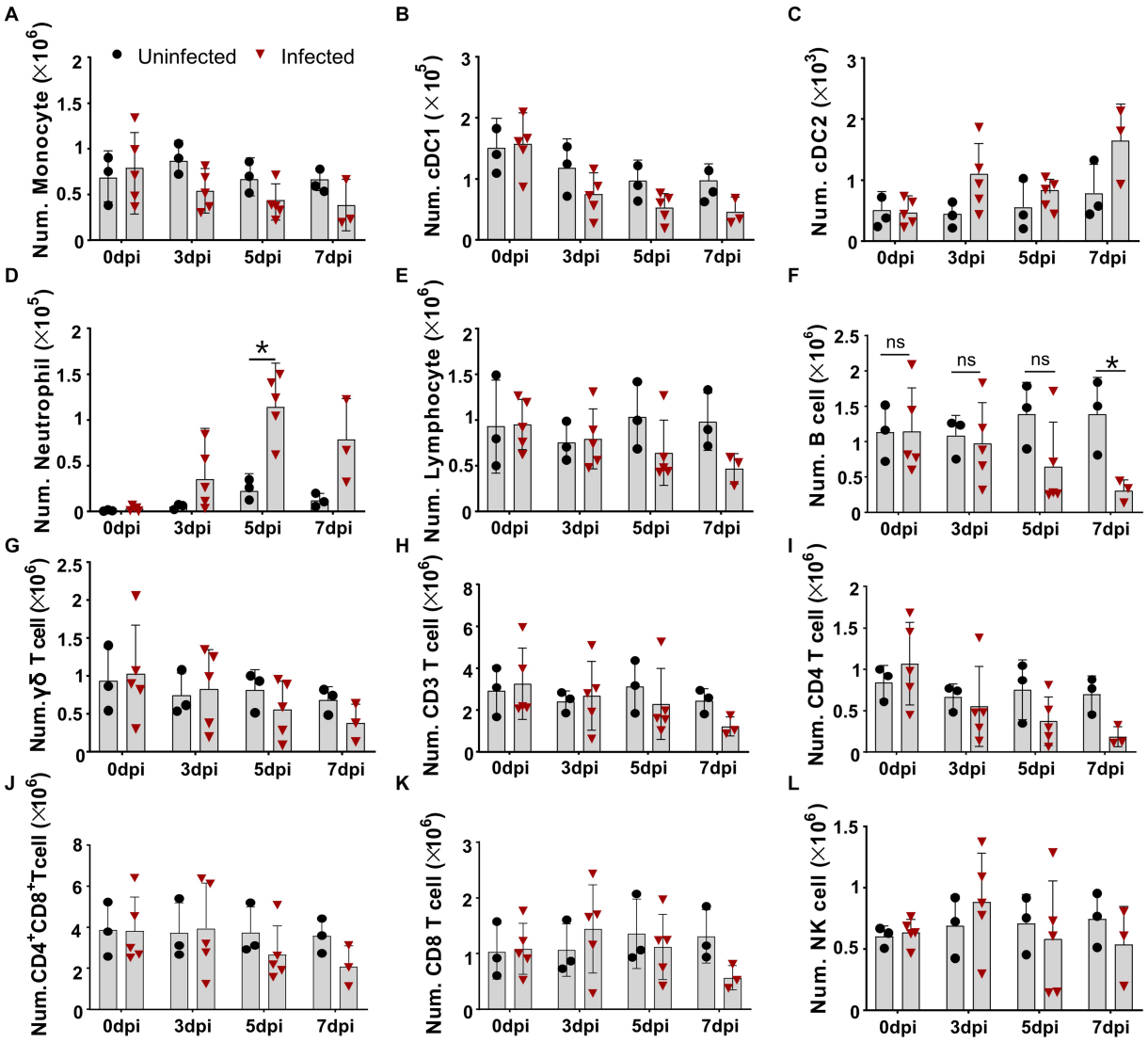

FIGURE 1
Virulent ASFV infection led to predominant reduction of B cells, CD4 T cells, monocytes, and DCs in periphery blood. At the indicated time points, PBMCs were prepared and stained for distinct leukocyte subsets and were analyzed by FCM. The absolute amount of each leukocyte subset per milliliter of blood was calculated based on the percentage of the specific cell type in live PBMCs. The numbers of monocyte **(A)**, cDC1 **(B)**, cDC2 **(C)**, neutrophil **(D)**, lymphocyte **(E)**, B cell **(F)**, γδ T cell **(G)**, CD3 T cell **(H)**, CD4 T cell **(I)**, $CD4^+CD8^+$ T cell **(J)**, CD8 T cell **(K)**, and NK cell **(L)** in 1 mL blood. Data shown are mean ± SD. $*p < 0.05$. $**p < 0.01$.

in Figure 3, all lymphocyte subsets of the infected animals showed different levels of apoptosis from 3 dpi on, compared to the control. The frequency of apoptotic B cells and NK cells increased to 6.78 ± 2.60% and 9.51 ± 4.79% (Figures 3A,B) at 3 dpi, respectively. The percentage of apoptotic γδ T cells gradually increased from 2.39 ± 2.55% at 3 dpi to 7.79 ± 3.71% at 7 dpi (Figure 3C), whereas αβ T cells showed higher proportional Annexin V-positive cells. Among these T cells, the frequencies of apoptotic $CD4^+$ T cells and $CD4^+CD8^+$ T cells peaked at 3 dpi, ranging from 10 to 30% with an average of 15% (Figures 3D,E), whereas Annexin V^+CD8^+ T cells showed relatively lower proportion, with an average of 10.59 ± 4.18% (Figure 3F) that sustained until 7 dpi.

Considering that acute virulent ASFV infection may cause more than one type of cell death, we detected the levels of IL-1β and IL-18, which are products of pyroptosis (He et al., 2015, Gao et al., 2022) in pig sera at 5 dpi. As shown in Supplementary Figure S3, the levels of IL-1β and IL-18 in infected pig sera increased compared with that of uninfected pig sera.

Virulent ASFV infection downregulated the expression of MHC II and CD21 molecules on APCs and B cells, respectively

The upregulation of the MHC II molecule on the cell surface is a hallmark of antigen-presenting cell (APC) maturation, especially DC maturation (Franzoni et al., 2019), and is associated with the capability of DCs to present antigen and prime T cells (Dalod et al., 2014). It was unclear whether ASFV infection affected the MHC II expression on APCs *in vivo*. Therefore, we examined the expression of SLA-DR/DQ molecules and their mean fluorescence intensity (MFI) on APCs by

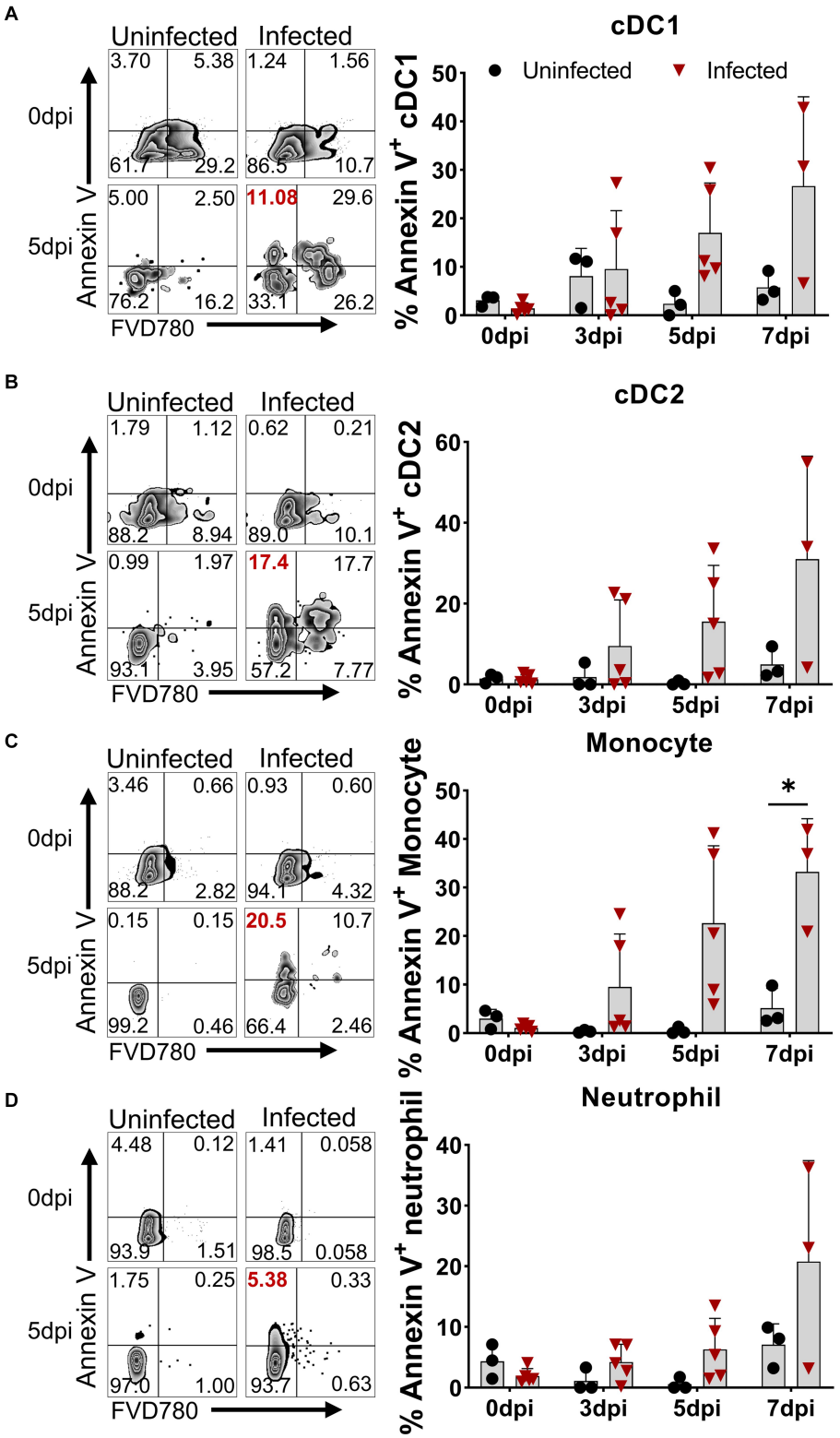

FIGURE 2
Apoptosis of DCs, monocytes, and neutrophils *in vivo* after ASFV infection. At the indicated time points, PBMCs of ASFV-infected and ASFV-uninfected piglets were prepared and stained for the apoptosis of cDC1, cDC2, monocytes, and neutrophils and were analyzed by FCM. Representative zebra plots (left panel) and kinetic changes (right panel) of the percentage of apoptotic (Annexin V$^+$) cDC1 **(A)**, cDC2 **(B)**, monocytes **(C)**, and neutrophils **(D)**. FVD780$^+$ cells, dead cells. Data shown are mean ± SD. *$p < 0.05$.

FCM. As shown in Figure 4, the MFI of SLA-DR/DQ on monocytes and cDC1 from infected piglets significantly decreased from 5 dpi on (Figures 4A,B), while the MFI of MHC II on cCD2 did not show any obvious change (Figure 4C). These results indicated that infection with ASFV CADC_HN09 strain may affect the antigen-presenting function of porcine monocytes and cDC1.

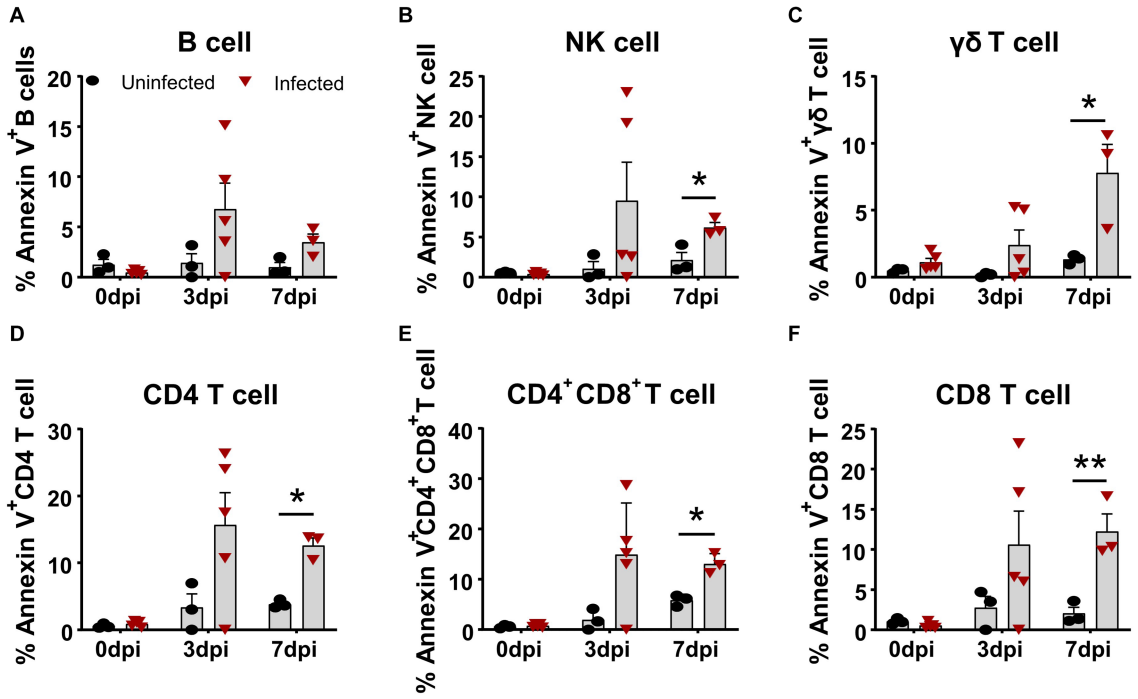

FIGURE 3
Apoptosis of T cell subsets *in vivo* after ASFV infection. At the indicated time points, PBMCs of ASFV-infected and ASFV-uninfected piglets were prepared and stained for apoptotic T cell subsets and were analyzed by FCM. Kinetic changes of the percentage of apoptotic (Annexin V$^+$) B cell **(A)**, NK cell **(B)**, γδ T cell **(C)**, CD4 T cell **(D)**, CD4$^+$CD8$^+$ T cell **(E)**, and CD8$^+$ T cell **(F)**. FVD780$^+$ cells, dead cells. Data shown are mean ± SD. *$p < 0.05$; **$p < 0.01$.

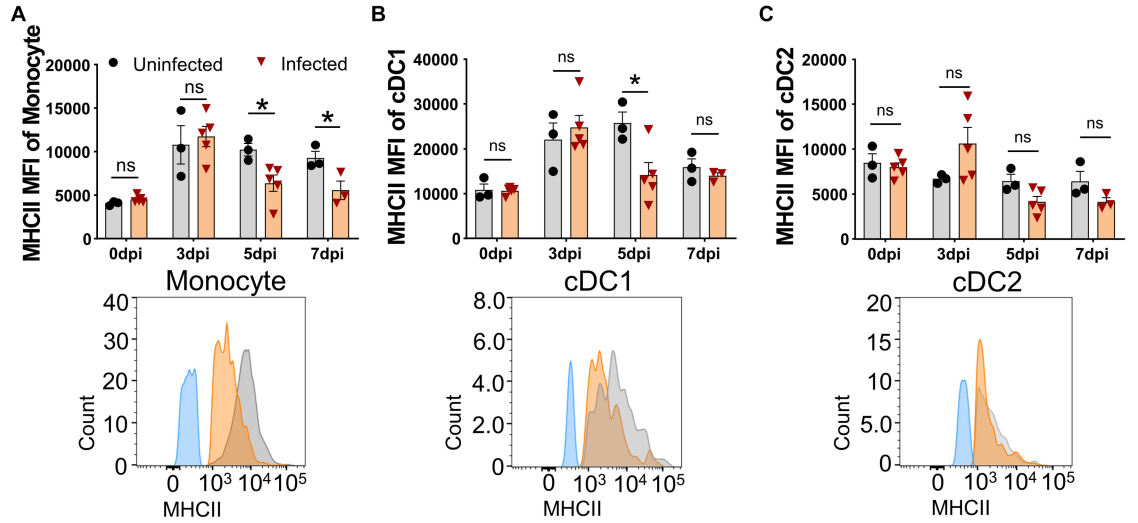

FIGURE 4
Downregulation of MHC II on APCs after ASFV infection. At the indicated time points, PBMCs of piglets infected with or without ASFV were prepared and stained for monocyte and DCs and were analyzed by FCM. MFI of MHC II on monocyte **(A)**, cDC1 **(B)**, and cDC2 **(C)** was calculated for assessment of the expression level on each subset (upper panel). Each point represents data from a single piglet, while bars represent the mean of each group. A representative histogram of the MHC II$^+$ APCs at 5 dpi (lower panel); the black line represents uninfected piglets and the orange line represents infected piglets, while the blue line means MHC II-FMO control. Data shown are mean ± SD. ns, no statistical significance. *$p < 0.05$; **$p < 0.01$.

Further analysis showed that CD21 MFI was significantly decreased as early as 5 dpi and further decreased at 7 dpi (Figure 5), while the percentage of CD21$^+$ B cells was reduced during ASFV infection. Given that CD21 is a marker for the maturation and activation of naive B cells and is associated with complement activation (Ahearn and Fearon, 1989), this result suggested that ASFV

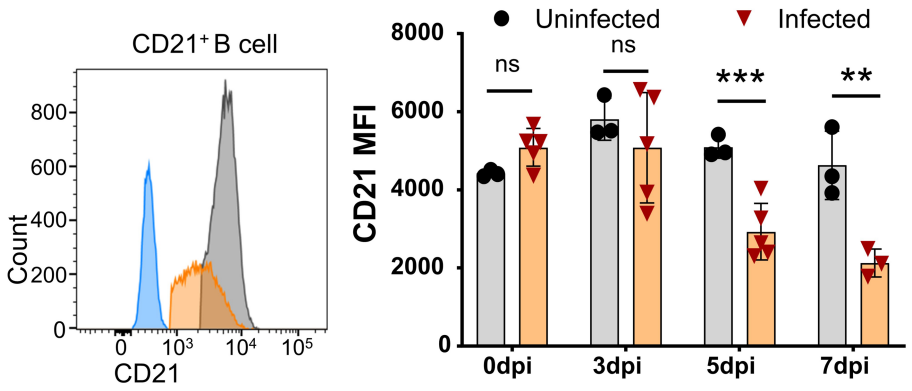

FIGURE 5
Downregulation of CD21 on B cells after ASFV infection. At the indicated time points, PBMCs of ASFV-infected or ASFV-uninfected piglets were separated and stained for FCM analysis of B cells. A representative histogram of CD21⁺ B cell at 5 dpi (left panel), and the black line represents uninfected piglets and the orange line represents infected piglets, while the closed blue histogram means FITC-CD21-FMO control. Dynamic changes of CD21 MFI on B cells (right panel). Each point represents data from a single pig, while the bars represent the mean of each group. Data shown are mean ± SD. ns, no statistical significance. $^{**}p < 0.01$; $^{***}p < 0.001$.

infection may potentially impair B cell development and complement activation.

African swine fever virus infection induced transient activation of T cells and NK cells

The ASF disease progression was so rapid that the infected pigs usually died within 7–14 days after infection (Zhao et al., 2019). It was debatable whether there is an activation of lymphocytes after virulent ASFV infection. Using porcine CD69 as the very early activation marker (Tian et al., 2022) and *ex vivo* cytokine staining, we examined the early activation of lymphocytes after ASFV infection. As shown in Figure 6, as early as 3 dpi, though no obvious early activation of lymphocytes was detected in PBMCs (Figure 6A), the percentages of CD69⁺ γδ T cells in both mLN (2.91 ± 0.63% vs. 1.01 ± 0.20%) and lungs (5.8 ± 1.38% vs. 1.57 ± 0.27%) were significantly increased in the ASFV-infected pigs, compared to the uninfected pigs (Figures 6B,C). Interestingly, the early activation of lymphocytes (3.22 ± 0.16% vs. 2.17 ± 0.15%) appeared first in the spleen of the infected pigs and was more significant than in other organs (Figure 6D). Among the activated lymphocytes, distinct T-cell subsets (CD4⁺, CD4⁺CD8⁺, and CD8⁺ T cells) showed obviously higher CD69 expression than those cells from the control. The activation of these cells became even more evident at 5 dpi and more pronounced in lymphoid organs than in periphery blood in terms of CD69 expression after infection, which was shown in our previous study (Tian et al., 2022).

To further identify whether the activated lymphocytes express cytokines *in vivo* upon ASFV infection, we performed an *ex vivo* intracellular cytokine staining of freshly isolated PBMCs at 5 dpi. We found that there were higher percentages of IFN-γ-secreting CD4⁺, CD8⁺ and CD4⁺CD8⁺ T cells, γδ T cells, and NK cells (Figures 7A–E; Supplementary Figure S2F), as well as TNF-α and IL-2-secreting γδ T cells (Figure 7F) in the ASFV-infected pigs, compared to the uninfected pigs, though the percentages were relatively low. In addition, more frequencies of TNF-α⁺IFN-γ⁺ CD8⁺ T cells and γδ T cells were observed in the ASFV-infected pigs (Figures 7B,E). These results indicated that there was *in vivo* activation of T cells and NK cells during virulent ASFV infection.

African swine fever virus infection impaired the capability of αβ T cells to produce cytokines

Even though the lymphocytes of the infected pigs were activated, these animals died in 7 to 9 days after infection in this study, suggesting the adaptive immunity to ASFV may be overridden by the immunosuppression caused by ASFV. Therefore, we compared the capability of lymphocytes from the infected and uninfected pigs to produce cytokines upon mitogenic stimulation by flow cytometry. The results showed that CD4⁺CD8⁺ T cells from the infected piglets were less capable of producing IFN-γ (5.0 ± 3.0% vs 10.43 ± 2.3%) and TNF-α (3.61 ± 0.68% vs 9.72 ± 1.36%) at 7 dpi upon PMA/Ionomycin stimulation, compared to those from the uninfected pigs (Figures 8A,B). Moreover, the results also revealed that CD4⁺CD8⁺ T and CD4 T cells showed reduced polyfunctionality for producing both TNF-α and IL-2 (0.13 ± 0.16% vs 1.28 ± 0.48% and 0.44 ± 0.28% vs 3.20 ± 1.02%) at 7 dpi and 5 dpi, respectively (Figures 8C,D), while CD4⁺CD8⁺ T and CD8 T cells showed impaired polyfunctionality for producing both TNF-α and IFN-γ (2.31 ± 1.0% vs 8.66 ± 1.92% and 6.57 ± 3.04% vs 12.39 ± 3.52%) at 7 dpi and 5 dpi, respectively (Figures 8A,B,E) in infected pigs in comparison with those of uninfected pigs. These findings demonstrated that αβ T cells from the ASFV-infected pigs were less responsive to stimulation and may be functionally impaired in vivo. However, there were still increased frequencies of TNF-α⁺IFN-γ⁺ and TNF-α⁺IL-2⁺ double-positive γδ T cells in infected pigs (Supplementary Figures S4A,B), though with no statistical significance due to huge individual differences. Further analysis of lymphocyte proliferation using Ki67 as a surrogate marker showed that B cells from the infected pigs significantly proliferated only at 3 dpi and then decreased (Supplementary Figure S5A) whereas CD4 T cells were less proliferative from 5 dpi on, compared to the control (Supplementary Figure S5B). The proliferation of CD8⁺,

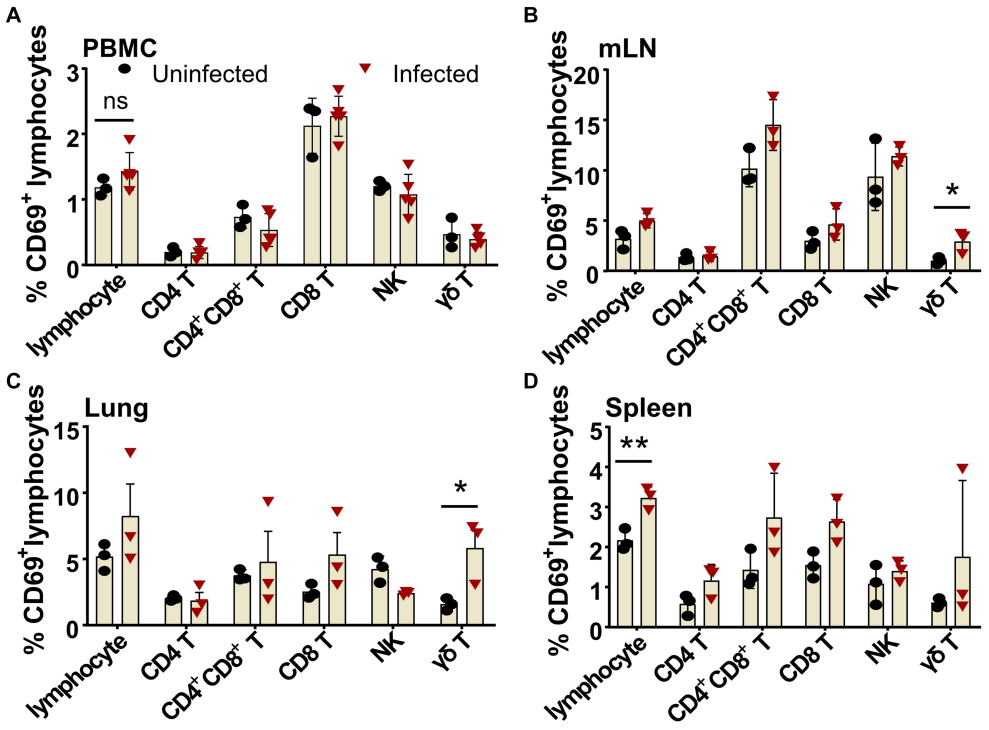

FIGURE 6
Early activation of different lymphocyte subsets after ASFV infection in blood and organs. Single-cell suspensions of peripheral blood, mLN, lung, and spleen were prepared at 3 dpi and stained for lymphocyte subsets and were analyzed by FCM. The percentages of CD69$^+$ lymphocyte subsets in PBMC **(A)**, mLN **(B)**, lung **(C)**, and spleen **(D)** were compared between ASFV-uninfected and ASFV-infected groups. Data shown are mean ± SD. *$p < 0.05$.

CD4$^+$CD8$^+$ T cells, γδ T cells and NK cells seemed not to be affected by ASFV infection (Supplementary Figures S5C–F).

Regulatory T cells were reduced in periphery blood after ASFV infection

Regulatory T cell (Treg) is believed to be involved in the immunopathogenesis of ASF and affects the long-term protection of an attenuated ASFV vaccine (Kaser et al., 2011; Sanchez-Cordon et al., 2020). We also examined the frequency changes of CD3$^+$CD4$^+$Foxp3$^+$ Tregs in periphery blood after ASFV CADC_HN09 infection. We found that the frequency of Tregs progressively decreased in the infected pigs and was significantly lower than that in the control group at 5 dpi (Supplementary Figures S6A,B), which is concomitant with the decreased proliferation of Treg (Ki67$^+$ Treg) (Supplementary Figure S6C).

Discussion

Virulent ASFV infection causes rapid death of the infected domestic pigs within 2 weeks (Zhao et al., 2019). Although the pathological changes of ASF have been extensively studied (Salguero et al., 2004; Wang et al., 2020; Li D. et al., 2021; Walczak et al., 2021), its immunopathogenesis remains incompletely understood. In addition to the cytokine storm that is believed to contribute to rapid death, *in vivo* death and activation of distinct immune cells have not been well tracked; moreover, it was unclear whether there was T-cell activation. In this study, we demonstrated that distinct immune cells underwent different levels of apoptosis kinetically *in vivo* over the course of infection and confirmed the cell types (B cells, CD4 T cells, monocytes, and dendritic cells) that were mainly affected by ASFV infection and accounted for the leukopenia documented in many studies (Carrasco de Lara et al., 1996a; Oura et al., 1998; Karalyan et al., 2012; Walczak et al., 2021). Interestingly, we found that T cells were transiently activated but eventually became less responsive to mitogenic stimulation, suggesting that the adaptive cellular immunity to ASFV might be initiated in the specific pathogen-unexperienced and pathogen-unimmunized piglets but somehow interrupted eventually. These findings improved our understanding of the immunopathogenesis of ASF.

The cellular immune response to the virulent ASFV strain has been examined in previous studies (Huhr et al., 2020; Schafer et al., 2021). CD4 T cells and CD79a$^+$ B cells were shown to account for the lymphopenia, while CD4$^+$CD8$^+$ T cells were increased at 7 dpi in domestic pigs, and no T-cell activation was detected in terms of Ki67 and T-bet expression (Huhr et al., 2020). Consistent with this study, we also observed that B cells and CD4 T cells were the major populations that contributed to lymphopenia, but why and how ASFV induces B cell and CD4 T cell reduction or death require further investigation. In addition, different from the previous study, we demonstrated that there was T-cell activation during virulent ASFV infection, based on CD69 expression and *ex vivo* IFN-γ expression by T cells. However, this early activation of T cells seemed not to contribute to the protection as the infected pigs eventually died.

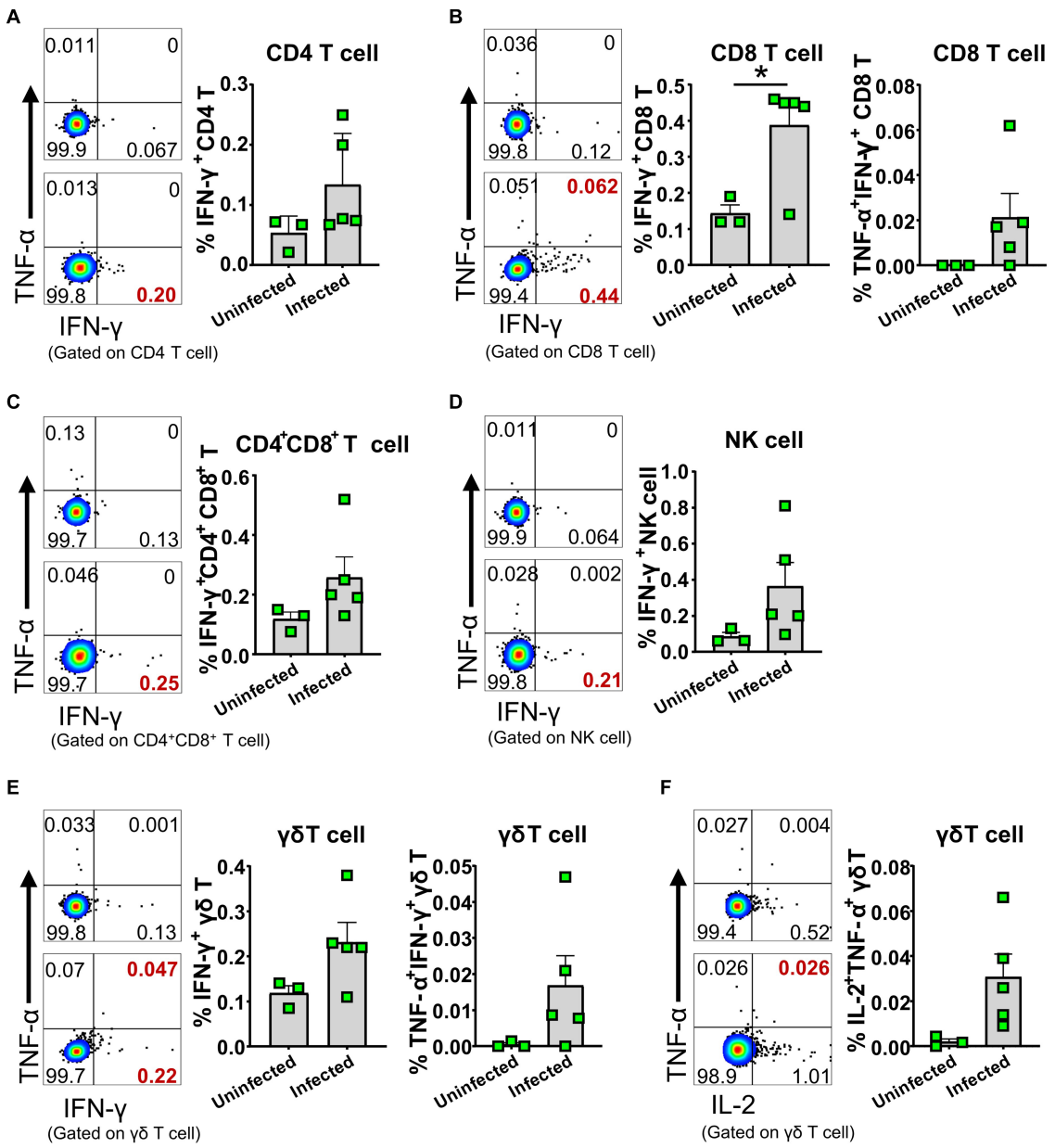

FIGURE 7
ASFV infection induced cytokine-secreting T cells and NK cells. PBMC of both ASFV-infected and ASFV-uninfected piglets were separated at 5 dpi and stained for lymphocyte subsets, followed by intracellular cytokine staining for TNF-α, IFN-γ, and IL-2, and then, the cells were analyzed by FCM. Representative pseudocolor plots (left panel: the upper one, uninfected; the lower one, infected) and increased frequencies of IFN-γ$^+$, IFN-γ$^+$TNF-α$^+$ or IL-2$^+$ CD4 T **(A)**, CD8 T **(B)**, CD4$^+$CD8$^+$ T **(C)**, NK **(D)** and γδ T cells **(E,F)** (right panel). Data shown are mean ± SD. *$p < 0.05$.

One of the reasons for this could be that the initiation of anti-ASFV T cell immunity was interrupted by the apoptosis and reductions of antigen-presenting cells (Figures 1A,B, 2A,C) or overridden by ASFV-induced immunosuppression. Cytotoxic CD8 T cells are of great importance in antiviral infection. We failed to examine if there was an increase of perforin$^+$ or granzyme$^+$ effector CD8 T cell in acute infection, which was described elsewhere (Lagumdzic et al., 2023), due to a lack of antibodies.

It was well reported that ASFV induced immunosuppression (Dixon et al., 2019). ASFV-encoded proteins, such as pE199L, p54, and A179L, have been shown to induce cell death via apoptosis or necroptosis in cell lines (Hernaez et al., 2004; Li T. et al., 2021; Shi et al., 2021). TNF-α from ASFV-infected macrophages caused the apoptosis of bystander lymphocytes during later stages (Dixon et al., 2019). Whether the reduction of distinct immune cell subsets is directly mediated *in vivo* by viral proteins or induced by inflammatory cytokines still needs to be answered. Cytokine IL-1β and IL-18 are typically products of cell pyroptosis (Church, 2014; Schneider et al., 2017). In this study, we found that the concentration of IL-1β and IL-18 in the sera of the infected pigs was significantly increased, implying that pyroptosis may also be induced during ASFV infection. However, how a single viral protein induces the cell death of immune cells *in vivo* remains to be demonstrated.

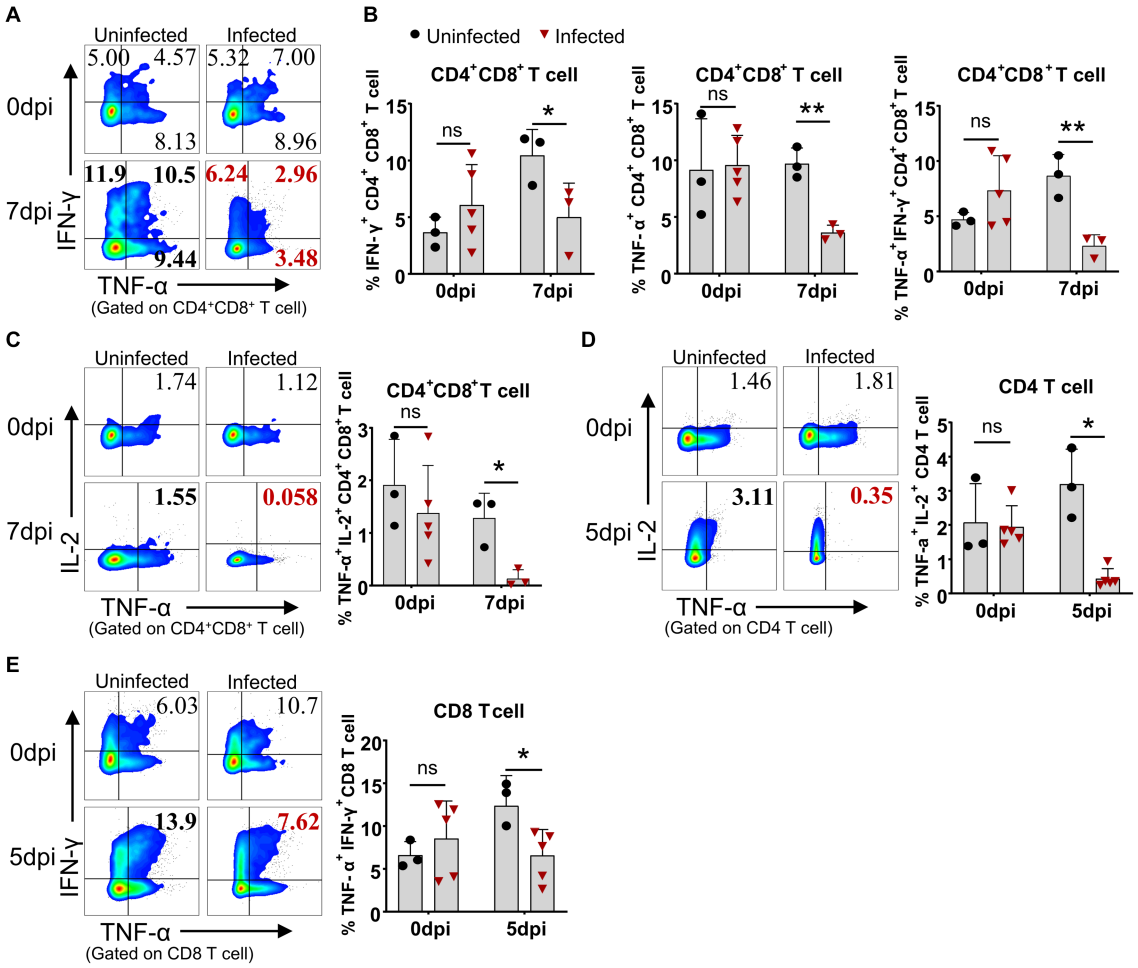

FIGURE 8
ASFV infection impaired the capability of T cells to produce cytokines. At the indicated time points, PBMC of ASFV-infected and uninfected piglets were separated and stimulated with mitogen and were stained for lymphocyte subsets, followed by an intracellular cytokine staining step and cells were determined by FCM. Representative pseudocolor plots **(A)** and the differential expression of cytokines in $CD4^+CD8^+$ T cell **(B)**. Representative pseudocolor plots (left panels) and the differential expression of cytokines in $CD4^+CD8^+$ T cell **(C)**, CD4 T cell **(D)** and CD8 T cell **(E)** (right panels). Each point represents data from a single pig while bars represent the mean of each group. Data shown are mean ± SD. ns, no statistical significance. *$p < 0.05$; **$p < 0.01$.

Treg is generally induced during acute infection and plays a role in counteracting immunopathological lesions caused by the excessive inflammatory response (Kaser et al., 2011). In this study, we did not observe the same increase of Treg in periphery blood as in previous studies (Huhr et al., 2020; Schafer et al., 2021), though strong cytokine storm and neutrophil increases were documented (Wang et al., 2020; Franzoni et al., 2023). It is reasonable to speculate that lacking Treg to dampen aberrant inflammatory response may promote or accelerate the death of the infected pigs. Of note, individual variation among pigs and operational variations including blood collection, PBMC isolation, and disease progression between each time-point, which severely affected data consistency and interpretations, were minimized in this study by setting the uninfected pigs as a control group, something that was missing in previous studies (Huhr et al., 2020; Schafer et al., 2021).

It is debatable whether there is activation of adaptive immunity after virulent ASFV infection as the ASF disease progresses so rapidly that the infected pigs die quickly (Zhao et al., 2019). In this study, using two methods, CD69 expression and *ex vivo* cytokine staining, we showed that early activation of lymphocytes indeed had taken place after ASFV CADC_HN09 infection. However, the capability of T cells to produce cytokines was impaired later. Apart from the cell death of activated T cells, the impairment of antigen presentation could be another possible reason. It was reported that ASFV infection did not significantly change the expression level of MHC II on mature pig bone marrow cells (pBM) and Mφ (Lithgow et al., 2014; Franzoni et al., 2017). However, we found that the expression of MHC II on monocyte and cDC1 was significantly decreased after ASFV infection (Figure 4), suggesting that antigen presentation by these cells may be impaired, thus disrupting the elicitation of effective adaptive immunity to ASFV. In addition, B cell reduction and CD21 downregulation on B cells may account for the failure of developing an effective humoral response as CD21 is involved in the regulation of B cell activation (Tedder et al., 1994).

Overall, in the present study, by examining the cellular changes of domestic pigs after infection with the highly virulent ASFV CADC_HN09 strain, we found that ASFV infection induced different levels of

apoptosis of distinct immune cells over the course of infection. There was early T-cell activation, but T-cell function was impaired later. The failure to develop an effective adaptive immunity to ASFV may be related to ASFV-induced immunosuppression or the impaired function of APCs, B cells, and T cells, leading to a dual impairment of humoral and cellular immune response. This study provides new insights into the rapid disease progression of ASF in domestic pigs, improves our understanding of the immunopathogenesis of ASF, and paves the way for further investigation.

Data availability statement

The original contributions presented in the study are included in the article/Supplementary material, further inquiries can be directed to the corresponding authors.

Ethics statement

The animal study was approved by the Animal Welfare and Ethics of China Animal Disease Control Center. The study was conducted in accordance with the local legislation and institutional requirements.

Author contributions

YT: Data curation, Formal analysis, Investigation, Methodology, Software, Validation, Visualization, Writing – original draft. DW: Data curation, Investigation, Validation, Writing – original draft. SH: Resources, Writing – original draft. ZC: Investigation, Writing – original draft. WL: Data curation, Writing – original draft. FJ: Data curation, Writing – original draft. YS: Data curation, Writing – original draft. YH: Data curation, Writing – original draft. XW: Investigation, Writing – original draft. QW: Investigation, Writing – original draft. SQ: Investigation, Writing – original draft. JWa: Data curation, Writing – original draft. TL: Data curation, Writing – original draft. XH: Methodology, Writing – original draft. JZ: Resources, Writing – original draft. JWu: Funding acquisition, Project administration, Supervision, Writing – review & editing. SS: Project administration, Supervision, Conceptualization, Funding acquisition, Writing – review & editing. XZ: Project administration, Supervision, Writing – original draft.

Funding

The author(s) declare financial support was received for the research, authorship, and/or publication of this article. This study was financially supported by the National Key Research and Development Program of China (2021YFD1800100), the National Natural Science Foundation of China (31941009), the Priority Academic Program Development of Jiangsu Higher Education Institutions (PAPD) and JSSCTD202224.

Acknowledgments

The authors thank Xiaohan Li at the China Animal Disease Control Center for her help in animal trials and single-cell preparation.

Conflict of interest

The authors declare that the research was conducted in the absence of any commercial or financial relationships that could be construed as a potential conflict of interest.

Publisher's note

Supplementary material

The Supplementary material for this article can be found online at: https://www.frontiersin.org/articles/10.3389/fmicb.2024.1328177/full#supplementary-material

References

Ahearn, J. M., and Fearon, D. T. (1989). Structure and function of the complement receptors, CR1 (CD35) and CR2 (CD21). *Adv. Immunol.* 46, 183–219. doi: 10.1016/S0065-2776(08)60654-9

Alejo, A., Matamoros, T., Guerra, M., and Andres, G. (2018). A proteomic atlas of the African swine fever virus particle. *J. Virol.* 92:18. doi: 10.1128/JVI.01293-18

Carrasco, L., de Lara, F. C., de las Mulas, J. M., Gómez-Villamandos, J. C., Pérez, J., Wilkinson, P. J., et al. (1996a). Apoptosis in lymph nodes in acute African swine fever. *J. Comp. Pathol.* 115, 415–428. doi: 10.1016/S0021-9975(96)80075-2

Carrasco, L., Gómez-Villamandos, J. C., Bautista, M. J., Martín de las Mulas, J., Villeda, C. J., Wilkinson, P. J., et al. (1996b). In vivo replication of African swine fever virus (Malawi '83) in neutrophils. *Vet. Res.* 27, 55–62.

Church, J. A. (2014). Cell death by Pyroptosis drives CD4 T-cell depletion in HIV-1 infection. *Pediatrics* 134:S184. doi: 10.1542/peds.2014-1817JJJJ

Cwynar, P., Stojkov, J., and Wlazlak, K. (2019). African swine fever status in Europe. *Viruses* 11:310. doi: 10.3390/v11040310

Dalod, M., Chelbi, R., Malissen, B., and Lawrence, T. (2014). Dendritic cell maturation: functional specialization through signaling specificity and transcriptional programming. *EMBO J.* 33, 1104–1116. doi: 10.1002/embj.201488027

Dixon, L. K., Chapman, D. A., Netherton, C. L., and Upton, C. (2013). African swine fever virus replication and genomics. *Virus Res.* 173, 3–14. doi: 10.1016/j.virusres.2012.10.020

Dixon, L. K., Islam, M., Nash, R., and Reis, A. L. (2019). African swine fever virus evasion of host defences. *Virus Res.* 266, 25–33. doi: 10.1016/j.virusres.2019.04.002

Franzoni, G., Dei Giudici, S., and Oggiano, A. (2018). Infection, modulation and responses of antigen-presenting cells to African swine fever viruses. *Virus Res.* 258, 73–80. doi: 10.1016/j.virusres.2018.10.007

Franzoni, G., Graham, S. P., Dei Giudici, S., and Oggiano, A. (2019). Porcine dendritic cells and viruses: an update. *Viruses* 11:445. doi: 10.3390/v11050445

Franzoni, G., Graham, S. P., Giudici, S. D., Bonelli, P., Pilo, G., Anfossi, A. G., et al. (2017). Characterization of the interaction of African swine fever virus with monocytes

and derived macrophage subsets. *Vet. Microbiol.* 198, 88–98. doi: 10.1016/j.vetmic.2016.12.010

Franzoni, G., Pedrera, M., and Sanchez-Cordon, P. J. (2023). African swine fever virus infection and cytokine response in vivo: an update. *Viruses* 15:233. doi: 10.3390/v15010233

Galindo, I., and Alonso, C. (2017). African swine fever virus: a review. *Viruses* 9:103. doi: 10.3390/v9050103

Gao, W., Li, Y., Liu, X., Wang, S., Mei, P., Chen, Z., et al. (2022). TRIM21 regulates pyroptotic cell death by promoting Gasdermin D oligomerization. *Cell Death Differ.* 29, 439–450. doi: 10.1038/s41418-021-00867-z

Ge, S., Li, J., Fan, X., Liu, F., Li, L., Wang, Q., et al. (2018). Molecular characterization of African swine fever virus, China, 2018. *Emerg. Infect. Dis.* 24, 2131–2133. doi: 10.3201/eid2411.181274

Gomez-Villamandos, J. C., Bautista, M. J., Sanchez-Cordon, P. J., and Carrasco, L. (2013). Pathology of African swine fever: the role of monocyte-macrophage. *Virus Res.* 173, 140–149. doi: 10.1016/j.virusres.2013.01.017

Gomez-Villamandos, J. C., Hervas, J., Mendez, A., Carrasco, L., de las Mulas, J. M., Villeda, C. J., et al. (1995). Experimental African swine fever: apoptosis of lymphocytes and virus replication in other cells. *J. Gen. Virol.* 76, 2399–2405. doi: 10.1099/0022-1317-76-9-2399

Hao, X., Li, S., Chen, L., Dong, M., Wang, J., Hu, J., et al. (2020). Establishing a multicolor flow cytometry to characterize cellular immune response in chickens following H7N9 avian influenza virus infection. *Viruses* 12:396. doi: 10.3390/v12121396

He, W. T., Wan, H., Hu, L., Chen, P., Wang, X., Huang, Z., et al. (2015). Gasdermin D is an executor of pyroptosis and required for interleukin-1beta secretion. *Cell Res.* 25, 1285–1298. doi: 10.1038/cr.2015.139

Hernaez, B., Diaz-Gil, G., Garcia-Gallo, M., Ignacio Quetglas, J., Rodriguez-Crespo, I., Dixon, L., et al. (2004). The African swine fever virus dynein-binding protein p54 induces infected cell apoptosis. *FEBS Lett.* 569, 224–228. doi: 10.1016/j.febslet.2004.06.001

Huhr, J., Schafer, A., Schwaiger, T., Zani, L., Sehl, J., Mettenleiter, T. C., et al. (2020). Impaired T-cell responses in domestic pigs and wild boar upon infection with a highly virulent African swine fever virus strain. *Transbound. Emerg. Dis.* 67, 3016–3032. doi: 10.1111/tbed.13678

Karalyan, Z., Zakaryan, H., Arzumanyan, H., Sargsyan, K., Voskanyan, H., Hakobyan, L., et al. (2012). Pathology of porcine peripheral white blood cells during infection with African swine fever virus. *BMC Vet. Res.* 8:18. doi: 10.1186/1746-6148-8-18

Karalyan, Z., Zakaryan, H., Sargsyan, K., Voskanyan, H., Arzumanyan, H., Avagyan, H., et al. (2012). Interferon status and white blood cells during infection with African swine fever virus in vivo. *Vet. Immunol. Immunopathol.* 145, 551–555. doi: 10.1016/j.vetimm.2011.12.013

Kaser, T., Gerner, W., and Saalmuller, A. (2011). Porcine regulatory T cells: mechanisms and T-cell targets of suppression. *Dev. Comp. Immunol.* 35, 1166–1172. doi: 10.1016/j.dci.2011.04.006

Lagumdzic, E., Pernold, C. P. S., Ertl, R., Palmieri, N., Stadler, M., Sawyer, S., et al. (2023). Gene expression of peripheral blood mononuclear cells and CD8(+) T cells from gilts after PRRSV infection. *Front. Immunol.* 14:1159970. doi: 10.3389/fimmu.2023.1159970

Li, D., Zhang, J., Yang, W., Li, P., Ru, Y., Kang, W., et al. (2021). African swine fever virus protein MGF-505-7R promotes virulence and pathogenesis by inhibiting JAK1- and JAK2-mediated signaling. *J. Biol. Chem.* 297:101190. doi: 10.1016/j.jbc.2021.101190

Li, T., Zhao, G., Zhang, T., Zhang, Z., Chen, X., Song, J., et al. (2021). African swine fever virus pE199L induces mitochondrial-dependent apoptosis. *Viruses* 13:240. doi: 10.3390/v13112240

Lithgow, P., Takamatsu, H., Werling, D., Dixon, L., and Chapman, D. (2014). Correlation of cell surface marker expression with African swine fever virus infection. *Vet. Microbiol.* 168, 413–419. doi: 10.1016/j.vetmic.2013.12.001

Maisonnasse, P., Bouguyon, E., Piton, G., Ezquerra, A., Urien, C., Deloizy, C., et al. (2016). The respiratory DC/macrophage network at steady-state and upon influenza infection in the swine biomedical model. *Mucosal Immunol.* 9, 835–849. doi: 10.1038/mi.2015.105

Oura, C. A., Powell, P. P., and Parkhouse, R. M. (1998). African swine fever: a disease characterized by apoptosis. *J. Gen. Virol.* 79, 1427–1438. doi: 10.1099/0022-1317-79-6-1427

Petrov, A., Forth, J. H., Zani, L., Beer, M., and Blome, S. (2018). No evidence for long-term carrier status of pigs after African swine fever virus infection. *Transbound. Emerg. Dis.* 65, 1318–1328. doi: 10.1111/tbed.12881

Pikalo, J., Zani, L., Huhr, J., Beer, M., and Blome, S. (2019). Pathogenesis of African swine fever in domestic pigs and European wild boar - lessons learned from recent animal trials. *Virus Res.* 271:197614. doi: 10.1016/j.virusres.2019.04.001

Portugal, R., Leitao, A., and Martins, C. (2009). Apoptosis in porcine macrophages infected in vitro with African swine fever virus (ASFV) strains with different virulence. *Arch. Virol.* 154, 1441–1450. doi: 10.1007/s00705-009-0466-x

Ramiro-Ibanez, F., Ortega, A., Brun, A., Escribano, J. M., and Alonso, C. (1996). Apoptosis: a mechanism of cell killing and lymphoid organ impairment during acute African swine fever virus infection. *J. Gen. Virol.* 77, 2209–2219. doi: 10.1099/0022-1317-77-9-2209

Salguero, F. J., Sanchez-Cordon, P. J., Sierra, M. A., Jover, A., Nunez, A., and Gomez-Villamandos, J. C. (2004). Apoptosis of thymocytes in experimental African swine fever virus infection. *Histol. Histopathol.* 19, 77–84. doi: 10.14670/HH-19.77

Sanchez-Cordon, P. J., Jabbar, T., Chapman, D., Dixon, L. K., and Montoya, M. (2020). Absence of long-term protection in domestic pigs immunized with attenuated African swine fever virus isolate OURT88/3 or BeninDeltaMGF correlates with increased levels of regulatory T cells and Interleukin-10. *J. Virol.* 94:20. doi: 10.1128/JVI.00350-20

Schafer, A., Zani, L., Pikalo, J., Huhr, J., Sehl, J., Mettenleiter, T. C., et al. (2021). T-cell responses in domestic pigs and wild boar upon infection with the moderately virulent African swine fever virus strain 'Estonia2014'. *Transbound. Emerg. Dis.* 68, 2733–2749. doi: 10.1111/tbed.14048

Schneider, K. S., Gross, C. J., Dreier, R. F., Saller, B. S., Mishra, R., Gorka, O., et al. (2017). The Inflammasome drives GSDMD-independent secondary Pyroptosis and IL-1 release in the absence of Caspase-1 protease activity. *Cell Rep.* 21, 3846–3859. doi: 10.1016/j.celrep.2017.12.018

Shi, J., Liu, W., Zhang, M., Sun, J., and Xu, X. (2021). The A179L gene of African swine fever virus suppresses virus-induced apoptosis but enhances necroptosis. *Viruses* 13:490. doi: 10.3390/v13122490

Takamatsu, H. H., Denyer, M. S., Lacasta, A., Stirling, C. M., Argilaguet, J. M., Netherton, C. L., et al. (2013). Cellular immunity in ASFV responses. *Virus Res.* 173, 110–121. doi: 10.1016/j.virusres.2012.11.009

Tedder, T. F., Zhou, L. J., and Engel, P. (1994). The CD19/CD21 signal transduction complex of B lymphocytes. *Immunol. Today* 15, 437–442. doi: 10.1016/0167-5699(94)90274-7

Tian, Y., Hao, Y., Dong, M., Li, S., Wang, D., Jiang, F., et al. (2022). Development of a monoclonal antibody to pig CD69 reveals early activation of T cells in pig after PRRSV and ASFV infection. *Viruses* 14:343. doi: 10.3390/v14061343

Walczak, M., Wasiak, M., Dudek, K., Kycko, A., Szacawa, E., Olech, M., et al. (2021). Blood counts, biochemical parameters, inflammatory, and immune responses in pigs infected experimentally with the African swine fever virus isolate Pol18_28298_O111. *Viruses* 13:521. doi: 10.3390/v13030521

Wang, S., Zhang, J., Zhang, Y., Yang, J., Wang, L., Qi, Y., et al. (2020). Cytokine storm in domestic pigs induced by infection of virulent African swine fever virus. *Front Vet Sci* 7:601641. doi: 10.3389/fvets.2020.601641

Zhao, D., Liu, R., Zhang, X., Li, F., Wang, J., Zhang, J., et al. (2019). Replication and virulence in pigs of the first African swine fever virus isolated in China. *Emerg. Microbes Infect.* 8, 438–447. doi: 10.1080/22221751.2019.1590128

Zheng, Y., Li, S., Li, S. H., Yu, S., Wang, Q., Zhang, K., et al. (2022). Transcriptome profiling in swine macrophages infected with African swine fever virus at single-cell resolution. *Proc. Natl. Acad. Sci. USA* 119:e2201288119. doi: 10.1073/pnas.2201288119

Zhou, X., Li, N., Luo, Y., Liu, Y., Miao, F., Chen, T., et al. (2018). Emergence of African swine fever in China, 2018. *Transbound. Emerg. Dis.* 65, 1482–1484. doi: 10.1111/tbed.12989

frontiers | Frontiers in Microbiology

TYPE Original Research
PUBLISHED 21 February 2024
DOI 10.3389/fmicb.2024.1362471

OPEN ACCESS

EDITED BY
Gang Wang,
Shandong Agricultural University, China

REVIEWED BY
Chao-Nan Lin,
National Pingtung University of Science and Technology, Taiwan
Jean-Pierre Frossard,
Animal and Plant Health Agency, United Kingdom
Onyekachukwu Henry Osemeke,
Iowa State University, United States

*CORRESPONDENCE
Yin Wang
10334@sicau.edu.cn

†These authors have contributed equally to this work

RECEIVED 28 December 2023
ACCEPTED 12 February 2024
PUBLISHED 21 February 2024

CITATION
Tu T, Li Y, Zhang G, Du C, Zhou Y, Jiang D, Luo Y, Yao X, Yang Z, Ren M and Wang Y (2024) Isolation, identification, recombination analysis and pathogenicity experiment of a PRRSV recombinant strain in Sichuan Province, China.
Front. Microbiol. 15:1362471.
doi: 10.3389/fmicb.2024.1362471

Isolation, identification, recombination analysis and pathogenicity experiment of a PRRSV recombinant strain in Sichuan Province, China

Teng Tu[1,2†], Yanwei Li[1,2†], Guidong Zhang[1,2], Chengchao Du[1,2], You Zhou[1,2], Dike Jiang[1,2], Yan Luo[1,2], Xueping Yao[1,2], Zexiao Yang[1,2], Meishen Ren[1,2] and Yin Wang[1,2*]

[1]Key Laboratory of Animal Disease and Human Health of Sichuan Province, Sichuan Agricultural University, Chengdu, China, [2]College of Veterinary Medicine, Sichuan Agricultural University, Chengdu, China

Since 2013, the porcine reproductive and respiratory syndrome virus type 2 (PRRSV-2), lineage 1.8 (NADC30-like PRRSV) has emerged and become widely prevalent in China. The NADC30-like PRRSV poses significant challenges for disease control, primarily because of its propensity for frequent mutations and recombinations. We successfully isolated and identified a NADC30-like strain, designated SCCD22, in Chengdu, Sichuan Province, China. We meticulously examined the genetic recombination properties and evaluated its pathogenicity in 28-day-old piglets. SCCD22 showed 93.02% nucleotide homology with the NADC30 PRRSV strain, and its non-structural protein 2 coding region showed the same 131 amino acid deletion pattern as that seen in NADC30. Furthermore, we identified two recombination events in SCCD22: one in the NSP2 region (1,028–3,290nt), where it was highly similar to the JXA1-like strain GZ106; and another in the NSP10~12 region (9,985–12,279nt), closely resembling the NADC30-like strain CY2-1604. Piglets infected with SCCD22 exhibited clinical symptoms such as elevated body temperature, prolonged fever, reduced appetite, and roughened fur. Postmortem examinations underscored the typical lung pathology associated with PRRSV, indicating that the lungs were the primary affected organs. Furthermore, extended viral shedding accompanied by progressive viremia was observed in the serum and nasal excretions of infected piglets. In summary, this study reports a domestic PRRSV recombination strain in the Sichuan Province that can provide critical insights into preventing and controlling PRRSV in this region.

KEYWORDS

porcine reproductive and respiratory syndrome virus (PRRSV), genetic recombination, lineage 1.8, pathogenicity, preventing and controlling

1 Introduction

Porcine reproductive and respiratory syndrome (PRRS) is a highly contagious disease caused by the porcine reproductive and respiratory syndrome virus (PRRSV). It differs from clinical manifestations caused by other pathogens such as African swine fever virus, classical swine fever virus, porcine parvo virus, and porcine circovirus type 2, and it leads to severe

reproductive disorders, delayed growth, respiratory symptoms, and high mortality rates in pigs (Kappes and Faaberg, 2015).

PRRSV is a single-stranded positive-sense RNA virus that belongs to the Arteriviridae family. The genome size of PRRSV ranges from 15 to 15.5 Kb, encoding approximately 10 open reading frames (ORFs), which include ORF1a, ORF1b, ORF2a, ORF2b, ORF3, ORF4, ORF5a, ORF5, ORF6, and ORF7. ORF1a and ORF1b together account for approximately 75% of the genome and encode at least 16 non-structural proteins (NSPs), such as NSP1a, NSPSP1β, NSP2, NSP2TF, NSP2N, NSP3-NSP6, NSP7α, NSP7β, and NSP8-NSP12 (Jiang et al., 2023). ORF2a, ORF2b, ORF3, ORF4, ORF5, ORF6, and ORF7 encode seven structural proteins: glycoprotein GP2a, small envelope protein E, glycoproteins GP3, GP4, and GP5, membrane protein (M protein), and nucleocapsid protein (N protein) (Meng et al., 1995; Kappes and Faaberg, 2015; Lunney et al., 2016).

Based on differences in genomic sequences and antigenic characteristics, the prevalence of PRRSV can be divided into PRRSV-1 (represented by the European type with the lelystadvirus strain) and PRRSV-2 (represented by the North American type with the VR-2332 strain) (Adams et al., 2016). Shi constructed a global classification system for PRRSV based on a comprehensive analysis of the complete ORF5 gene sequence (Shi et al., 2010b). According to this classification system, PRRSV-1 can be divided into three subtypes (sublineages 1–3). Although numerous reports have been published on the prevalence of PRRSV-1 in China in recent years, its clinical detection rate remains relatively low. As early as 1997, Chinese customs intercepted pigs infected with PRRSV-1 (B13, GenBank: AY633973) (Yun et al., 1998), indicating that the introduction of PRRSV-1 may have occurred more than 20 years ago.

PRRSV-2 is divided into nine lineages, each with several sub-lineages (Shi et al., 2010a,b). The virulence and antigenicity of each lineage vary owing to genetic diversity. Five lineages of PRRSV-2 have been reported in China, namely lineages 1 (sublineages 1.5 and 1.8), 3, 5 (sublineage 5.1), 8 (sublineage 8.7), and 9 (Chen et al., 2019; Han et al., 2020). Lineage 1 of PRRSV includes representative strains such as NADC30, JL580, NADC34, and RFLP1-4-4; lineage 3 is mainly prevalent in southern China, with relatively low pathogenicity, including representative strains QYYZ and GM; lineage 5 mainly contains the classic PRRSV strain represented by VR-2332; lineage 8 contains highly pathogenic strains represented by TJ, JXA1, TA-12, and the classic strain represented by CH-1a; lineage 9 was discovered in Xinjiang in 2011.

Sublineage 1.8 (NADC30-like) of PRRSV-2 has been reported in China since 2013 (Zhou F. et al., 2015). Similar to the American NADC30 isolates MN184A and NADC30, the Chinese NADC30-like virus strains exhibit the same NSP2 deletion pattern, including a discontinuous deletion of 131 amino acids (Feng et al., 2014; Zhao et al., 2015; Zhou L. et al., 2015; Li et al., 2016). Recently, multiple novel recombinant PRRSV strains from NADC30-like outbreaks in China have recently been reported to exhibit different pathogenicities (Zhao et al., 2015; Liu et al., 2017; Chen et al., 2018). Compared with other PRRSV lineages in China, the NADC30-like strain has a higher potential for recombination and pathogenic diversity. Numerous recent studies (Zhao et al., 2015; Zhang et al., 2016; Liu et al., 2018; Sui et al., 2018; Han et al., 2019; Zhang et al., 2019; Li et al., 2021; Liu et al., 2022; Ma et al., 2022; Wu et al., 2022; Chang et al., 2023) have indicated that the virulence of NADC30-like PRRSV strains is related to the recombination regions and segments derived from the parental strains. Currently, all NADC30-like PRRSV strains induce typical clinical symptoms and pathological changes in piglets following infection, with their pathogenicity tending toward intermediacy between the parental strains (Yu et al., 2021).

This study aims to elucidate the genetic and pathogenic features of PRRSV in Sichuan Province, through the isolation, recombination analysis and pathogenicity experiment of a NADC30-like PRRSV strain. In this study, the Pams-163 (PRRSV receptor CD163 was expressed and transfected into primary alveolar macrophage passage cell line 3D4/21 (CRL-2843). The Pams-163 was maintained and provided by the Animal Quarantine Laboratory of Sichuan Agricultural University) was used to isolate and identify prevalent PRRSV strains from suspected PRRSV-infected samples, resulting in the isolation of an NADC30-like PRRSV strain. The isolated strain underwent whole-genome sequencing, genetic evolution analysis, and pathogenicity testing in piglets to clarify the genetic evolutionary relationship and recombination events of the isolated strain and to assess its pathogenicity in 28-day-old piglets. The results of this study lay the foundational scientific groundwork for future prevention and control strategies against PRRSV in Sichuan Province. Firstly, our comprehensive genome-wide analysis of the isolated strains holds promise for identifying novel genetic markers. These markers could be instrumental in developing specific vaccines and diagnostic assays, meticulously tailored to combat potential NADC30 PRRSV outbreaks. Secondly, a deeper understanding of the unique mutation and recombination patterns of this virus could inform the creation of more targeted antiviral therapeutics. Furthermore, the pathogenicity assessment conducted in this study offers valuable insights into the virulence of this newly identified PRRSV variant, which is crucial for formulating effective disease management strategies.

2 Materials and methods

2.1 Sample collection and processing

In 2022, samples suspected of PRRSV infection, including serum, lung tissue, saliva swabs, semen, were collected from a pig farm in Chengdu, Sichuan Province, China. After subjecting the samples to three freeze–thaw cycles, where each cycle involved freezing at −80°C for 15 min followed by thawing at room temperature (26°C), 2 mL of PBS was added to the samples. They were then centrifuged at 12,000 rpm for 5 min at 4°C. Following centrifugation, the samples were stored in an ultra-low temperature freezer at −80°C for subsequent pathogen detection and virus isolation.

2.2 RNA extraction and reverse transcription

Total RNA was extracted from the samples using the AG RNAex Pro RNA extraction reagent (Accurate Biology Co., Ltd., Hunan, China), following the manufacturer's instructions. Subsequently, cDNA was synthesized using the Evo M-MLV RT Kit (Accurate Biology Co., Ltd., Hunan, China) according to the manufacturer's protocol. The reverse transcription reaction system and conditions are listed in Supplementary Table S1.

TABLE 1 Information for detection primer.

Type of virus	Sequence (5′-3′)	Target gene	Length of products (bp)	References
NADC34-like PRRSV	F: CCTGTGTGACTCATATTGTCTCC R: CGGCGTAAATGCTACTCAAGAC P: FAM-CGCCCTCACCACCAGCCATTTCCT-BHQ1	ORF5	129	Tu et al. (2023)
HP-PRRSV	F: GACGTGCCCCCAAGCTGAT R: GGATGCCCATGTTCTGCGA P: FAM-CGTAGAACTGTGACAACAACGCTGAC-BHQ1	*NSP2*	171	Qiu et al. (2020)
NADC30-likePRRSV	F: CGTATTGGACACCTCTTTTGACTG R: AACTGGACCTAATCTTCCTGCG P: ROX-CCCAAAGGTCTTCGTCGGTATTCC-BHQ2	*NSP2*	218	Qiu et al. (2020)
Classical PRRSV	F: GCAATTGTGTCTGTCGTC R: CTTATCCTCCCTGAATCTGAC	ORF5	81	Chai (2009)

2.3 Primer design and PRRSV detection

The cDNA obtained from 2.2 was detected using RT-qPCR to confirm PRRSV positive. All primers used are listed in Table 1. All primers were synthesized by TsingkeBiotechnology Co., Ltd. (Chengdu, China).

2.4 Isolation and identification of PRRSV

To increase the volume of viral fluid for the isolation of PRRSV, we meticulously selected approximately 5 g of lung tissue that was confirmed to be PRRSV-positive using RT-qPCR. This tissue was finely minced using scissors and ground in a mortar. After adding PBS and undergoing three freeze–thaw cycles, the supernatant was collected and sterilized using a 0.22 μm filter, then stored at −80°C for later use. A 500 μL aliquot of the treated supernatant was added to a monolayer of Pams-163 (constructed, maintained and provided by the Animal Quarantine Laboratory of Sichuan Agricultural University) with a confluence of approximately 90%. After a one-hour incubation period, the supernatant was meticulously removed. The cells were subsequently incubated for 48 h in a 5% CO_2 incubator at 37°C. Following this incubation, PRRSV was detected using a fluorescein isothiocyanate-labeled polyclonal antibody specifically targeting the PRRSV N protein (Bioss, Beijing, China).

In the subsequent phase, the purified viral fluid was subjected to a 10-fold serial dilution and inoculated onto a 96-well cell culture plate. Following a 5-day incubation at 37°C in a CO_2-controlled environment, the cytopathic effect (CPE) induced by PRRSV was meticulously evaluated using an inverted microscope (Olympus Corporation, Tokyo, Japan). The CPE was characterized by notable changes in Pams-163 cells, including cell shrinkage, detachment, and the blurring of cellular boundaries. The 50% tissue culture infectious dose ($TCID_{50}$) of PRRSV was calculated using the Reed-Muench formula based on the number of wells with CPE.

Purified viral isolates were used to sequence their entire genomes. To investigate the effect of multiplicity of infection (MOI) on the growth of PRRSV in Pams-163, we infected cells with MOI = 0.01 in triplicate. We incubated them for 1.5 h at 37°C. RPMI 1640 medium containing 2% serum was added for maintenance, and virus fluid was collected every 24 h and frozen at −80°C. After 144 h, the CPE induced by PRRSV was assessed. Subsequently, the $TCID_{50}$ of PRRSV was determined using the Reed-Muench formula. A viral growth curve was constructed based on the titration results. The PRRSV strain isolated from Sichuan Province was designated as SCCD22.

2.5 Whole-genome sequencing and genetic evolution analysis of SCCD22

PRRSV RNA was extracted, and cDNA was prepared according to the above procedures. Subsequently, RT-qPCR was conducted to verify that the tested sample contained an adequate number of viral copies, thus ensuring its suitability for further analysis (the qPCR cycle threshold value was <25). Once confirmed, the sample was sent to Beijing Tsingke Biotech Company (Beijing, China) for whole-genome sequencing. Illumina sequencing technology was used with a coverage of 5,000, and the assembly method used was FastPlast v1.2.6. The complete genome sequence of SCCD22 was annotated and visualized using CGView.[1] Phylogenetic tree was constructed using the distance-based neighbor-joining method with 1,000 bootstrap replicates in MEGAX software (Tempe, AZ, United States) for the purpose of genetic evolutionary analysis.

2.6 Genetic recombination analysis of SCCD22

The SCCD22 strain was compared with the full-genome sequences of representative strains from various lineages in Genbank for recombination analysis using RDP5.1 and SimPlot 3.5.1. Recombination breakpoints in the sequences were predicted using RDPv5.1. A recombination event was confirmed if it was supported by at least three of the following methods: RDP, GENECONV, MAXCHI, CHIMAERA, Bootscan, Siscan, and 3SEQ. Similarity comparisons were further performed using SimPlot 3.5.1 within a

1 https://proksee.ca/

200 bp sliding window along the genomic alignment (20-bp step), and the complete SCCD22 genome was selected as the query sequence, and the reference sequences were strains GZ106, ISU18, NADC 30, and CY2-1604.

2.7 Pathogenicity analysis of SCCD22

To strike a balance between statistical significance and practical limitations, we opted for a sample size of 10 piglets for the pathogenicity experiment. Ten weaned piglets (five males and five females, breed Yorkshire, approximately 4 weeks old), were purchased from Chengdu Wangjiang Agriculture and Animal Husbandry Technology Co., Ltd., and the weight variance among all piglets in the study was within a range of 500 g. After testing negative for both PRRSV antibodies and antigens, the piglets were randomly divided into two groups and housed in separate rooms. Their breed, number and grouping in the experiment with the 3R principle. All animals were housed under controlled conditions with a temperature of 26°C, humidity of 60%, and 12 h of light per day, with *ad libitum* access to water. Group 1 (infection group): five piglets received intranasal inoculation with virus solution ($TCID_{50} = 10^5$/mL), 2 mL per piglet. Group 2 (control group): five piglets received an intranasal inoculation of 2 mL of RPMI 1640 medium per piglet.

Following the virus inoculation, daily recordings were made of the rectal temperatures of the pigs, and their clinical manifestations were observed, such as appetite, mental state (presence of unconsciousness/coma), and respiratory condition. Clinical symptom scoring (Jiang et al., 2023) is detailed in Supplementary Table S2. Additionally, on days 3, 7, 10, and 14 post-inoculation, the pigs were weighed to calculate the average daily weight gain. These comprehensive assessments aimed to evaluate the impact of the viral infection on the health and welfare of the piglets and to provide insights into potential treatment strategies for this specific strain.

Blood samples were drawn from the anterior vena cava of the piglets using a 5 mL syringe at 0, 3, 5, 7, 10, and 14 days post-infection. Concurrently, nasal secretions were collected using cotton swabs. Subsequently, the shedding of the virus was detected using RT-qPCR. On days 7, 10, and 14, viremia was measured using the $TCID_{50}$ method. This study aimed to gain a deeper understanding of the viral shedding and clearance mechanisms in piglets, thereby enhancing our understanding of how this specific virus strain interacts with its host.

Throughout the experiment, the survival of the piglets in each group was monitored. On day 14 post-infection, all piglets were humanely euthanized. Necropsies were immediately performed on the dead piglets to observe gross pathological changes in various organs. Lung tissues were collected and fixed in a 4% paraformaldehyde solution. After fixation, tissue embedding, paraffin sectioning, and hematoxylin and eosin (H&E) staining were performed for pathological examination. Additionally, the spleen, lungs, thymus, and lung lymph nodes were collected from each dissected piglet, and RT-qPCR was used to measure the viral load in these organs. The animal study was approved by the Animal Ethics Committee of Sichuan Agricultural University (Approval Number: 20220261).

2.8 Statistical analysis

Statistical analysis was performed with GraphPad Prism 8.0.2 (GraphPad Software, San Diego, CA, United States). All data were subjected to one-way ANOVA followed by t-tests to determine statistical significance. A value of p of less than 0.05 was considered statistically significant.

3 Results

3.1 Virus isolation and identification

PRRSV-positive specimens were inoculated onto monolayer Pams-163 and cultured in a 37°C CO_2 incubator for 4–5 days. At 48 h post-inoculation with PRRSV, Pams-163 exhibited CPE, including cell shrinkage, irregular cell margins, increased refraction, and partial detachment (Figure 1A). In contrast, the control cells remained healthy and maintained distinct cell boundaries (Figure 1B). Pams-163 supernatant, which showed 80% CPE after six continuous passages, was subjected to RT-qPCR testing for PRRSV using the primers listed in Table 1. The isolated strain was identified as an NADC30-like strain (Figure 1C). PRRSV proliferation on Pams-163 was confirmed through immunofluorescence assay (IFA), which demonstrated green fluorescence surrounding the cell nuclei, while the negative control showed no fluorescence signal, indicating that the isolated PRRSV strain could proliferate on Pams-163 (Figure 1D).

3.2 Results of $TCID_{50}$ determination

The CPE observed in each well of the 96-well plate was meticulously recorded. Subsequently, the $TCID_{50}$ was calculated based on these observations using the Reed-Muench formula. As shown in Supplementary Table S3, the $TCID_{50}$ of the PRRSV isolate was determined to be $10^{-6.5}$/0.1 mL.

3.3 Plotting of viral multi-step growth curves

By quantifying the $TCID_{50}$ of the viral fluid at various time points, we constructed a correlation between the viral titers and time, thereby generating a multi-step growth curve for the virus (Figure 2). Our findings indicate that the titer of the isolate peaked at 72 h, reaching a value of $10^{-6.74}$/mL (MOI = 0.01), followed by a decreasing trend over time.

3.4 Phylogenetic and recombination analysis of PRRSV SCCD22

3.4.1 Whole-genome sequencing and annotation of PRRSV SCCD22

Utilizing Illumina sequencing technology, the whole genome of SCCD22 was sequenced, measuring 15,016 base pairs in length (GenBank accession number: OR670493.1). Visualization of the

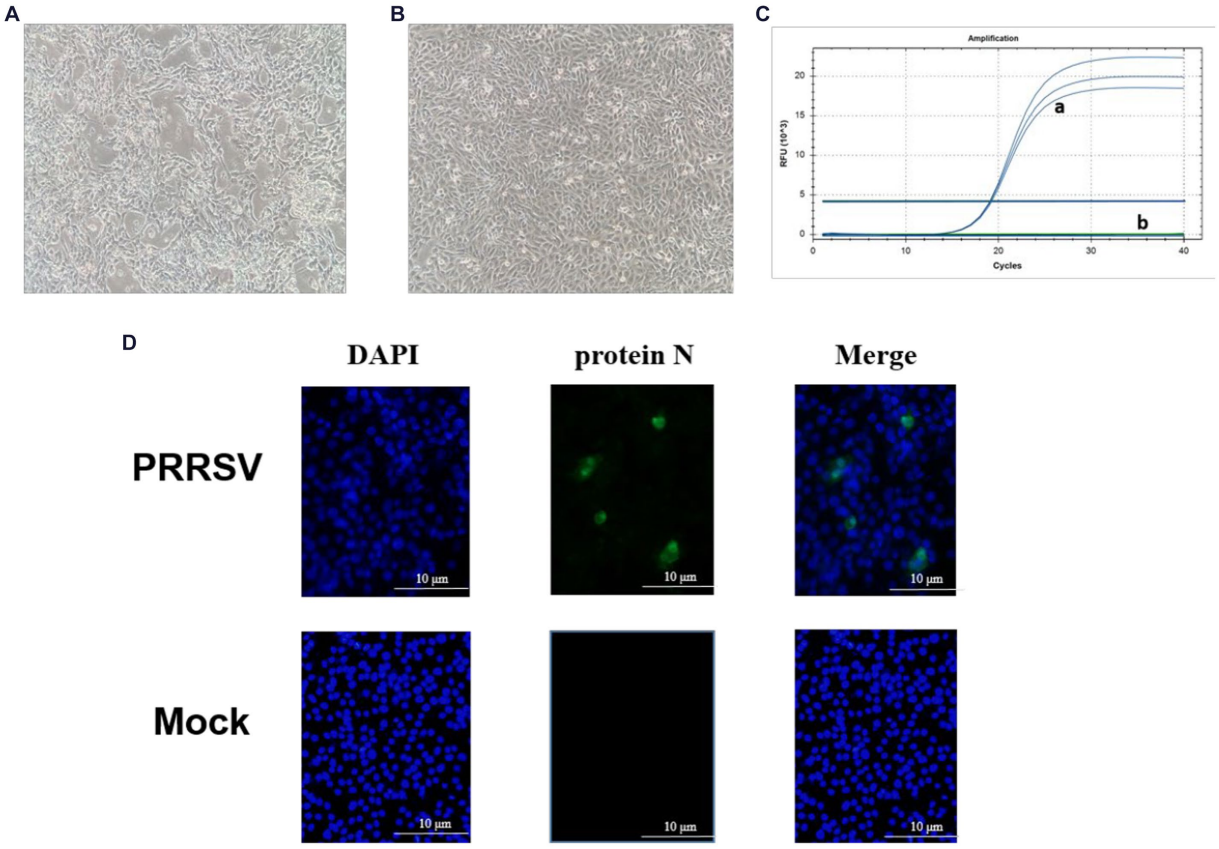

FIGURE 1
Isolation and Identification of the PRRSV isolate. **(A)** CPE diagram of Pams-163 infected with PRRSV isolate; **(B)** Blank control; **(C)** RT-qPCR results of the PRRSV isolate: (a) Amplification results of NADC30-like PRRSV (3 Replicates). (b) Amplification results for Highly Pathogenic-PRRSV, Classical PRRSV, NADC34-like PRRSV; **(D)** Results of indirect immunofluorescence assay.

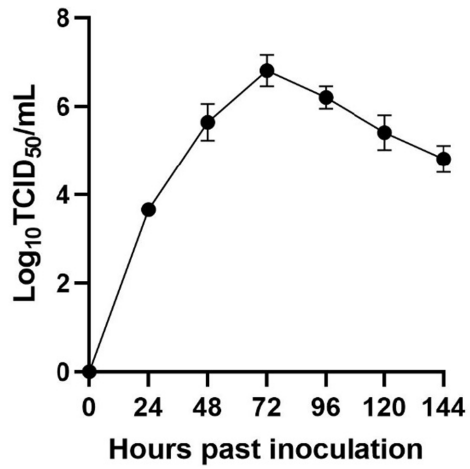

FIGURE 2
Viral multi-step growth curves.

SCCD22 sequencing results using CGView revealed a GC content of 52.64% (Figure 3). The ORF1a and ORF1b regions constitute 75% of the entire PRRSV genome and are translated into two polyproteins, pp1a and pp1ab. The ORF2, ORF2b, ORF3, ORF4, ORF5a, ORF5, ORF6, and ORF7 regions encode the envelope proteins (E, GP2, GP3, GP4, GP5a, GP5, and M protein) and the nucleocapsid protein (N protein), respectively.

3.4.2 Genetic evolution analysis of PRRSV SCCD22

To evaluate the genetic evolutionary relationships of PRRSV SCCD22 with reference strains from different lineages, we compared the nucleotide homology of SCCD22 with representative strains across various lineages (Table 2). The results indicated that SCCD22 shares a nucleotide identity ranging from 79.84 to 93.02% with strains CH-1a, JXA1, NADC30, NADC34, VR2332, and QYYZ, but only 58.60% with the LV strain, suggesting that SCCD22 belongs to PRRSV-2. Further comparative analysis revealed a close relationship between PRRSV SCCD22 and NADC30, with nucleotide and amino acid sequence identities in ORF1a, ORF1b, ORF3, ORF4, ORF5, ORF6, ORF7, and the 3' UTR ranging between 81.70–97.30% and 84.38–98.85%, respectively.

A phylogenetic tree was constructed based on the ORF5 gene sequences (Figure 4), revealing that aside from PRRSV-2 strains, the remaining strains could be divided into four lineages based on the ORF5 gene. SCCD22 was classified within Lineage 1.8, showing the closest phylogenetic relationship with the CH/SCYB-1/2018 isolate from Yibin, China.

Comparison of the NSP2 amino acid sequence of SCCD22 with representative strains indicated that SCCD22, compared to

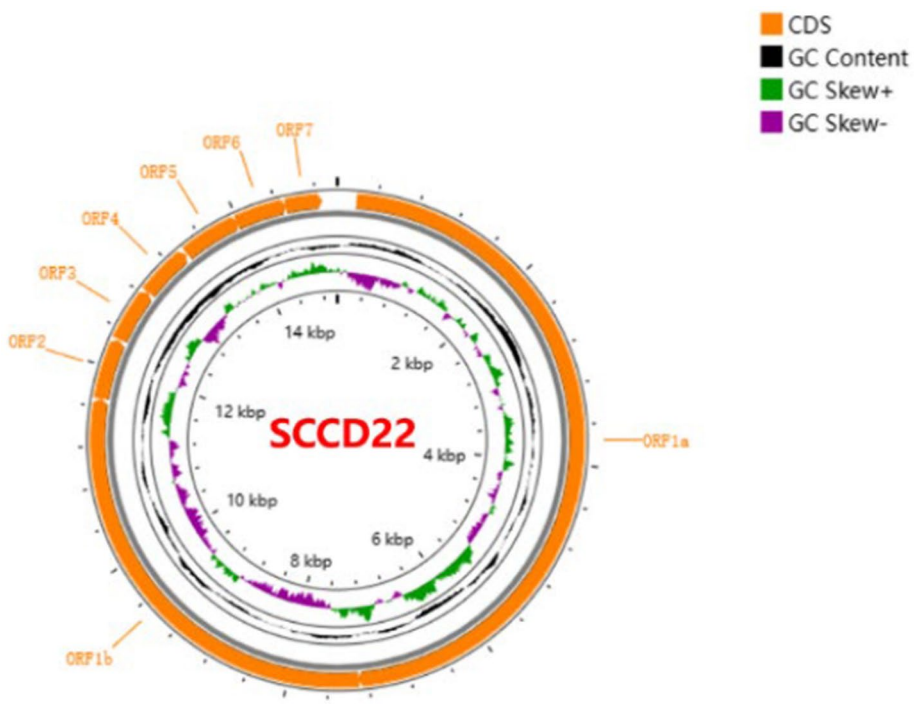

FIGURE 3
Whole genome sequencing and annotation of PRRSV SCCD22.

TABLE 2 Sequence comparison results (in percentages) between PRRSV SCCD22 and other reference strains.

	CH-1a		JXA1		LV		NADC30		NADC34		VR2332		QYYZ	
	nt	aa	nt	aa	nt	aa	nt	aa	nt	aa	nt	aa	nt	aa
Complete genome	83.02	–	82.75	–	58.60	–	93.02	–	84.49	–	81.91	–	79.84	–
5' UTR	94.24	–	95.79	–	52.91	–	93.19	–	92.63	–	92.11	–	92.15	–
ORF1a	78.71	77.83	78.98	78.94	53.21	45.78	91.11	89.33	79.88	80.07	78.81	78.63	74.23	74.34
ORF1b	75.51	82.77	74.40	82.67	54.42	58.30	81.70	84.38	76.91	83.12	75.67	82.50	73.55	81.95
ORF2	86.38	87.11	86.51	87.89	65.24	63.67	74.42	73.48	85.75	83.98	87.29	68.69	66.77	69.30
ORF3	84.05	82.28	83.79	81.89	63.17	56.39	94.38	94.88	85.74	84.65	83.92	84.65	82.48	83.64
ORF4	87.34	88.20	86.22	87.64	65.22	66.67	95.16	93.82	95.16	94.94	87.34	85.39	85.29	85.96
ORF5	86.73	85.50	85.74	85.50	59.22	50.99	92.21	92.50	87.56	90.00	85.74	85.50	83.91	83.50
ORF6	88.19	92.53	88.38	93.68	70.48	79.89	96.76	98.85	93.14	93.68	90.10	94.83	89.33	93.68
ORF7	91.40	92.68	90.32	91.06	60.86	57.25	95.43	98.37	95.70	97.56	92.47	95.12	87.63	91.87
3' UTR	88.08	–	75.84	–	50.91	–	97.30	–	94.04	–	55.41	–	81.63	–

the VR-2332 strain, exhibited three discontinuous deletions in NSP2 (111aa, 1aa, and 19aa) (Supplementary Figures S1A,B), aligning it with other NADC30-like strains.

Representative strains of different PRRSV lineages were selected to analyze ORF5 amino acid sequence variation. As shown in Figure 5, the results indicated that compared with the NADC30 strain, SCCD22 exhibits the greatest variation in the hypervariable region (HVR) 2, with a mutation in the 56-58aa NEH to QER. Additionally, a serine deletion was observed at position 33 in the hypervariable region 1 (HVR1).

3.4.3 Recombination analysis of PRRSV SCCD22

Recombination events were predicted using RDPv5.1 and supported by at least three assays. Sequence similarity plotting was also performed using SimPlot 3.5.1 within a sliding window of 200 bp. The results (Table 3 and Figure 6) indicate two recombination events in the isolate SCCD22. In the first event, with GZ106 (sublineage 8.7) and ISU18 (sublineage 1.5) as the major and minor parents respectively, SCCD22 demonstrated a high sequence similarity to GZ106 in the 1,028–3,290 nt region. This region included a portion of the NSP2 coding area, where all seven detection methods of RDP5

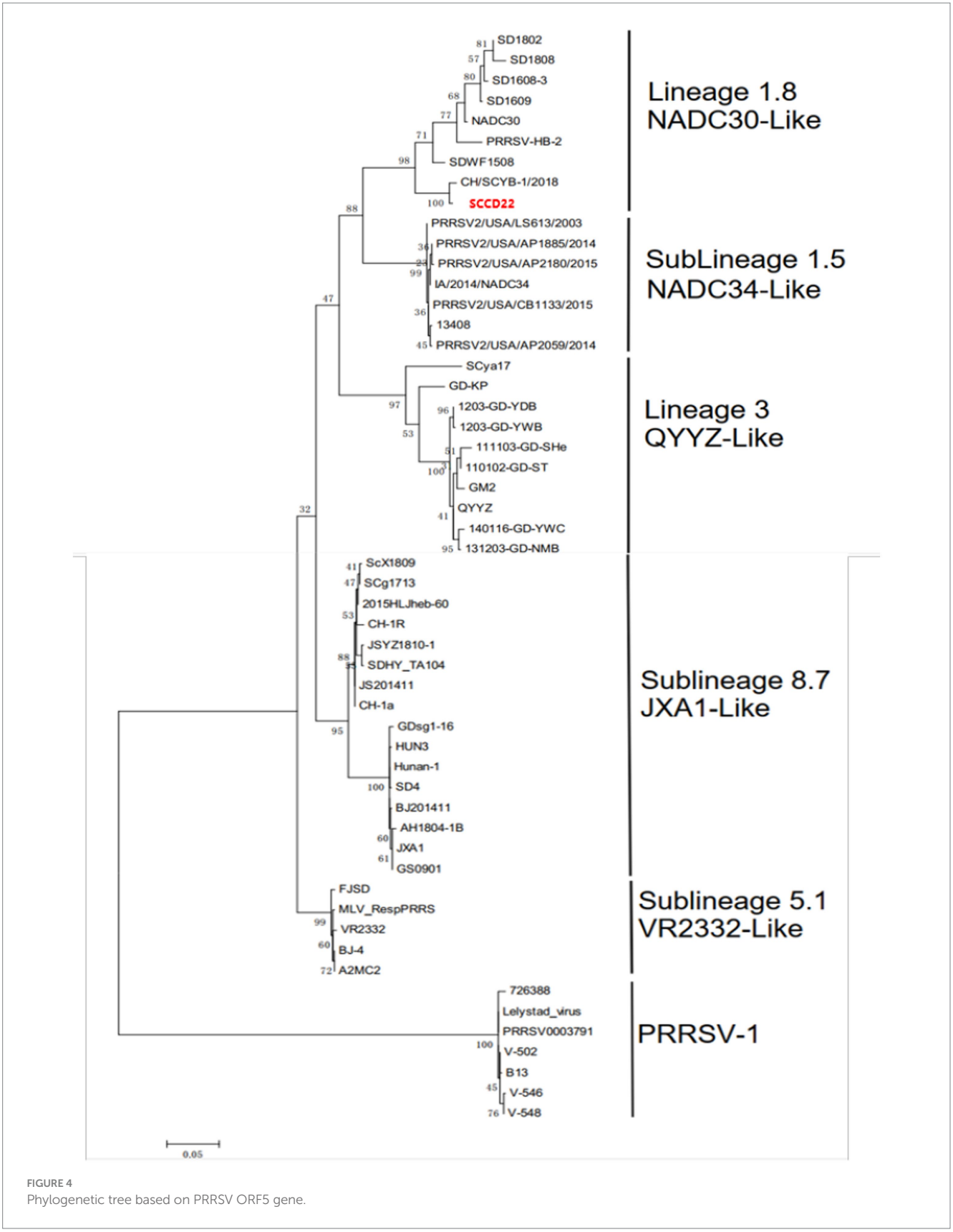

FIGURE 4
Phylogenetic tree based on PRRSV ORF5 gene.

identified significant *p* values. In the second event, with NADC30 (lineage 1.8) and CY2-1604 (lineage 1.8) as the major and minor parents, SCCD22 showed high similarity to CY2-1604 in the 9,985–12,279 nt region, which encompasses parts of the NSP10 to NSP12 coding areas, with all seven RDP5 detection methods again detecting *p* values.

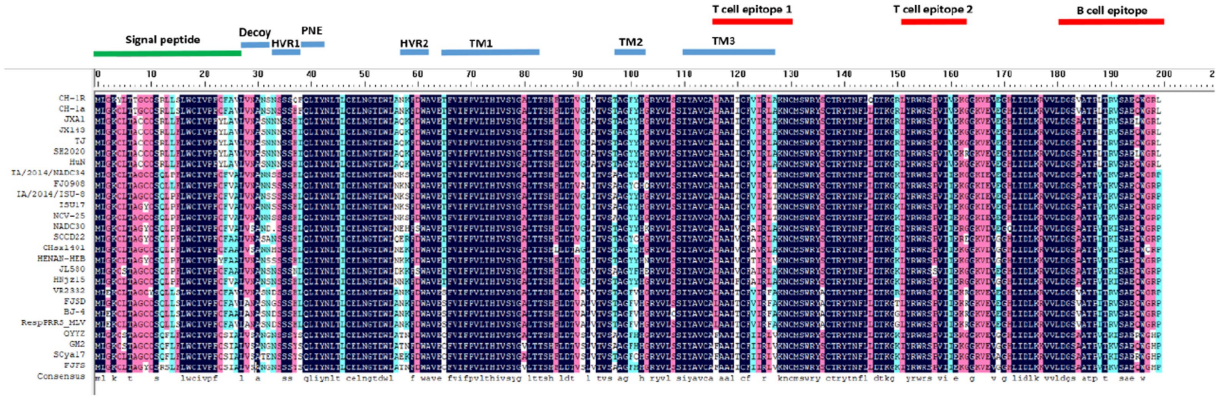

FIGURE 5
Comparison of ORF5 amino acid sequences among representative strains of PRRSV from different lineages.

3.5 Pathogenicity analysis of SCCD22

3.5.1 Changes in clinical symptoms of piglets

After inoculation, a significant increase in body temperature was observed in the piglets, commencing from day 1 (Figure 7A). The temperature peaked at 41.2°C on the fourth day. Starting from day 4, all piglets in the inoculated group experienced sustained fever for 8 days, with temperatures consistently above 40°C. After day 12, there was a noted decline in the body temperature of the inoculated piglets. In contrast, the control group piglets exhibited no abnormal temperature fluctuations throughout the experiment.

Body weight measurements were conducted on days 3, 7, and 14 post-inoculation (Figure 7B). In the initial 3 days following inoculation, the body weights of the control and challenge groups showed no significant differences. However, from day 7, the body weight of the challenge group was significantly lower than that of the control group ($p < 0.05$). By day 14, the average weight of the control group piglets was 2.544 Kg heavier than the challenge group. These findings indicate that the isolate SCCD22 is capable of inhibiting weight gain in piglets.

After the challenge, we meticulously tracked and recorded the clinical symptoms in piglets from each group (Figure 7C). The challenge group piglets exhibited increasingly severe symptoms over time. In contrast, the control group piglets displayed no significant clinical symptoms (Figure 7D). From day 3, the challenge group piglets began showing decreased appetite and intermittent, mild coughing. On day 7, these piglets started clustering together, with a notable reduction in appetite, and some exhibited symptoms such as coughing, lethargy, and disheveled fur. Individual piglets showed distinct symptoms, including redness around the ears and abdominal breathing. On day 14, the piglets in the challenge group were characterized by rapid breathing, unkempt fur, and minimal food intake. Among them, one piglet displayed particularly severe symptoms, including emaciation, cessation of feeding, and respiratory distress (Figure 7E).

3.5.2 Shedding of virus and changes in blood virus titers in piglets

The process of viral shedding in piglets and the changes in blood viral titers are shown in Figure 8. The serum viral load peaked on the fifth day post-infection at 3.65×10^5 copies/mL, subsequently stabilizing above 8.69×10^4 copies/mL until the end of the experiment (Figure 8A). Nasal swabs showed a peak viral concentration of 1.32×10^4 copies/mL on the seventh day post-infection, followed by a decline (Figure 8B). The viral titers in serum on days 7, 10, and 14 post-infection were $10^{-4.2}$, $10^{-4.4}$, and $10^{-4.8}$ $TCID_{50}$/mL, respectively, indicating a progressive intensification of viremia in piglets (Figure 8C).

3.5.3 Assessment of viral loads in organs post-dissection and pathological observations

In the control group, the piglets exhibited no visible lung abnormalities upon visual inspection (Figure 9A). Pathological section analysis revealed a normal lung structure with clear alveolar architecture. There were no signs of marked alveolar collapse or thickening of the alveolar walls, nor was there any congestion or expansion in the interstitial spaces or infiltration of inflammatory cells (Figure 9A).

In contrast, piglets in the challenge group predominantly displayed clear signs of pneumonia, characterized by either focal or diffuse distribution of lesions. The lesions varied in color from tan to dark purple, with some lung tissues undergoing consolidation and displaying a fish-scale pattern due to widened pulmonary interstitium (Figure 9B). Histopathological examination revealed an abnormal overall lung tissue structure. There was a significant increase in the width of the alveolar septa, resulting in substantial thickening, as indicated by yellow arrows. Additionally, conspicuous infiltration of inflammatory cells was observed, as indicated by black arrows (Figure 9B).

Viral loads in the spleen, lungs, thymus, and lung lymph nodes were quantified using RT-qPCR (Figure 9C). The highest viral concentration was observed in the lungs, followed by the lung lymph nodes and thymus, with the spleen registering the least viral presence. These results provide pivotal insights into the distribution and replication of the NADC30-like PRRSV recombinant strain in piglet organs, thereby advancing our understanding of its pathogenesis and transmission dynamics.

4 Discussion

Since its initial report in China in 2013, NADC30-like PRRSV has become widespread and shown an increasing annual clinical detection

10.3389/fmicb.2024.1362471

TABLE 3 Summary of crossover events in SCCD22 identified by RDP5.

Recombined virus	Major parent	Minor parent	Region of recombination	*P* values for the seven assays in RDP5						
				RDP	GENECONV	Bootscan	Maxchi	Chimaera	Siscan	3seq
SCCD22	GZ106	ISU18	1,028–3,290 nt	4.197×10^{-7}	1.888×10^{-7}	3.130×10^{-4}	8.222×10^{-14}	1.461×10^{-10}	9.976×10^{-20}	3.290×10^{-8}
	NADC 30	CY2-1604	9,985–12279 nt	2.026×10^{-21}	7.431×10^{-20}	4.308×10^{-15}	1.748×10^{-11}	5.262×10^{-10}	1.509×10^{-18}	6.367×10^{-9}

rate (Wang et al., 2017; Tu et al., 2023). Notable representative strains within China included HENAN-XINX (GenbankID: KF611905) and JL580 (GenbankID: KR706343). These strains exhibit a genomic homology of 86.7–87.8% with the U.S. isolate MN184A from 2001 (GenbankID: DQ176019), and 92.8–95.4% with the U.S. isolate NADC30 from 2008. Moreover, when compared with other strains like CH1a, jb-4, JXA1, and QYYZ, their homology varied between 82.2 and 87.2%. Similar to the U.S. isolates MN184A and NADC30, the Chinese NADC30-like strains also demonstrated the same NSP2 deletion pattern, including a discontinuous deletion of 131 amino acids (Zhao et al., 2015; Zhou L. et al., 2015; Li et al., 2016). The recurrence of this specific deletion across different geographic isolates may suggests its significance in the viral biology and pathogenesis, offering insights into potential targets for vaccine development and disease management strategies.

Several studies have demonstrated that recombination plays a pivotal role in the pathogenicity and genetic diversity of NADC30-like PRRSV in China. Notably, the virulence of these recombinant strains tends to be intermediate compared to their parental strains (Yu et al., 2021). Recombinant mutations observed in China's NADC30-like PRRSV strains have undermined the cross-protective efficacy of existing vaccines, thereby posing significant challenges to the control and prevention of PRRSV in the region. Over recent years, our team has focused on collecting a wide array of PRRSV clinical samples to investigate the prevalence of the virus. Previous studies have reported an annual increase in the prevalence of NADC30-like PRRSV, particularly in Sichuan Province, China (Tu et al., 2022, 2023; Jiang et al., 2023). In a notable development, we isolated a mutant PRRSV strain from a clinical sample collected in 2022. This strain was named SCCD22 and contained recombinant fragments. Full genome sequencing revealed that SCCD22 is 15,016 bp in length, with a 93.02% genomic identity to NADC30. An evolutionary tree constructed based on ORF5 was used to classify SCCD22 into lineage 1.8 (NADC30-like PRRSV). This discovery adds a new dimension to our understanding of the viral evolution and spread, highlighting the need for continued surveillance and research in this field.

The NSP2 is one of the most variable regions in the PRRSV genome and is frequently targeted for monitoring genetic mutations in PRRS. Compared with VR2332, HP-PRRSV exhibits a discontinuous deletion of 30 amino acids (1aa + 29aa) in the NSP2 coding region (Tian et al., 2007), while NADC30-like PRRSV shows a discontinuous deletion of 131 amino acids (111aa + 1aa + 19aa) (Brockmeier et al., 2012), and NADC34-like has a continuous deletion of 100 amino acids (Bao and Li, 2021). In our analysis of the NSP2 amino acid sequence of the SCCD22 strain, we observed three discontinuous deletions (111aa, 1aa, and 19aa) compared with VR2332. This deletion pattern aligns with that of the NADC30-like PRRSV. This pattern merits further investigation as a marker for PRRSV surveillance and as a target in recombinant strain vaccine design. Additionally, the analysis of the amino acid sequence derived from the ORF5 gene showed significant variations in SCCD22 compared with the NADC30 strain, with the most substantial variation in HVR2, where amino acids 56–58 NEH were mutated to QER; and a Serine was deleted at position 33 in HVR1. These mutations and deletions highlight the ongoing and complex variability of PRRSV strains. This continuous genetic evolution presents a persistent challenge to the development and efficacy of control measures in the swine industry, particularly in China. Our study

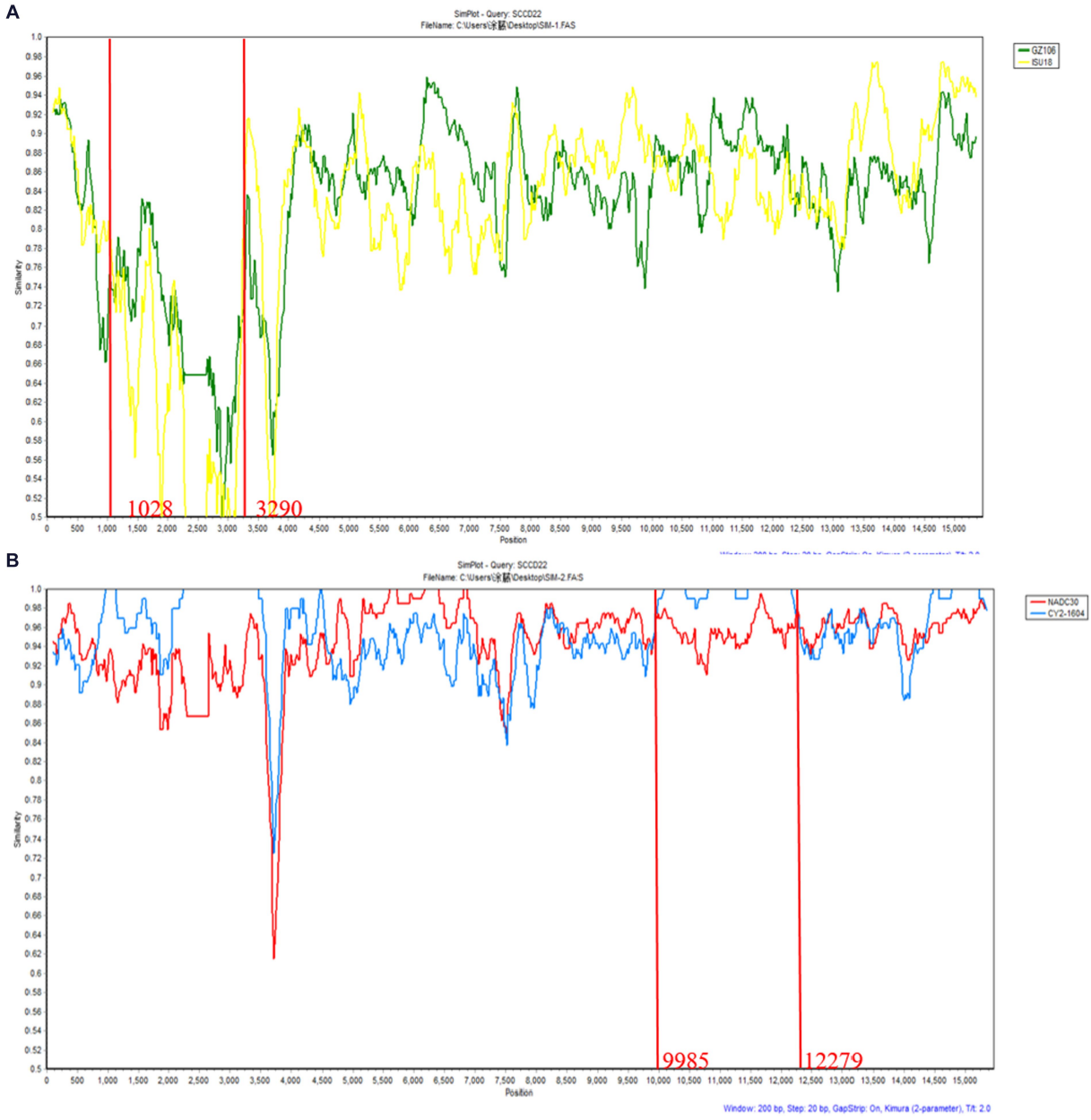

FIGURE 6
Genomic recombination analysis of SCCD22 using SimPlot. **(A)** GZ106 and ISU18were used as major and minor parents, respectively; **(B)** NADC30 and CY2-1604 were used as major and minor parents, respectively. Solid red lines indicate the recombination breakpoints; the locations are shown at the bottom.

identified novel amino acid deletions and mutations in the SCCD22 strain, which have not been previously reported in the literature. These genetic alterations are potentially crucial for understanding the dynamic evolution of the virus's pathogenicity. Furthermore, they could provide invaluable insights for the development of more effective vaccines and diagnostic methods, enhancing our ability to combat this evolving pathogenic threat.

Relative to other prevalent strains of PRRSV in China, the lineage 1.8, also known as NADC30-like PRRSV, demonstrates a heightened propensity for recombination and diverse pathogenicity. A review analyzing the pathogenicity of recombinant NADC30-like PRRSV prevalent in China indicated that the virulence of these domestic NADC30-like PRRSV is closely linked to their recombinant regions and the inherent virulence of the parental strains contributing to these segments (Yu et al., 2021). This study identified two notable recombination events in the SCCD22 isolate, specifically at 1028–3290 nt in the NSP2 and 9,985–12,279 nt in the NSP10 ~ 12. Concurrently, SCCD22 shows high similarity to GZ106 (sublineage 8.7) in the 1,028–3,290 nt, and to CY2-1604 (lineage 1.8) in the 9,985–12,279 nt, suggesting that the isolate SCCD22 may be a recombinant derivative of domestic NADC30-like (lineage 1.8) and JXA1-like (sublineage 8.7) strains. This intermingling of genetic traits from different lineages underscores the dynamic and complex nature of PRRSV evolution in China and highlights the continuous need for

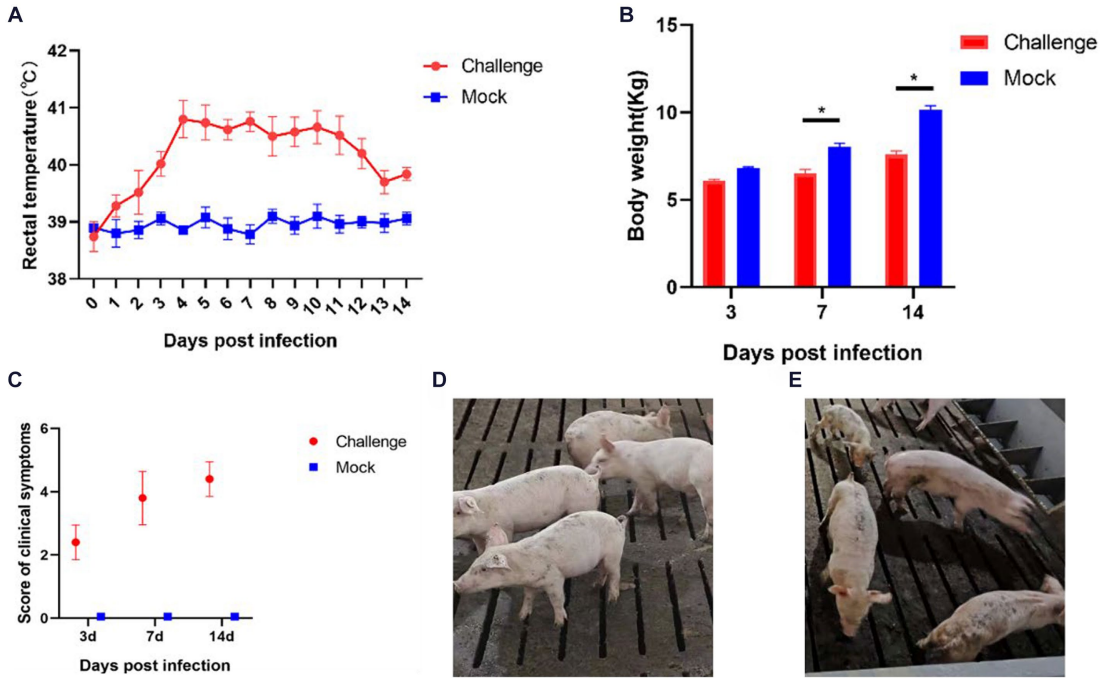

FIGURE 7
Clinical symptoms of the pathogenicity test in piglets. **(A)** Rectal temperature changes of piglets; **(B)** Body weight of piglets; **(C)** Clinical scores of piglets in each group during the whole experiment **(D)** Pigs in the Control group; **(E)** Pigs in the Challenge group. Significant differences are marked with asterisks, *$p < 0.05$.

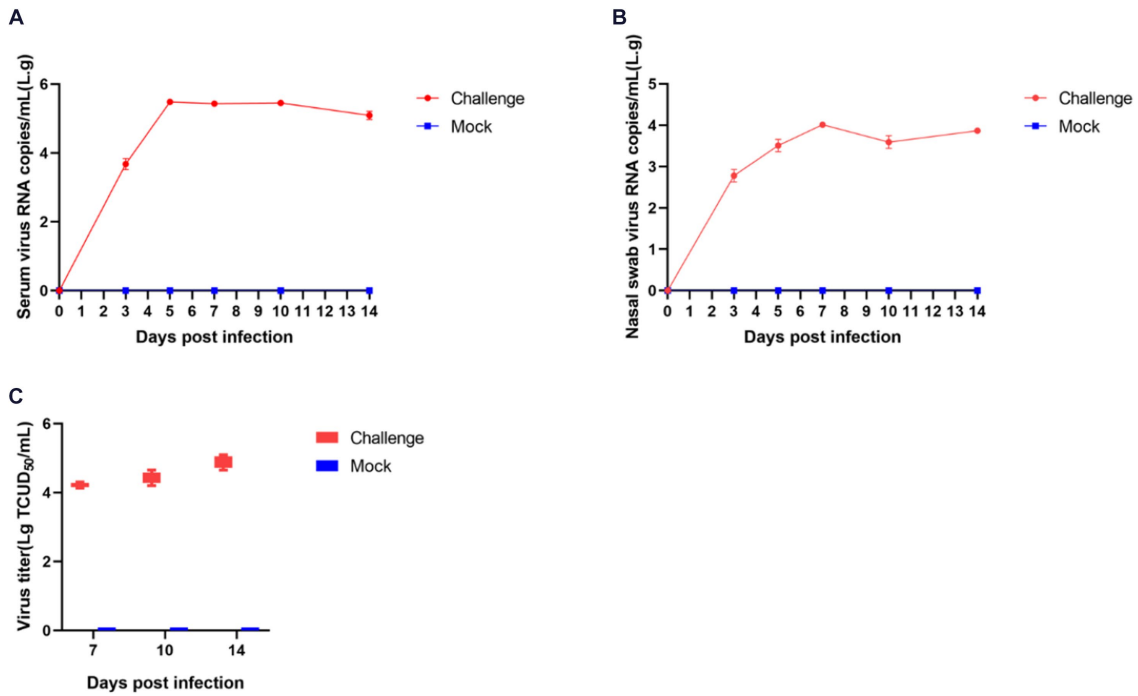

FIGURE 8
Shedding of virus and changes in blood virus titers in piglets after challenge. The amount of virus in serum **(A)** and nasal swabs **(B)**; Virus titers in the serum **(C)**.

vigilant monitoring and in-depth genomic analyses to effectively manage and control this virus. In addition, this underscores the necessity for broadened surveillance, encompassing multiple lineages, to prevent and manage recombinant strain emergence effectively. Our investigation led to the discovery of novel recombination events in the NADC30-like PRRSV strain that have been previously undocumented

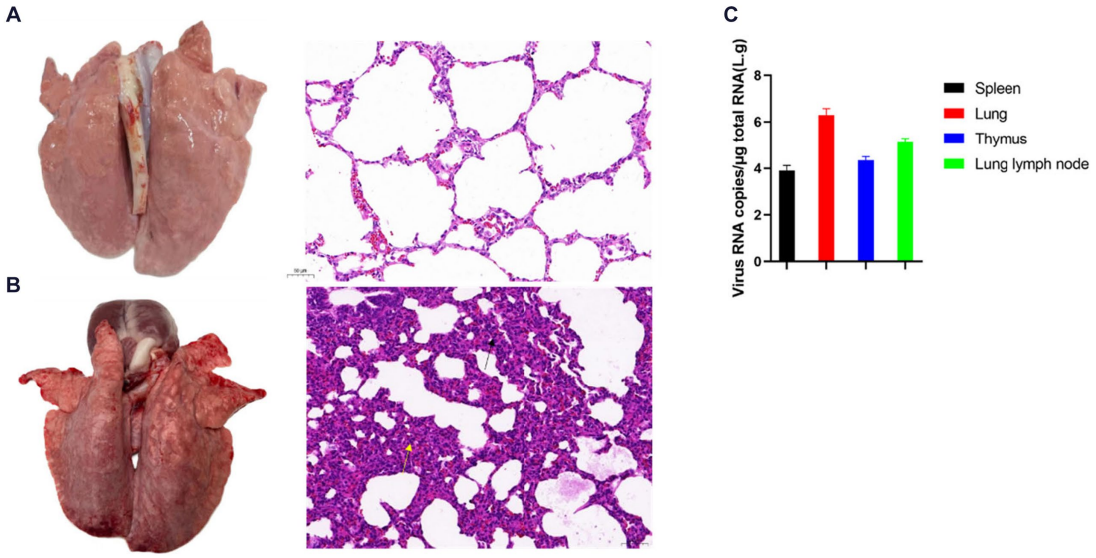

FIGURE 9
The pathological changes in the piglets' lungs and the results of viral load testing after SCCD22 challenge. **(A)** Lung and histopathological sections from the control group; **(B)** Lung and histopathological sections from the challenged group; **(C)** Results of viral load in the organs of piglets from the challenge group.

in the scientific literature. These unique recombination events are important for elucidating the evolution of viral pathogenicity.

We further investigated the pathogenicity of SCCD22 in piglets. Our findings indicated that piglets in the challenge group exhibited elevated body temperatures with prolonged fever, reduced appetite, and rough coat conditions. Despite these clinical manifestations, there was no mortality was observed in piglets throughout the duration of the challenge. However, it was evident that the SCCD22 had a significant impact on the overall growth performance and weight gain of the piglets. This observation suggests that, in the absence of secondary infections, SCCD22 may not be directly responsible for post-weaning mortality in piglets. This finding is particularly relevant for understanding the clinical impact of PRRSV strains. Necropsies and histopathological examinations revealed that infection with SCCD22 in piglets led to typical pulmonary pathological changes characteristic of PRRSV infection. These changes included discernible alterations in the lung tissues, reinforcing the understanding that the lungs are the primary target organ for PRRSV. Moreover, after challenge, the piglets' serum and nasal swabs showed prolonged viral shedding, and there was a gradual exacerbation of viremia. These findings underscore the persistence and potential for transmission of SCCD22, providing valuable insights into the pathogenic nature of this particular PRRSV variant. NSP2, a key component associated with viral packaging, manifests in various subtypes on the viral envelope and plays a pivotal role in the fusion process during the packaging of the Porcine Reproductive and Respiratory Syndrome Virus (PRRSV) (Zhao et al., 2018). NSP10, functioning as a helicase in PRRSV, is crucial for the unwinding of double-stranded RNA (dsRNA) and RNA synthesis during the virus's replication cycle, thus being indispensable for effective virus replication (Bautista et al., 2002). NSP11 exhibits RNA endoribonuclease activity and deubiquitinating functions (Nedialkova et al., 2009; Fang and Snijder, 2010; Wang et al., 2015), while NSP12 promotes viral replication (Wang et al., 2015; 2019; Bai et al., 2020). In the case of SCCD22, the identified recombination events involving NSP2 and NSP10-12 are likely to have significant implications for the packaging and replication processes of PRRSV. This understanding is a critical part of our ongoing research on the behavior and pathogenicity of the virus. Our future research will aim to conduct *in vivo*/vitro studies to determine how these recombination events affect the pathogenicity of NADC30-like PRRSV. Furthermore, by acknowledging the coexistence of multiple PRRSV lineages, our study focused on investigating the epidemiology of PRRSV. This includes closely monitoring of the viral potential for recombination and its pathogenicity in the aftermath of such genetic exchanges. These efforts are crucial for advancing our understanding of PRRSV and developing more effective strategies for its control and management. Additionally, our challenge experiment design faced certain limitations. In the control group, the use of RPMI 1640 medium to inoculate piglets was not the optimal approach. A suspension of uninfected Pams-163 cells would have been a more appropriate choice. However, the swine-feeding site is characterized by a lack of facilities suitable for cell culture and preservation. Moreover, the significant distance between our laboratory and the swine-feeding site introduced logistical complexity. This is particularly relevant because extended transportation can detrimentally affect the viability of Pams-163 cells. In our methodology, the RPMI 1640 medium was employed as the foundational medium for both the viral cultures and the Pams-163 cell cultures in the negative control group, aligned with our experimental design parameters. Given these considerations, and to maintain consistency and control within our experimental framework, we used the RPMI 1640 medium as a negative control.

In summary, we successfully isolated and reported a new strain of NADC30-like PRRSV, which we designated as SCCD22. Our research encompassed a thorough analysis of this strain, delving into its genetic evolution, conducting a detailed recombination analysis, and assessing its pathogenicity. The insights gained from this study lay a crucial theoretical foundation for future advancement in this field. These findings are important for guiding the development of vaccines that specifically target

NADC30-like PRRSV strains. Our research contributes valuable knowledge for broader efforts to control and prevent PRRSV infection. First, our findings can aid in the refinement of diagnostic assays. By incorporating newly identified genetic markers, these assays can become more sensitive and specific for detecting NADC30-like strains, enabling early detection and more effective management of outbreaks. Second, the unique genetic characteristics of the SCCD22 strain provide markers that can be used in molecular epidemiological studies. This can help track the spread and evolution of the virus, informing public health decisions and strategies for disease management. Third, understanding the specific mutations and recombination patterns in SCCD22 can guide the development of antiviral drugs that are more effective against these specific genetic profiles.

Data availability statement

The datasets presented in this study can be found in online repositories. The names of the repository/repositories and accession number(s) can be found in the article/Supplementary material.

Ethics statement

The animal study was approved by Sichuan Agricultural University Institutional Animal Care and Use Committee. The study was conducted in accordance with the local legislation and institutional requirements.

Author contributions

TT: Conceptualization, Writing – original draft, Writing – review & editing. YLi: Conceptualization, Writing – review & editing. GZ: Writing – review & editing, Methodology. CD: Formal analysis, Writing – review & editing. YZ: Formal analysis, Writing – review & editing. DJ: Software, Writing – review & editing. YLuo: Funding acquisition, Writing – review & editing. XY: Writing – review & editing. ZY: Writing – review & editing. MR: Writing – review & editing. YW: Conceptualization, Funding acquisition, Writing – review & editing.

Funding

The author(s) declare financial support was received for the research, authorship, and/or publication of this article. This project was supported by the Sichuan Province Science and Technology Planning Program (2021ZDZX0010 and 2021YFSY0005).

Conflict of interest

The authors declare that the research was conducted in the absence of any commercial or financial relationships that could be construed as a potential conflict of interest.

Publisher's note

All claims expressed in this article are solely those of the authors and do not necessarily represent those of their affiliated organizations, or those of the publisher, the editors and the reviewers. Any product that may be evaluated in this article, or claim that may be made by its manufacturer, is not guaranteed or endorsed by the publisher.

Supplementary material

The Supplementary material for this article can be found online at: https://www.frontiersin.org/articles/10.3389/fmicb.2024.1362471/full#supplementary-material

References

Adams, M. J., Lefkowitz, E. J., King, A. M. Q., Harrach, B., Harrison, R. L., Knowles, N. J., et al. (2016). Ratification vote on taxonomic proposals to the international committee on taxonomy of viruses (2016). *Arch. Virol.* 161, 2921–2949. doi: 10.1007/s00705-016-2977-6

Bai, Y., Li, L., Shan, T., Zhang, Y., Chen, X., Gao, F., et al. (2020). Proteasomal degradation of nonstructural protein 12 by RNF114 suppresses porcine reproductive and respiratory syndrome virus replication. *Vet. Microbiol.* 246:108746. doi: 10.1016/j.vetmic.2020.108746

Bao, H., and Li, X. (2021). Emergence and spread of NADC34-like PRRSV in China. *Transbound. Emerg. Dis.* 68, 3005–3008. doi: 10.1111/tbed.14316

Bautista, E. M., Faaberg, K. S., Mickelson, D., and McGruder, E. D. (2002). Functional properties of the predicted helicase of porcine reproductive and respiratory syndrome virus. *Virology* 298, 258–270. doi: 10.1006/viro.2002.1495

Brockmeier, S. L., Loving, C. L., Vorwald, A. C., Kehrli, M. E. Jr., Baker, R. B., Nicholson, T. L., et al. (2012). Genomic sequence and virulence comparison of four type 2 porcine reproductive and respiratory syndrome virus strains. *Virus Res.* 169, 212–221. doi: 10.1016/j.virusres.2012.07.030

Chai, Z. (2009). Establishment of a differential method of highly pathogenic strain and classical strain of PRRSV by SYBR green-I real-time PCR assay. *Chinese Acad. Agric. Sci.* Master Dissertation. Available at: https://kns.cnki.net/kcms2/article/abstract?v=l-44aStnccA0rYkiHg-T1494lCovwWk_gYWY2msMVR6-FpXns01hrukCZjIXuDvQlwP1rbC8W7QxcBxjetD_7otM7GElyZnGsB7n_xe-ngSeBGFq-qPs7VYPa_OvAXPPdHEArMtu-5pBhkHzbjtlQw==&uniplatform=NZKPT&language=CHS

Chang, H., Zheng, J., Qiu, Y., Chen, C., Li, Q., Wu, Q., et al. (2023). Isolation, identification, and pathogenicity of a NADC30-like porcine reproductive and respiratory disorder syndrome virus strain affecting sow production. *Front. Vet. Sci.* 10:1207189. doi: 10.3389/fvets.2023.1207189

Chen, N., Ye, M., Li, S., Huang, Y., Zhou, R., Yu, X., et al. (2018). Emergence of a novel highly pathogenic recombinant virus from three lineages of porcine reproductive and respiratory syndrome virus 2 in China 2017. *Transbound. Emerg. Dis.* 65, 1775–1785. doi: 10.1111/tbed.12952

Chen, N., Ye, M., Huang, Y., Li, S., Xiao, Y., Li, X., et al. (2019). Identification of Two Porcine Reproductive and Respiratory Syndrome Virus Variants Sharing High Genomic Homology but with Distinct Virulence. *Viruses.* 11:875. doi: 10.3390/v11090875

Fang, Y., and Snijder, E. J. (2010). The PRRSV replicase: exploring the multifunctionality of an intriguing set of nonstructural proteins. *Virus Res.* 154, 61–76. doi: 10.1016/j.virusres.2010.07.030

Feng, Z., Hongtao, C., Jun, Z., Lu, C., Xinwei, W., Hongying, L., et al. (2014). Identification and molecular epidemiology of porcine reproductive and respiratorsyndrome virus prevailing in Henan province from 2012 to 2013. *Chinese J. Vet. Sci.* 34, 1398–1410. doi: 10.16303/j.cnki.1005-4545.2014.09.002

Han, G., Lei, K., Xu, H., and He, F. (2020). Genetic characterization of a novel recombinant PRRSV2 from lineage 8, 1 and 3 in China with significant variation in replication efficiency and cytopathic effects. *Transbound. Emerg. Dis.* 67, 1574–1584. doi: 10.1111/tbed.13491

Han, G., Xu, H., Wang, K., and He, F. (2019). Emergence of two different recombinant PRRSV strains with low neutralizing antibody susceptibility in China. *Sci. Rep.* 9:2490. doi: 10.1038/s41598-019-39059-8

Jiang, D., Tu, T., Zhou, Y., Li, Y., Luo, Y., Yao, X., et al. (2023). Epidemiological investigation and pathogenicity of porcine reproductive and respiratory syndrome virus in Sichuan, China. *Front. Microbiol.* 14:1241354. doi: 10.3389/fmicb.2023.1241354

Kappes, M. A., and Faaberg, K. S. (2015). PRRSV structure, replication and recombination: origin of phenotype and genotype diversity. *Virology* 479-480, 475–486. doi: 10.1016/j.virol.2015.02.012

Li, Y., Xu, G., Du, X., Xu, L., Ma, Z., Li, Z., et al. (2021). Genomic characteristics and pathogenicity of a new recombinant strain of porcine reproductive and respiratory syndrome virus. *Arch. Virol.* 166, 389–402. doi: 10.1007/s00705-020-04917-8

Li, C., Zhuang, J., Wang, J., Han, L., Sun, Z., Xiao, Y., et al. (2016). Outbreak investigation of NADC30-like PRRSV in South-East China. *Transbound. Emerg. Dis.* 63, 474–479. doi: 10.1111/tbed.12530

Liu, Y., Li, J., Yang, J., Zeng, H., Guo, L., Ren, S., et al. (2018). Emergence of different recombinant porcine reproductive and respiratory syndrome viruses, China. *Sci. Rep.* 8:4118. doi: 10.1038/s41598-018-22494-4

Liu, J., Liu, C., Xu, Y., Yang, Y., Li, J., Dai, A., et al. (2022). Molecular characteristics and pathogenicity of a novel recombinant porcine reproductive and respiratory syndrome virus strain from NADC30-, NADC34-, and JXA1-like strains that emerged in China. *Microbiol. Spectr.* 10:e0266722. doi: 10.1128/spectrum.02667-22

Liu, J. K., Zhou, X., Zhai, J. Q., Li, B., Wei, C. H., Dai, A. L., et al. (2017). Emergence of a novel highly pathogenic porcine reproductive and respiratory syndrome virus in China. *Transbound. Emerg. Dis.* 64, 2059–2074. doi: 10.1111/tbed.12617

Lunney, J. K., Fang, Y., Ladinig, A., Chen, N., Li, Y., Rowland, B., et al. (2016). Porcine reproductive and respiratory syndrome virus (PRRSV): pathogenesis and interaction with the immune system. *Annu. Rev. Anim. Biosci.* 4, 129–154. doi: 10.1146/annurev-animal-022114-111025

Ma, X., Wang, P., Zhang, R., Zhao, Y., Wu, Y., Luo, C., et al. (2022). A NADC30-like PRRSV causes serious intestinal infections and tropism in piglets. *Vet. Microbiol.* 268:109397. doi: 10.1016/j.vetmic.2022.109397

Meng, X. J., Paul, P. S., Halbur, P. G., and Lum, M. A. (1995). Phylogenetic analyses of the putative M (ORF 6) and N (ORF 7) genes of porcine reproductive and respiratory syndrome virus (PRRSV): implication for the existence of two genotypes of PRRSV in the U.S.A. and Europe. *Arch. Virol.* 140, 745–755. doi: 10.1007/BF01309962

Nedialkova, D. D., Ulferts, R., van den Born, E., Lauber, C., Gorbalenya, A. E., Ziebuhr, J., et al. (2009). Biochemical characterization of arterivirus nonstructural protein 11 reveals the nidovirus-wide conservation of a replicative endoribonuclease. *J. Virol.* 83, 5671–5682. doi: 10.1128/JVI.00261-09

Qiu, W., Meng, K., Liu, Y., Zhang, Y., Wang, Z., Chen, Z., et al. (2020). Simultaneous detection of classical PRRSV, highly pathogenic PRRSV and NADC30-like PRRSV by TaqMan probe real-time PCR. *J. Virol. Methods* 282:113774. doi: 10.1016/j.jviromet.2019.113774

Shi, M., Lam, T. T., Hon, C. C., Hui, R. K., Faaberg, K. S., Wennblom, T., et al. (2010a). Molecular epidemiology of PRRSV: a phylogenetic perspective. *Virus Res.* 154, 7–17. doi: 10.1016/j.virusres.2010.08.014

Shi, M., Lam, T. T., Hon, C. C., Murtaugh, M. P., Davies, P. R., Hui, R. K., et al. (2010b). Phylogeny-based evolutionary, demographical, and geographical dissection of north American type 2 porcine reproductive and respiratory syndrome viruses. *J. Virol.* 84, 8700–8711. doi: 10.1128/JVI.02551-09

Sui, X., Guo, X., Jia, H., Wang, X., Lin, W., Li, M., et al. (2018). Genomic sequence and virulence of a novel NADC30-like porcine reproductive and respiratory syndrome virus isolate from the Hebei province of China. *Microb. Pathog.* 125, 349–360. doi: 10.1016/j.micpath.2018.08.048

Tian, K., Yu, X., Zhao, T., Feng, Y., Cao, Z., Wang, C., et al. (2007). Emergence of fatal PRRSV variants: unparalleled outbreaks of atypical PRRS in China and molecular dissection of the unique hallmark. *PLoS One* 2:e526. doi: 10.1371/journal.pone.0000526

Tu, T., Pang, M., Jiang, D., Zhou, Y., Wu, X., Yao, X., et al. (2023). Development of a real-time TaqMan RT-PCR assay for the detection of NADC34-like porcine reproductive and respiratory syndrome virus. *Vet. Sci.* 10:279. doi: 10.3390/vetsci10040279

Tu, T., Wang, Y., Liao, C. Y., Zhang, P. F., Xiang, M. Y., Yang, Z. X., et al. (2022). Isolation and bioinformatics analysis of the NADC30_Like CJS01 strain of the porcine reproductive and respiratory syndrome virus. *Vet. Ital.* 58, 47–55. doi: 10.12834/VetIt.2182.14564.1

Wang, D., Fan, J., Fang, L., Luo, R., Ouyang, H., Ouyang, C., et al. (2015). The nonstructural protein 11 of porcine reproductive and respiratory syndrome virus inhibits NF-κB signaling by means of its deubiquitinating activity. *Mol. Immunol.* 68, 357–366. doi: 10.1016/j.molimm.2015.08.011

Wang, T. Y., Fang, Q. Q., Cong, F., Liu, Y. G., Wang, H. M., Zhang, H. L., et al. (2019). The Nsp12-coding region of type 2 PRRSV is required for viral subgenomic mRNA synthesis. *Emerg. Microbes Infect.* 8, 1501–1510. doi: 10.1080/22221751.2019.1679010

Wang, L. J., Xie, W., Chen, X. X., Qiao, S., Zhao, M., Gu, Y., et al. (2017). Molecular epidemiology of porcine reproductive and respiratory syndrome virus in Central China since 2014: the prevalence of NADC30-like PRRSVs. *Microb. Pathog.* 109, 20–28. doi: 10.1016/j.micpath.2017.05.021

Wu, Y., Peng, O., Xu, Q., Li, Q., Li, W., Lin, L., et al. (2022). Characterization and pathogenicity of two novel PRRSVs recombined by NADC30-like and NADC34-like strains in China. *Viruses* 14:2174. doi: 10.3390/v14102174

Yu, Y., Zhang, Q., Cao, Z., Tang, Y. D., Xia, D., Wang, G., et al. (2021). Recent advances in porcine reproductive and respiratory syndrome virus NADC30-like research in China: molecular characterization, pathogenicity, and control. *Front. Microbiol.* 12:791313. doi: 10.3389/fmicb.2021.791313

Yun, Z., Zhixiong, L., Ru, C., and Changbao, L. (1998). Molecular cloning and identification of the ORF7gene of Chinese isolates B13 of porcine reproductive and respiratory syndrome virus. *Chinese J. Vet. Med.* 24, 3–5.

Zhang, Q., Jiang, P., Song, Z., Lv, L., Li, L., and Bai, J. (2016). Pathogenicity and antigenicity of a novel NADC30-like strain of porcine reproductive and respiratory syndrome virus emerged in China. *Vet. Microbiol.* 197, 93–101. doi: 10.1016/j.vetmic.2016.11.010

Zhang, H., Leng, C., Ding, Y., Zhai, H., Li, Z., Xiang, L., et al. (2019). Characterization of newly emerged NADC30-like strains of porcine reproductive and respiratory syndrome virus in China. *Arch. Virol.* 164, 401–411. doi: 10.1007/s00705-018-4080-7

Zhao, K., Ye, C., Chang, X. B., Jiang, C. G., Wang, S. J., Cai, X. H., et al. (2015). Importation and recombination are responsible for the latest emergence of highly pathogenic porcine reproductive and respiratory syndrome virus in China. *J. Virol.* 89, 10712–10716. doi: 10.1128/JVI.01446-15

Zhao, J., Zhiwen, X., and Ling, Z. (2018). Research advances in non-structural protein 2 of porcine reproductive and respiratory syndrome virus. *Acta Agric. Zhejiangensis* 30, 350–356. doi: 10.3969/j.issn.1004-1524.2018.02.23

Zhou, F., Zhao, J., Chen, L., Chang, H., Li, Y., Liu, H., et al. (2015). Complete genome sequence of a novel porcine reproductive and respiratory syndrome virus that emerged in china. *Genome Announc.* 3, e00702–e00715. doi: 10.1128/genomeA.00702-15

Zhou, L., Wang, Z., Ding, Y., Ge, X., Guo, X., and Yang, H. (2015). NADC30-like strain of porcine reproductive and respiratory syndrome virus, China. *Emerg. Infect. Dis.* 21, 2256–2257. doi: 10.3201/eid2112.150360

frontiers | Frontiers in Microbiology

TYPE Original Research
PUBLISHED 10 May 2024
DOI 10.3389/fmicb.2024.1359970

OPEN ACCESS

EDITED BY
Taofeng Du,
Northwest A&F University, China

REVIEWED BY
Andrew Robert Kick,
United States Military Academy West Point, United States
Tor Gjøen,
University of Oslo, Norway

*CORRESPONDENCE
Jianchao Wei
✉ jianchaowei@shvri.ac.cn
Zhiyong Ma
✉ zhiyongma@shvri.ac.cn

†These authors have contributed equally to this work

RECEIVED 22 December 2023
ACCEPTED 22 April 2024
PUBLISHED 10 May 2024

CITATION
Lin Y, Zhou L, Xiao C, Li Z, Liu K, Li B, Shao D, Qiu Y, Ma Z and Wei J (2024) Development and biological characterization of an infectious cDNA clone of NADC34-like PRRSV.
Front. Microbiol. 15:1359970.
doi: 10.3389/fmicb.2024.1359970

Development and biological characterization of an infectious cDNA clone of NADC34-like PRRSV

Yafang Lin†, Lujia Zhou†, Changguang Xiao, Zongjie Li, Ke Liu, Beibei Li, Donghua Shao, Yafeng Qiu, Zhiyong Ma* and Jianchao Wei*

Shanghai Veterinary Research Institute, Chinese Academy of Agricultural Sciences, Shanghai, China

Introduction: Porcine Reproductive and Respiratory Syndrome virus (PRRSV) causes high abortion rates in gestating sows and stillbirths, as well as high piglet mortality, seriously jeopardizing the pig industry in China and worldwide.

Methods: In this study, an infectious clone containing the full-length genome of NADC34-like PRRSV was constructed for the first time using reverse genetic techniques. The gene was amplified segmentally onto a plasmid, transfected into BHK-21 cells, and the transfected supernatant was harvested and transfected into PAM cells, which showed classical cytopathic effects (CPE).

Results: The virus rJS-KS/2021 was successfully rescued which could be demonstrated by Western Blot and indirect immunofluorescence assays. Its growth curve was similar to the original strain. Replace the 5′UTR and 3′UTR of rJS-KS/2021 with 5′UTR and 3′UTR of HP-PRRSV (strain SH1) also failed to propagate on MARC-145.

Discussion: In this study, an infectious clone of NADC34-like was constructed by reverse genetics, replacing the UTR and changing the cellular tropism of the virus. These findings provide a solid foundation for studying the recombination of different PRRSVs and the adaption of PRRSVs on MARC-145 in the future.

KEYWORDS

porcine reproductive and respiratory syndrome virus, NADC34-like, infectious clones, biological characteristics, recombinant virus

1 Introduction

Porcine reproductive and respiratory syndrome (PRRS) is an acute infectious ailment primarily recognized by clinical manifestations such as late abortion, stillbirth, respiratory distress (interstitial pneumonia), and high mortality rates among pigs, particularly piglets in affected sows (An et al., 2020). This virus causes persistent infections characterized by prolonged viremia, escalated macrophage phagocytosis, and dependence on antibody response (Ouyang et al., 2019). PRRSV is an enveloped and single positive-stranded RNA virus classifying in the family *Arteriviridae*, together with Equine Arteritis Virus, Lactate Dehydrogenase Elevating Virus and Simian Hemorrhagic Fever Virus (Tian, 2017). With an approximate genome length of 15 kilobases (kb), it comprises a minimum of 10 open reading frames (ORFs) and flanking untranslated regions at the 5′ and 3′ ends of the

genome (Shanmukhappa and Kapil, 2001; Sun et al., 2018). Secondary structures in the 5'UTR and 3'UTR of PRRSV have important effects on PRRSV replication and transcription (Wootton et al., 2000). ORF1a and ORF1b encode a minimum of 16 non-structural proteins (Nsps) linked to replication. ORF2a, ORF2b, ORF3–5, ORF5a, ORF6, and ORF7 encode eight viral structural proteins (Pujhari and Zakhartchouk., 2016; Liu et al., 2019). Notably, ORF5 has been extensively used in molecular epidemiologic research, as well as for the classification of PRRSV field strains due to its marked genetic variation (Larochelle et al., 2003; Zhu et al., 2021; Yim-Im et al., 2023). Owing to this genetic divergence, PRRSV was divided into two primary genotypes—genotypes 1 and 2, recognized as the European type and the North American type, respectively (Bálint et al., 2021; Wang et al., 2021). Although the clinical symptoms and onset time of these two genotypes are similar, the genome sequences of these two genotypes are only 60% homologous (Li et al., 2022).

PRRSV was first isolated in North America in 1987 and subsequently in the Netherlands, exerting a significant impact on the global swine industry for nearly four decades (Zhao et al., 2018; Wu et al., 2022). Recently, NADC34-like PRRSV has been reported in the United States, China, and Peru and is agreed to be the cause of a large number of clinical abortions (Trevisan et al., 2021; Zhao H. Z. et al., 2022). The pathogenicity of NADC34-like PRRSV in piglets within the United States exhibits a significant degree of variability (Xu et al., 2020). A strain belonging to sublineage 1.5 named NADC34 appear in the United States in 2014 (Kim et al., 2022), which resulting in mass abortion of sows and high mortality of piglets (Xu et al., 2023). It is worth noting that the Nsp2 (non-structural protein 2) gene of the NADC34 strain carries a sustained deletion spanning 100 amino acids (Zhenhua et al., 2018; Xie et al., 2021). The continuous introduction of foreign breeding pigs has led to the recombination of new strains with locally prevalent strains, promoting the diversity of PRRSV (Zhang et al., 2018; Tu et al., 2023). Currently, NADC34-like strains in China account for 11.5 and 28.6% of positives in 2020 and 2021, respectively, demonstrating their pervasive dissemination across at least nine provinces, including Liaoning, Heilongjiang, Fujian, Henan, Sichuan, Jiangsu, Jilin, Hebei, and Shandong (Yuan et al., 2022; Zhao J. et al., 2022). Those indicate the prevalence of NADC34-like PRRSV in China. Intriguingly, The NADC34-like PRRSV strains in Sichuan have different molecular genetic characteristics from other NADC34-like PRRSV strains in China (Xu H. et al., 2022), displaying divergent patterns of amino acid deletion beyond the previously noted 100-amino acid deletion in Nsp2 (Zhang H. et al., 2023). This intricacy contributes to the increased complexity of NADC34-like PRRSV in its native environment (van Geelen et al., 2018). Apart from the documented recombination events, the pathogenicity of NADC34-like PRRSV in the Chinese setting remains elusive. The NADC34-like variant, characterized by substantial mutational alterations, significantly reduced homology, and complex recombination with native Chinese strains, displays a nuanced and intricate landscape for further research (Zhou et al., 2023). Chinese NADC34-like PRRSV exhibits a complex recombination pattern, but as of 2019, it has not recombined with native Chinese strains (Zhao J. et al., 2022). Since 2020, recombination events between NADC34-like viruses and native strains of other lineages have occurred in China. NADC34-like strains have undergone rapid mutations in the Nsp2 region (Xue et al., 2021; Xia et al., 2023). An intricate deletion pattern in the Nsp2 region further distinguishes Chinese NADC34-like strains.

In modern virology, reverse genetic technology is an important tool for the study of RNA viruses, which can produce the genome of the virus from cDNA, and replicate and transcribe it. Technological advancements in PRRSV genome manipulation via reverse genetics have enabled the precise introduction of mutations and deletions in particular genomic areas (Chae et al., 2023). In 1998, the reverse genetic platform of PRRSV-I classical LV strain has been successfully constructed. The full-length LV strain genome was inserted into the pOK12 vector, containing the T7 promoter, as part of the construction strategy. This construction was further transfected into baby hamster kidney-21 (BHK-21) cells. Subsequently, transfected supernatant was harvested and inoculated into MARC-145 cells, resulting in typical cytopathic effects (CPE) following several generations of culture (Meulenberg, 2000). Currently, this system has been widely used in viral genome replication and transcription, virulence, target cell infection, pathogenesis, and immune response, opening up new avenues for molecular research on PRRSV. Several studies have reported that a number of reverse genetic platforms of PRRSV-2 strains have been successfully constructed, including VR-2332, HuN4-F112, and JXwn06 (Zhengda et al., 2022).

In order to further understand the growth characteristics of the virulent strains as well as the pathogenic mechanism, we constructed an infectious clone of NADC34-like PRRSV by reverse genetics to provide a platform for the subsequent study of the vaccine.

2 Materials and methods

2.1 Cells, strains, and vectors

The MARC-145 and BHK-21 cells were cultured in Dulbecco's Modified Eagle Medium (DMEM) supplemented with 10% fetal bovine serum (FBS) and antibiotics. Porcine alveolar macrophages (PAMs), the primary target cell for PRRSV, were prepared from lung lavage of specific pathogen-free piglets. PAMs were maintained in Roswell Park Memorial Institute 1,640 medium (RPMI-1640, Gibco, ThermoFisher Scientific, Waltham, MA, United States) supplemented with 10% FBS and antibiotics. The PRRSV isolates [JS-KS/2021 (Zhou et al., 2022)] and the pACYC177 vector were stored at-80°C.

2.2 Construction of a full-length cDNA clone

The total RNA from the supernatants of PAM cells at 72 h post-infection (hpi) was used by AG RNAex Pro Reagent (Accurate Biology, Hangzhou, China). The cDNA was synthesized using a M-MLV(H-) Reverse Transcriptase. Specific primer pairs (Table 1) were designed based on the whole genome length to amplify five fragments covering the entire JS-KS/2021 strain genome using a 2× Hieff polymerase chain reaction (PCR) Master Mix (Yeasen Biotechnology, Shanghai, China). The amplification method was performed per the manufacturer's instructions, and the PCR-amplified fragments were

TABLE 1 Primers used in this study.

Primer name	Primer sequence (5′-3′)	Location	Length
JS-KS/2021-P1F	ATTTGCGGCCGCATGACGTATAGGTGTTGGCTCTATGCCACGACATTTGTATTGTCGGGAGCTGTGAC	1–41	1
JS-KS/2021-P1R	GTATTTCTCCTTTACCTCTCGGAGGTGCCC	2,945–2,975	
JS-KS/2021-P2F	GGGCACCTCCGAGAGGTAAAGGAGAAATAC	2,945–2,975	2
JS-KS/2021-P2R	TCTCCACAGGAGAAAAAACACACAAAGAAG	5,906–5,936	
JS-KS/2021-P3F	CTTCTTTGTGTGTTTTTTCTCCTGTGGAGA	5,906–5,936	3
JS-KS/2021-P3R	ATCAGGGGCTGGACCTTAAGCATGTCCTCAA	8,829–8,859	
JS-KS/2021-P4F	TTGAGGACATGCTTAAGGTCCAGCCCCTGAT	8,829–8,859	4
JS-KS/2021-P4R	TCTGTCGCGCACGAAACGCGTCATTGTAAT	11,612–11,642	
JS-KS/2021-P5F	ATTACAATGACGCGTTTCGTGCGCGACAGA	11,612–11,642	5
JS-KS/2021-P5R	GAAGGGCTAATGACGCCGGCGAACTTGTTTATTGCAG	14,910–14,940	
SH1-5'UTR-F	ATGACGTATAGGTGTTGGC	1–19	5'UTR
SH1-5'UTR-R	GGTTAAAGGGGTGGAGAGACCG	168–189	
SH1-3'UTR-F	TGGGCTGGCATTCTTTGGCACC	15,171–15,193	3'UTR
SH1-3'UTR-R	AATTACGGCCGCATGGTTC	15,107–15,226	

gel-purified. Further, four fragments of the viral genome were fused to produce two new fragments by two-step fusion PCR. Following double digestion of the pACYC177 vector with the appropriate restriction enzymes, the three fragments of the viral genome were inserted into the pACYC177 vector using a homologous recombination kit following the instructions. The scheme used for the construction of a full-length cDNA clone of the JS-KS/2021 strain is indicated in Figure 1A. On the pACYC177 vector, the cytomegalovirus (CMV) promoter was added before the target fragment insertion position, and hepatitis delta virus ribozyme (HDVRz) was added at a subsequent position using primers. Eventually, the completely assembled full-length cDNA clone was sequenced to verify its accuracy and integrity.

2.3 Construction of recombinant strains with 5'UTR and 3'UTR substitutions

Replace the 5'UTR and 3'UTR of rJS-KS/2021 with 5'UTR and 3'UTR of HP-PRRSV (strain SH1). The 5'UTR and 3'UTR fragments of HP-PRRSV SH1 were amplified by PCR (Figure 1C). The plasmid of the infectious clone constructed was named pJS-KS/2021–53. The scheme of construction could be seen in Figure 1E.

2.4 Virus rescue

BHK-21 cells at ~80% confluence in a 24-well culture plate were transfected with 1 μg of a full-length cDNA clone using TurboFect™ transfection reagent (ThermoFisher Scientific, Waltham, MA, United States) according to the manufacturer's instructions. At 24 h post-transfection (hpt), culture supernatant was harvested to infect PAMs seeded in a 24-well culture plate 1 days ahead. CPE were monitored daily to identify the successful rescue of the virus. Around 4 days post-infection (dpi), the culture supernatant was harvested as F1 virus and stored at-80°C.

2.5 Viral growth curve

The confluent PAMs cells in a 24-well culture plate were inoculated with JS-KS/2021, rJS-KS/2021 and rJS-KS/2021–53 at a multiplicity of infection (MOI) of 0. 1. Cells were incubated with virus supernatant diluted with RPMI-1640 for 2 h, then washed twice with 1 × PBS, and cultured with 500 μL RPMI-1640 supplemented with 2% FBS. Virus supernatants were harvested at 0, 12, 24, 36, 48, 60, 72, 84 and 96 hpi for virus titration by $TCID_{50}$. The viral growth curves were created with GraphPad Prism 8.

2.6 Indirect immunofluorescence assay

BHK-21 cells were infected with PRRSV at a multiplicity of infection (MOI) of 0.1 and subjected to immunofluorescence assays at 48 hpi. The cells were fixed with 4% paraformaldehyde at room temperature for 30 min and blocked with 5% bovine serum albumin at room temperature for 1 h. For the detection of N protein expression, cells were incubated with an anti-N monoclonal antibody (Lu et al., 2020) at 37°C for 1 h. After three washes, the cell monolayers were stained with FITC-labeled goat anti-mouse IgG. Cell nuclei were counterstained with 4′,6-diamidino-2-phenylindole (DAPI) solution (Solarbio Life Sciences, Beijing, China) for 5 min at room temperature. After extensive washes with 1 × PBS, fluorescent images were captured with epifluorescence microscope.

2.7 Western blot

Cellular specimens were harvested and lysed using radioimmunoprecipitation assay buffer comprising 50 mM Tris, pH 7.2, 150 mM NaCl, 1% sodium deoxycholate, and 1% Triton X-100. Following lysate preparation, protein samples were separated on 12% sodium dodecyl sulphate-polyacrylamide gel electrophoresis (SDS-PAGE) gels and were subsequently transferred onto nitrocellulose

10.3389/fmicb.2024.1359970

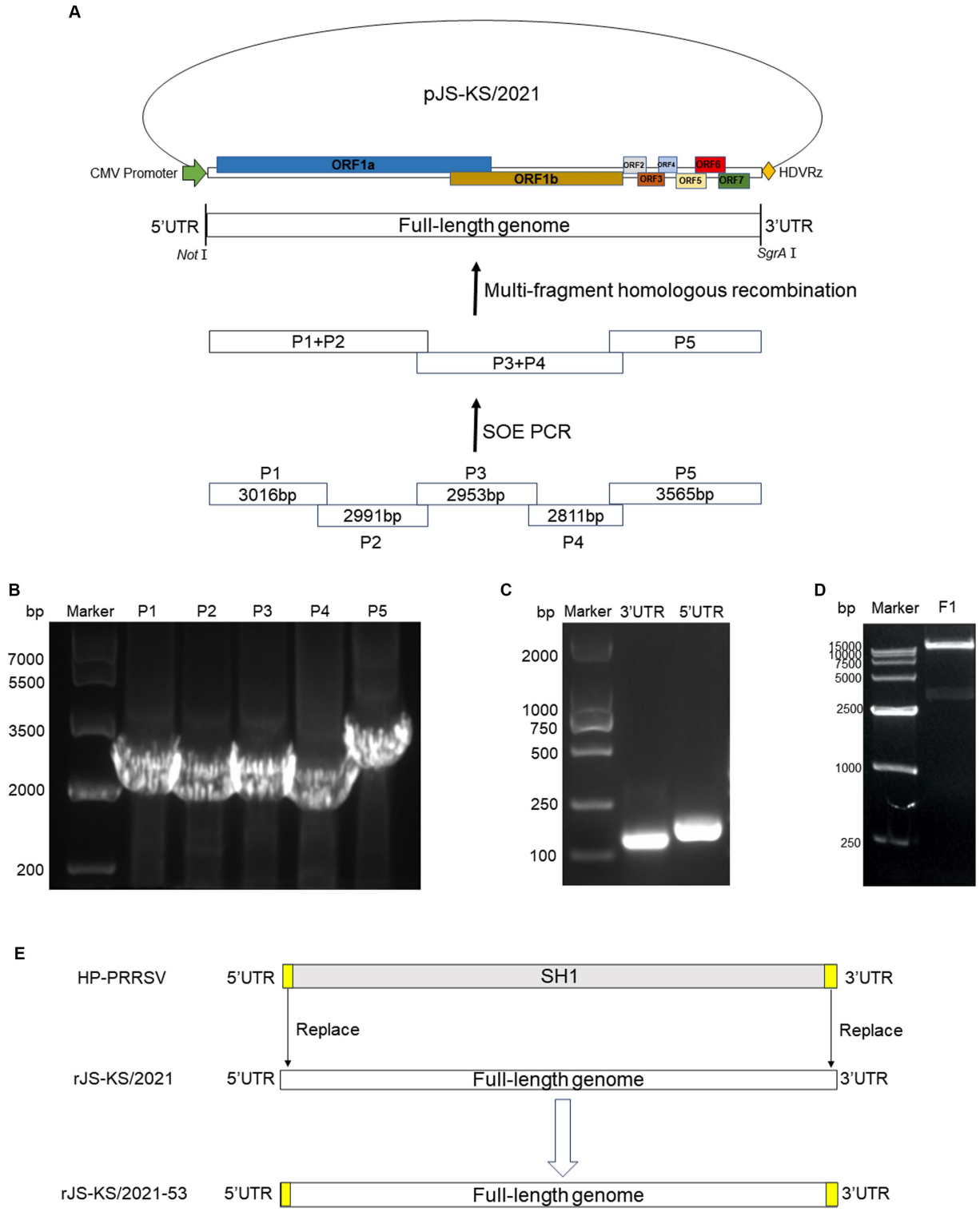

FIGURE 1
Strategy to construct the full-length cDNA clone of NADC34-Like PRRSV JS-KS/2021 strain. **(A)** Scheme of the NADC34-like PRRSV JS-KS/2021 genome and assembly strategy. The NADC34-like PRRSV JS-KS/2021 genome was divided into five fragments and synthesized. CMV: cytomegalovirus promoter; HDVRz: hepatitis delta virus ribozyme. **(B)** Gel analysis of the five purified cDNA fragments. The P1-P5 fragments were obtained by polymerase chain reaction (PCR) amplification and gel purification. **(C)** The 5'UTR (189bp) and 3'UTR (155bp) of HP-PRRSV SH1 were extracted by PCR. **(D)** Infectious clones were verified by *NotI* and *SgrAI* digestion. **(E)** Scheme of pJS-KS/2021–53 by replace the 5'UTR and 3'UTR of rJS-KS/2021 with 5'UTR and 3'UTR of HP-PRRSV strain SH1.

filter membranes (NC, Cytiva, Washington, United States). The purified blots were incubated with mouse anti-PRRSV N protein (N) antiserum (1,500) at 4°C overnight, followed by treatment with HRP-conjugated goat anti-mouse IgG (1,500 in TBST, TransGen, Beijing, China) at 37°C for 50 min. Signals were detected using the ECL chemiluminescent detection system (Tanon, Shanghai, China) per the manufacturer's instructions, and resultant images were captured using the Western Blotting imaging system (Tanon, Shanghai, China).

2.8 Statistical analysis

The experimental procedures were performed through at least three independent replicates. All acquired data were analyzed using GraphPad Prism 8. The quantified values were indicated as the mean ± standard deviation. Differences were analyzed for statistical significance using two-tailed unpaired t test for two groups or multiple comparison one-way variance (ANOVA) for more than two groups. $p < 0.05$ was considered statistically significant.

3 Results

3.1 Construction of the full-length infectious cDNA clone

The extraction of viral genomic RNA from the JS-KS/2021 strain followed by reverse transcription to synthesize cDNA, then initiated the generation of a full-length infectious cDNA clone. The resulting viral genome was partitioned into five fragments, denoted as P1-P5, with lengths of 3,016, 2,991, 2,953, 2,811, and 3,565 bp, respectively, as visually presented in Figure 1A. Notably, the observed fragment sizes matched with the anticipated values, as indicated by the congruence displayed in Figure 1B. Following this validation, the fragments were incorporated into a pACYC177 vector, resulting in the successful construction of a full-length cDNA viral plasmid, thereafter referred to as pJS-KS/2021. Its aggregate length was approximately 18.8 kb. Enzymatic digestion of pJS-KS/2021 was verified with *NotI* and *SgrAI* restriction endonucleases, yielding a viral genome of approximately 15 kb (Figure 1D). The results showed that the full-length genome of JS-KS/2021 was successfully inserted into the vector. The efficacy of the reverse genetics system was further validated by the successful rescue of the infective rJS-KS/2021 virus.

3.2 The infective rJS-KS/2021 virus was successfully rescued using the reverse genetics system

The full-length infectious clone of pJS-KS/2021 was transfected into BHK-21 cells by DNA transfection. At 48 hpi, N protein expression was detected by IFA in cells transfected with rJS-KS/2021 clone (Figure 2B). The N protein expression of the rescued virus and the parental virus was analyzed in PAM cells, the target cells of PRRSV. The findings reveal these viruses could exhibit specific green fluorescence in PAM cells (MOI = 0.1). This finding substantiates the robust expression of the N protein in the target cells by the rJS-KS/2021.

The harvested virus supernatants were further passaged to target cells. MARC-145 cells were used to isolated the virus, but no CPE was observed after incubation for 5 days. After three passages in MARC-145 cells, there was still no CPE. The Reverse Transcription-Polymerase Chain Reaction (RT-PCR) analysis showed that the cell culture was PRRSV-negative. PAMs were then used to isolate the virus with the same sample. At 72hpi, the PAMs showed clustering, detachment, and partial lysis (Figure 2A). In contrast, PAM cells in the blank control group were singly dispersed and morphologically intact. The RT-PCR analysis showed that the cell culture was PRRSV-positive, which was shown to amplify the target bands of the expected size. The sequence of ORF5 of rJS-KS/2021 F3 was verified by sequencing to be the same as ORF5 of the primary virus. The virus was then tried to culture in MARC-145 cells again, but no obvious CPE was observed even after five blind passages. The result indicated that rJS-KS/2021 was unable to propagate in MARC-145 cells.

3.3 *In vitro* characterization of the rescued virus rJS-KS/2021

Next, a multiple-step growth curve was performed to characterize the rescued virus. Virus supernatants harvested at 0, 12, 24, 36, 48, 60, 72, 84, and 96 hpi were titrated in PAMs. Based on virus titration results, the parent virus JS-KS/2021 and rescued virus rJS-KS/2021 exhibited similar growth trends and reached their peak titers ($10^{4.34}$ $TCID_{50}$/mL and $10^{4.61}$ $TCID_{50}$/mL) at 72 hpi, although virus titers of JS-KS/2021 were about 0.3 logs lower than these of rJS-KS/2021 at each time (Figure 3A).

Following infection of PAM cells with rJS-KS/2021, cellular samples were harvested at 24 hpi for subsequent western blot assays. The findings of these assays revealed minimal disparity in N protein expression between the rescued virus and the parental virus, JS-KS/2021, as depicted in Figure 3B.

3.4 Characterization of the recombinant virus

The recombinant virus was rescued by DNA transfection of BHK-21 cells. By replacing the 5'UTR and 3'UTR associated with replication capacity, with a view to improving the replication capacity of the virus on PAMs as well as its adaptation at MARC-145. A representative schematic for construction of full-length cDNA clone of rJS-KS/2021–53 was denoted in Figure 1E. Thereafter, the growth characteristics of the recombinant strain were determined. Similarly, the observed band sizes after gel electrophoresis were in accordance with the expected values (Figure 1C). At 72 hpi, typical CPE similar to rJS-KS/2021 were seen on PAMs (Figure 2A), however, no obvious CPE was observed on MARC-145.

The recombinant strain expressed slightly more N protein than rJS-KS/2021(Figure 2B), and we obtained the same result when virus supernatants were harvestred from infected PAMs 24 hpi for western blot assay. This shows that the recombinant strain has a slightly higher replication ability than rJS-KS/2021 at the early stage of viral infection.

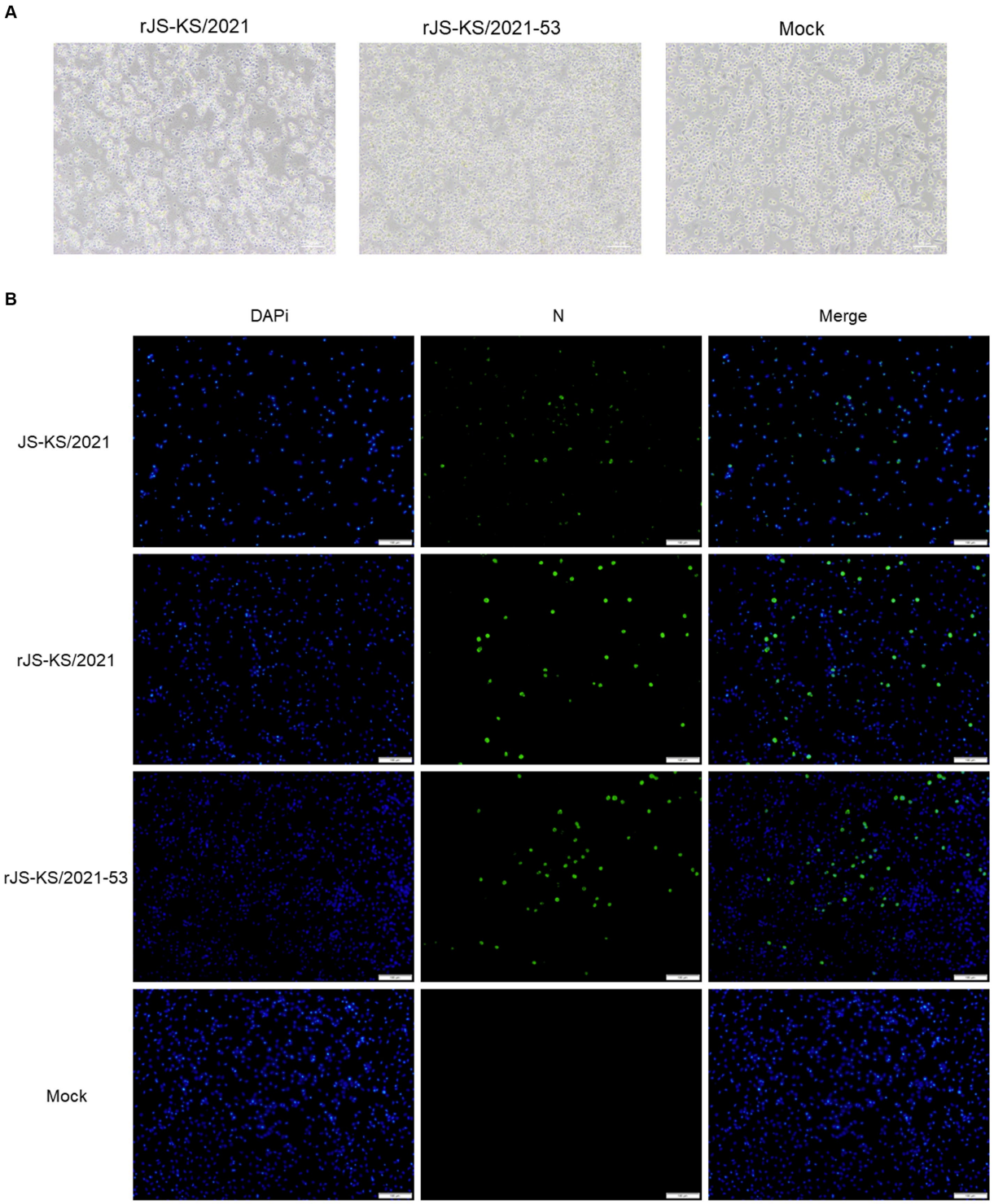

FIGURE 2
Validation of rJS-KS/2021 and rJS-KS/2021–53. **(A)** Cytopathic effects (CPE) in porcine alveolar macrophages (PAM) cells were observed with rJS-KS/2021 and rJS-KS/2021–53. Classical CPE was observed at 72 hpi compared to negative controls. **(B)** Immunofluorescence staining against the N protein in PAM cells at 48 hpi with JS-KS/2021, rJS-KS/2021 and rJS-KS/2021–53 (MOI = 0.1); mock-infected cells (PAM cells) were used as a negative control. Scale bar =100 μm.

But when PAMs cells were infected at MOI = 0.1 for the growth curve analysis, the recombinant strain replicates faster at the early stage and reaches a high titer at 72 hpi compared to rJS-KS/2021. The viral titer after 72 hpi tends to stabilize, and higher than rJS-KS/2021. These results demonstrate that replacing the 5'UTR and 3'UTR of HP-PRRSV improves the replication ability of the recombinant strain, but does not change the fitness of the recombinant strain on MARC-145.

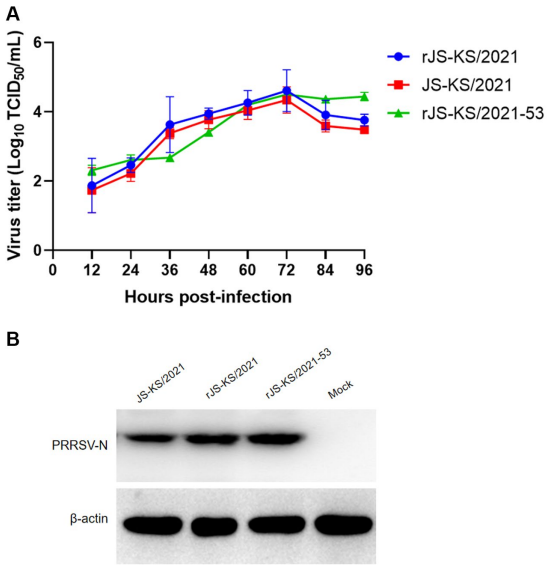

FIGURE 3
Viral characteristic analysis for rJS-KS/2021 and rJS-KS/2021–53. **(A)** Virus growth kinetics in porcine alveolar macrophages (PAMs). Data are represented by mean ± standard deviation of three independent experiments. **(B)** Western blot analysis of N protein in the virus with JS-KS/2021, rJS-KS/2021 and rJS-KS/2021–53 with specific antibodies against N proteins.

4 Discussion

NADC34-like PRRSV was reported for the first time in 2017 in the pig farms of Liaoning Province in China (An et al., 2020). The virus was identified as the causal agent of the symptoms of late abortion, stillbirth, dry or weak fetuses, respiratory distress (interstitial pneumonia) and high mortality in pigs of different ages, especially piglets (Xu Y. et al., 2022). Another way PRRSV affects pigs is through an increased incidence of secondary bacterial infections, including Haemophilus parvum, Pseudomonas multiforme, and Pseudomonas pleuropneumoniae (Bao and Li, 2021; Zhang W. et al., 2023). To date, infections and outbreaks caused by PRRSV have not been well controlled and prevented and thus remain prevalent in numerous countries, and particularly, the emergence of mutants or new strains occasionally causes outbreaks and re-emergence of the disease (Ma et al., 2022). The continuous introduction of foreign breeds has resulted in the recombination of new strains with locally prevalent strains, promoting the diversity of PRRSV (Xia et al., 2023). However, the pathogenicity of NADC34-like PRRSV in China remains elusive (Rawal et al., 2023).

The detection rate of NADC34-Like PRRSV has been on the rise in recent years. In 2017–2019, the PRRSV positivity rate was less than 3%, which gradually increased to 11.5% in 2020. It finally reaches a staggering 28.6% positivity rate. It can be seen that NADC34-Like and NADC30-Like (35.4%) together with highly pathogenic (HP)-PRRSV (31.2%) have become the major strains in some areas of China and are becoming more and more prevalent (Zhao J. et al., 2022). The NADC34 strain has been mainly isolated in the northern provinces of Heilongjiang, Henan, Shandong, Hebei, Jilin, Jiangsu, and Liaoning. Thus, the southern provinces must closely monitor the epidemic trend of this strain (Kappes and Faaberg., 2015; Zhao J. et al., 2022). The NADC34-like PRRSV strains in Sichuan differ from other NADC34-like PRRSV strains in China in terms of molecular genetic characteristics (Xu et al., 2020). The variation in pathogenicity across various NADC34 may be attributed to the different recombination patterns with different PRRSV strains (Nanhua et al., 2013; Pamornchainavakul et al., 2022). Recombination is a common phenomenon among PRRSV isolates and a significant genetic variation that is observed in PRRSV (Wang et al., 2018; Yu et al., 2020; Zhou et al., 2023). A distinct pattern of amino acid (aa) deletion was observed in addition to recombination events, in contrast to the 100-aa deletion in NSP2 (Xie et al., 2022). Consequently, in the wild, NADC34-like PRRSV is more complex (Bao and Li, 2021). To date, there have been no reports of experimental infections of NADC34 in sows and gilts.

Within the realm of molecular biology, reverse genetics is significant techniques, particularly in the fundamental investigation of RNA viruses. Consequently, this technology is extremely important for the advancement of molecular research on PRRSV (Chae et al., 2023). The conventional approach to constructing infectious cDNA molecular clone entails segmenting the genome according to the distribution of restriction sites, amplifying the corresponding viral genome segments, and ligating them with appropriate vectors. This is responsible for controlling the complete cDNA of the PRRSV genome under the influence of robust transcription promoters. Frequently employed promoters encompass bacteriophage T7, T3, SP6, and CMV promoters. Initially, the full-length genome is synthesized, transcribed *in vitro* (T7, T3, and SP6 promoters), and transfected, and subsequently, infectious virus particles are regenerated. It is crucial to note that mutations in fragment nucleotides during the construction and reverse transcription process can impede the successful recovery of infectious clones. Since 1998, infectious clones have been successfully produced using the LV strain as a template, causing successive acquisition of multiple infectious clones (Meulenberg, 2000; Shin et al., 2022). In recent endeavors, numerous infectious clones of both classical-and HP-PRRSV have been carefully engineered in the scientific community of China. Reverse genetic systems have become an important tool in the field of picornavirus research, particularly supporting the investigation of NADC34-like PRRSV. This advanced technology provides a strong technical basis for examining diverse facets such as viral replication, pathogenic mechanisms, virulence genes, molecular details of viral-host interactions, *in vivo* functionality of viral proteins, the creation of live viral vectors, and the development of recombinant genetically engineered vaccines (Zhengda et al., 2022).

CMV is generally recognized as the most powerful promoter of eukaryotic gene expression. Compared with H1/U6 promoter, which is a prokaryotic promoter and has very low initiation efficiency in eukaryotic cells, CMV is a triple-type promoter, which can be initiated in both short and long lengths, and can initiate sequences with PolyA tails. Generally, the CDS region of a gene is inserted downstream of the CMV promoter, and the CMV is responsible for initiating the expression of the gene, so as to increase the expression of the gene. It is most used in the construction of adenovirus and lentivirus overexpression vectors. In contrast to the high specificity of the T7 promoter, which can only be initiated by T7 polymerase binding, the CMV promoter can be initiated by a wide range of polymerases, including *E.coli* RNA polymerase and T7 RNA polymerase. In order to produce stable and generous viruses,

we constructed a full-length infectious cDNA clone (Figure 1A), rescued the virus of the NADC34-like strain, JS-KS/2021. In this study, constructing an infectious clone with a low copy plasmid and placing the CMV promoter in front of the viral genome allowed strict control of viral genome replication and reduced toxicity to cells. The rescued virus rJS-KS/2021 was able to propagate well on PAMs cells (Figure 2A). The biological characteristics of the rescued virus was further evaluated (Figures 2, 3). The results show that rJS-KS/2021 was able to express more N proteins than the parental strain JS-KS/2021. In the analysis of growth curves, rJS-KS/2021 had similar growth characteristics to the parental strain JS-KS/2021 and the viral titer was about 0.3 logs higher than that of the parental strain at each time point.

It is known that the 5′ and 3' UTRs of PRRSV both play critical roles in replication, subgenomic RNA transcription, and infectivity (Verheije et al., 2002; Yin et al., 2013). Shanmukhappa et al. (2007) firstly indicated that 3'UTR RNA of PRRSV is responsible for the interaction with CD151 receptor. CD151 has been identified as another important PRRSV cellular receptor. CD151 is expressed in all PRRSV permissive cell lines, including PAMs, MA-104, MARC-145, Vero, COS-7 and SJPG cells (Shanmukhappa et al., 2007; Provost et al., 2012), while the PRRSV nonpermissive cell lines, such as BHK-21 and MDBK cells, do not express CD151 protein (Shanmukhappa et al., 2007). In 2007, Shanmukhappa et al. (2007) reported that they identified CD151 plays a significant role during PRRSV infection of target cells by a serial of experiments. By the transfection of CD151 clone into BHK-21, the non-susceptible cells became permissive to PRRSV infection. In our study, in view of the replication looping of the 5'UTR and 3'UTR of PRRSV, replace the 5'UTR and 3'UTR of rJS-KS/2021 with the 5'UTR and 3'UTR of HP-PRRSV (strain SH1). The recombinant strain rJS-KS/2021–53 could stably express more N proteins in the early stage of viral infection, which demonstrated by indirect immunofluorescence and western blot assays (Figures 2B, 3B). The growth curve can also support this result (Figure 3A). However, the viral titer after 72 hpi tends to stabilize, higher than the rescued virus rJS-KS/2021 and the parental virus JS-KS/2021. Most importantly, the recombinant strain infected PAMs well, but also failed to propagate on MARC-145. These infectious clones constructed of NADC34-like PRRSV prove reverse genetics becoming more and more important techniques in study of PRRSVs. Moreover, provide a platform for further research on cellular tropism of PRRSV through replacement and mutation.

5 Conclusion

In the present study, we successfully established a reverse genetics system for NADC34-Like PRRSV. Next, we demonstrated that a full-length cDNA clone was able to replicate and infect PAM cells. Also, we replaced the 5'UTR and 3'UTR of rJS-KS/2021 with these of HP-PRRSV (strain SH1). Unfortunately, rJS-KS/2021 and the recombinant virus could not propagate on MARC-145. We believe that this rJS-KS/2021 infectious clone and the information generated in the present study will make a significant contribution to future studies on basic viral biology and to the development of NADC34-Like PRRSV control measures.

Data availability statement

The raw data supporting the conclusions of this article will be made available by the authors, without undue reservation.

Author contributions

YL: Formal analysis, Methodology, Validation, Writing – original draft. LZ: Formal analysis, Investigation, Methodology, Validation, Writing – original draft. CX: Formal analysis, Visualization, Writing – original draft, Writing – review & editing. ZL: Investigation, Validation, Writing – review & editing. KL: Investigation, Validation, Writing – review & editing. BL: Investigation, Validation, Writing – review & editing. DS: Investigation, Validation, Writing – review & editing. YQ: Investigation, Validation, Writing – review & editing. ZM: Conceptualization, Funding acquisition, Project administration, Writing – review & editing. JW: Conceptualization, Formal analysis, Funding acquisition, Methodology, Writing – review & editing.

Funding

The author(s) declare that financial support was received for the research, authorship, and/or publication of this article. This work was supported by grants from the Shanghai Agriculture Applied Technology Development Program, China (no. X2022-02-08-00-12-F01195 and no. X2021-02-08-00-12-F00770, awarded to JW); Cooperation on Animal Biosecurity Prevention and Control in Lancang Mekong Countries (no. 125161035, awarded to JW); Shanghai Municipal Science and Technology Major Project (no. ZD2021CY001, awarded to ZM); and the Agricultural Science and Technology Innovation Program (CAAS-ZDRW202203, awarded to ZM).

Conflict of interest

The authors declare that the research was conducted in the absence of any commercial or financial relationships that could be construed as a potential conflict of interest.

Publisher's note

Supplementary material

The Supplementary material for this article can be found online at: https://www.frontiersin.org/articles/10.3389/fmicb.2024.1359970/full#supplementary-material

References

An, T. Q., Li, J. N., Su, C. M., and Yoo, D. (2020). Molecular and cellular mechanisms for PRRSV pathogenesis and host response to infection. *Virus Res.* 286:197980. doi: 10.1016/j.virusres.2020.197980

Bálint, Á., Molnár, T., Kecskeméti, S., Kulcsár, G., Soós, T., Szabó, P. M., et al. (2021). Genetic variability of PRRSV vaccine strains used in the National Eradication Programme, Hungary. *Vaccine* 9:849. doi: 10.3390/vaccines9080849

Bao, H., and Li, X. (2021). Emergence and spread of NADC34-like PRRSV in China. *Transbound. Emerg. Dis.* 68, 3005–3008. doi: 10.1111/tbed.14316

Chae, H., Roh, H. S., Jo, Y. M., Kim, W. G., Chae, J. B., Shin, S. U., et al. (2023). Development of a one-step reverse transcription-quantitative polymerase chain reaction assay for the detection of porcine reproductive and respiratory syndrome virus. *PLoS One* 18:e0293042. doi: 10.1371/journal.pone.0293042

Kappes, M. A., and Faaberg, K. S. (2015). PRRSV structure, replication and recombination: origin of phenotype and genotype diversity. *Virology* 479, 475–486. doi: 10.1016/j.virol.2015.02.012

Kim, S. C., Moon, S. H., Jeong, C. G., Park, G. S., Park, J. Y., Jeoung, H. Y., et al. (2022). Whole-genome sequencing and genetic characteristics of representative porcine reproductive and respiratory syndrome virus (PRRSV) isolates in Korea. *Virol. J.* 19:66. doi: 10.1186/s12985-022-01790-6

Larochelle, R., D'Allaire, S., and Magar, R. (2003). Molecular epidemiology of porcine reproductive and respiratory syndrome virus (PRRSV) in Québec. *Virus Res.* 96, 3–14. doi: 10.1016/S0168-1702(03)00168-0

Li, Y., Jiao, D., Jing, Y., He, Y., Han, W., Li, Z., et al. (2022). Genetic characterization and pathogenicity of a novel recombinant PRRSV from lineage 1, 8 and 3 in China failed to infect MARC-145 cells. *Microb. Pathog.* 165:105469. doi: 10.1016/j.micpath.2022.105469

Liu, J., Wei, C., Lin, Z., Xia, W., Ma, Y., Dai, A., et al. (2019). Full genome sequence analysis of a 1-7-4-like PRRSV strain in Fujian Province, China. *PeerJ* 7:e7859. doi: 10.7717/peerj.7859

Lu, Y., Zhang, Y., Xiang, X., Sharma, M., Liu, K., Wei, J., et al. (2020). Notch signaling contributes to the expression of inflammatory cytokines induced by highly pathogenic porcine reproductive and respiratory syndrome virus (HP-PRRSV) infection in porcine alveolar macrophages. *Dev. Comp. Immunol.* 108:103690. doi: 10.1016/j.dci.2020.103690

Ma, X., Wang, P., Zhang, R., Zhao, Y., Wu, Y., Luo, C., et al. (2022). A NADC30-like PRRSV causes serious intestinal infections and tropism in piglets. *Vet. Microbiol.* 268:109397. doi: 10.1016/j.vetmic.2022.109397

Meulenberg, J. (2000). PRRSV, the virus. *Vet. Res.* 31, 11–21. doi: 10.1051/vetres:2000103

Nanhua, C., Xiuling, Y., Lilin, W., Jiajun, W., Zhi, Z., Jianqiang, N., et al. (2013). Two natural recombinant highly pathogenic porcine reproductive and respiratory syndrome viruses with different pathogenicities. *Virus Genes* 46, 473–478. doi: 10.1007/s11262-013-0892-4

Ouyang, T., Zhang, X., Liu, X., and Ren, L. (2019). Co-infection of swine with porcine circovirus type 2 and other swine viruses. *Viruses* 11:185. doi: 10.3390/v11020185

Pamornchainavakul, N., Kikuti, M., Paploski, I. A. D., Makau, D. N., Rovira, A., Corzo, C. A., et al. (2022). Measuring how recombination re-shapes the evolutionary history of PRRSV-2: a genome-based Phylodynamic analysis of the emergence of a novel PRRSV-2 variant. *Front Vet Sci* 9:846904. doi: 10.3389/fvets.2022.846904

Provost, C., Jia, J. J., Music, N., Lévesque, C., Lebel, M., del Castillo, J. R., et al. (2012). Identification of a new cell line permissive to porcine reproductive and respiratory syndrome virus infection and replication which is phenotypically distinct from MARC-145 cell line. *Virol. J.* 9:267. doi: 10.1186/1743-422X-9-267

Pujhari, S., and Zakhartchouk, A. N. (2016). Porcine reproductive and respiratory syndrome virus envelope (E) protein interacts with mitochondrial proteins and induces apoptosis. *Arch. Virol.* 161, 1821–1830. doi: 10.1007/s00705-016-2845-4

Rawal, G., Almeida, M. N., Gauger, P. C., Zimmerman, J. J., Ye, F., Rademacher, C. J., et al. (2023). In vivo and in vitro characterization of the recently emergent PRRSV 1–4-4 L1C variant (L1C.5) in comparison with other PRRSV-2 lineage 1 isolates. *Viruses* 15:2233. doi: 10.3390/v15112233

Shanmukhappa, K., and Kapil, S. (2001). Cloning and identification of MARC-145 cell proteins binding to 3'UTR and partial nucleoprotein gene of porcine reproductive and respiratory syndrome virus. *Adv. Exp. Med. Biol.* 494, 641–646. doi: 10.1007/978-1-4615-1325-4_95

Shanmukhappa, K., Kim, J. K., and Kapil, S. (2007). Role of CD151, a tetraspanin, in porcine reproductive and respiratory syndrome virus infection. *Virol. J.* 4:62. doi: 10.1186/1743-422X-4-62

Shin, G. E., Park, J. Y., Lee, K. K., Ko, M. K., Ku, B. K., Park, C. K., et al. (2022). Genetic diversity of porcine reproductive and respiratory syndrome virus and evaluation of three one-step real-time RT-PCR assays in Korea. *BMC Vet. Res.* 18:327. doi: 10.1186/s12917-022-03407-0

Sun, Y. F., Zhou, L., Bian, T., Tian, X.-X., Ren, W.-K., Lu, C., et al. (2018). Efficacy evaluation of two commercial modified-live virus vaccines against a novel recombinant type 2 porcine reproductive and respiratory syndrome virus. *Vet. Microbiol.* 216, 176–182. doi: 10.1016/j.vetmic.2018.02.016

Tian, K. (2017). NADC30-like porcine reproductive and respiratory syndrome in China. *Open Virol. J.* 11, 59–65. doi: 10.2174/1874357901711010059

Trevisan, G., Li, G., Moura, C. A. A., Coleman, K., Thomas, P., Zhang, J., et al. (2021). Complete coding genome sequence of a novel porcine reproductive and respiratory syndrome virus 2 restriction fragment length polymorphism 1-4-4 lineage 1C variant identified in Iowa, USA. *Microbiol. Resour. Announc.* 10:e0044821. doi: 10.1128/MRA.00448-21

Tu, T., Pang, M., Jiang, D., Zhou, Y., Wu, X., Yao, X., et al. (2023). Development of a real-time TaqMan RT-PCR assay for the detection of NADC34-like porcine reproductive and respiratory syndrome virus. *Vet. Sci.* 10:279. doi: 10.3390/vetsci10040279

van Geelen, A. G. M., Anderson, T. K., Lager, K. M., Das, P. B., Otis, N. J., Montiel, N. A., et al. (2018). Porcine reproductive and respiratory disease virus: evolution and recombination yields distinct ORF5 RFLP 1-7-4 viruses with individual pathogenicity. *Virology* 513, 168–179. doi: 10.1016/j.virol.2017.10.002

Verheije, M. H., Olsthoorn, R. C., Kroese, M. V., Rottier, P. J., and Meulenberg, J. J. (2002). Kissing interaction between 3′ noncoding and coding sequences is essential for porcine arterivirus RNA replication. *J. Virol.* 76, 1521–1526. doi: 10.1128/JVI.76.3.1521-1526.2002

Wang, H. M., Liu, Y. G., Tang, Y. D., Liu, T. X., Zheng, L. L., Wang, T. Y., et al. (2018). A natural recombinant PRRSV between HP-PRRSV JXA1-like and NADC30-like strains. *Transbound. Emerg. Dis.* 65, 1078–1086. doi: 10.1111/tbed.12890

Wang, S., Liu, Y., Yu, L., Liang, T., Zhang, P., Dong, J., et al. (2021). A strain of highly pathogenic porcine reproductive and respiratory syndrome virus: genomic characterization, pathogenicity, and construction of an infectious full-length cDNA clone. *Arch. Virol.* 166, 3127–3141. doi: 10.1007/s00705-021-05212-w

Wootton, S., Yoo, D., and Rogan, D. (2000). Full-length sequence of a Canadian porcine reproductive and respiratory syndrome virus (PRRSV) isolate. *Arch. Virol.* 145, 2297–2323. doi: 10.1007/s007050070022

Wu, Y., Peng, O., Xu, Q., Li, Q., Li, W., Lin, L., et al. (2022). Characterization and pathogenicity of two novel PRRSVs recombined by NADC30-like and NADC34-like strains in China. *Viruses* 14:2174. doi: 10.3390/v14102174

Xia, Y., Zhang, T., Gong, D., Qi, J., Jiang, S., Yang, H., et al. (2023). Recombination and mutation in a new HP-PRRSV strain (SD2020) from China. *Viruses* 15:165. doi: 10.3390/v15010165

Xie, C. Z., Tao, Y. M., Ha, Z., Zhang, P., Zhang, Y., Zhang, H., et al. (2022). Characterization of a new NSP2-deletion NADC34-like porcine reproductive and respiratory syndrome virus in China. *Res. Vet. Sci.* 152, 212–218. doi: 10.1016/j.rvsc.2022.08.001

Xie, C. Z., Wang, Z., Ha, Z., Zhang, Y., Xie, Y. B., Zhang, H., et al. (2021). Genetic characterization of a new NSP2-deletion porcine reproductive and respiratory syndrome virus in China. *Microb. Pathog.* 150:104729. doi: 10.1016/j.micpath.2021.104729

Xu, H., Li, C., Gong, B., Li, W., Guo, Z., Sun, Q., et al. (2023). Protective efficacy of a candidate live-attenuated vaccine derived from the SD-R strain against NADC34-like porcine reproductive and respiratory syndrome virus. *Vaccine* 11:1349. doi: 10.3390/vaccines11081349

Xu, H., Li, C., Li, W., Zhao, J., Gong, B., Sun, Q., et al. (2022). Novel characteristics of Chinese NADC34-like PRRSV during 2020-2021. *Transbound. Emerg. Dis.* 69, e3215–e3224. doi: 10.1111/tbed.14485

Xu, H., Song, S., Zhao, J., Leng, C., Fu, J., Li, C., et al. (2020). A potential endemic strain in China: NADC34-like porcine reproductive and respiratory syndrome virus. *Transbound. Emerg. Dis.* 67, 1730–1738. doi: 10.1111/tbed.13508

Xu, Y., Ye, M., Sun, S., Cao, Q., Luo, J., Wang, Y., et al. (2022). CD163-expressing porcine macrophages support NADC30-like and NADC34-like PRRSV infections. *Viruses* 14:2056. doi: 10.3390/v14092056

Xue, R. X., Sun, S. F., Li, Y. G., Wang, M. L., Wang, G. S., Li, Y. J., et al. (2021). Diversity of porcine reproductive and respiratory syndrome virus in Shandong, China. *Acta Virol.* 65, 303–306. doi: 10.4149/av_2021_305

Yim-Im, W., Anderson, T. K., Paploski, I. A., VanderWaal, K., Gauger, P., Krueger, K., et al. (2023). Refining PRRSV-2 genetic classification based on global ORF5 sequences and investigation of their geographic distributions and temporal changes. *Microbiol. Spectr.* 11:e0291623. doi: 10.1128/spectrum.02916-23

Yin, Y., Liu, C., Liu, P., Yao, H., Wei, Z., Lu, J., et al. (2013). Conserved nucleotides in the terminus of the 3' UTR region are important for the replication and infectivity of porcine reproductive and respiratory syndrome virus. *Arch. Virol.* 158, 1719–1732. doi: 10.1007/s00705-013-1661-3

Yu, F., Yan, Y., Shi, M., Liu, H. Z., Zhang, H. L., Yang, Y. B., et al. (2020). Phylogenetics, genomic recombination, and NSP2 polymorphic patterns of porcine reproductive and respiratory syndrome virus in China and the United States in 2014-2018. *J. Virol.* 94:e01813-19. doi: 10.1128/JVI.01813-19

Yuan, L., Zhu, Z., Fan, J., Liu, P., Li, Y., Li, Q., et al. (2022). High pathogenicity of a Chinese NADC34-like PRRSV on pigs. *Microbiol. Spectr.* 10:e0154122. doi: 10.1128/spectrum.01541-22

Zhang, H., Luo, Q., Zheng, Y., Sha, H., Li, G., Kong, W., et al. (2023). Genetic variability and recombination of the NSP2 gene of PRRSV-2 strains in China from 1996 to 2021. *Vet. Sci.* 10:325. doi: 10.3390/vetsci10050325

Zhang, W., Ma, W., Pan, Y., Wang, X., Wang, M., Zhang, H., et al. (2023). Characterization of Rongchang piglets after infection with type 2 porcine reproductive and respiratory syndrome virus strains differing in pathogenicity. *Front. Microbiol.* 14:1283039. doi: 10.3389/fmicb.2023.1283039

Zhang, H.-L., Zhang, W.-L., Xiang, L.-R., Leng, C.-L., Tian, Z.-J., Tang, Y.-D., et al. (2018). Emergence of novel porcine reproductive and respiratory syndrome viruses (ORF5 RFLP 1-7-4 viruses) in China. *Vet. Microbiol.* 222, 105–108. doi: 10.1016/j.vetmic.2018.06.017

Zhao, K., Gao, J. C., Xiong, J. Y., Guo, J. C., Yang, Y. B., Jiang, C. G., et al. (2018). Two residues in NSP9 contribute to the enhanced replication and pathogenicity of highly pathogenic porcine reproductive and respiratory syndrome virus. *J. Virol.* 92:e02209-17. doi: 10.1128/JVI.02209-17

Zhao, H. Z., Wang, F. X., Han, X. Y., Guo, H., Liu, C. Y., Hou, L. N., et al. (2022). Recent advances in the study of NADC34-like porcine reproductive and respiratory syndrome virus in China. *Front. Microbiol.* 13:950402. doi: 10.3389/fmicb.2022.950402

Zhao, J., Xu, L., Xu, Z., Deng, H., Li, F., Sun, X., et al. (2022). Emergence and spread of NADC34-like PRRSV in Southwest China. *Transbound. Emerg. Dis.* 69, e3416–e3424. doi: 10.1111/tbed.14463

Zhengda, C., Jinxia, C., Liwei, L., Jiachen, L., Wu, T., Yanjun, Z., et al. (2022). A rescued NADC30-like virus by reverse genetic manipulation exhibits moderate virulence and a promising application perspective. *Virus Res.* 316:198801. doi: 10.1016/j.virusres.2022

Zhenhua, G., Xin-Xin, C., Rui, L., Songlin, Q., and Gaiping, Z. (2018). The prevalent status and genetic diversity of porcine reproductive and respiratory syndrome virus in China: a molecular epidemiological perspective. *Virol. J.* 15:2. doi: 10.1186/s12985-017-0910-6

Zhou, L., Yang, Y., Xia, Q., Guan, Z., Zhang, J., Li, B., et al. (2022). Genetic characterization of porcine reproductive and respiratory syndrome virus from eastern China during 2017-2022. *Front. Microbiol.* 13:971817. doi: 10.3389/fmicb.2022.971817

Zhou, L., Yu, J., Zhou, J., Long, Y., Xiao, L., Fan, Y., et al. (2023). A novel NADC34-like porcine reproductive and respiratory syndrome virus 2 with complex genome recombination is highly pathogenic to piglets. *Infect. Genet. Evol.* 112:105436. doi: 10.1016/j.meegid.2023.105436

Zhu, Z., Yuan, L., Hu, D., Lian, Z., Yao, X., Liu, P., et al. (2021). Isolation and genomic characterization of a Chinese NADC34-like PRRSV isolated from Jiangsu province. *Transbound. Emerg. Dis.* 69, e1015–e1027. doi: 10.1111/tbed.14392

Frontiers in Microbiology

Explores the habitable world and the potential of microbial life

The largest and most cited microbiology journal which advances our understanding of the role microbes play in addressing global challenges such as healthcare, food security, and climate change.

Discover the latest Research Topics

See more →

Frontiers

Avenue du Tribunal-Fédéral 34
1005 Lausanne, Switzerland
frontiersin.org

Contact us

+41 (0)21 510 17 00
frontiersin.org/about/contact